Analysis of *Epichloë festucae* membrane lipid composition and its role in Nox complex assembly

A thesis presented in partial fulfilment of the requirements for the degree of

Master of Science

in

Genetics

At Massey University, Palmerston North

New Zealand

Alyesha Valerie Joy Candy

2018

Abstract

Epichloë festucae is a filamentous fungus that forms a highly regulated mutualistic symbiosis with perennial ryegrass. The spatially and temporally controlled production of reactive oxygen species (ROS) by the fungal NADPH oxidase (Nox) complex regulates this interaction by restricting fungal growth *in planta*. Whilst much is known about the importance of ROS in plant-fungal interactions, comparatively little is known about how its production is regulated. In plant and mammalian systems, production of ROS by the Nox complex is regulated via lipid signalling. Cytosolic Nox components containing lipid-binding domains are targeted to specific phosphoinositide enriched at certain locations within in the plasma membrane. Once assembled, specific lipids then directly activate the Nox complex. It is hypothesised that similar regulation also occurs in fungi. This study investigated whether lipid signalling could play a role in regulating the fungal Nox complex. The lipid-binding PH domain of Nox protein Cdc24 was found to be necessary for membrane localisation, supporting a role for lipid signalling in fungal Nox complex regulation. To identify potential lipid targets for the cytosolic Nox proteins, a comprehensive analysis of *E. festucae* membrane lipid composition was carried out using a suite of biosensors. These biosensors consisted of mammalian lipid binding domains of known specificity fused to a fluorophore, enabling live cell imaging of phosphoinositide localisation both in culture and *in planta* via fluorescence microscopy. Phosphatidylinositol 4,5-bisphosphate was detected in the plasma membrane and septa in culture and *in planta*. A striking asymmetric gradient was observed at the hyphal tip, with enriched fluorescence in the sub-apical region. Similar to yeast, phosphatidylinositol 4-phosphate was localised to golgi vesicles in culture. In contrast, phosphatidylinositol 3-phosphate was found in vacuolar and endosomal membranes. Biosensors for phosphatidylinositol 3,4-bisphosphate and phosphatidylinositol 3,4,5-triphosphate, localised to the cytoplasm in culture and *in planta*, suggesting that these phospholipids were absent under the growth conditions examined. These results confirm a role for lipid signalling in fungal Nox complex assembly and provide insight into membrane lipid composition, identifying candidate phosphoinositide targets for assembly.

Acknowledgements

To start off I would like to thank my fantastic supervisors. Carla Eaton, you have provided me with invaluable advice and cautionary tales of past, some of which I learnt from some of which I repeated (agar vs agarose... whoops). Thank you so much for your bottomless support and encouragement. You never failed to lighten the mood and ease my worries with a hilarious story, while providing top-notch scientific guidance. Barry Scott, you helped me an incredible amount in not only guiding my research, but also in providing great tramping and climbing recommendations, and most importantly in showing me that even as a Prof you can be the life of a party. Thank you so much for your help and support.

To Eaton Lab and ScottBase members, Ellie, Kim, Berit, Yonathan, Nazanin, Taryn, Dan, and Katrin. Thank you so much for all the advice, chats, and lending of solutions.

To Arvina, you really are the heart and soul of the lab. From day one you took me under your wing and have provided me with an incredible amount of help and support. You were always around for a causal chat, last minute advice, lending of sterilised equipment, and most importantly provision of chocolate. Thank you so very much.

To the staff at MMIC, especially Matthew, thank you so much for all of your guidance and expert knowledge.

To my family, thank you for all the love and support. Mum with an endless supply of pep talks, Dad with the steady advice, and Gab with the constant chats and offers of solace down in Dunedin.

To Greg, thank you for all the times you brought me dinner on late nights, all the times you helped me with those 'wee' tasks that would end up taking three hours, and for everything else.

To MUAC members, especially my fellow committee members, thank you for being my adventure buddies. All the awesome adventures from bush balls to mountain

climbs to general camping are such treasured memories and provided me with much needed breaks from Palmy.

Finally to the Royal Society of New Zealand Marsden Fund and Bio-protection Research Centre who have funded my research and myself. Thank you very much. In addition to you making this research possible, you have enabled me to travel across the world and to various places around New Zealand meeting other fantastic scientists and gaining invaluable experience in communicating my research with a broad range of people.

Table of contents

List of figures

List of tables

List of abbreviations

Amp	ampicillin
Amp^R	ampicillin resistant
bp	base pair
BLAST	basic local alignment search tool
BLASTp	search of protein databases with a protein query
cDNA	complementary DNA
Cp	crossing point
CR	contractile ring
d	day(s)
DIC	differential interference contrast
DMSO	dimethyl sulfoxide
DNA	deoxyribonucleic acid
dNTP	deoxynucleotide triphosphate
EDTA	ethylenediaminetetraacetic acid
eGFP	enhanced green fluorescent protein
EM	electron microscopy
g	gram
gDNA	genomic DNA
Gen	geneticin
Gen^R	geneticin resistant
H	hour
Hyg	hygromycin
Hyg^R	hygromycin resistant
HPLC	high performance liquid chromatography
Kb	kilobase
L	litre
LBD	lipid-binding domain
LB	Luria-Bertani
M	Molar
MAP	mitogen-activated protein
µg	microgram

µL	microlitre
µm	micrometre
µM	micromolar
mg	milligram
mL	millilitre
mm	millimetre
mM	millimolar
min	minute
mRNA	messenger RNA
MVB	multi-vesicular body
N/A	not applicable
NADPH	nicotinamide adenine dinucleotide phosphate
Ng	nannogram
nM	nannomolar
Nox	NADPH oxidase
OE	overexpression
PCR	polymerase chain reaction
PD	potato dextrose
PEG	polyethylene glycol
PIK	phosphatidylinositol kinase
PI[3]P	phosphatidylinositol 3-phosphate
PI[3,4]P_2	phosphatidylinositol 3,4-bisphosphate
PI[3,4,5]P_3	phosphatidylinositol 3,4,5-triphosphate
PI[4]P	phosphatidylinositol 4-phosphate
PI[4,5]P_2	phosphatidylinositol 4,5-bisphosphate
PM	plasma membrane
PPI	phosphoinositide
qRT-PCR	quantitative reverse transcription PCR
RG	regeneration
RNA	ribonucleic acid
ROS	reactive oxygen species
rpm	revolutions per minute
RT-PCR	reverse transcriptase PCR

s	second
SDS	sodium dodecyl sulphate
SNX	sorting nexin
spp.	species
TBE	Tris/Borate/EDTA
tBLASTn	search of translated nucleotide databases with a protein query
TGN	*trans*-Golgi network
UV	ultraviolet
V	volt
v / v	volume to volume
vol	volume
w / v	weight to volume
WT	wild-type

1. Introduction

Plants and fungi have an interconnected history in the natural ecosystem, with interactions ranging from beneficial to pathogenic (1). Originally, only pathogenic interactions were documented and the idea of beneficial symbiosis wasn't proposed until 1898 when fungal hyphae were identified in seeds (2). These beneficial interactions are now recognised as one of the most successful strategies employed by plants, allowing them to adapt to a variety of environmental niches and withstand environmental change (3). Fossil records and molecular data revealed that beneficial interactions have existed since the Paleozoic era, where fungal associations aided plants in the colonisation of land (4). Most plants studied in natural ecosystems form symbiotic associations with fungal endophytes resulting in increased fitness (5, 6). The term 'endophyte' being a generic term for any organism that lives within ('endo-') a plant ('-phyte') (7, 8). The *Epichloë* fungal endophyte genus (Ascomycota, Clavicipitaceae) form symbiotic interactions with cool season grasses of the sub family Pooideae, including perennial ryegrass (*Lolium perenne*), the most commonly sown grass in New Zealand pastures and a globally important pasture grass (9). These endophytes increase the tolerance of the host plant against biotic and abiotic stresses (9-11). The production of secondary metabolites by *Epichloë festucae* protects the host plant from biotic stresses, such as insect and mammalian herbivory (11-14). In addition, *E. festucae* affects the osmotic balance of the host plant, increasing the tolerance to abiotic stresses, such as drought (15, 16). In return, the host plant provides *E. festucae* with a stable environment, a continuous supply of nutrients, and source of dissemination *via* colonisation of seeds (17).

1.1 The *E. festucae – L. perenne* model system

Epichloë endophytes were originally classified into two distinct genera: *Neotyphodium*, which has a strictly asexual life cycle; and *Epichloë*, which has both sexual and asexual life cycles. In response to fungal nomenclature changes in 2011, these genera have been merged and are now collectively placed in the *Epichloë* genus (18, 19). Both *E. festucae* and its asexual derivative *E. festucae* var. *lolii* form beneficial mutualistic interactions with perennial ryegrass, *Lolium perenne*. While *E. festucae* var. *lolii* is the predominant symbiont of *L. perenne* in nature, the artificially induced interaction with *E. festucae* is better suited for laboratory

experimentation (20). *E. festucae* grows relatively fast, forming a consistent white fluffy mycelial colony in culture in one week, compared to *E. festucae* var. *lolii* which has an unstable colony morphology and requires multiple weeks to grow (21, 22). Additionally, *E. festucae* can be easily manipulated using molecular techniques yielding good transformation frequencies (23) and inoculations with strain Fl1 typically achieve a 90% infection rate with *L. perenne* in the laboratory (24). Furthermore, the genomic sequence of two *E. festucae* strains, Fl1 and E2368, are now available (Schardl et al, 2013; Winter et al, 2018), assisting genetic analysis and manipulation and making *E. festucae* an ideal model organism for studying mutualistic symbiotic interactions.

1.2 *E. festucae* life cycle

E. festucae has the ability to undergo both sexual and asexual life cycles (Figure 1.1).

1.2.1 Asexual life cycle

The *E. festucae* life cycle is primarily asexual. In this mode of reproduction, there are no external reproductive structures as the fungus is vertically transmitted through the seeds of the infected plant. During vegetative development of the host plant, hyphae colonise the intercellular regions of the true stem via polarized tip growth. From here hyphae spread into the leaf primordia and axillary buds to infect the growing leaves (11). When the host undergoes reproductive development the hyphae colonise the inflorescence tissues including the ovary and ovules. Immediately after fertilisation, hyphae gain entry to the embryo sac and as the embryo matures, hyphae become widespread throughout the embryo and surrounding tissues (20). When seed germination occurs, hyphae infect all plant tissues above ground, with the pattern of growth very dependent on the tissue being colonised (1, 25, 26).

1.2.2 Sexual life cycle

When *Epichloë* enters the sexual life cycle, the formation of the host inflorescence primordia results in a switch from restricted mutualistic hyphal growth to

Figure 1.1. **The two different life cycles of *Epichloë festucae*.** Reproduced from Oberhofer (27).

proliferative pathogenic growth and initiation of stromata (sexual structure) formation (9). This results in a disease called 'choke' where the emergence of the host inflorescence is blocked (Figure 1.2) (28). Conidia, which act as spermatia, are abundant on these structures. Female flies of the genus *Botanophila* consume and transfer conidia in their gut and ovipositor. Oviposition occurs on stromata formed on different host plants, and the flies also excrete conidia through faeces onto these tissues. If a different mating type is present, fruiting structures, called perithecia, containing asci with eight ascospores will develop (13). Ascospores are released into the air and will infect neighbouring plants through the florets. *Epichloë* benefit from flies as reliable vectors, while fly larvae benefit by using the fertilised stroma as a food source (13, 29, 30).

Figure 1.2. ***Epichloë festucae*** **stromata on fine fescue causing 'Choke' disease.** Reproduced from Scott, Becker (20).

While *E. festucae* is capable of entering the sexual lifecycle, in its natural hosts, including *Festuca rubra* (fine fescue) and *Festuca longifolia* (hard fescue), there have been no reports of 'choke' in associations with perennial ryegrass (20).

1.3 Growth of *E. festucae*

1.3.1 Growth in axenic culture

E. festucae is predominantly cultivated on potato dextrose agar and forms a white fluffy colony expanding at 1 to 3 mm per day. It can utilise a range of carbon and nitrogen sources and often starts to senesce 2 to 3 weeks after cultivation when nutrients become limiting (20). Young hyphae at the edge of the colonies grow in parallel-unbranched bundles, which appear to be stuck together by an unknown adhesive (31). When stained with Calcofluor white, both the tips and septa fluoresce brightly, indicative of active chitin synthesis (20). Towards the middle of the colony, hyphae branch frequently and are found in two distinct layers: one attached to the agar, for continued access to nutrients; and another forming bunches of at least 10 hyphae growing on top of one another. In this region, coiled structures that often produce conidiospores are common, although in *E. festucae* Fl1 formation of conidiospores is sparse and sporadic (32). Older hyphae in the centre of the colony frequently fuse with each other to form an interconnected hyphal network. This is necessary for colony formation enabling nutrient transfer and signal transduction (20, 33).

1.3.2 Conidiogenesis and conidiospore germination in culture

The ability of *E. festucae* to sporulate is variable between different strains. For example, strain Fl1 produces very few conidiospores, whereas strain E2368, derived from a backcross of progeny E189 and E464, was selected on the basis of its ability to sporulate and readily produces conidiospores (34, 35). To increase sporulation in Fl1, nutrient limitations and specific media can be employed; however, this normally reduces the growth rate of the fungus (36). Instead, E2368 is preferentially used for conidiospore studies. The mature conidiophore is a unicellular phialide, which forms either at the tips of long, thin, unbranched hyphae or from branches radiating off hyphal coils (20). Oval shaped conidia

develop at the tip of a phialide and are released through either the production of a new conidium or mechanical shear as seen in *Epichloë typhina* (37). Spores germinate readily on both PD and water agar. Initially a single germ tube emerges from one end of the conidium, then either a branch will form or a second germ tube will emerge from the opposite end. After 15-24 hours a range of germ tube lengths are observed. At 72 hours a three dimensional mycelial net forms including phialides which produce more conidiospores (20).

1.3.3 Growth *in planta*

E. festucae systematically colonises all vegetative and reproductive tissues above ground, including leaf blade, sheath, and pseudostem tissues (20). When introduced through vertical transmission or artificial inoculation *E. festucae* grows within the apoplastic spaces, initially via tip growth, forming a branched mycelial net in the shoot meristem. Once hyphae colonise the leaf primordia they attach to the plant cell wall (38, 39). Host leaf cell expansion triggers a switch to stretch via intercalary growth effectively synchronising the growth of the fungi with the plant (25, 38). This switch is essential as it avoids mechanical shear and hyphal breakage when the leaf tissue rapidly expands (9). Leaf tissue can expand by 1 cm a day, whereas the growth rate of *E. festucae* on potato dextrose agar is just 1-3 mm per day (20). Such closely co-ordinated growth requires strict regulation that involves communication between the fungus and host plant resulting in restricted fungal growth. Unlike obligate biotrophic ascomycetes, *E. festucae* has no specialised feeding structures, such as haustoria. Instead, it relies on direct uptake of nutrients from the apoplastic space or by transport between the fungus and its host plant. This is likely because *E. festucae* has maintained a number of genes involved in primary metabolism so is less reliant on the host plant for key nutrients (16). In addition to endophytic growth, *E. festucae* is also observed growing epiphytically. Endophytic hyphae form expressoria which breach the cuticle allowing the fungi to grow and form conidia from coiled structures on the plant surface, as seen in culture (40). The presence of epiphyllous hyphal nets is thought to increase the resistance of the plant host to fungal pathogens through ‘niche exclusion’ or by biosynthesis of bioprotective metabolites (41).

1.4 Regulation of fungal growth *in planta*

Establishment and maintenance of an *E. festucae* symbiotic network in *L. perenne* is dependent on a number of signalling pathways, including the cell wall integrity (CWI) (42), pheromone response/invasive growth (PR/IG), and stress-activated mitogen-activated protein (MAP) kinase pathways (43); cAMP/PKA signalling (44); calcineurin signalling (45); and reactive oxygen species (ROS) signalling from the NADPH oxidase (Nox) complex (12, 23, 46-48). Together these pathways achieve two main objectives: suppression or evasion of plant defence responses (12, 46) and regulation of fungal growth inside the host plant (14, 49, 50). Disruption of *E. festucae* genes in these signalling pathways frequently leads to a severe host phenotype characterised by fungal senescence and host stunting.

In particular, ROS produced by the Nox complex has been identified as an important regulator of symbiosis in filamentous fungi, enabling both beneficial and pathogenic infection (46, 51). In *E. festucae* the timed and localised production of ROS by the Nox complex is necessary for the regulation of hyphal growth *in planta* (46). Nox catalysed ROS production is a universal signalling system among multi-cellular organisms and the reactive nature of H_2O_2 makes it an ideal second messenger for signalling (52). Two ROS producing Nox isoforms have been identified in *E. festucae*, NoxA and NoxB (46). Tanaka, Christensen (46) showed that *noxA* mutants lose apical dominance and the ability to fuse resulting in unrestricted pathogen-like growth with a significant increase in fungal biomass indicative of an antagonistic interaction. This causes severe host plant stunting, precocious senescence, and an increased mortality rate. Deletion of *noxB* similarly causes host stunting; however, unlike Δ*noxA*, Δ*noxB* retains the ability to fuse in culture (40). The ability of Δ*noxB* mutants to fuse is significant because cell-cell fusion is essential for an endophyte to develop a stable hyphal network *in planta* (42). This indicates that NoxB regulates the association between *E. festucae* and perennial ryegrass in a different way to NoxA, as seen in *Magnaporthe oryzae* (36, 40, 51). It is proposed that ROS produced by the NoxA isoform are an important regulator of fungal growth, where bursts of ROS negatively regulate hyphal tip growth preventing excessive colonisation (23). Despite its importance, very little is known about how the complex itself is regulated. Insights into potential

mechanisms for regulation of the fungal Nox complex can be gained based on conserved mammalian and plant systems (23, 53, 54).

1.5 Lipid signalling in Nox complex assembly and activation

The Nox enzymes are most well characterised in mammalian systems, where they are divided into three sub families: Nox1-Nox4, Nox5, and Duox. Fungal NoxA and NoxB isoforms are both homologues of the mammalian Nox2 isoform (Figure 1.3). Nox2, found in the membranes of phagocytes and neutrophils, is responsible for the oxidative burst response to invading pathogens. Due to the important role Nox2 plays in the immune system the regulation of the complex is well established (53, 55).

A key mechanism for regulating Nox2 in mammals is through lipid signalling. Interactions between specific phosphoinositides (PPIs) and cytosolic Nox proteins, p47*phox*, p67*phox*, and p40*phox*, enable the assembly of the cytosolic proteins with the membrane bound, gp91*phox* and p22*phox* (56-58). Upon an unknown activation signal, the cytosolic Nox proteins are phosphorylated resulting in a conformational change. Protein interaction domains and lipid-binding PX domains are exposed allowing p47*phox*, p67*phox*, and p40*phox* to interact and translocate to the membrane bound proteins (53).

p67*phox*, does not contain any lipid-binding domains (LBDs), instead it is likely recruited via interaction with the other cytosolic proteins p47*phox* and p40*phox* (59). Protein kinase C (PKC) also plays an important role in recruiting p67*phox*. PKC is a lipid-regulated kinase that is activated by second messengers DAG and inositol triphosphate. PKC isoform, PKCβ, is necessary for p47phox and p67phox phosphorylation and translocation in human meningeal cells (60). Overexpression of PKCδ in human neuroblastoma cells leads to increased recruitment of p67*phox* and increased ROS production (61). While, inhibition of PKC *in vivo* leads to reduced p67*phox* phosphorylation, suggesting PKC likely induces p67*phox* membrane translocation (62).

Figure 1.3. Composition of the mammalian Nox2 complex (left) and fungal Nox complexes containing NoxA and NoxB isoforms. Reproduced from Scott (58).

PX domains in p40^{phox} and p47^{phox} are crucial for the recruitment of these cytosolic proteins in the mammalian Nox2 complex (53). The PX domain of p47^{phox} has several potential lipid targets. It preferentially binds to vesicles containing phosphoinositide 4-phosphate (PI[4]P) and phosphoinositide 3,4-bisphosphate (PI[3,4]P_2) (63-65). Additionally, the PX domain may be capable of binding acidic phospholipids, such as phosphatidic acid (PA) (64, 66-68). The p40^{phox} PX domain has one lipid target, specifically binding phosphoinositide 3-phosphate (65, 68).

E. festucae does not contain homologues of p40^{phox} and p47^{phox}. Instead, BemA is thought to be a functional homologue of both mammalian proteins (48). The BemA protein is a strong candidate to fulfil this function given that it physically interacts with NoxR and contains protein interaction domains, SH3, PB1, and PX, similar to those found in p47^{phox} and p40^{phox}. These domains would facilitate interactions with other proteins and the plasma membrane (PM), necessary for complex assembly and activation (48, 69, 70). In yeast, Bem1p binds PI[4]P in the PM, making PI[4]P a potential target for Nox activation (65). However, the BemA PX domain is not required for membrane localisation in *Neurospora crassa* (71), suggesting that BemA is dispensable for NoxA function. Takemoto, Kamakura (48) found that yeast polarity protein Cdc24 is also part of the Nox complex. It contains both PB1 and PH domains and also physically interacts with NoxR and BemA, exhibiting specific co-localisation at the hyphal tip and septa. Previous work by Toenjes, Sawyer (72) additionally identified that the localisation of Cdc24 is dependent on its lipid-binding PH domain in yeast. While the lipid target of the Cdc24 PH domain remains unclear, Cdc24 is likely the central protein in the recruitment of cytosolic Nox proteins in fungi, responsible for the membrane localisation of BemA and NoxR.

1.6 Fungal membrane lipid composition

Very little is known about the fungal membrane lipid composition making it difficult to predict the target of the PH domain of Cdc24. Fungi are known to generate PI[4]P, phosphoinositide 4,5-bisphosphate (PI[4,5]P_2), and phosphoinositide 3-phosphate (PI[3]P) (73, 74). However, based on homology of

mammalian PIKs, PI[3,4]P_2 and phosphoinositide 3,4,5-triphosphate (PI[3,4,5]P_3) may also be present in the membranes of *E. festucae*.

1.6.1 PI[4]P

In plants, mammals, yeast, and fungi PI[4]P exists in two separate pools generated and maintained by different phosphatidylinositol kinases (PIKs) (75-79). Yeast possesses two PIKs, Pik1 and Stt4, which are both essential for viability and unable to substitute for each other (80). Pik1 produces PI[4]P in *trans*-Golgi vesicles and is proposed to have a role in Golgi-to-PM transport (81). Mutants with impaired Pik1 kinase activity exhibit defects in the secretion of newly synthesised proteins (82, 83). Stt4 produces PI[4]P in the PM and has a role in actin organisation and integrity of the yeast cell wall (75, 84). In *Candida albicans* PI[4]P in the Golgi and PM have distinct functional roles, both crucial in the transition from yeast to filamentous growth. PI[4]P in the Golgi is required for membrane trafficking, while PI[4]P at the PM forms an asymmetric gradient along the hyphal tip where it is concentrated in a tight cap at the tip apex (78). It is very likely that this PPI is present and important in *E. festucae* as homologues for both PIKs are present (Figure 1.4). As mammalian $p47^{phox}$ and Bem1 both have a strong affinity for PI[4]P, this PPI may play an important role in assembly of the Nox complex in *E. festucae*.

1.6.2 PI[4,5]P_2

PI[4,5]P_2 is present in the inner leaflet of the PM in plants, mammals, and yeast (85-91). This PPI controls many cellular processes in yeast and mammals including, endocytosis, exocytosis, establishment of cell polarity, and actin polymerisation (90, 92-94). In *Saccharomyces cerevisiae*, PI[4,5]P_2 is generated by the essential protein Mss4p which converts PI[4]P to PI[4,5]P_2 (84, 95). PI[4,5]P_2 and Mss4p are mainly localised along the PM, where they are required for actin organisation (84, 95). Similarly, in *C. albicans* PI[4,5]P_2 and Mss4 are both localised long the PM and are required for the yeast-to-hyphal growth transition (96). Furthermore, PI[4,5]P_2 and MssD are asymmetrically distributed in both budding and filamentous cells, maintained by Stt4 and the actin cytoskeleton (96). In *N.*

crassa, MSS-4 is proposed to have a key role in establishing polarised growth through the production of

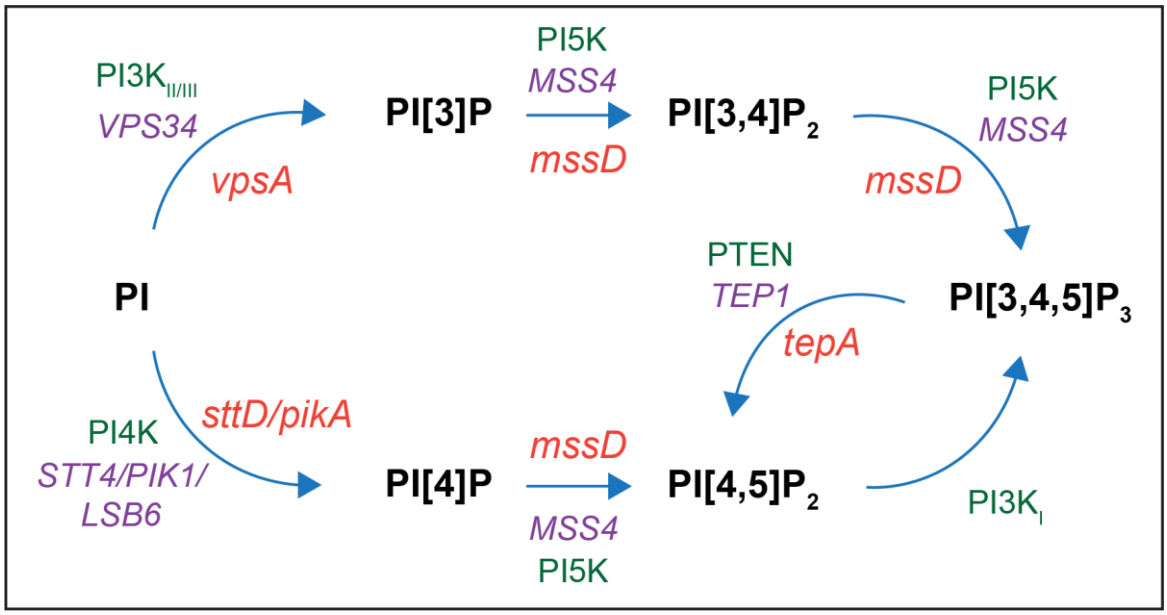

Figure 1.4. Predicted PPIs in *Epichloë festucae*. Phosphoinositides found in mammalian systems (bold type), enzymes involved in their production (green), genes that encode these enzymes in yeast (purple), and genes predicted to encode these enzymes in filamentous fungi (orange). Adapted from Eaton (97).

$PI[4,5]P_2$ (96). $PI[4,5]P_2$ was distributed along the PM as seen in *S. cerevisiae* and *C. albicans* and also at hyphal septa (98). MSS-4 was found to localise in a ring-like membrane domain immediately behind the apex of growing hyphae. The PM localisation appeared patchy possibly indicating association with membrane microdomains (98). A similar result was also seen in *A. thaliana* (99) and tobacco (100) pollen tubes, where Mss4 localised in the apical region of the tube tip. The conservation of localisation of $PI[4,5]P_2$ and Mss4 homologues across the kingdoms emphasises the important role this PPI plays in mammals, yeast, and fungi. *E. festucae* has a Mss4 homologue, MssD, so it is highly likely that $PI[4,5]P_2$ is produced (Figure 1.4). While there is no record of mammalian cytosolic Nox proteins having an affinity for $PI[4,5]P_2$, the addition of exogenous $PI[4,5]P_2$ is able to stimulate ROS production in tobacco pollen tubes (101).

1.6.3 PI[3]P

PI[3]P plays a major role in endocytic trafficking (81). Previous studies in yeast and mammals, indicate that PI[3]P is highly enriched on early endosomes and in the internal vesicles of both multi-vesicular endosomes and vacuoles (102-105) and additionally to the *trans*-Golgi network (TGN) in plant cells (106). Yeast possess only one PIK to generate PI[3]P, Vps34p, while mammals possess three classes of PI3Ks, two of which (type-III and type-II) produce PI[3]P (80, 107, 108). In yeast, PI[3]P is crucial in TGN-to-vacuole transport and is essential for protein sorting, with point mutations in Vps34p resulting in a severe defect in vacuolar protein sorting (109). Turnover of PI[3]P by dephosphorylation, phosphorylation, or degradation is equally important (81). Wurmser and Emr (103) found that PI[3]P must be transported from the cytoplasmic membrane leaflet where it is synthesized to the lumen of the vacuole to be degraded by resident hydrolases. *E. festucae* possesses a homologue for yeast Vps34p, VpsA, which is predicted to generate PI[3]P (Figure 1.4). In mammals, PI[3]P can directly bind the PX domain of $p40^{phox}$ (65, 68, 110, 111). Despite the absence of $p40^{phox}$ PI[3]P is a promising target for lipid signalling in fungi. PI3K suppression by inhibitors prevents the translocation of cytosolic proteins in plants, resulting in low ROS generation and disruption of seed germination (112). Additionally, exogenous PI[3]P can rescue ROS production in *Arabidopsis* root hairs as well as in broad bean guard cells (63-65, 113, 114).

1.6.4 PI[3,4]P_2

PI[3,4]P_2 is present in the mammalian PM with several specific binding proteins including TAPP1 and TAPP2, lamellipodin, and Akt, which regulate processes like cell adhesion, chemotaxis, and migration (115-119). This PPI is well studied in mammals due to its role in cancer metastasis where binding of lamellipodin to PI[3,4]P_2 at the leading edge of the cell enhances cell mobility and tumour metastasis (120, 121). PI[3,4]P_2 has also been implicated in the late stages of clathrin-mediated endocytosis where synthesis of the PPI by PI3KC2α at the invagination neck recruits PX-BAR domain protein sorting nexin (SNX) 9 and its close homologue SNX18 which mediate membrane constriction and progression of

the endocytic pathway (122-127). Levels of this PPI are regulated through the action of kinases, such as class I PI3Ks, and phosphatases, such as SHIP2 (PI[3,4,5]P_3 to PI[3,4,]P_2) and INPP4A (PI[3,4]P_2 to PI[3]P) (115). It is predicted that this PPI is produced by MssD in *E. festucae*, as yeast Mss4p has dual substrate specificity *in vitro*, also converting PI[3]P to PI[3,4]P_2 (Figure 1.4) (84). PI[3,4]P_2 is a potential target of the fungal cytosolic Nox proteins as mammalian Nox protein, p47^{phox}, binds PI[3,4]P_2 (63-65).

1.6.5 PI[3,4,5]P_3

PI[3,4,5]P_3 is found at the PM of the leading edge in mammalian cells (80, 89), where it serves as a potent signal for survival and proliferation (91, 128, 129), and is associated with cytoskeletal rearrangements (130). It is produced by a class I PI3K (91) and is rapidly turned over by phosphatases like PTEN, which converts PI[3,4,5]P_3 to PI[4,5]P_2 to inhibit cell growth and survival (131). This PPI was thought to be absent in yeast due to the absence of any class I PI3K homologues and an inability to detect PI[3,4,5]P_3. However, deletion of the PI[3,4,5]P_3 phosphatase Ptn1p, PTEN homologue, made the PPI detectable in levels comparable to those found in mammalian cells (131). PI[3,4,5]P_3 synthesis in *Schizosaccharomyces pombe* requires vps34p and its3p, suggesting a novel biosynthetic pathway evolved before the appearance of class I PI3Ks (131). *E. festucae*, like yeast, do not possess class I PI3Ks but do have a mammalian PTEN homologue, TepA, suggesting fungi also use an alternative pathway for PI[3,4,5]P_3 synthesis (Figure 1.4) (131, 132).

1.7 Methods for measuring PPI composition

Many methods have been developed to investigate membrane lipid composition in mammals, plants, and fungi, the most common being; high performance liquid chromatography (HPLC) (74, 84, 131, 133-135), electron microscopy (EM) (102), and biosensors (96, 136-139). Each of these has distinct advantages and limitations. In HPLC, lipids are extracted from whole cells, deacylated, and analysed by anion exchange HPLC (140, 141). Lipids are identified through various methods, such as co-chromatography with [^{3}H] standards or by an online detector

(74, 142). The advantage of this method is that it reveals all PPIs present and relative quantities. However, the main limitations are that you do not know where the lipid is localised nor can you visualise the lipid dynamics. EM analyses fixed cells, which are cut into thin sections and labelled with a specific probe (102). The high resolution of this method allows identification of the PPI in specific organelles, and can detect PPI in organelles that other probes may not be able to access (102). The main limitation of EM is that you are unable to visualise the lipid dynamics, as the cells are fixed. It is also possible that you will not detect lipids already bound to proteins (102). The biosensor method is now the most commonly used due to the advantage of viewing lipid dynamics in living cells, crucial for understanding lipid signalling. Additionally, biosensors may be able to compete with PPI binding proteins revealing a localisation overlooked in EM. However, this method has some limitations: light microscopy used to visualise the biosensors is comparatively low resolution compared to EM; the biosensor must be overexpressed to detect sufficient fluorescence, which may interfere with PPI distribution; and PPIs may be masked or inaccessible to the biosensor so will appear incorrectly absent (102, 131).

1.8 Aims of this study

Given both plant and mammalian Nox complexes are regulated by lipid signalling, it is hypothesised that the regulatory mechanisms are likewise conserved in fungi. To explore the role lipid signalling plays in assembling the fungal Nox complex this study addressed the following aims and objectives:

1. Investigate whether the putative lipid-binding PH domain of Cdc24 is necessary for its localisation to the hyphal tip.
   - examine localisation of Cdc24 with and without the PH domain in axenic culture
2. Using a suite of LBD biosensors, identify which PPIs are present in the membranes of *E. festucae* under various conditions.
   - examine biosensor localisation in axenic culture
   - examine biosensor localisation during conidiospore germination
   - examine biosensor localisation *in planta*

3. Assess whether altering the levels of PI[4,5]P_2 has an effect on growth in culture or on the mutualistic fungal-plant symbiosis.
   - overexpress *mssD*
   - analyse impact on axenic culture phenotype
   - analyse impact on PPI distribution
   - analyse impact on fungal-plant symbiosis

2. Materials and methods

2.1 Biological materials

Plasmids, bacterial strains, fungal strains, and plant material used in this study are listed in Tables 2.1 and 2.2.

Table 2.1. Plasmids used in this study

Plasmids	Relevant characteristic(s)	Source or Reference
pRS426	Amp^R/*URA3*	Christianson, Sikorski (143)
pSF16.17	P*trpC-nptII*-T*trpC*; Amp^R; Gen^R	Saikia and Scott (144)
pSF15.15	P*trpC-nptII*-T*trpC*; Amp^R; Hyg^R	Saikia and Scott (144)
pPN83	pBlueScriptII® KS(+) containing P*gpd*-EGFP-T*trpC*; Amp^R	Tanaka, Christensen (46)
pCE105	pRS426 containing P*gpdA*- PLC PH domain-eGFP-T*trpC*; Amp^R	This study
pCE106	pRS426 containing P*gpdA*- HGS FYVE domain-eGFP-T*trpC*; Amp^R	This study
pCE107	pRS426 containing P*gpdA*- BTK PH domain-eGFP-T*trpC*; Amp^R	This study
pCE108	pRS426 containing P*gpdA*- PLEKHA2 PH domain-eGFP-T*trpC*; Amp^R	This study
pCE109	pRS426 containing P*gpdA*- PLEKHA3 PH domain-eGFP-T*trpC*; Amp^R	This study
pCE110	pRS426 containing P*gpdA*-mCherry-PLC PH domain-T*trpC*; Amp^R	This study
pCE111	pRS426 containing P*gpdA*-mCherry-HGS FYVE domain-T*trpC*; Amp^R	This study
pCE112	pRS426 containing P*gpdA*-mCherry-BTK PH domain-T*trpC*; Amp^R	This study
pCE113	pRS426 containing P*gpdA*-mCherry-PLEKHA2 PH domain-T*trpC*; Amp^R	This study
pCE114	pRS426 containing P*gpdA*-mCherry-PLEKHA3 PH domain-T*trpC*; Amp^R	This study

pCE125	pRS426 containing P*gpdA*-eGFP-T*trpC*; Amp^R	This study
pCE126	pRS426 containing P*gpdA*-mCherry-T*trpC*; Amp^R	This study
pCE101	pRS426 containing P*gpdA*-*mssD*-T*trpC*; Amp^R	This study
pCE127	pRS426 containing P*gpdA*-*cdc24*-eGFP-T*trpC*; Amp^R	This study
pCE124	pRS426 containing P*gpdA*-*cdc24*ΔPH-eGFP-T*trpC*; Amp^R	This study

Table 2.2. Organisms used in this study

Organism/Strain	Relevant characteristic(s)	Description	Source or Reference
E. coli			
DH5α	F-, φ80*lac*Z, ΔM15, Δ(*lacZYA-argF*), U169, *recA1*, *endA1*, *hsdR17* (r_k-. M_k-), *phoA*, *supE44*, *λ*-, *thi-1*, *gryA96*, *relA1*	N/A	Invitrogen
ES10	DH5α/pCE105	PLC-eGFP (PI[4,5]P_2) biosensor	This study
ES11	DH5α/pCE106	HGS-eGFP (PI[3]P) biosensor	This study
ES12	DH5α/pCE107	BTK-eGFP (PI[3,4,5]P_3) biosensor	This study
ES13	DH5α/pCE108	Plekha2-eGFP (PI[4]P) biosensor	This study
ES14	DH5α/pCE109	Plekha3-eGFP (PI[3,4]P_2) biosensor	This study
ES15	DH5α/pCE110	mCherry-PLC (PI[4,5]P_2) biosensor	This study
ES16	DH5α/pCE111	mCherry-HGS (PI[3]P) biosensor	This study
ES17	DH5α/pCE112	mCherry-BTK (PI[3,4,5]P_3) biosensor	This study
ES18	DH5α/pCE113	mCherry-Plekha2 (PI[4]P) biosensor	This study
ES19	DH5α/pCE114	mCherry-Plekha3 (PI[3,4]P_2) biosensor	This study
ES34	DH5α/pCE125	eGFP control	This study
ES35	DH5α/pCE126	mCherry control	This study

ES36	DH5α/pCE127	cdc24-eGFP	This study
ES32	DH5α/pCE124	cdc24ΔPH-eGFP	This study
ES6	DH5α/pCE101	*mssD* over expression	This study
ES3	DH5α/pCE98	*mssD* knockout cassette	This study
E. festucae			
PN2278	Wild-type Fl1	N/A	Young, Bryant (145)
PN2734	Wild-type E2368	N/A	Wilkinson, Siegel (34), Young, Aiken (35)
PN4175	PN2278/pCT74	eGFP control	Lorang, Tuori (146)
EFS1-EFS3	PN2278/pCE105	PH_{PLC}-eGFP ($PI[4,5]P_2$) biosensor	This study
EFS4-EFS6	PN2278/pCE106	$FYVE_{HGS}$-eGFP (PI[3]P) biosensor	This study
EFS7-EFS9	PN2278/pCE107	PH_{BTK}-eGFP ($PI[3,4,5]P_3$) biosensor	This study
EFS10-EFS12	PN2278/pCE108	$PH_{Plekha2}$-eGFP (PI[4]P) biosensor	This study
EFS13-EFS15	PN2278/pCE109	$PH_{Plekha3}$-eGFP ($PI[3,4]P_2$) biosensor	This study
EFS16, EFS17	PN2278/pCE110	mCherry-PH_{PLC} ($PI[4,5]P_2$) biosensor	This study
EFS18-EFS20	PN2278/pCE111	mCherry-$FYVE_{HGS}$ (PI[3]P) biosensor	This study
EFS 21-EFS24	PN2278/pCE112	mCherry-PH_{BTK} ($PI[3,4,5]P_3$) biosensor	This study
EFS25-EFS27	PN2278/pCE113	mCherry-$PH_{Plekha2}$ (PI[4]P) biosensor	This study
EFS 28-EFS31	PN2278/pCE114	mCherry-$PH_{Plekha3}$ ($PI[3,4]P_2$) biosensor	This study

EFS32, EFS33	PN2278/pCE125	eGFP control	This study
EFS34, EFS35	PN2278/pCE126	mCherry control	This study
EFS88-EFS90	PN2278/ pCE127	cdc24-eGFP #3, #9, #10	This study
EFS92-EFS94	PN2278/pCE124	cdc24ΔPH-eGFP #11, #23, #24	This study
EFS85-EFS87	PN2278/pCE101	*mssD* OE #17, #20, #53	This study
EFS75, EFS76	PN2734/pCE105	PH_{PLC}-eGFP ($PI[4,5]P_2$) biosensor	This study
EFS59-EFS61	PN2734/pCE106	$FYVE_{HGS}$-eGFP (PI[3]P) biosensor	This study
EFS69-EFS71	PN2734/pCE108	$PH_{Plekha2}$-eGFP (PI[4]P) biosensor	This study
EFS65	PN2734/pCE109	$PH_{Plekha3}$-eGFP ($PI[3,4]P_2$) biosensor	This study
EFS77, EFS78	PN2734/pCE110	mCherry-PH_{PLC} ($PI[4,5]P_2$) biosensor	This study
EFS62-EFS64	PN2734/pCE111	mCherry-$FYVE_{HGS}$ (PI[3]P) biosensor	This study
EFS79	PN2734/pCE112	mCherry-PH_{BTK} ($PI[3,4,5]P_3$) biosensor	This study
EFS72-EFS74	PN2734/pCE113	mCherry-$PH_{Plekha2}$ (PI[4]P) biosensor	This study
EFS66-EFS68	PN2734/pCE114	mCherry-$PH_{Plekha3}$ ($PI[3,4]P_2$) biosensor	This study
EFS80-EFS83	PN2734/pCE125	eGFP control	This study
EFS84	PN2734/pCE126	mCherry control	This study
L. perenne			
A11104	*L. perenne* cv. Samson; endophyte free		AgResearch

2.2 Media, growth, and storage conditions

All media were prepared using ultrapure water from the Barnstead Nanopure water purification system (Thermo Scientific™ Barnstead™ Nanopure™) and sterilised by autoclaving at 121°C for 20 mins. All methods involving live cultures or substances used in conjunction with live cultures were performed under sterile conditions.

2.2.1 *Escherichia coli*

2.2.1.1 Luria-Bertani (LB) medium

LB medium contained 1% (w/v) tryptone, 0.5% (w/v) yeast extract, 0.5% NaCl, and pH adjusted to 7–7.5 with NaOH (147). LB agar additionally contained 1.5% (w/v) agar.

2.2.1.2 Solid Culture

E. coli cultures were incubated overnight on plates containing ~25 mL LB agar (Section 2.2.1.1) at 37°C, supplemented with antibiotic when appropriate (Section 2.3.1.4).

2.2.1.3 Liquid culture

A single colony from solid culture (Section 2.2.1.2) was inoculated into a sterile test tube containing 5 mL LB medium (Section 2.2.1.1) and grown over night at 37°C, with shaking at 200 rpm. Antibiotics were added when appropriate (Section 2.3.1.4).

2.2.1.4 Antibiotic concentrations

Ampicillin was added to liquid or molten media, post-autoclaving, under sterile conditions to a final concentration of 100 μg/mL.

2.2.2 *E. festucae*

2.2.2.1 Potato dextrose (PD) medium

PD medium contained 2.4% (w/v) potato dextrose. PD agar additionally contained 1.5% (w/v) agar.

2.2.2.2 Regeneration (RG) medium

RG medium contained 2.4% PD and 0.8 M sucrose; pH adjusted to 6.5 with NaOH. RG agar additionally contained 1.5% (w/v) agar for plates and 0.8% (w/v) agar for transformation overlays.

2.2.2.3 Solid culture

Cultures were grown at 22°C for 5-10 days on plates containing ~25 mL PD agar (Section 2.2.2.1) or RG agar (Section 2.2.2.2). When antibiotic was required, hygromycin or geneticin was added post-autoclaving to a final concentration of 150 μg/mL or 200 μg/mL, respectively.

2.2.2.4 Liquid culture

Approximately 1 cm^2 of mycelia were diced and scraped off the surface of a freshly grown solid culture colony (Section 2.2.2.3). For DNA isolation and protoplasting, mycelia were added to sterile 125 mL flasks containing 50 mL PD medium (Section 2.2.2.1). For long-term storage, the mycelia were added to a sterile bijou bottle containing 2.5 mL PD medium (Section 2.2.2.1). Both were then incubated at 22°C for approximately 4 days, shaking at 200 rpm.

2.2.2.5 Short-term storage

Solid cultures plates were stored at 4°C for up to 6 months.

2.2.2.6 Long-term storage

2.2.2.6.1 Mineral oil slants

Slants were prepared by setting 5 mL PD agar at an angle in a 15 mL falcon tube and inoculated with a small piece of mycelium. The slants were incubated at 22°C until 50% was covered (~7 days), then sterile mineral oil was pipetted over the mycelia until fully submerged (~4 mL). The lid was closed to the first stop, sealed with Parafilm, and stored at 4°C.

2.2.2.6.2 Glycerol stocks

After mycelia were grown in liquid culture (Section 2.2.2.4), 2.5 mL of 30% glycerol was added to the bijou bottle. 1 mL of the mycelia mixture was added to a 1 mL cryotube in duplicate. Cryotubes were then placed in a Nalgene™ Mr. Frosty freezing container and put in the -80°C freezer overnight. Tubes were then moved to a cryobox and stored at -80°C.

2.3 DNA isolation

2.3.1 Isolation of plasmid DNA from *E. coli*

E. coli cells were grown as previously described (Section 2.2.1.3), and plasmid DNA isolated using the GeneJet Miniprep Kit (Thermoscientific) according to the manufacturer's instructions.

2.3.2 Isolation of crude genomic DNA (gDNA) from *E. festucae*

E. festucae cultures were grown on PD agar plates (Section 2.2.2.1) for 7-10 days. Mycelia from an entire colony were scraped off using a scalpel, placed in a Eppendorf tube containing 150 µL of lysis buffer (100 mM Tris-HCl adjusted to pH 8.0, 100 mM EDTA, 1% SDS), and incubated at 70°C for 30 mins while the cellular contents are released. 150 µL of 5 M potassium acetate was then added to each tube, inverted 6 times, and incubated on ice for 15 mins to precipitate any proteins present. Tubes were then centrifuged for 20 mins at 17,000 x g at 4°C, pelleting the cell debris and proteins. Using a pipette, the supernatant was transferred to a fresh

sterile Eppendorf tube containing 200 µL chilled isopropanol, inverted 6 times, and incubated overnight in a -20°C freezer to precipitate as much DNA as possible. The tubes were then centrifuged for 15 mins at 17, 000 x g to pellet the crude gDNA, the supernatant carefully discarded using a pipette. The DNA pellet was then washed by adding 300 µL of chilled 70% ethanol, centrifuging at 17, 000 x g for 5 mins, then removing the supernatant with a pipette. The pellet was left to air-dry for 30 mins then resuspended in 30 µL sterile deionised water. To improve the quality of the gDNA, the tubes were incubated at 70°C for 15 mins, centrifuged at 17, 000 x g for 15 mins, and the supernatant, containing crude gDNA, was transferred to a fresh sterile tube leaving behind any impurities. Samples were stored at -20°C.

2.3.3 Isolation of pure gDNA from *E. festucae*

The method for small-scale isolation of gDNA from fungal liquid cultures was adapted from Byrd, Schardl (148). Mycelia were grown up in liquid culture as previously described (Section 2.2.2.4) and harvested by pouring each culture through a fabric liner. The mycelia were rinsed three times with deionised water and blotted dry. Each strain was scraped into a 15 mL Falcon tube and freeze dried for 24-48 hours. The mycelia were then ground to a fine powder under liquid nitrogen. 10-20 mg of each strain were added to a 2 mL Eppendorf tube and resuspended in 800 µL extraction buffer (150 mM EDTA, 50 mM Tris-HCl, 1% SLS; pH 8.0). Proteinase K was added to each tube to a final concentration of 2 mg/mL and incubated at 37°C for 20 mins. Tubes were then centrifuged at 17, 000 x g for 10 mins. The supernatant was then transferred to a new 2 mL Eppendorf tube. 0.5/0.5 volumes of phenol/chloroform were added to each tube and mixed thoroughly. Samples were then centrifuged at 17, 000 x g for 10 mins and the upper aqueous phase was carefully transferred to a new tube. The phenol/chloroform steps were repeated twice more, followed by a final chloroform step using 1 volume of chloroform. The upper aqueous phase was then transferred to a tube containing 1 volume of chilled isopropanol to precipitate the DNA and incubated for at least an hour at -20°C. The DNA was then pelleted by centrifugation for 10 mins at 17, 000 x g. The pellet was washed with 1 mL of chilled 70% (v/v) ethanol and centrifuged for 5 mins at 17, 000 x g. The

supernatant was discarded, and the pellet air-dried at room temperature. The pellet was then resuspended in 100 µL sterile deionised water and stored at -20°C.

2.4 DNA manipulation

2.4.1 DNA quantification

Crude gDNA was quantified using the NanoPhotometer (Implen) according to the manufacturer' s instructions.

Pure gDNA was quantified using the Qubit® 2.0 fluorometer (Thermo Fisher Scientific) according to the manufacturer's instructions.

2.4.2 Restriction endonuclease digestion

To confirm the identity of an extracted plasmid, plasmid DNA was digested using commercial restriction enzymes (Roche and NEB) in an appropriate buffer. The digests were carried out in 10 µL reaction volumes, containing 10 units of enzyme, 1X buffer, and 1 µg of DNA. Each digest was then incubated for 1 hour at 37°C and the fragment sizes were then identified by gel electrophoresis (Section 2.4.3) and compared to expected values.

2.4.3 Agarose gel electrophoresis

DNA samples were separated on gels prepared from molten agarose, 0.8% (w/v) - 1.8% (w/v) depending on the size of the DNA fragments. Gels were immersed in 1x Tris/Borate/EDTA (TBE) buffer (89 mM Tris, 89 mM boric acid, 2 mM Na_2EDTA, pH adjusted to 8.2) and loaded with DNA samples mixed with 2-5 µL loading dye (20% (w/v) sucrose, 5 mM EDTA, 1% (w/v) SDS, and 0.2% (w/v) bromophenol blue) depending on the amount of DNA loaded. Gels were then run at 100-110 volts/cm, until the dye front was approximately 1 cm from the bottom of the gel.

To visualise DNA, the molten agarose was either mixed with 1 µL SYBR™ safe per 1 mL molten agarose prior to pouring the gel, or the gel was post-stained by immersion in 0.2% ethidium bromide for 15-20 mins. A UV Transilluminator Gel Documentation System (Bio-Rad) was used to visualise and photograph the gel.

2.4.4 Gel purification

DNA fragments for sub-cloning were purified from agarose gels (Section 2.4.3.) using the Wizard® SV Gel and PCR Clean-UP system (Promega), as per the manufacturer's instructions.

2.5 RNA isolation and manipulation

2.5.1 Isolation of total RNA from fungal mycelia

Mycelia grown in liquid culture (Section 2.2.2.4) were filtered through sterile fabric liners and washed three times with sterile deionised water, mycelia were pressed between paper towels to remove as much water as possible and then flash frozen with liquid nitrogen. Samples were ground into a fine powder with a mortar and pestle and 1.2 mL of TRIzol® reagent (Invitrogen) was immediately added and mixed well to protect from RNases. After the resulting mixture reached room temperature, 1 mL was transferred to an Eppendorf tube and centrifuged for 5 mins at 12, 000 x g at 4°C. 1 mL of supernatant was moved to a new tube containing 0.2 mL chloroform, mixed well, incubated at room temperature for 2-3 mins, and centrifuged for 15 mins as above. 0.6 mL of the aqueous phase was transferred to a new tube containing 0.6 mL isopropanol and 0.3 mL high salt solution (0.8 M sodium citrate, 1.2 M NaCl, in DEPC-treated H_2O), inverted 6 times, and incubated at room temperature for 10 mins to precipitate the RNA. Tubes were then centrifuged as above for 10 mins to pellet the RNA. The supernatant was discarded using a pipette then the pellet was washed by adding 75% ethanol (in DEPC H_2O), centrifuging for 5 mins at 7, 500 x g at 4°C, and removing as much supernatant as possible using a pipette leaving the pellet to air dry. The pellet was then resuspend in 100 µL RNAsecure solution (Ambion), incubated at 60°C for at least 10 mins to inactivate any RNases, and stored at -80°C.

2.5.2 RNA quantification

RNA was quantified using the NanoPhotometer (Implen) according to the manufacturer' s instructions.

2.5.3 DNase I treatment

RNA used for RT-PCR (Section 2.6.2) was first treated with RNase-free DNase I (NEB). 5 µg RNA was treated with 1 unit of DNase in a 50 µL reaction volume with 1x DNase Reaction Buffer and incubated at 37°C for 10 min. DNase I was subsequently inactivated by the addition of 3 M NaOAc and 250 µL absolute ethanol and stored at -20°C overnight. The mixture was then centrifuged for 15 mins at 17, 000 x g, 4°C to pellet the RNA. The pellet was then washed with 70% ethanol, centrifuged for a further 30 mins, dried, and re-suspended in 30 µL RNase-free water. RNA concentration was re-determined following DNase I treatment.

2.5.4 Determining RNA quality

Electrophoresis of total RNA samples to check quality was performed on denaturing SDS agarose gels (0.3% SDS, 1.2% agarose). Gels were stained using ethidium bromide and visualised as described in Section 2.4.3. High quality RNA samples displayed two distinct ribosomal RNA bands.

2.6 Polymerase chain reaction (PCR)

PCR was performed using a Biometra® T1 Thermocycler. Primers used in this study are listed in Table 2.3.

Table 2.3. PCR primers used in this study

Name	Sequence (5' – 3')	Target sequence	Used for
pRS426-Pgpd-F	GTAACGCCAGGGTTTTCCCAGTCACGACGAATTCCCTTGTATCTCTACA	*gpdA* promoter, Fwd	Screening biosensor strains
Pgpd-R	GGCGGATTTTAGGCTCAAGTC	*gpdA* promoter, Rev	
Pgpd-F	GACTTCAGCAACATCTCCTGG	*gpdA* promoter, Fwd	
pRS426-TtrpC-R	GCGGATAACAATTTCACACAGGAAACAGCCCATCTTAGTAGGAATGATTTTCG	*trpC* terminator, Rev	
hgs1	AGATTCGTCAAGCTGTTTGATGATTTCAGCTACTTCTTGTTGAGCTGCTC	*trpC* terminator, Rev	
hgs2	ACAGCTACCCCGCTTGAGCAGACATCACCATGGAGCGCGCCCCCGACTGGGTCG	HGS FYVE domain, Fwd	
hgs3	CCCTTGCTCACCATTCCTCCTCCTCCTCCCTTCTTGTTGAGCTGCTCGTAGC	HGS FYVE domain, Rev	
mCherry-F	ACAGCTACCCCGCTTGAGCAGACATCACCATGGTGAGCAAGGGCGAGGAG	mCherry, 5' Fwd	
btk1	AGATTCGTCAAGCTGTTTGATGATTTCAGCTACTCGAGGATCTGGCAGCC	*trpC* terminator, Rev	
plekha3-1	AGATTCGTCAAGCTGTTTGATGATTTCAGCTAGGTGAGGCAGGCCTTGC	*trpC* terminator, Rev	
mss5	ACAGCTACCCCGCTTGAGCAGACATCACCATGCCCTCGTTTCTCAACGAC	*mssD*, Fwd	Screening *mssD* OE strains
mss6	AGATTCGTCAAGCTGTTTGATGATTTCAGCTAAACCATGCGTACGCCGCT	*mssD*, Rev	
mss7	GCAAGCAAGCGGAAGATTCTC	*mssD*, Fwd	

mss12	CCAGTTTGGAAGTGCTTTAGC	*Mssmss7D*, Fwd	*mssD* KO screen
mss13	AGAAATCGGTCGTCACTCTCG	*mssD*, Rev	
cdc1	ACAGCTACCCCGCTTGAGCAGACATCACCATGGCCCATGCTCCCCTCCTTC	*cdc24*, Fwd	Cdc24 construct screen
cdc3	GCACCCCGACATTCCCAGAGC	*cdc24*, Fwd	
cdc4	TTGGCCCTCGCCAACGCAGAAG	*cdc24*, Rev	

2.6.1 Standard PCR amplifications

Standard PCR reactions werem performed using One*Taq*® DNA polymerase (New England Biolabs, Inc.) in 12.5 µL reaction volumes with 1x OneTaq standard buffer, 200 µM dNTPs, 0.2 µM forward primer, 0.2 µM reverse primer, 1.25 units One*Taq* DNA polymerase, and <1000 ng DNA template. Reaction conditions were: one cycle at 94°C for 30 s; 29-35 cycles at 94°C for 30 s, 50°C for 30 s, 68°C for 1 min/1kb product; one cycle at 68°C for 5 min.

2.6.2 Reverse-transcription PCR (RT-PCR)

For quantitative reverse transcription PCR (qRT-PCR), reactions were performed with the QuantiTect Transcription Kit (Qiagen), according to the manufacturer's instructions. 1 µg of DNase treated RNA was used in a 20 µL reaction volume. cDNA synthesised from RNA was either directly used in qRT-PCR or stored at -20°C.

2.6.3 Quantitative reverse transcription PCR (qRT-PCR)

qRT-PCR reactions were prepared in 384-well plates using a 10 µL reaction volume containing 1 µL DNA (diluted to 10 ng/µL), 1x SsoFast™ EvaGreen® Supermix (Bio-Rad), and 0.5 µM of each forward and reverse primer. Two technical replicates were included in each experiment for reproducibility. Primers used for qRT-PCR in this study are listed in Table 2.3.

Table 2.4. qRT-PCR primers used in this study

Name	Sequence (5' – 3')	Target sequence
TC399	AAAAAGCAACCGAATGCAAG	EF-2 Fwd
TC400	CGAGACGACATAACTACATGTATCAAA	EF-2 Rev
TC407	TAGCTGGCGTTATGGAAAGG	S22 Fwd
TC408	CGATTGTGCGACTACTACCTCA	S22 Rev
AC33	TGCGTGACAAAACTCTCCAG	MSSD OE Fwd
AC34	AGCCTTTCTCACGTTCTCCA	MSSD OE Rev

2.6.3.1 Cycling conditions

qRT-PCR was performed using the LightCycler® 480 Instrument II (Roche). Reaction conditions were: one cycle at 95°C for 30 s; 40 cycles at 96 for 5 s and 60°C for 10 s; melt curve at 65-95°C with a ramp of 0.4°C/ s. Signal was acquired at the end of each extension step and during the melt curve.

2.6.3.2 Data analysis

Relative amounts of cDNA between target and reference genes were calculated by comparison of the two concentration values calculated using the $2^{(\Delta Cp)}$ method (149), reflecting degree of expression. Fold difference was then calculated by comparing the relative expression of the gene of interest in over expression strains to that in the wild-type (WT) Fl1 strain.

2.7 Transformation techniques

2.7.1 Preparation of *E. festucae* protoplasts

Mycelia were grown in liquid culture as previously described (Section 2.2.2.4), harvested by filtering through a sterile fabric liner, and washed using sterile water followed by OM buffer (1.2 M $MgSO_4.7H_2O$, 100 mM Na_2HPO_4, pH adjusted to 5.8 using 100 mM $NaH_2PO_4.2H_2O$). 50 mL of 0.45 µm filtered-sterilised *Trichoderma harzianum* lysing enzyme (Sigma-Aldrich L1412; 10 mg/mL in OM buffer) was added to flasks containing approximately 4 g of mycelia in each. The flasks were incubated at 22°C overnight, shaking at 80 rpm. The mixture was then filtered using a sterile fabric liner and the filtrate, containing the protoplasts, was divided into 5 mL aliquots, and carefully overlaid with 2 mL of ST buffer (0.6 M sorbitol, 1 M Tris-HCl, pH adjusted to 8). Tubes were centrifuged at 2375 x g for 5 mins at 4°C and the interface which forms between the lysing enzyme solution and ST buffer, containing the protoplasts, was removed into a fresh tube using a pipette. 5 mL of STC buffer (1 M sorbitol; 1 M Tris-HCl, pH adjusted to 8; 50 mM $CaCl_2$) was added, mixed gently, and centrifuged at 2, 375 x g. This step was then repeated, pooling the samples together after each repetition, halving the number of tubes each time until one tube remained, which contained all the protoplasts. 500 µL of STC buffer

was used to resuspend the protoplasts in this tube. The concentration of protoplasts present was calculated using a haemocytometer and the mixture was then diluted as to contain 1.25 x 10^8 protoplasts/mL using STC buffer. 20 µL of 40% PEG (w/v) was then added to 80 µL aliquots of protoplast solution and the tubes stored at -80°C.

2.7.2 Co-transformation of *E. festucae* protoplasts

Protoplasts were transformed using a method adapted from Itoh, Johnson (150). One tube of protoplasts per sample DNA and two extra tubes for controls were thawed on ice (Section 2.7.1). 3 µg of sample plasmid and 2 µg of antibiotic resistance-encoding plasmid were added to each sample tube along with 2 µL of 50 mM spermidine (Sigma) and 5 µL of 5 mg/mL heparin (Sigma). To another tube only the antibiotic resistance-encoding plasmid as well as spermidine and heparin were added (positive control); and to the last tube, nothing was added (no DNA control). The tubes were incubated on ice for 30 mins, then 900 µL of 40% (w/v) PEG solution was added. The tubes were mixed well and returned to ice for a further 20 mins. For the sample transformations, five 200 µL aliquots of each transformation mixture were suspended in 3.5 mL of 0.8% soft RG overlay pre-warmed to 50°C and poured over thin 1.5% RG plates of known volume (Section 2.2.2.2). For the no DNA control, two 100 µL aliquots were resuspended and plated as above (antibiotic resistance negative control and neat cell viability control). A serial dilution was then made using STC buffer producing 10^1, 10^2, and 10^3 dilutions, 100 µL aliquots of each were then plated as above (cell viability 10^1, 10^2, and 10^3 dilutions). For the positive control, a 100 µL aliquot was suspended in agar and plated as above. Plates were incubated at 22°C overnight then overlaid with 0.8% soft RG agar containing appropriate antibiotic selection (Section 2.2.2.3), or no antibiotic for the cell viability controls. Plates were then incubated at 22°C for up to 14 days. Isolated colonies growing through the antibiotic overlay were picked from the sample plates and placed on PD plates containing antibiotic (Section 2.2.2.3). Colonies were nuclear purified by three successive subculturing rounds, only taking a very small amount of fresh mycelia from the colony edge each time.

2.8 Isolation of *E. festucae* spores

Five *E. festucae* colonies were subcultured onto five PD agar plates (Section 2.2.2.1) and grown for 6-8 days at 22°C. To the first plate, 2 mL of sterile deionised water was added and a glass spreader was used to scrub the colonies for approximately 1 minute. The plate was then tilted and the liquid transferred to the next plate. This was repeated for all plates adding more deionised water if necessary. The liquid from the last plate was filtered through sterile glass wool into an Eppendorf tube and plated for microscopy (Section 2.10.2). Both Fl1 and E2368 *E. festucae* strains were used. E2368 biosensor strains were specifically generated as they produced more spores.

2.9 Plant inoculation and growth

2.9.1 Seed sterilisation

Endophyte-free *L. perenne* seeds were surface sterilised using an adaptation of the method of Latch and Christensen (151). Seeds were soaked in 50% (v/v) H_2SO_4 with 2% (w/v) available chlorine for 30 mins, rinsed in water three times, soaked in 50% (v/v) chlorine bleach for 30 mins, and rinsed in sterile deionised water three times. The seeds were left to air-dry in the laminar flow cabinet.

2.9.2 Seedling germination and inoculation

Surface-sterilised *L. perenne* seedlings (Section 2.9.1) were placed on water agar plates (3% (w/v)) and incubated at 22°C for 7 days in continuous darkness. Germinated seedlings were then inoculated with *E. festucae* mycelia, freshly grown on PD agar (Section 2.2.2.3), using the method of Latch and Christensen (151). In this method, fungal mycelia are introduced to the seedling via a small incision along the shoot apical meristem. Seedlings were incubated at 22°C for the next two weeks, 7 days in continuous darkness followed by 7 days in light conditions. The seedlings were then planted into root trainers containing pre-watered commercial potting mix and grown in a temperature (19°C) and light (16 h light / 8 h dark) controlled growth room. Light was provided with Gro-lux bulbs (Sylvania). Plants were watered when necessary.

2.9.3 Endophyte detection *in planta*

To screen for systemic endophyte infection, *L. perenne* plants were immunoblotted 6-8 weeks after planting. Tillers were cut close to the base of the pseudostem and pressed onto a nitrocellulose membrane (NCM). The NCM was then immersed in blocking solution (20 mM Tris, 10 mM HCl, 50 mM NaCl, 0.5% non-fat milk powder, pH adjusted to 7.5) for 2 hours with gentle shaking at room temperature. Blocking solution was decanted off and 15 mL of fresh blocking solution mixed with 5 µL primary rabbit polyclonal antibody raised to *E. festucae* var *lolii* (AgResearch) was added and incubated over night at 4°C with gentle shaking. The membrane was well rinsed with fresh blocking solution and incubated for 2 hours with 15 mL blocking solution mixed with 1.5 µL anti-rabbit alkaline phosphatase-conjugated secondary antibody (Santa Cruz Biotechnology, INC) at room temperature. The membrane was again thoroughly washed with fresh blocking solution and developed with Fast Red chromogen (Sigma-Aldrich, F4648) for 15 mins. The spots from infected tillers changed from green to dark pink, whereas those from uninfected plants appeared light pink.

2.10 Microscopy

2.10.1 In culture hyphal analysis

Slide plates were made by pouring a thin layer of 3% (w/v) water agar as a base. When the layer solidified a sterile slide was placed on top and overlayed with 8-10 mL 1.5% (w/v) water agar. One colony of an *E. festucae* strain was subcultured either side of the slide (42). After 6-9 days, a thin section of agar was excised using a scalpel and transferred to a clean glass slide where a coverslip was applied. The hyphal morphology and localisation of fluorescent constructs was examined in culture using the Olympus IX83- based Multidimensional Imaging Platform. Images were acquired using the QImaging Retiga 6000M camera, using the 60x, numerical aperture (NA) 1.42 lens. Data was acquired using Olympus CellSens Dimensions V1.13, using a bin of 2x2. Hyphae were imaged using Differential Interference Contrast (DIC) optics. eGFP tagged constructs were imaged using a standard FITC filter set (excitation, BP460-495; emission, BP510-550; and dichroic filter,

DM575). Strains containing mCherry tagged constructs were imaged with a altered of red filter (excitation, BP520-550; emission, LP565; and dichroic filter, DM565). Samples stained with Calcofluor white were imaged using a modified DAPI filter set (excitation, BP330-385; emission, LP420; and dichroic filter, DM400). Images were further optimised using ImageJ.

2.10.2 Conidia analysis

Three spots of conidia solution (Section 2.8) were pipetted along the length of a slide plate (Section 2.10.1). Two more spots were applied on top of each of these three spots, allowing time for each spot to dry in between. Slide plates were then incubated at 22°C for approximately 19 hours. A thin section of agar was excised using a scalpel and transferred to a clean glass slide where a coverslip was applied. The hyphal morphology and localisation of fluorescent constructs was examined in culture using the Olympus IX83- based Multidimensional Imaging Platform. Images were acquired using the QImaging Retiga 6000M camera, using the 60x, numerical aperture (NA) 1.42 lens (phialides) and the 100x, NA 1.4 lens (conidia). Data was acquired using Olympus CellSens Dimensions V1.13, using a bin of 2x2. Hyphae were imaged using Differential Interference Contrast (DIC) optics. Fluorophores eGFP and mCherry, and Calcofluor white were excited with a mercury lamp using standard FITC filter cubes. Images were further optimised using ImageJ.

2.10.3 *In planta* hyphal analysis

Tillers were freshly harvested and sections of sheath tissue, approximately 0.5 x 1 cm, were taken from the innermost leaf at the base of the pseudostem. These sections were mounted in approximately 20 µL of deionised water and covered with a glass cover slip. *In planta* localisation of biosensor constructs was examined using the Leica SP5 DM6000B Scanning Confocal Microscope driven by LAS AF V2.7.3.9723. Images were acquired using 40x oil immersion objective, NA 1.25 lens. eGFP biosensors were excited at 488 nm by a laser and emission was captured from 495 nm – 600 nm. mCherry biosensors were excited at 561 nm by a laser and emission was captured from 571 nm – 612 nm. Images were further optimised using ImageJ.

2.11 Bioinformatics

E. festucae genomic and protein sequence were accessed from the *E. festucae* Genome Project at the University of Kentucky (http://www.endophyte.uky.edu; (152)). Other fungal gene and protein sequences were retrieved from the NCBI (https://www.ncbi.nlm.nih.gov) and FungiDB (http://fungidb.org/fungidb/) databases. Multiple amino acid sequence alignments were generated by ClustalW using the Gonnet matrix with an open gap penalty of 10.0, an extended gap penalty of 0.02, and a 30% delay divergent. Pairwise alignment identity scores were generated through a global alignment with free end gaps using the Blosum62 matrix.

3. Results

3.1 Cdc24 localisation

Lipid signalling in mammalian and plant cells involves localised synthesis of specific PPIs to form lipid domains for recruitment of enzyme complexes such as the Nox complex, through binding of individual components that contain LBDs such as PH and PX domains. Interaction of these LBDs with the membrane combined with their ability to form protein-protein interactions with each other leads to recruitment and assembly of the complex at the membrane (53, 153). One key cytosolic component of the fungal Nox complex is the guanine nucleotide exchange factor Cdc24. This protein is known to preferentially localise to tips of growing hyphae and to septa in *E. festucae* (48). However, the mechanism responsible for this specific localisation is unknown. InterProScan analysis predicts that Cdc24 had three domains: a calponin homology domain (CH) at the N-terminus, potentially involved in actin binding (IPR036872); a pleckstrin homology domain (PH), involved in binding PPIs (IPR033511); and a Phox and Bem1 domain (PB1) at the C-terminus, which functions as a protein binding module through PB1-mediated heterodimerization or homo-oligomerization (IPR000270) (Figure 3.1A). PH domains generally have a strong affinity for a specific PPI with lower affinity for other PPIs (154, 155), suggesting that the PH domain of Cdc24 may crucial for localisation of this protein in *E. festucae*, as it is in yeast (72).

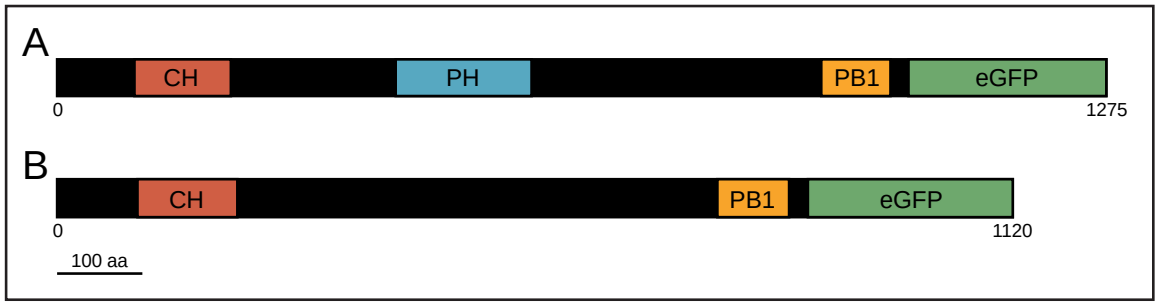

Figure 3.1. Cdc24-eGFP and Cdc24ΔPH-eGFP localisation constructs. Polypeptide structure of Cdc24-eGFP (A) and Cdc24ΔPH-eGFP, with amino acids (aa) 425-580 removed (B). InterProScan identified three domains; the Calponin homology (CH, IPR036872; purple), Pleckstrin homology (PH, IPR033511; blue), and Phox and Bem1 interaction (PB1, IPR000270; yellow) domains. Both polypeptides are C-terminally fused to enhanced green fluorescent protein (eGFP; green) with a 5x Glycine linker, enabling visualisation of the protein *in vivo*.

3.1.1 Generation of transformants

To investigate whether the PH domain of Cdc24 is indeed necessary for its localisation, two constructs were prepared by Dr Carla Eaton (Appendix 6.2.1), one with the WT gene fused to eGFP (pCE127) and the other with the internal PH domain deleted also fused to eGFP (pCE124) (Figure 3.1; Appendices 6.3.1.1 and 6.3.1.2). Transformants were generated by co-transforming WT *E. festucae* strain Fl1, protoplasts with each construct and pSF16.17 for antibiotic selection (Section 2.7.2; Appendix 6.3.4.1). Geneticin resistant transformants were picked and nuclear purified with three rounds of sub-culturing. Crude genomic DNA was extracted (Section 2.3.2) and used as template to PCR screen the transformants for presence of the construct. Three primer pairs spanning the 5', middle and 3' regions of the construct were used to confirm successful integration of each construct (Section 2.6.1; Figure 3.2). Transformants found to contain bands corresponding to the predicted sizes for each of these reactions were selected for further analysis.

3.1.2 Culture analysis

Strains were sub-cultured onto 1.5% (w/v) water agar slide plates, grown for 6-9 days, and analysed on the fluorescent microscope (Section 2.10.1). The construct expressing the WT gene fused to eGFP, Cdc24-eGFP, localised to the centre of hyphal septa and infrequently at the PM of hyphal tips as seen in previous studies (48), (Figure 3.3A; Appendix 6.4.1). There was also high level of background fluorescence possibly due to overexpression of the construct but most likely from free eGFP, as a previous western has shown that eGFP is prone to cleavage (Appendix 6.5). The construct expressing Cdc24 with the PH domain removed fused to eGFP, Cdc24ΔPH-eGFP, mislocalised and was not present in any hyphal tips analysed or at the centre of septa (Figure 3.3B; Appendix 6.4.2). The intensity of fluorescence was stronger across some septa than in the cytoplasm, however, it is unclear whether this was due to specific localisation or due to compression of the cytoplasm against the septa by vacuoles. Importantly, these results suggest that the PH domain of Cdc24 is essential for normal localisation to the hyphal tip and is likely also important for localisation to septa.

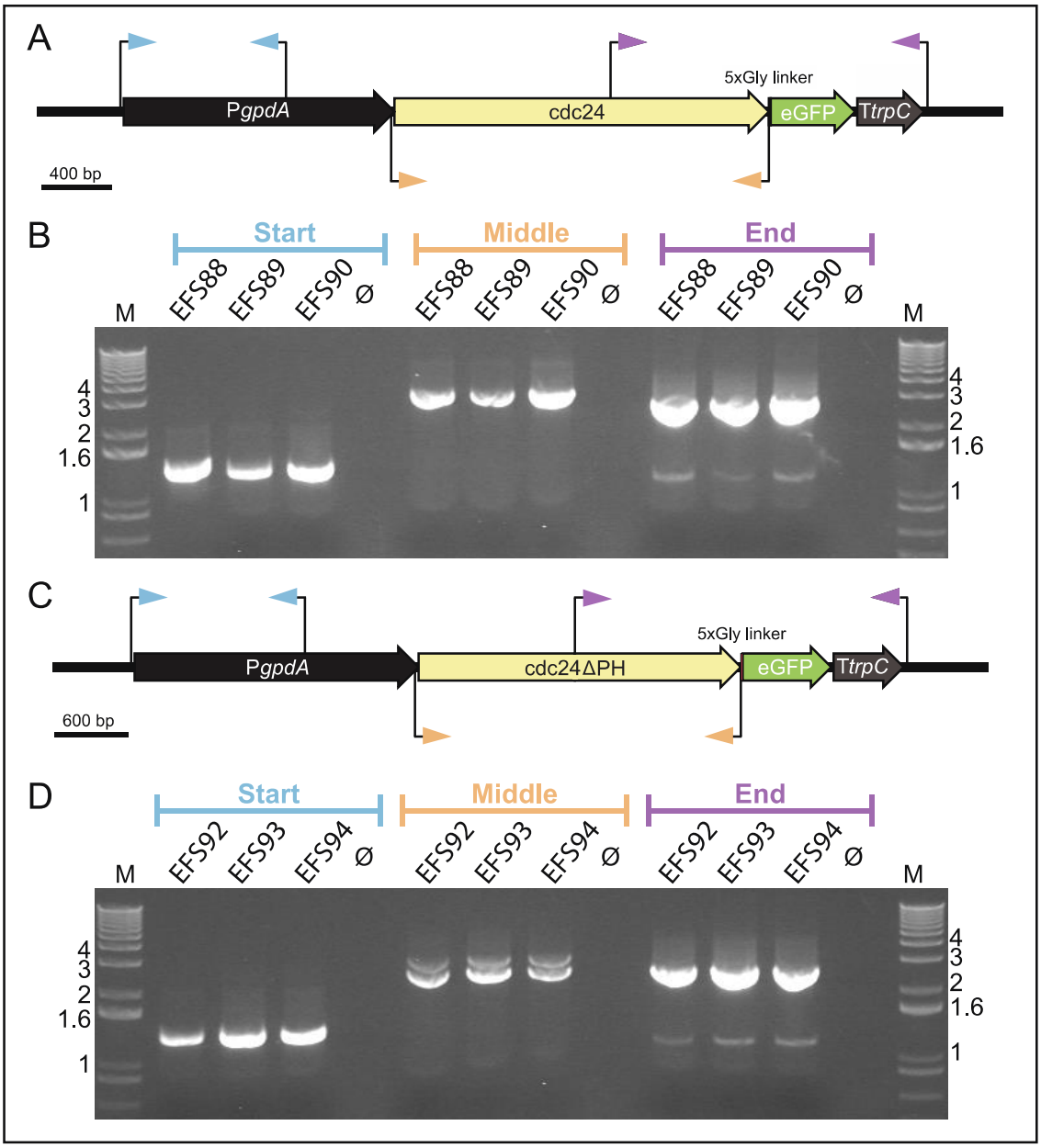

Figure 3.2. PCR screen of Cdc24-eGFP and Cdc24ΔPH-eGFP transformants. (A) Strategy for screening the cdc24-eGFP construct, pCE127, using three primer pairs covering the start (pRS426-Pgpd-F/Pgpd-R, 1412 bp; blue arrows), middle (cdc1/cdc4, 3222 bp; orange arrows), and end (cdc3/pRS426-TtrpC, 2702 bp; purple arrows) of the construct. (B) Gel electrophoresis of PCR screen with primers pairs amplifying the start, middle, and end of the cdc24-eGFP construct for strains EFS88-90. Ø = negative control. M = 1kb plus ladder. Approximate fragment sizes are given in kilobases. (C) Strategy for screening the cdc24ΔPH-eGFP construct, pCE124, using three primer pairs covering the start (pRS426-Pgpd-F/Pgpd-R, 1412 bp; blue arrows), middle (cdc1/cdc4, 2650 bp; orange arrows), and end (cdc3/pRS426-TtrpC, 2702 bp; purple arrows) of the construct. (D) Gel electrophoresis of PCR screen with primers pairs amplifying the start, middle, and end of the cdc24ΔPH-eGFP construct for strains EFS92-94. Ø = negative control. M = 1kb plus ladder. Approximate fragment sizes are given in kilobases.

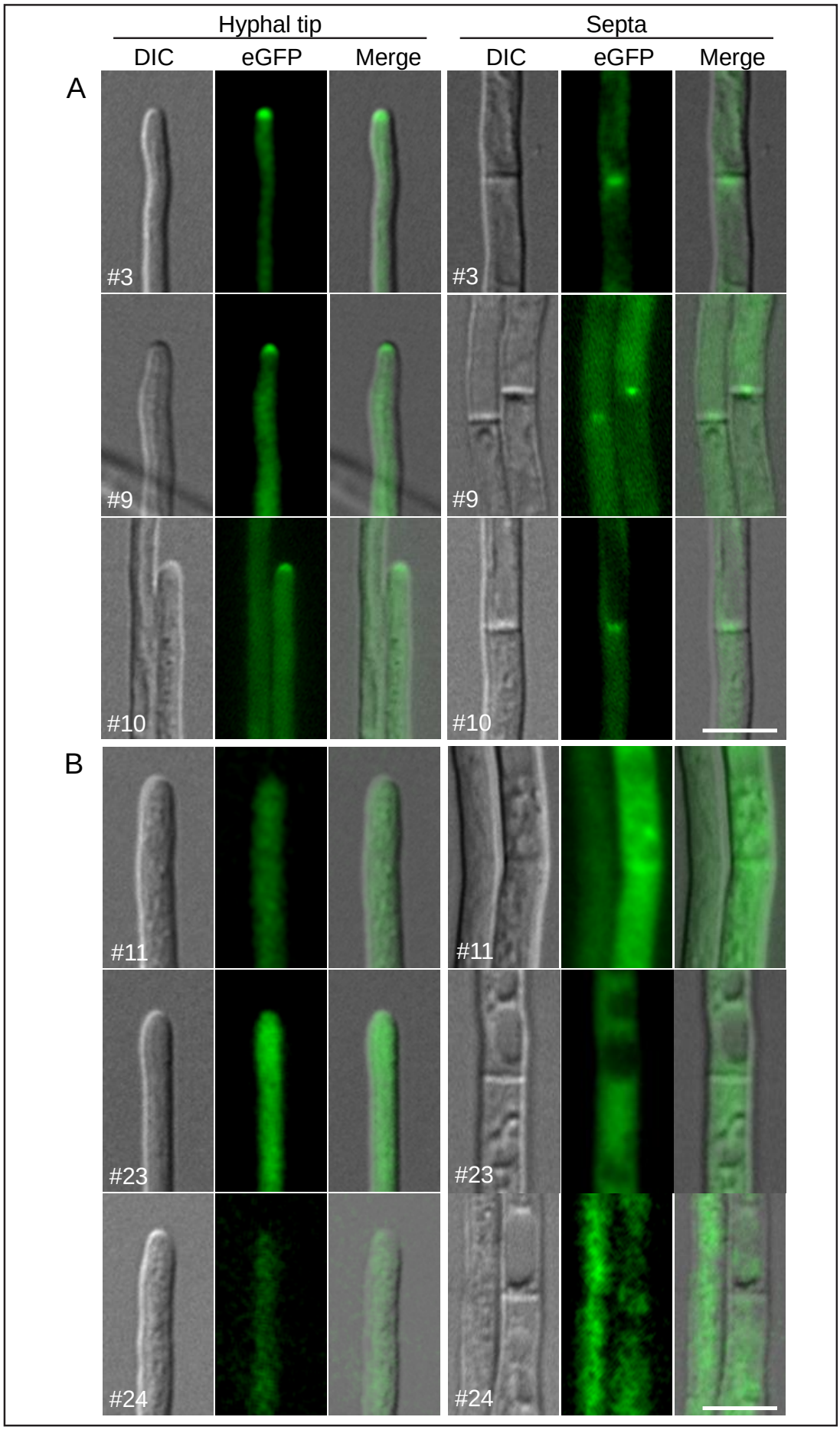
Hyphal tip
Septa
DIC
eGFP
Merge
DIC
eGFP
Merge
A
#3
#3
#9
#9
#10
#10
B
#11
#11
#23
#23
#24
#24

Figure 3.3. Localisation of Cdc24-eGFP and Cdc24ΔPH-eGFP. Differential interference contrast (DIC) and fluorescent microscopy (eGFP) images of hyphal tips and septa from three independent transformants of (A) Cdc24-eGFP (#3, EFS88; #9, EFS89; and #10, EFS90) and (B) Cdc24ΔPH-eGFP (#11, EFS92; #23, EFS 93; and #24, EFS94). Fluorescence signals have been pseudocoloured green and the DIC signal appears in grey scale. Mycelia were grown on 1.5% (w/v) water agar for 6 days at 22°C. Bars = 5 μm.

3.2 Localisation of lipid-binding domain biosensors in *Epichloë festucae*

To identify potential PPIs involved in lipid signalling, a comprehensive analysis was carried out to detect and localise predicted PPIs present in *E. festucae*.

A suite of LBD biosensors was designed *in silico* by Dr Carla Eaton (Appendix 6.2.2). Each was designed to target a specific PPI, including PI[3]P, PI[3,4]P_2, PI[3,4,5]P_3, PI[4]P, and PI[4,5]P_2, through a mammalian (*Mus musculus*) lipid-binding protein domain of known specificity (Appendix 6.1), fused either N-terminally to mCherry or C-terminally to eGFP (Appendix 6.3.2). In addition, control constructs were generated to express free mCherry and eGFP and confirm the fluorophore did not influence the biosensor localisation (Appendix 6.3.2). Each construct was codon optimised based on *E. festucae* codon bias as determined from a codon bias matrix generated by Dr Pierre-Yves Dupont.

3.2.1 Generation and screening of biosensor transformants

Transformants were generated by co-transforming WT *E. festucae* strain Fl1 protoplasts with each construct and a plasmid for geneticin resistance, pSF16.17 (Section 2.7; Appendix 6.3.4.1). Geneticin resistant transformants were picked then nuclear purified with three rounds of sub-culturing. Some transformants had reduced radial growth, likely due to overexpression of the construct interfering with normal cellular activity, so were discarded. Both crude and pure gDNA were extracted from strains with WT morphology (Sections 2.3.2 and 2.3.3) and used as template to PCR screen the transformants. Two or three primer pairs spanning the construct were used to confirm the successful integration of the biosensor construct (Section 2.6.1; Figures 3.4 to 3.9).

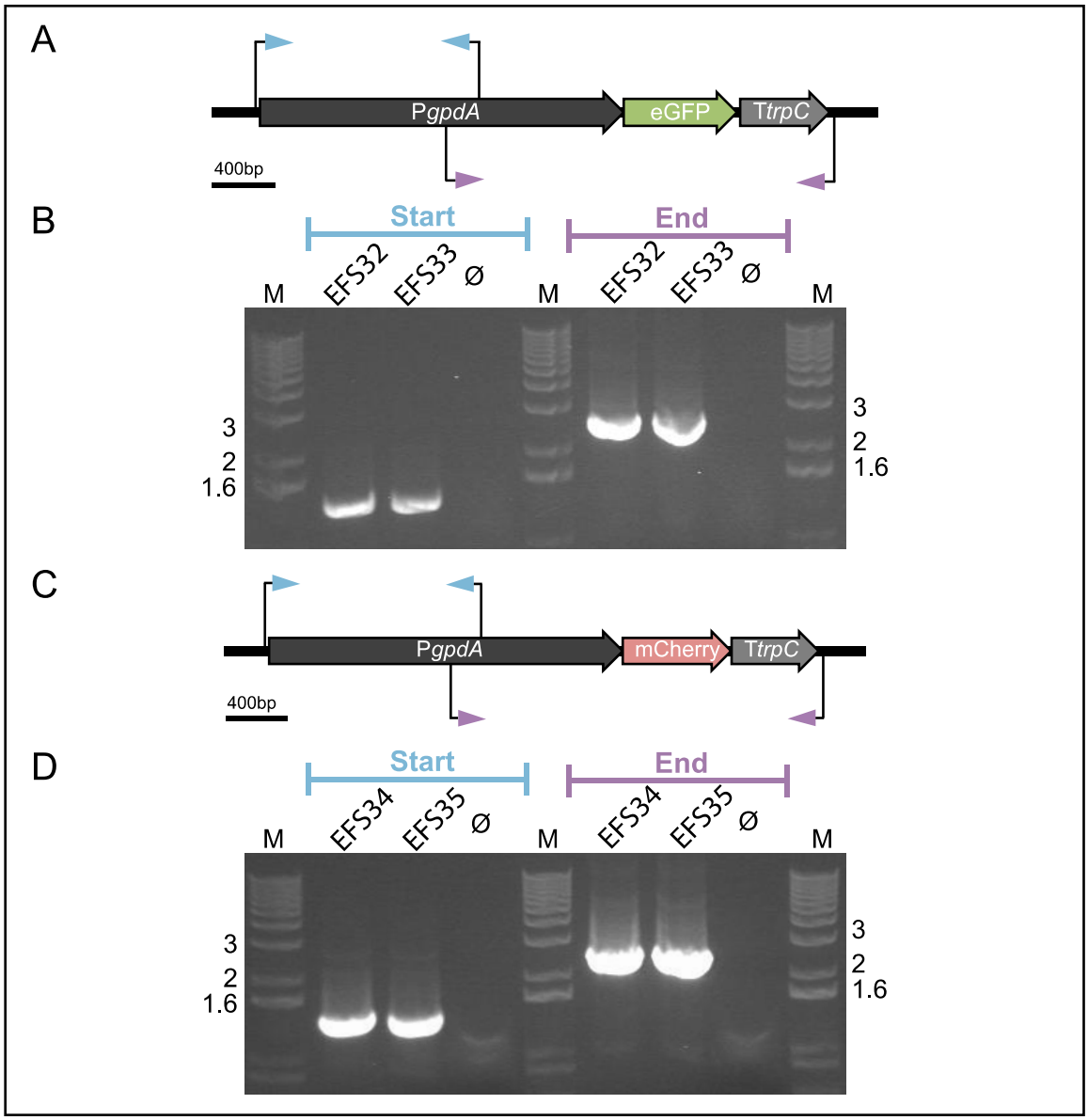

Figure 3.4. PCR screen of eGFP and mCherry control transformants. (A) Strategy for screening the eGFP construct, pCE125, using two primer pairs covering the start (pRS426-Pgpd-F/Pgpd-R, 1412 bp; blue arrows) and end (Pgpd-F/pRS426-TtrpC, 2764 bp; purple arrows) of the construct. (B) Gel electrophoresis of PCR screen with primers pairs amplifying the start and end of the eGFP construct. Ø = negative control. M = 1kb plus ladder. Approximate fragment sizes are given in kilobases. (C) Strategy for screening the mCherry construct, pCE126, using two primer pairs covering the start (pRS426-Pgpd-F/Pgpd-R, 1412 bp; blue arrows) and end (Pgpd-F/pRS426-TtrpC-R, 2461 bp; purple arrows) of the construct. (D) Gel electrophoresis of PCR screen with primers pairs amplifying the start and end of the mCherry construct. Ø = negative control. M = 1kb plus ladder. Approximate fragment sizes are given in kilobases.

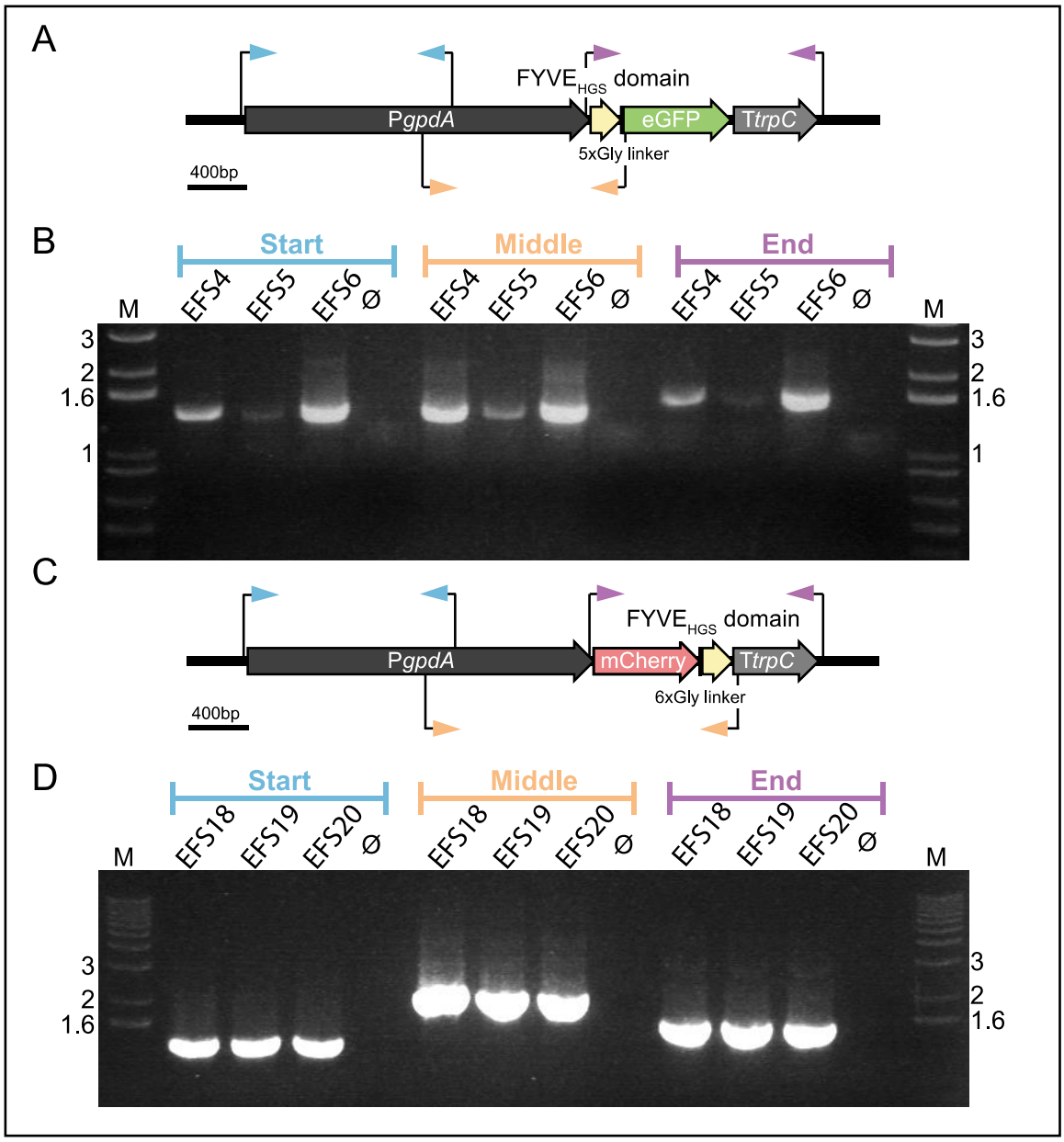

Figure 3.5. PCR screen of PI[3]P lipid-binding domain biosensor transformants. (A) Strategy for screening the HGS-eGFP construct, pCE106, using three primer pairs covering the start (pRS426-Pgpd-F/Pgpd-R, 1412 bp; blue arrows), middle (Pgpd-F/hgs3, 1359 bp; orange arrows), and end (hgs2/pRS426-TtrpC-R, 1588 bp; purple arrows) of the construct. (B) Gel electrophoresis of PCR screen with primers pairs amplifying the start, middle, and end of the eGFP construct. Ø = negative control. M = 1kb plus ladder. Approximate fragment sizes are given in kilobases. (C) Strategy for screening the mCherry-HGS construct, pCE111, using three primer pairs covering the start (pRS426-Pgpd-F/Pgpd-R, 1412 bp; blue arrows), middle (Pgpd-F/hgs1, 2169bp; orange arrows), and end (mCherry-F/pRS426-TtrpC-R, 1643bp; purple arrows) of the construct. (D) Gel electrophoresis of PCR screen with primers pairs amplifying the start, middle, and end of the mCherry construct. Ø = negative control. M = 1kb plus ladder. Approximate fragment sizes are given in kilobases.

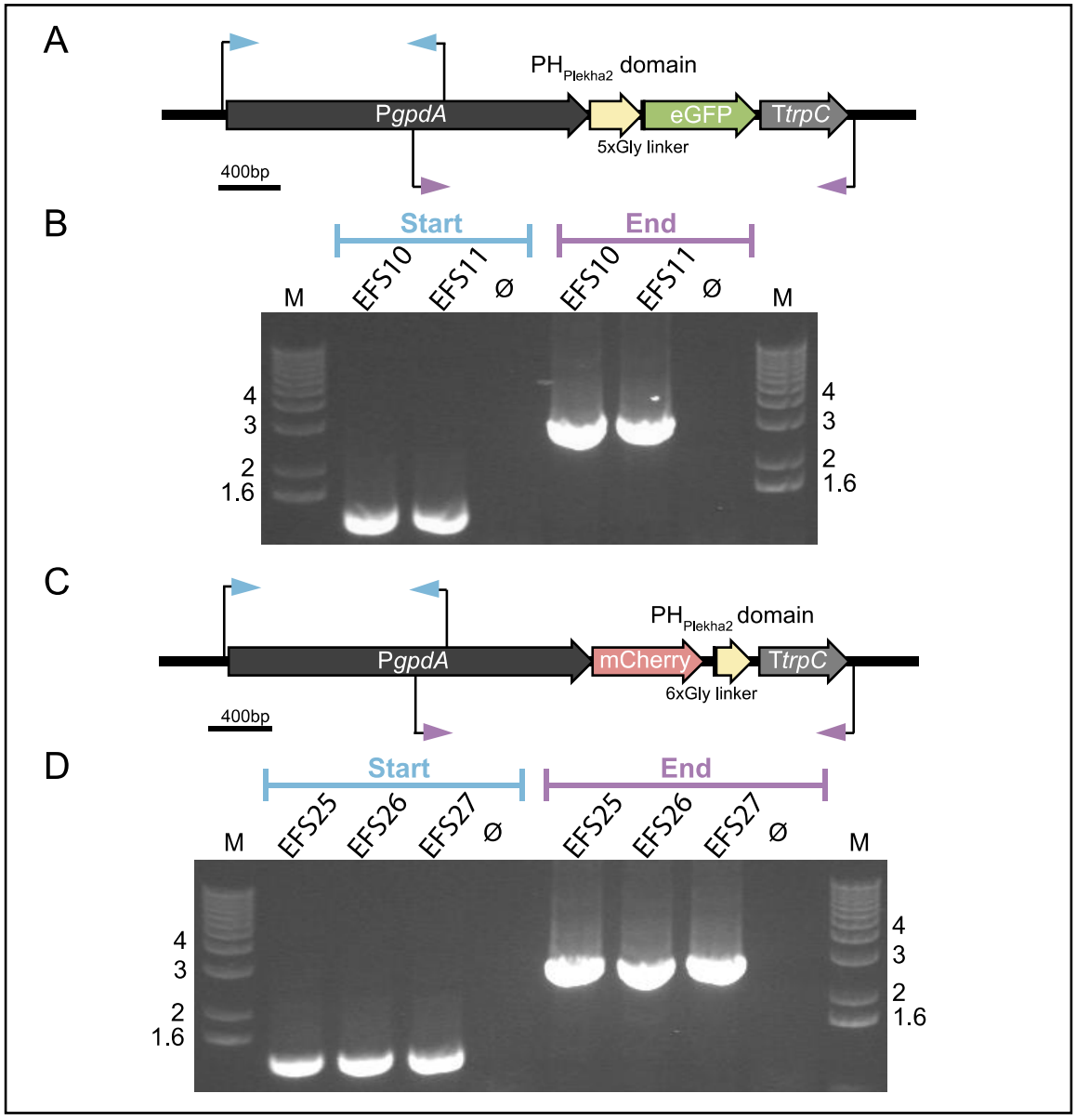

Figure 3.6. PCR screen of PI[3,4]P_2 lipid-binding domain biosensor transformants. (A) Strategy for screening the Plekha2-eGFP construct, pCE108, using two primer pairs covering the start (pRS426-Pgpd-F/Pgpd-R, 1412 bp; blue arrows) and end (Pgpd-F/pRS426-TtrpC, 2809 bp; purple arrows) of the construct. (B) Gel electrophoresis of PCR screen with primers pairs amplifying the start and end of the eGFP construct. Ø = negative control. M = 1kb plus ladder. Approximate fragment sizes are given in kilobases. (C) Strategy for screening the mCherry-Plekha2 construct, pCE113, using two primer pairs covering the start (pRS426-Pgpd-F/Pgpd-R, 1412 bp; blue arrows) and end (Pgpd-F/pRS426-TtrpC-R, 2780 bp; purple arrows) of the construct. (D) Gel electrophoresis of PCR screen with primers pairs amplifying the start and end of the mCherry construct. Ø = negative control. M = 1kb plus ladder. Approximate fragment sizes are given in kilobases.

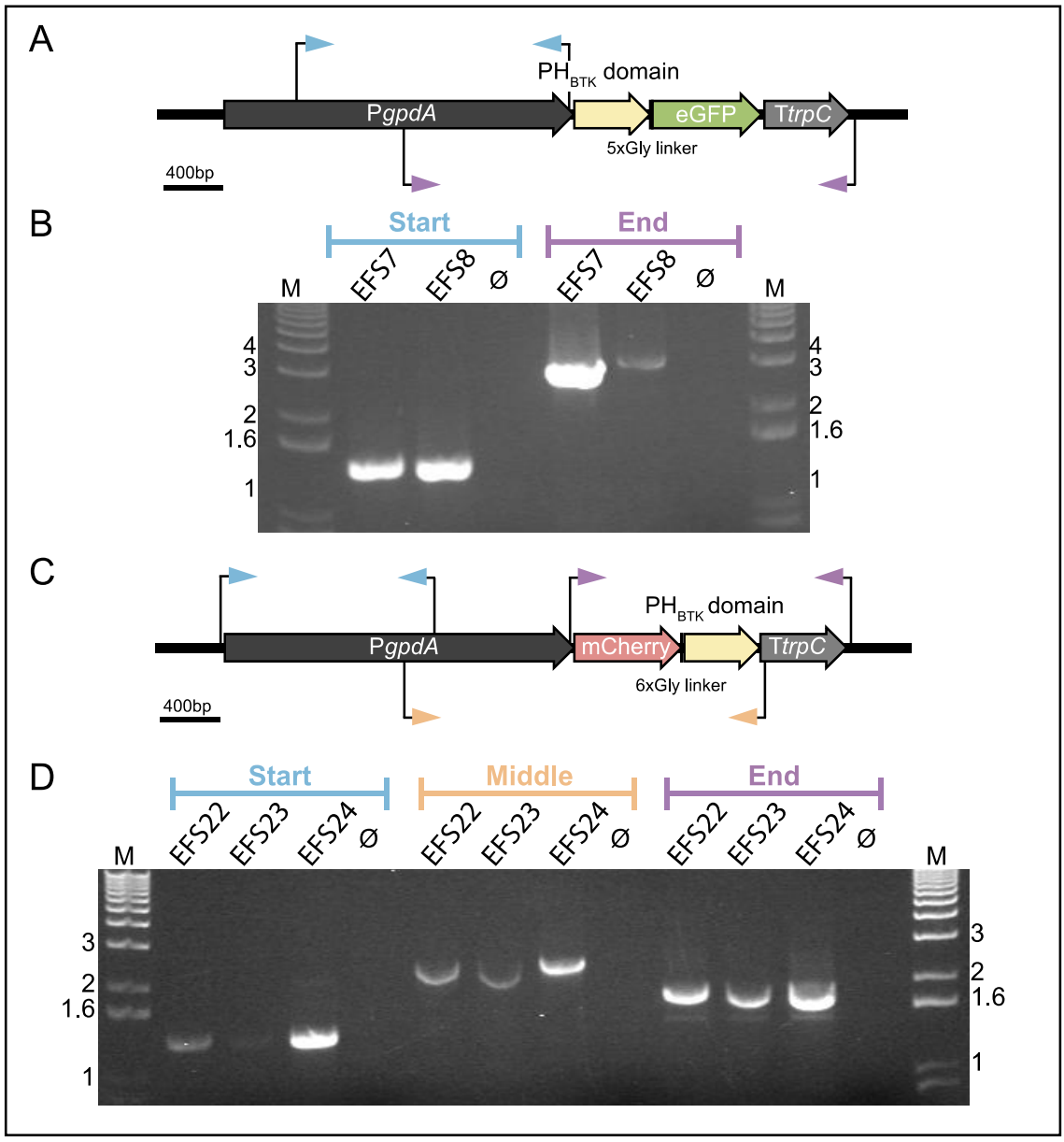

Figure 3.7. PCR screen of PI[3,4,5]P$_3$ lipid-binding domain biosensor transformants. (A) Strategy for screening the BTK-eGFP construct, pCE107, using two primer pairs covering the start (pRS426-Pgpd-F/Pgpd-R, 1412 bp; blue arrows) and end (Pgpd-F/pRS426-TtrpC, 2764 bp; purple arrows) of the construct. (B) Gel electrophoresis of PCR screen with primers pairs amplifying the start and end of the eGFP construct. Ø = negative control. M = 1kb plus ladder. Approximate fragment sizes are given in kilobases. (C) Strategy for screening the mCherry-BTK construct, pCE112, using three primer pairs covering the start (pRS426-Pgpd-F/Pgpd-R, 1412 bp; blue arrows), middle (Pgpd-F/btk1, 2382 bp; orange arrows), and end (mCherry-F/pRS426-TtrpC-R, 1643 bp; purple arrows) of the construct. (D) Gel electrophoresis of PCR screen with primers pairs amplifying the start, middle, and end of the mCherry construct. Ø = negative control. M = 1kb plus ladder. Approximate fragment sizes are given in kilobases.

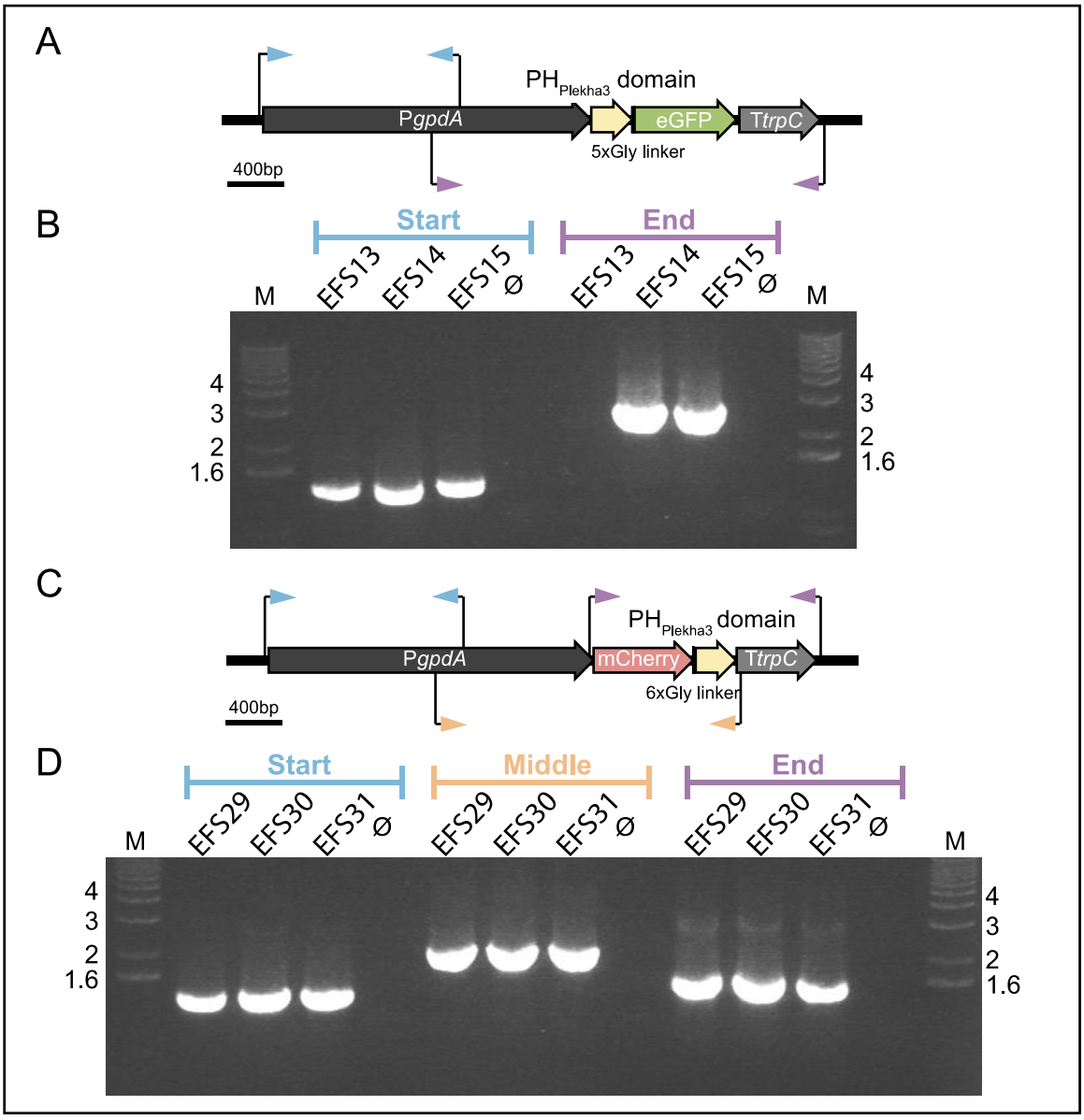

Figure 3.8. PCR screen of PI[4]P lipid-binding domain biosensor transformants. (A) Strategy for screening the Plekha3-eGFP construct, pCE109, using two primer pairs covering the start (pRS426-Pgpd-F/Pgpd-R, 1412 bp; blue arrows) and end (Pgpd-F/pRS426-TtrpC, 2764 bp; purple arrows) of the construct. (B) Gel electrophoresis of PCR screen with primers pairs amplifying the start and end of the eGFP construct. Ø = negative control. M = 1kb plus ladder. Approximate fragment sizes are given in kilobases. (C) Strategy for screening the mCherry-Plekha3 construct, pCE114, using three primer pairs covering the start (pRS426-Pgpd-F/Pgpd-R, 1412 bp; blue arrows), middle (Pgpd-F/Plekha3-1, 2169 bp; orange arrows), and end (mCherry-F/pRS426-TtrpC-R, 1643 bp; purple arrows) of the construct. (D) Gel electrophoresis of PCR screen with primers pairs amplifying the start, middle, and end of the mCherry construct. Ø = negative control. M = 1kb plus ladder. Approximate fragment sizes are given in kilobases.

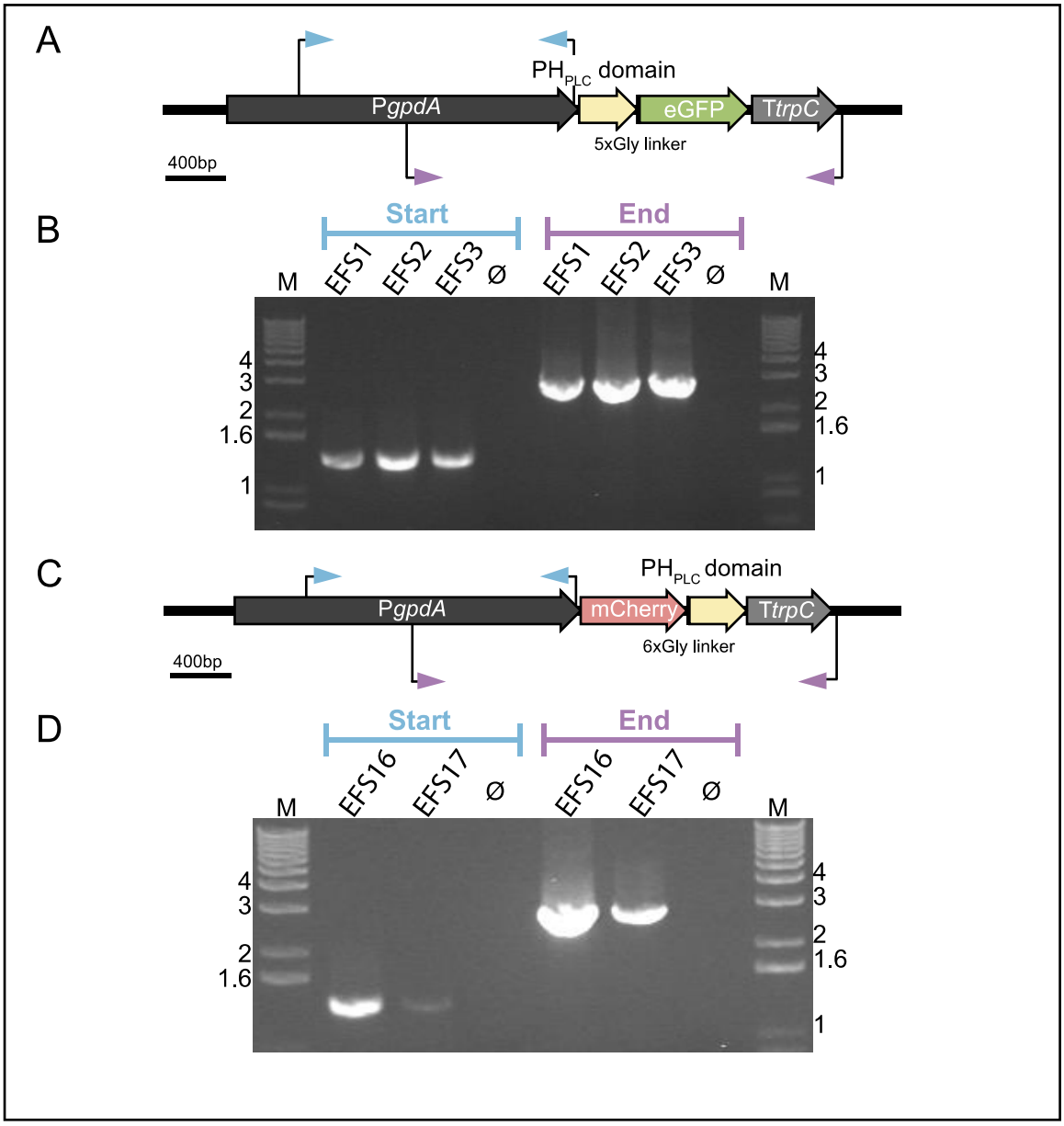

Figure 3.9. PCR screen of PI[4,5]P₂ lipid-binding domain biosensor transformants. (A) Strategy for screening the PLC-eGFP construct, pCE105, using two primer pairs covering the start (pRS426-Pgpd-F/Pgpd-R, 1412 bp; blue arrows) and end (Pgpd-F/pRS426-TtrpC, 2860 bp; purple arrows) of the construct. (B) Gel electrophoresis of PCR screen with primers pairs amplifying the start and end of the eGFP construct. Ø = negative control. M = 1kb plus ladder. Approximate fragment sizes are given in kilobases. (C) Strategy for screening the mCherry-PLC construct, pCE110, using two primer pairs covering the start (pRS426-Pgpd-F/Pgpd-R, 1412 bp; blue arrows) and end (Pgpd-F/pRS426-TtrpC-R, 2831 bp; purple arrows) of the construct. (D) Gel electrophoresis of PCR screen with primers pairs amplifying the start and end of the mCherry construct. Ø = negative control. M = 1kb plus ladder. Approximate fragment sizes are given in kilobases.

Transformants with bands corresponding to the correct size, suggestive of full construct integration, were selected for further analysis. Arvina Ram carried out western blot analyses to check for expression of each fusion protein (Appendix 6.5). The molecular weight (MW) of free eGFP and eGFP fused to the LBD was predicted using https://www.bioinformatics.org/sms/prot_mw.html. Bands corresponding to the predicted MW were detected in all transformants analysed (Appendix 6.5.1). Similarly, strains shown to contain the LBD-mCherry sequences were also analysed. Bands corresponding to free mCherry and biosensor fused to mCherry were detected (Appendix 6.5.2). The presence of free fluorophore in all biosensor strains was likely the result of cleavage of the LBD from the fluorophore as seen in previous studies (156). Transformants found to express the intact fusion protein were selected for further analysis.

The lipid composition of fungal membranes is known to change or fluctuate in response to different environmental conditions and growth stages (157, 158). To get a comprehensive picture of the PPIs present in *E. festucae*, biosensor localisation was analysed under three different conditions: vegetative growth in culture, asexual conidiation and phialide development, and intercalary growth *in planta*.

3.2.2 Localisation during vegetative growth in culture

The lipid composition was first analysed in four different regions of the mycelium growing in culture: the young hyphal tip, with active apical growth; hyphal fusion sites, where hyphae growing side by side fuse; branch points, with polarisation changes in both new and established branches; and mature hyphae. Biosensor strains were sub-cultured onto 1.5% (w/v) water agar slide plates, grown for 6-9 days, and analysed on an fluorescent microscope (Section 2.10.1). Representative images of control strains were selected to show localisation of the free fluorophore in all figures (Figures 3.10-3.14; Appendix 6.6).

3.2.2.1 PI[3]P biosensor

In hyphal tip cells the LBD of both the mCherry and eGFP PI[3]P biosensors localised to small mobile structures, likely vesicles, which rapidly oscillated

between directed movement and random 'wriggling', an observation consistent with trafficking along the cytoskeleton (Figure 3.10A; Video 3.1) (159). In the older hyphal structures, the PI[3]P biosensor localisation changed. In addition to the

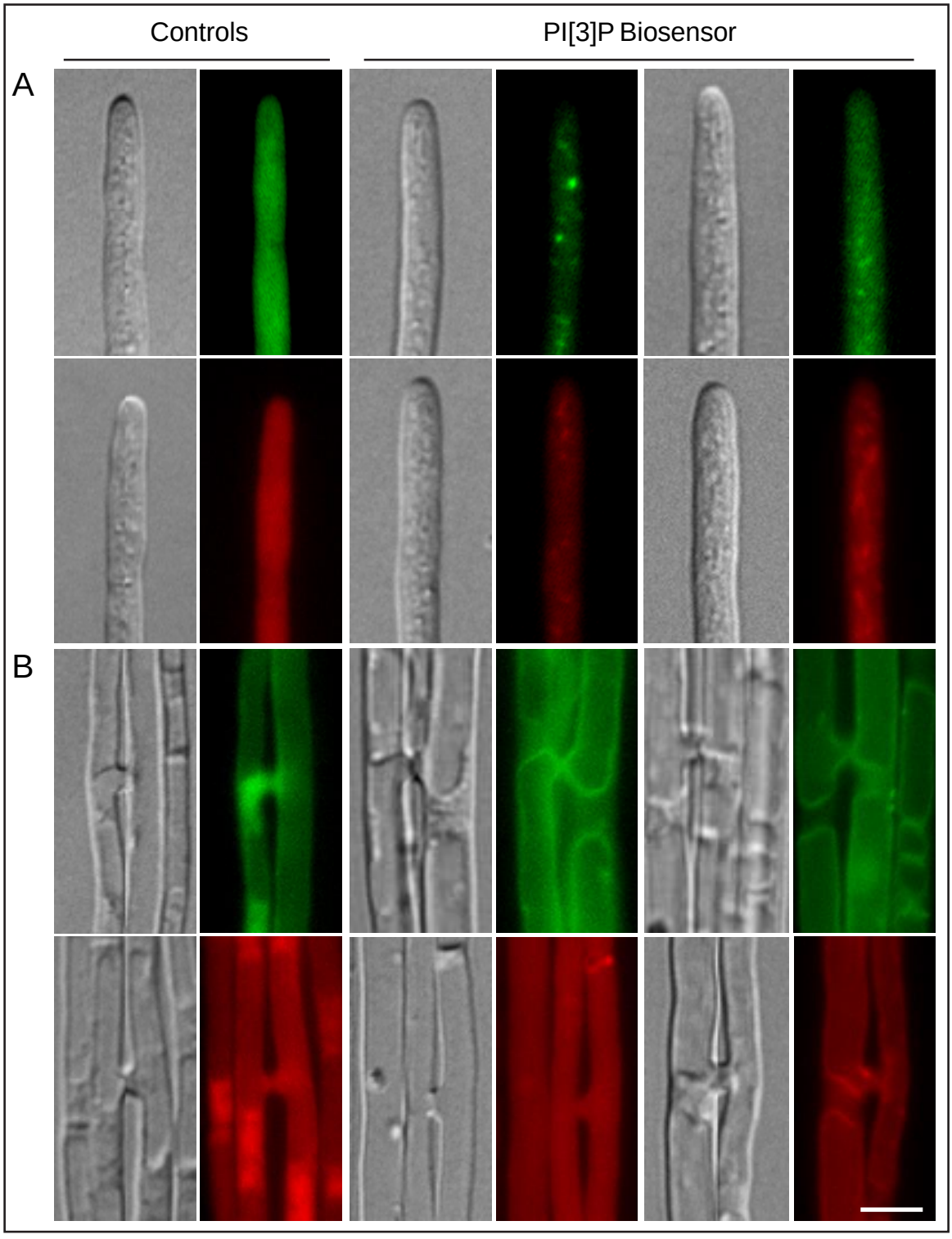

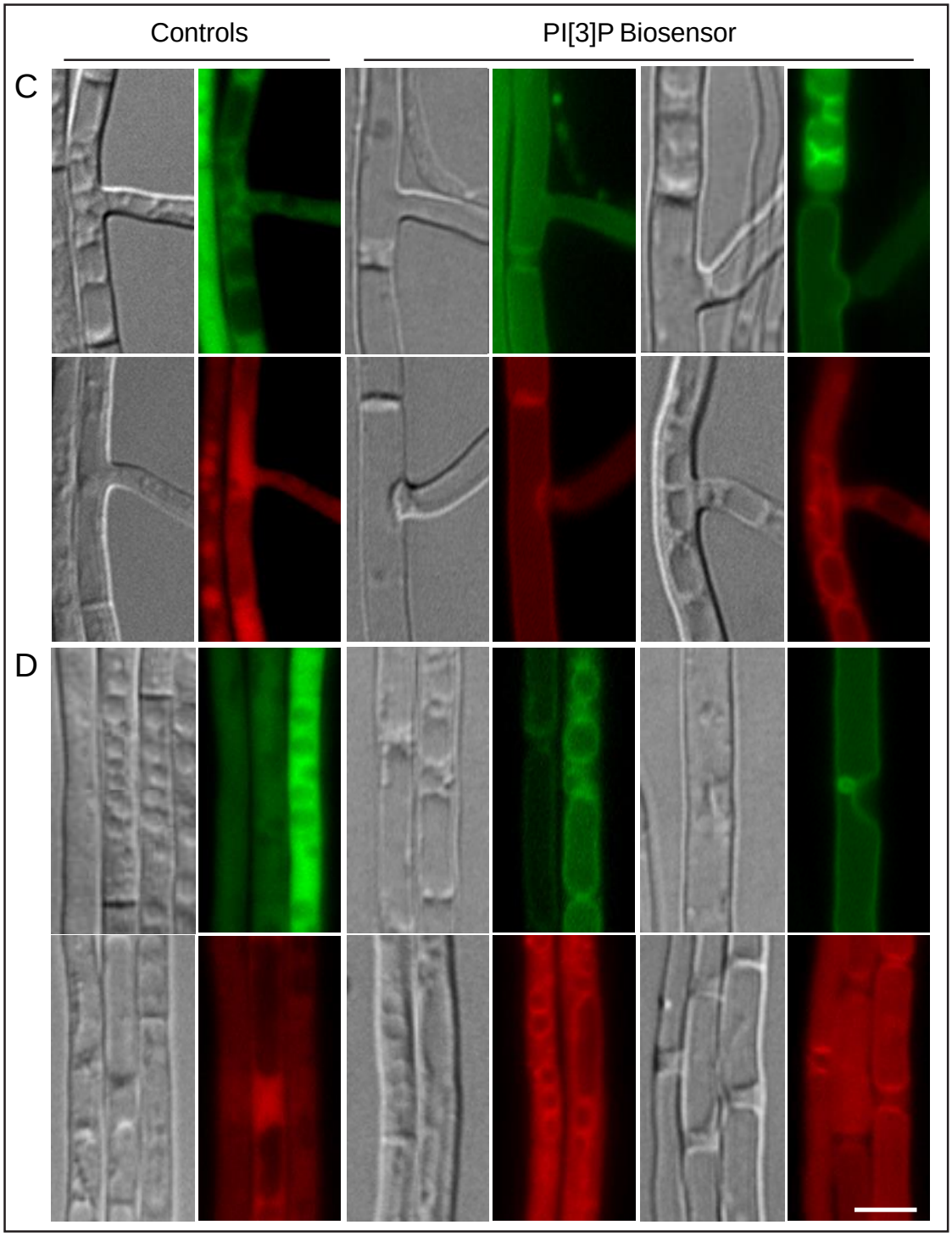

Figure 3.10. PI[3]P biosensor localisation in *Epichloë festucae* axenic cultures. Differential interference contrast and fluorescent microscopy images of the PI[3]P biosensor localisation in (A) hyphal tips, (B) fusion points, (C) branch points, and (D) mature hyphae. Representative images from control strains expressing cytoplasmic mCherry (EFS34 and EFS35) and eGFP (EFS33) and independent transformants expressing the PI[3]P biosensor either N-terminally fused mCherry (EFS18 and EFS20) or C-terminally fused to eGFP (EFS4 and EFS6) have been included. Fluorescence signals have been pseudocoloured green or red and the DIC signal appears in grey scale. Cultures were grown on 1.5% (w/v) water agar for 6-9 days. Bar = 5 µm.

vesicle-like structures seen in the hypha tip, the PI[3]P LBD localised to the periphery of rounded structures of varying sizes, likely vacuoles and endosomes as is seen in plants, mammals, and yeast (Figure 3.10B-D; Video 3.2) (102, 106). Background cytoplasmic fluorescence is seen throughout all hyphal structures, likely due to the cleaved fluorophore (Appendices 6.6.3 and 6.6.4). While the identity of these structures was not determined, the mobility and form of the two structures suggested they were vesicles and vacuoles.

3.2.2.2 PI[3,4]P_2 biosensor

Fluorescence in the PI[3,4]P_2 biosensor strains was observed throughout the cytoplasm in all hyphal tips, fusion sites, branch points, and mature cells analysed (Figure 3.11). This suggests that either this PPI was not present or inaccessible to the biosensor under vegetative growth conditions. The observed fluorescence is likely due to the cleaved free fluorophore as the grainy fluorescence seen within the cytoplasm was also seen in the control strains (Figure 3.11B, C; Appendices 6.6.5 and 6.6.6), as were the spots of fluorescence associated with damaged or abnormally thin hyphae.

3.2.2.3 PI[3,4,5]P_3 biosensor

Similar to the results for the PI[3,4]P_2 biosensor, fluorescence in the PI[3,4,5]P_3 biosensor strains was indistinguishable to that of the free fluorophore controls (Figure 3.12; Appendices 6.6.7 and 6.6.8). This suggests that this PPI was either absent under the conditions tested or inaccessible to the biosensor in these cells.

3.2.2.4 PI[4]P biosensor

In all hyphal structures examined, the LBD biosensor for PI[4]P localised to mobile structures in the cytoplasm. These are likely to be Golgi vesicles, where the moment is consistent with the stop-and-go cytoskeleton trafficking commonly associated with Golgi transport (Figure 3.13; Video 3.3) (160). Additionally, PI[4]P accumulates in Golgi vesicles in both mammalian cell lines and *C. albicans* (78, 161). In older hyphae, fewer vesicles were present and the biosensor was more frequently

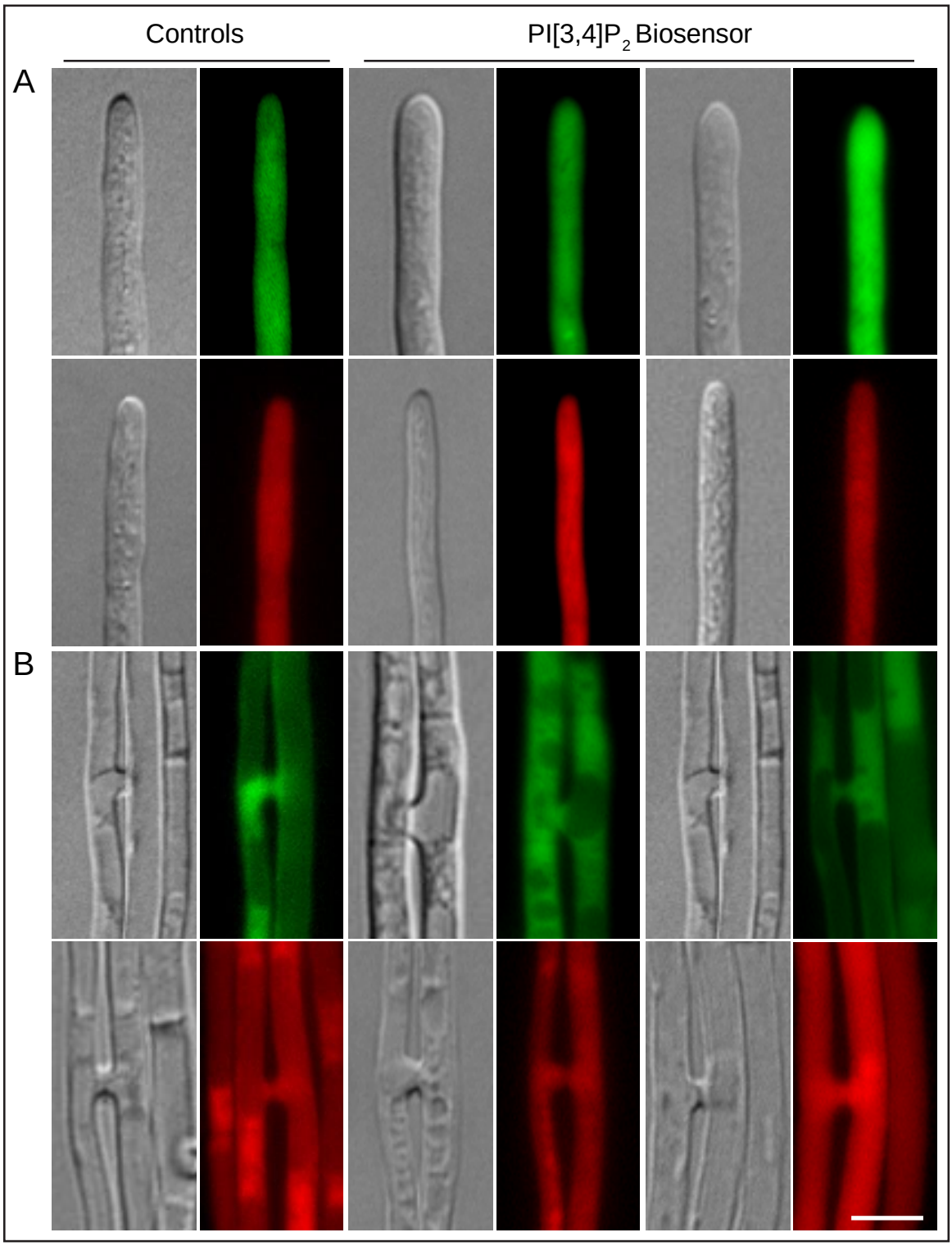
Controls
PI[3,4]P2 Biosensor
A
B

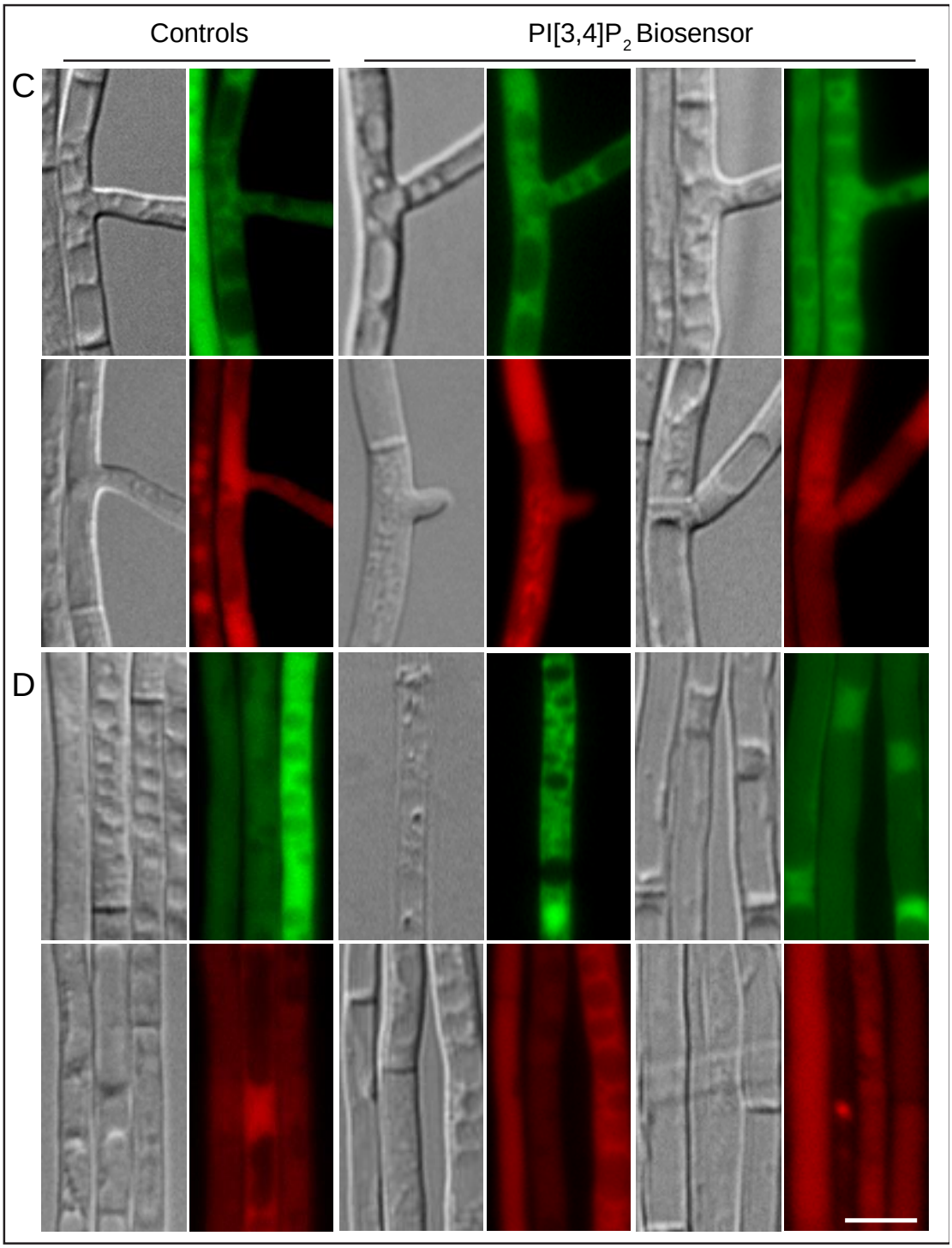

Figure 3.11. PI[3,4]P_2 biosensor localisation in *Epichloë festucae* axenic cultures. Differential interference contrast and fluorescent microscopy images of the PI[3,4]P_2 biosensor localisation in (A) hyphal tips, (B) fusion points, (C) branch points, and (D) mature hyphae. Representative images from control strains expressing cytoplasmic mCherry (EFS34 and EFS35) and eGFP (EFS33) and independent transformants expressing the PI[3,4]P_2 biosensor either N-terminally fused mCherry (EFS25, EFS26, and EFS27) or C-terminally fused to eGFP (EFS10 and EFS11) have been included. Fluorescence signals have been pseudocoloured green or red and the DIC signal appears in grey scale. Cultures were grown on 1.5% (w/v) water agar for 6-9 days. Bar = 5 µm.

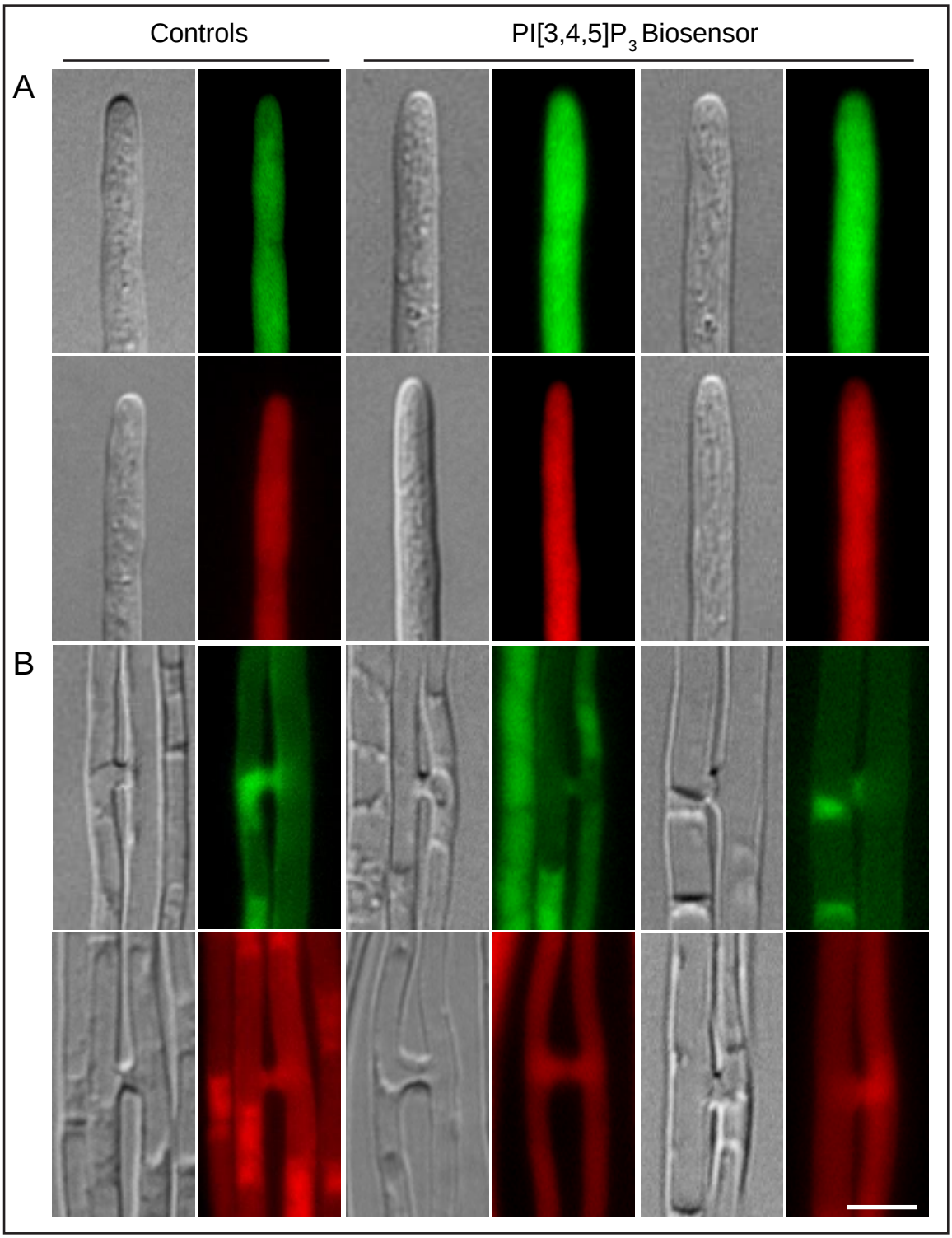
Controls
PI[3,4,5]P3 Biosensor
A
B

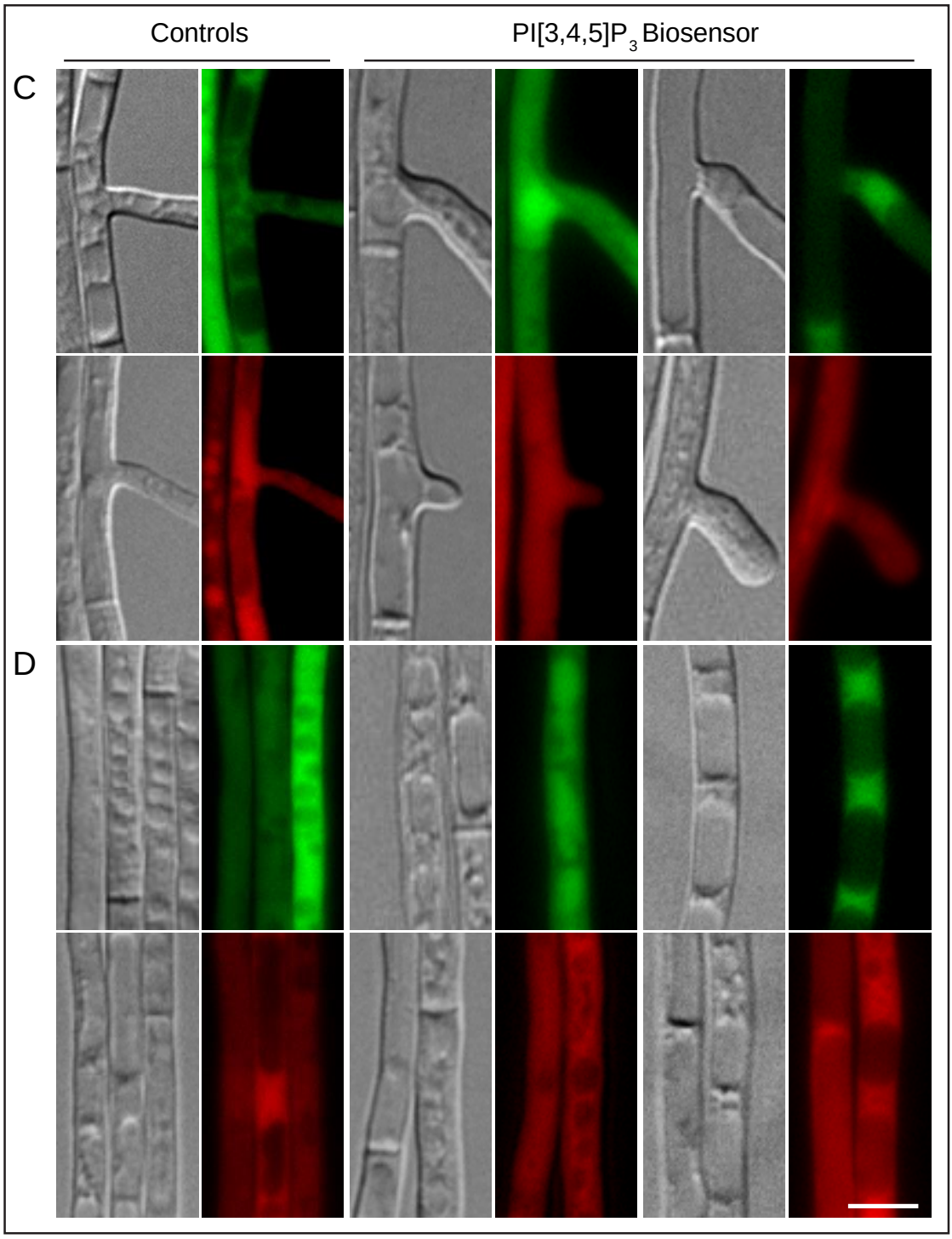

Figure 3.12. PI[3,4,5]P_3 biosensor localisation in *Epichloë festucae* axenic cultures. Differential interference contrast and fluorescent microscopy images of the PI[3,4,5]P_3 biosensor localisation in (A) hyphal tips, (B) fusion points, (C) branch points, and (D) mature hyphae. Representative images from control strains expressing cytoplasmic mCherry (EFS34 and EFS35) and eGFP (EFS33) and independent transformants expressing the PI[3,4,5]P_3 biosensor either N-terminally fused mCherry (EFS22, EFS23, and EFS24) or C-terminally fused to eGFP (EFS7 and EFS8) have been included. Fluorescence signals have been pseudocoloured green or red and the DIC signal appears in grey scale. Cultures were grown on 1.5% (w/v) water agar for 6-9 days. Bar =

5 μm.

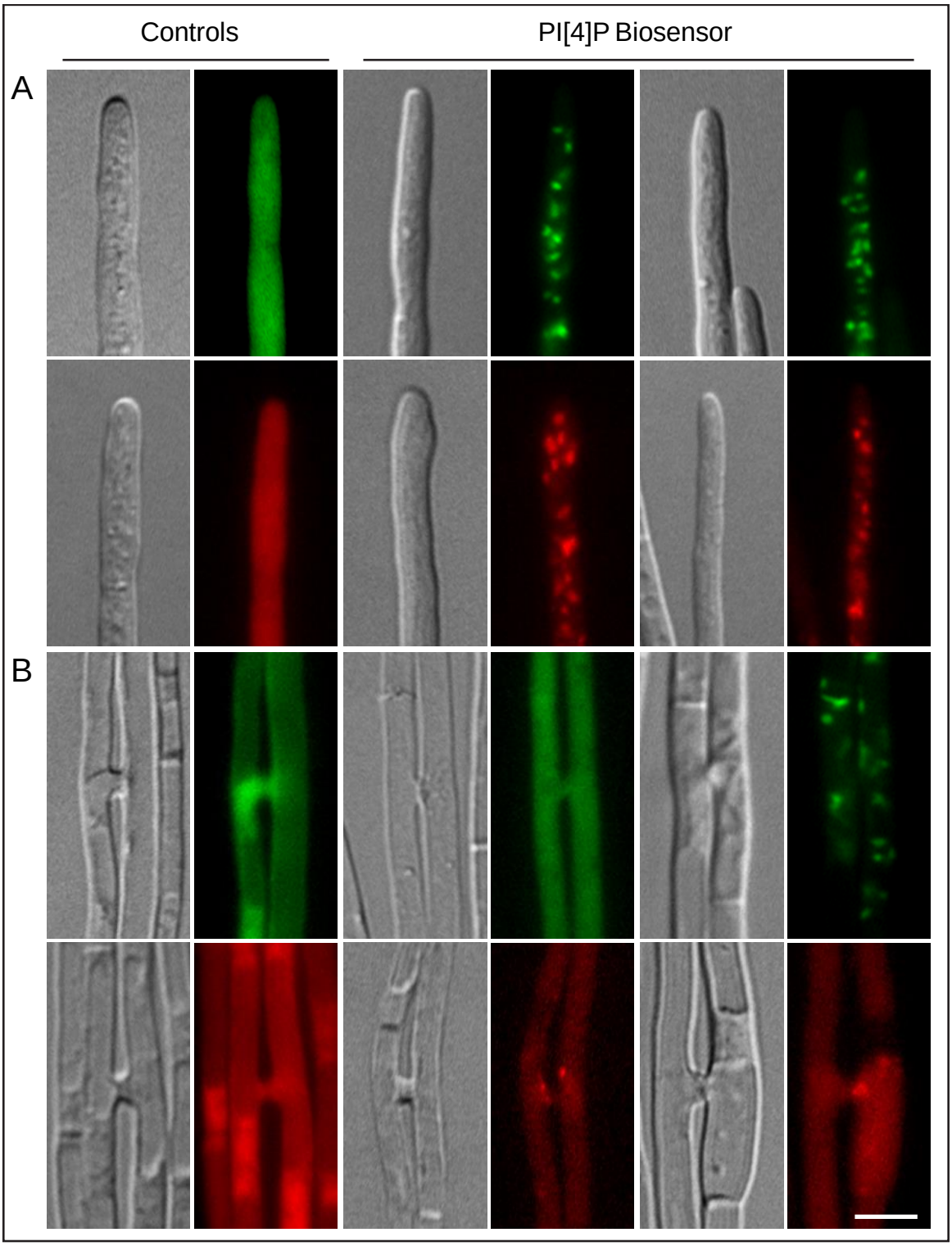

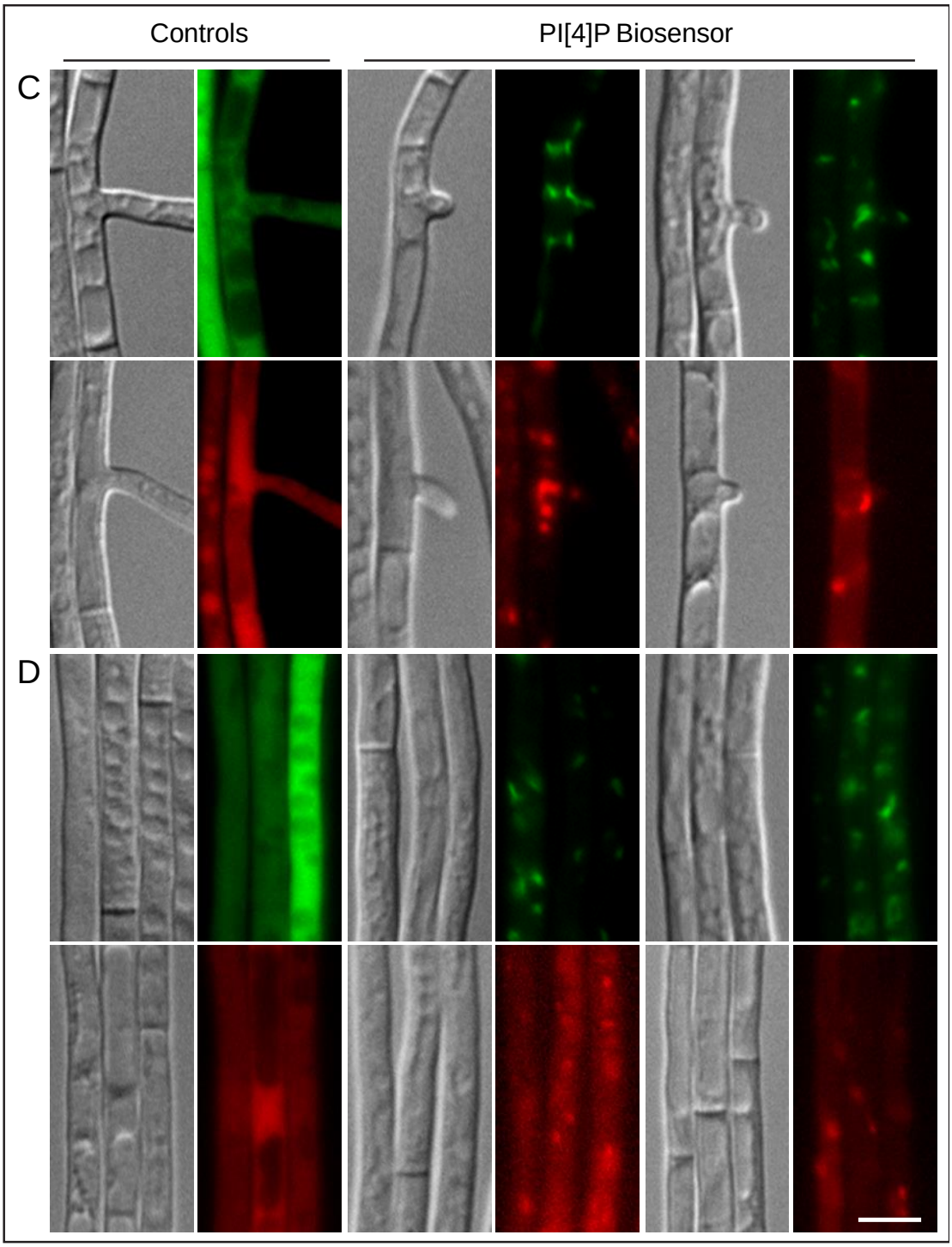

Figure 3.13. PI[4]P biosensor localisation in *Epichloë festucae* axenic cultures. Differential interference contrast and fluorescent microscopy images of the PI[4]P biosensor localisation in (A) hyphal tips, (B) fusion points, (C) branch points, and (D) mature hyphae. Representative images from control strains expressing cytoplasmic mCherry (EFS34 and EFS35) and eGFP (EFS33) and independent transformants expressing the PI[4]P biosensor either N-terminally fused mCherry (EFS29, EFS30, and EFS31) or C-terminally fused to eGFP (EFS13 and EFS14) have been included. Fluorescence signals have been pseudocoloured green or red and the DIC signal appears in grey scale. Cultures were grown on 1.5% (w/v) water agar for 6-9 days. Bar = 5 μm.

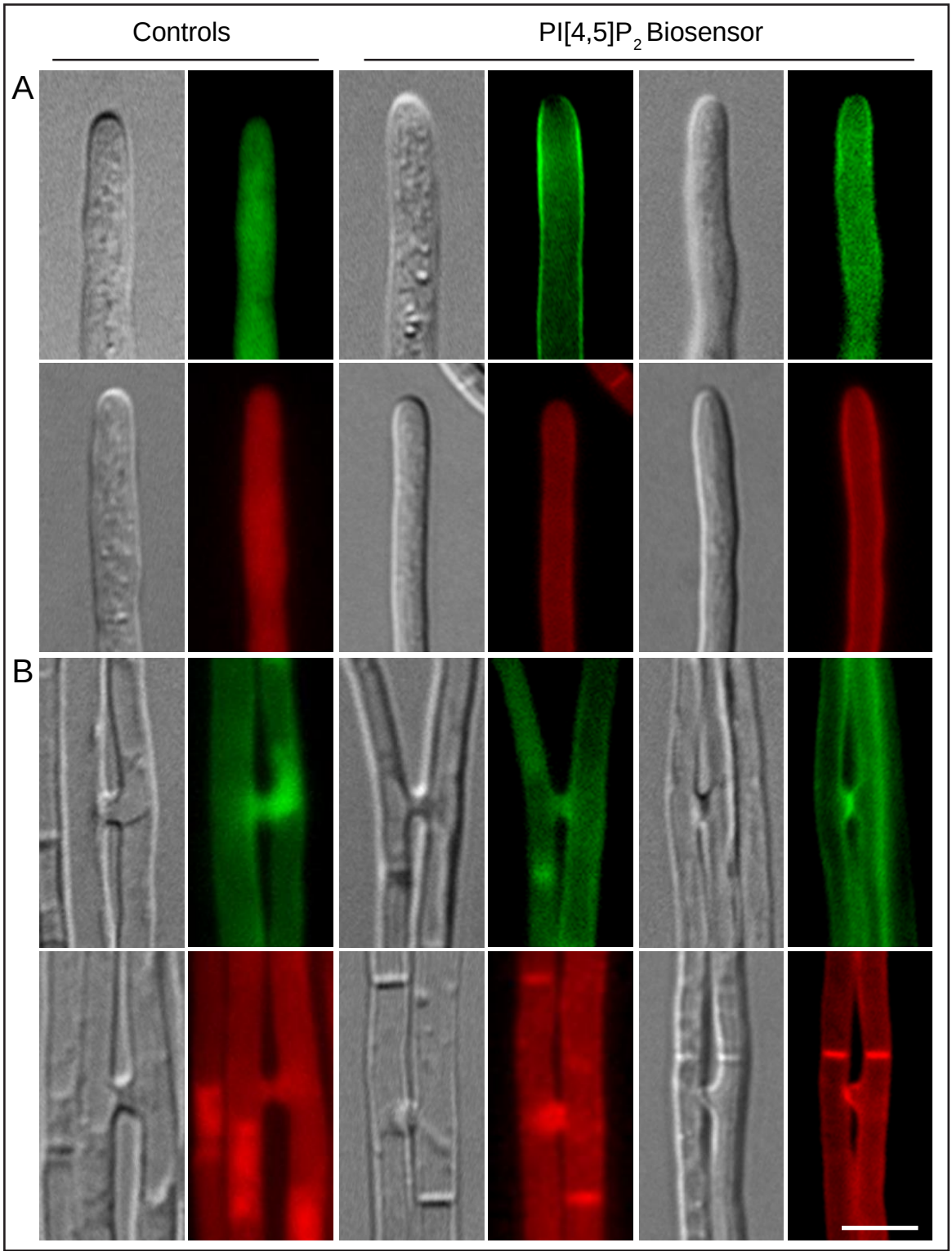
Controls
PI[4,5]P2 Biosensor
A
B

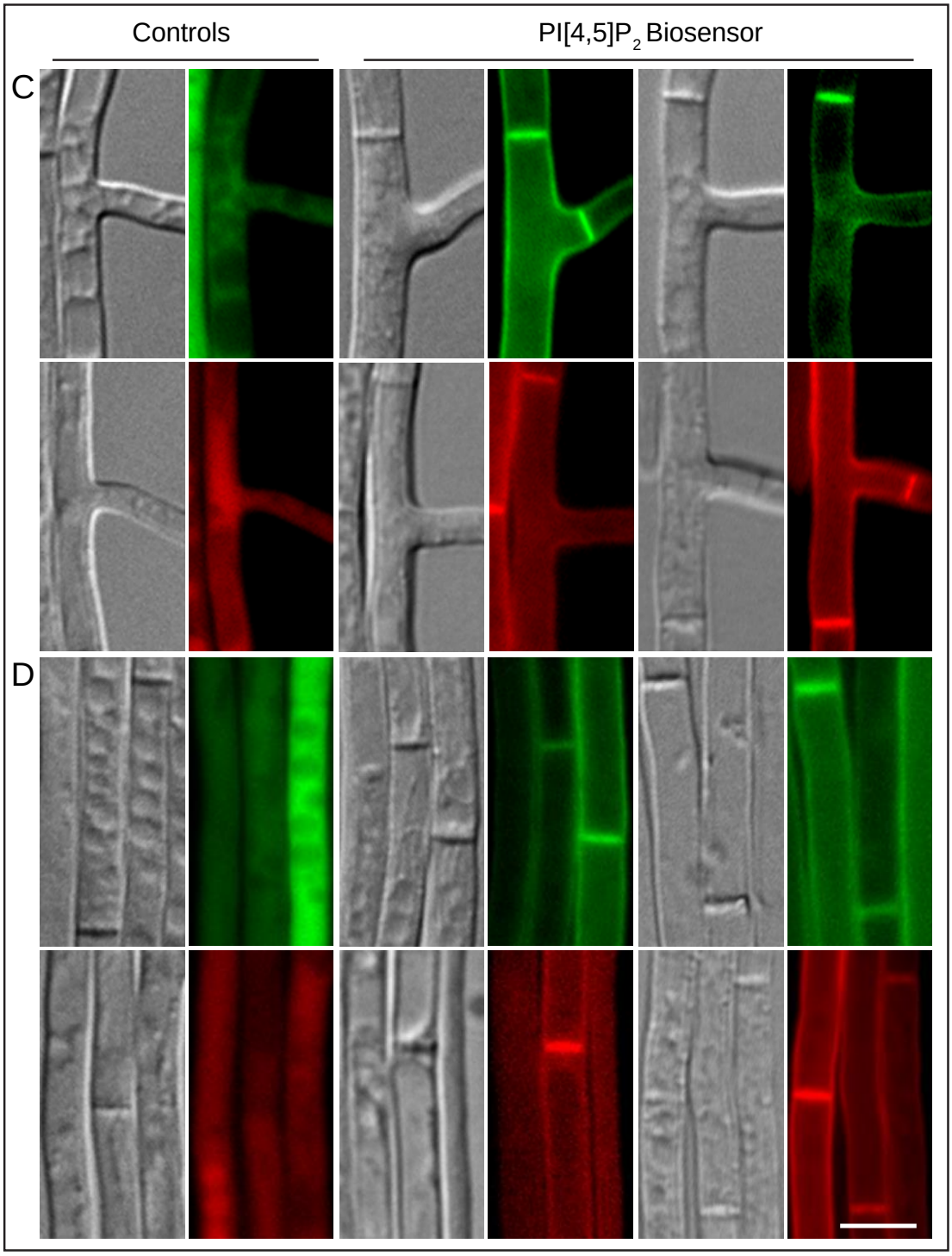

Figure 3.14. PI[4,5]P_2 biosensor localisation in *Epichloë festucae* axenic cultures. Differential interference contrast and fluorescent microscopy images of the PI[4,5]P_2 biosensor localisation in (A) hyphal tips, (B) fusion points, (C) branch points, and (D) mature hyphae. Representative images from control strains expressing cytoplasmic mCherry (EFS34 and EFS35) and eGFP (EFS33) and independent transformants expressing the PI[4,5]P_2 biosensor either N-terminally fused mCherry (EFS16 and EFS17) or C-terminally fused to eGFP (EFS1, EFS2, and EFS3) have been included. Fluorescence signals have been pseudocoloured green or red and the DIC signal appears in grey scale. Cultures were grown on 1.5% (w/v) water agar for 6-9 days. Bar = 5 µm.

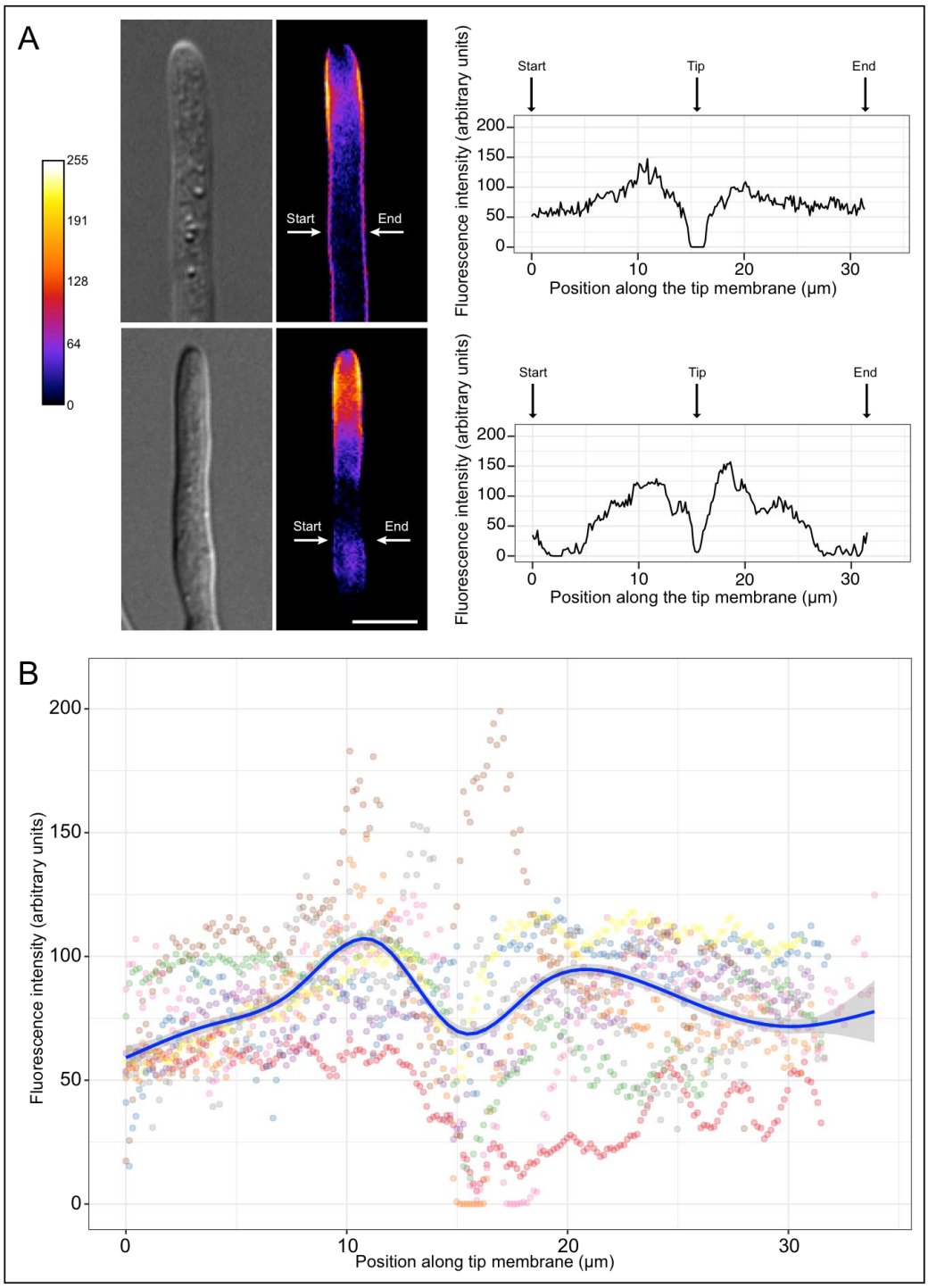

Figure 3.15. PI[4,5]P_2 biosensor gradient at the apical and sub-apical regions of the hyphal tip. (A) Representative differential interference contrast and fluorescent microscopy images of the PI[4,5]P_2 biosensor at hyphal tips, pseudocoloured to indicate the saturation of each pixel from 0 to 255 (fully saturated). A three pixel wide line was drawn along the cell membrane from the start arrow around the tip to the end arrow. Graphs represent the concentration of biosensor along this line. Cultures were grown on 1.5% (w/v) water agar for 6-9 days. Bar = 5µm. (B) Scatter graph summarising the concentration of the PI[4,5]P_2 biosensor along the cell membrane of 24 hyphal tips. Blue line = trend line. Grey shading = 95% confidence interval.

found in the cytoplasm, which could be due to the absence of the PPI or increased cleavage of the fluorophore from the fusion protein (Section 3.2.1; Figure 3.13B-D; Appendices 6.6.9 and 6.6.10).

3.2.2.5 PI[4,5]P_2 biosensor

Under vegetative mycelial growth conditions, the LBD of the PI[4,5]P_2 biosensor localised to septa and the PM (Figure 3.14). Septa fluoresced very strongly in all samples (Figure 3.14B-D). While this could indicate an enrichment of PI[4,5]P_2 in this region of the cell, it may have been due to other factors like ease of access of the biosensor to PPI at the septa, more rapid photobleaching of the PM than the septa, or the binding of the biosensor to both sides of the septa, effectively doubling the fluorescent signal. A low level of cytoplasmic fluorescence was seen in all hyphal stages, likely due to cleavage of the fluorophore from the LBD (Section 3.2.1; Appendices 6.6.11 and 6.6.12). Strikingly there was a distinct pattern of fluorescence at the hyphal tip; at the apex there was little to no signal, but a strong signal was observed in the sub-apical region, which became uniform in intensity further down the sides of the tip (Figure 3.14A; Figure 3.15A). This fluorescence pattern was measured along 24 tips all of which showed this same asymmetric pattern of lipid distribution (Figure 3.15B).

3.2.3 Localisation analysis in asexual conidiospores and phialides

To determine if the hyphal lipid composition changes during asexual reproduction, localisation of the biosensors was analysed in germinating asexual conidiospores and phialides. Phialides are flask shaped cells that a project from the hyphae and form conidiospores at their tips (37). Protoplasts from the hyper-conidiating *E. festucae* strain E2368 were prepared and co-transformed with biosensor or control constructs and pSF16.17 (Section 2.7; Appendix 6.3.4.1). Transformants were picked and screened for fluorescence, initially on the darkreader blue light transilluminator then on the fluorescent microscope. Where possible, up to 3 fluorescing strains were selected per construct for analysis. Spores were isolated (Section 2.8), plated on to 1.5% (w/v) water agar slide plates, and grown over night for 15-20 hours at 22°C (Section 2.10.1.3). Plates were then left a further 3-4

days for phialides to develop. Both conidia and phialides were analysed on the fluorescent microscope (Section 2.10.2).

3.2.3.1 PI[3]P biosensor

In germinating conidia, the PI[3]P biosensor localised in two distinct patterns, to static circular spots or to mobile vesicle-like structures. The circular spots were likely nuclei as one spot was present per cell and was frequently seen in conidia expressing the LBD-eGFP biosensor. However, this pattern was rarely seen in the mCherry-LBD biosensor (Figure 3.16A-C), where localisation was solely to mobile vesicle-like structures (Video 3.4) with movement suggestive of random Brownian motion. While the controls showed a mix of cytoplasmic and vesicular localisation (Video 3.5), the LBD biosensor had very little cytoplasmic fluorescence suggesting the vesicular localisation may be a result of specific binding to PI[3]P. In phialides the biosensor localised to distinct vesicle-like structures and to the periphery of vacuole-like structures, as seen in vegetative cells (Figure 3.16C; Section 3.2.2.1).

3.2.3.2 PI[3,4]P_2 biosensor

In both conidia and phialides the localisation of the LBD was no different from that seen in the controls, with both showing fluorescence in the cytoplasm and in small vesicle-like structures in conidia and in the cytoplasm of phialides (Figure 3.17). This suggests the PPI was either not present or inaccessible in the conidiospores and phialides under these conditions.

3.2.3.3 PI[3,4,5]P_3 biosensor

Transformants were only obtained for the mCherry-LBD biosensor as the LBD-eGFP transformations did not yield any fluorescing strains. Transformants containing the mCherry-LBD showed fluorescence throughout the cytoplasm and in vesicle-like structures, as seen in the controls, in both germinating conidia and phialides (Figure 3.18), suggesting the PI[3,4,5]P_3 was either absent or inaccessible under these conditions.

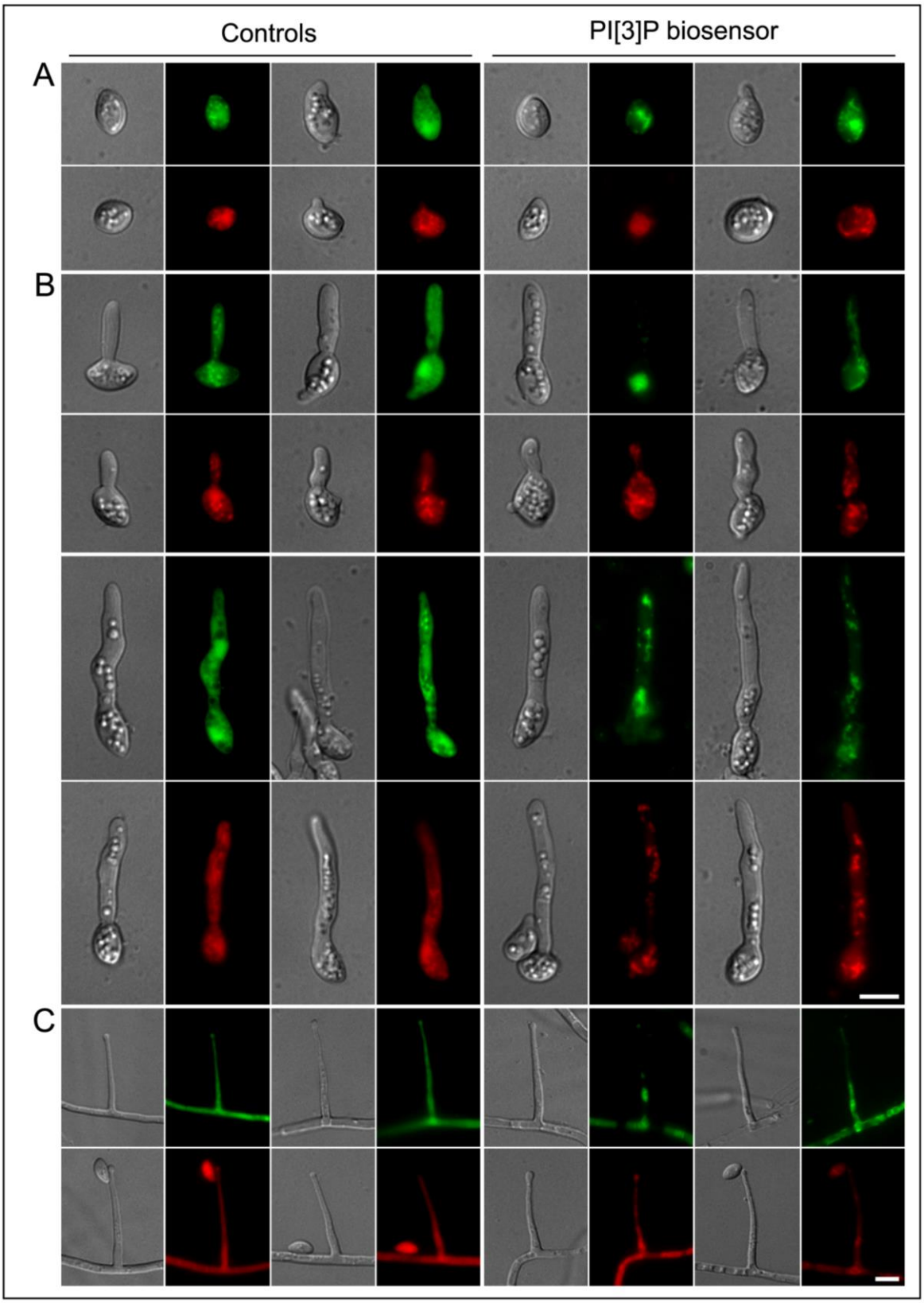

Figure 3.16. Localisation of PI[3]P in *Epichloë festucae* asexual conidia and phialides. Differential interference contrast and fluorescent microscopy images of the PI[3]P biosensor localisation in conidia (A), germinating conidia (B), and phialides (C). Images from control strains expressing cytoplasmic mCherry (EFS84) and eGFP (EFS80, EFS81, EFS82, and EFS83) and

independent transformants expressing the PI[3]P biosensor either N-terminally fused mCherry (EFS62, EFS63, and EFS64) or C-terminally fused to eGFP (EFS59, EFS60, and EFS61) have been included. Fluorescence signals have been pseudocoloured green or red and the DIC signal appears in grey scale. Conidia were obtained by scrubbing fungal colonies grown on PD agar for 7-9 days, plating onto 1.5% (w / v) water agar, and grown over night for 15-20 hours at 22°C. Plates were then left a further 3-4 nights for phialides to develop. Bars = 5 μm. Bar in (B) also applies to (A).

3.2.3.4 PI[4]P biosensor

The PI[4]P biosensor localised to small mobile vesicle-like structures that were distributed throughout germinating conidia and in phialides (Figure 3.19). This contrasted with the control strains, which had fluorescence throughout the cytoplasm of both the conidia and phialides. As seen in vegetative culture, the movement of the vesicles is consistent with cytoskeleton trafficking, though no general direction of movement could be identified (Section 3.2.2.4; Video 3.6).

3.2.3.5 PI[4,5]P_2 biosensor

The PI[4,5]P_2 biosensor localised at the plasma membrane and at the septa of conidia and phialides (Figure 3.20). The fluorescence at the septa was more intense compared to the plasma membrane, as seen in vegetative mycelia (Section 3.2.2.5; Figure 3.20C). There appeared to be a gradient of fluorescence along the axis of the germinating hyphae as seen in hyphal tips in culture (Figure 3.14A; 3.15; 3.20A and B), however, this was inconclusive as the three dimensional nature of conidia germination would cause the fluorescence intensity to naturally decrease as the spore became out of focus. A similar gradient can be observed in the conidia forming on a phialides (Figure 3.20D), where the conidium had greater fluorescence intensity than the membrane of the phialide. As the phialide structures are flatter, the gradient observed is likely to be the result of PI[4,5]P_2 enrichment.

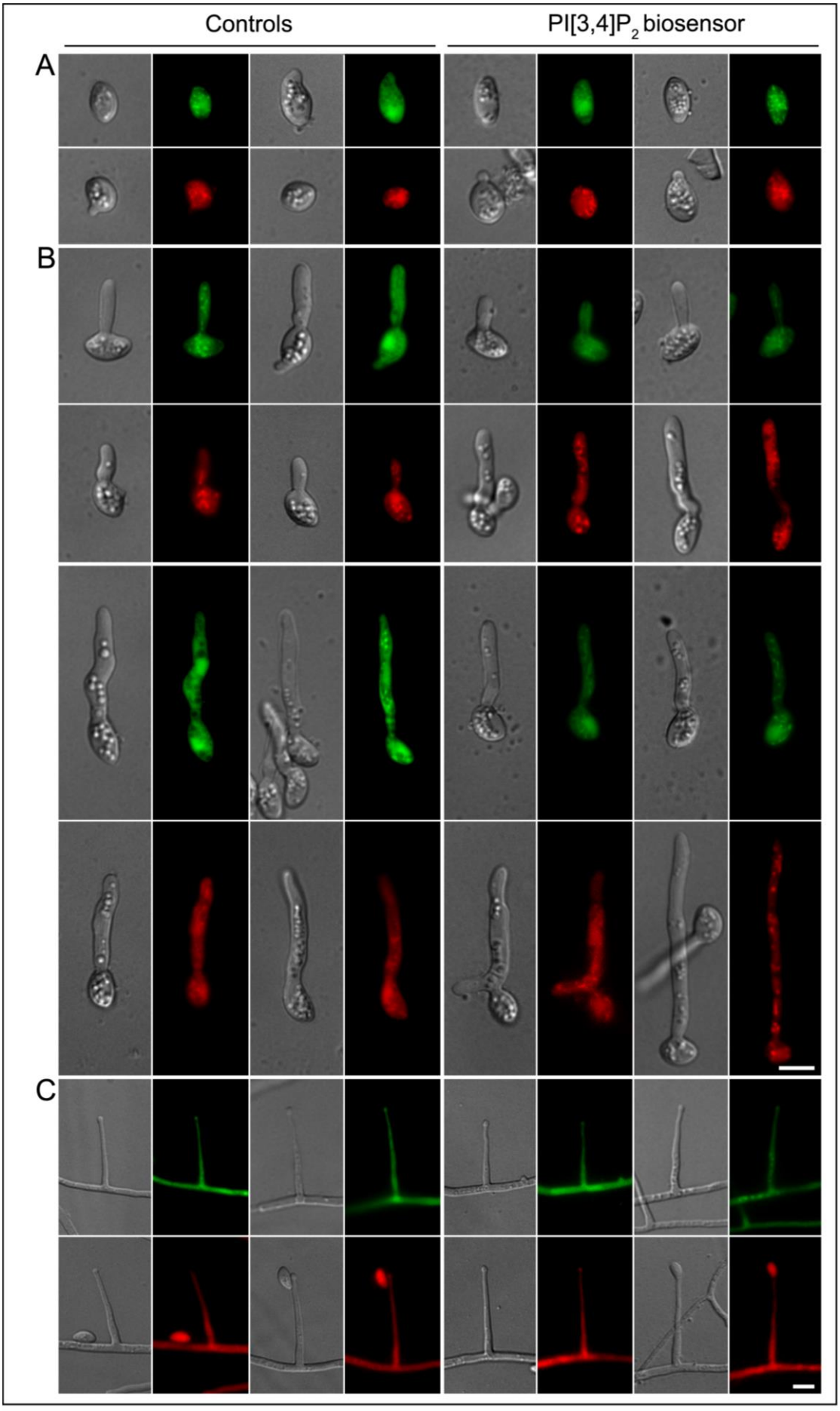
Controls
PI[3,4]P2 biosensor
A
B
C

Figure 3.17. Localisation of PI[3,4]P_2 in *Epichloë festucae* asexual conidia and phialides. Differential interference contrast and fluorescent microscopy images of the PI[3,4]P_2 biosensor localisation in conidia (A), germinating conidia (B), and phialides (C). Images from control strains expressing cytoplasmic mCherry (EFS84) and eGFP (EFS80, EFS81, EFS82, and EFS83) and independent transformants expressing the PI[3,4]P_2 biosensor either N-terminally fused mCherry (EFS72, EFS73, and EFS74) or C-terminally fused to eGFP (EFS69, EFS70, and EFS71) have been included. Fluorescence signals have been pseudocoloured green or red and the DIC signal appears in grey scale. Conidia were obtained by scrubbing fungal colonies grown on PD agar for 7-9 days, plating onto 1.5% (w / v) water agar, and grown over night for 15-20 hours at 22°C. Plates were then left a further 3-4 nights for phialides to develop. Bars = 5 µm. Bar in (B) also applies to (A).

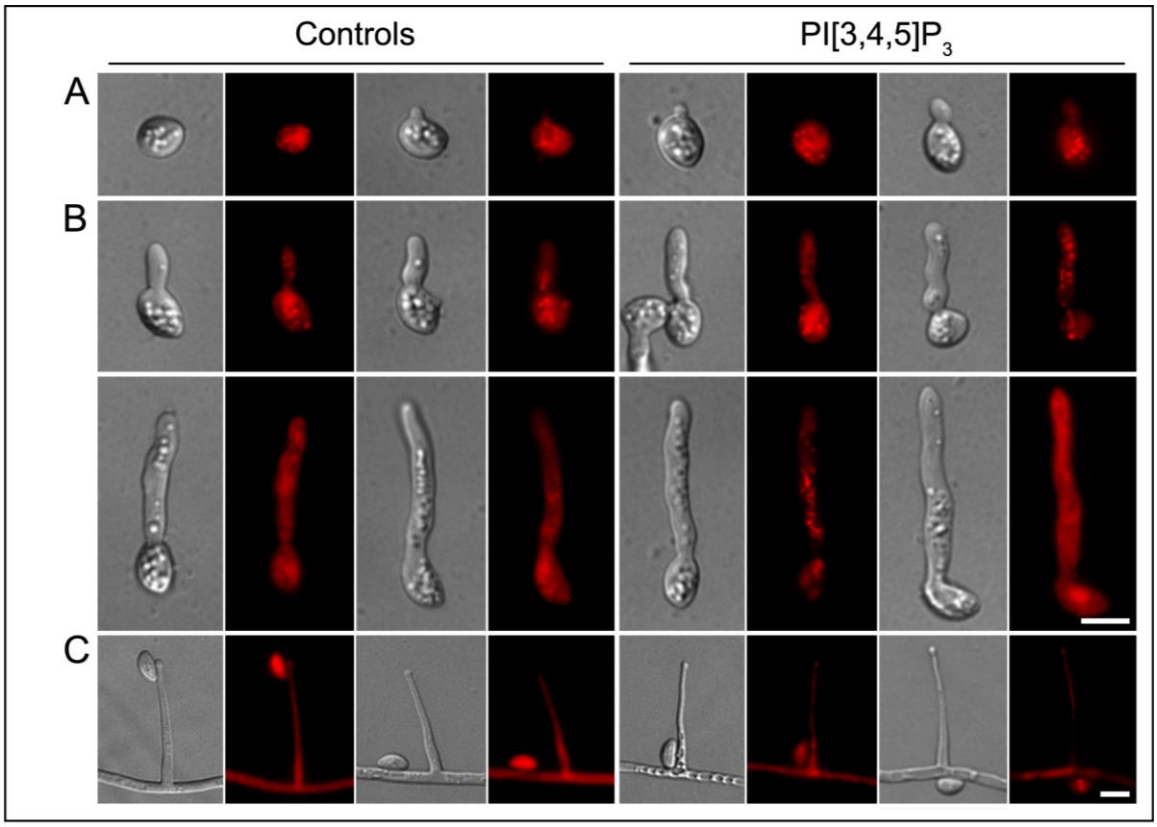

Figure 3.18. Localisation of PI[3,4,5]P_3 in *Epichloë festucae* asexual conidia and phialides. Differential interference contrast and fluorescent microscopy images of the PI[3,4,5]P_3 biosensor localisation in conidia (A), germinating conidia (B), and phialides (C). Images from control strains expressing cytoplasmic mCherry (EFS84) and an independent transformant expressing the PI[3,4,5]P_3 biosensor N-terminally fused mCherry (EFS79) have been included. Fluorescence signals have been pseudocoloured red and the DIC signal appears in grey scale. Conidia were obtained by scrubbing fungal colonies grown on PD agar for 7-9 days, plating onto 1.5% (w / v) water agar, and grown over night for 15-20 hours at 22°C. Plates were then left a further 3-4 nights for phialides to develop. Bars = 5 µm. Bar in (B) also applies to (A).

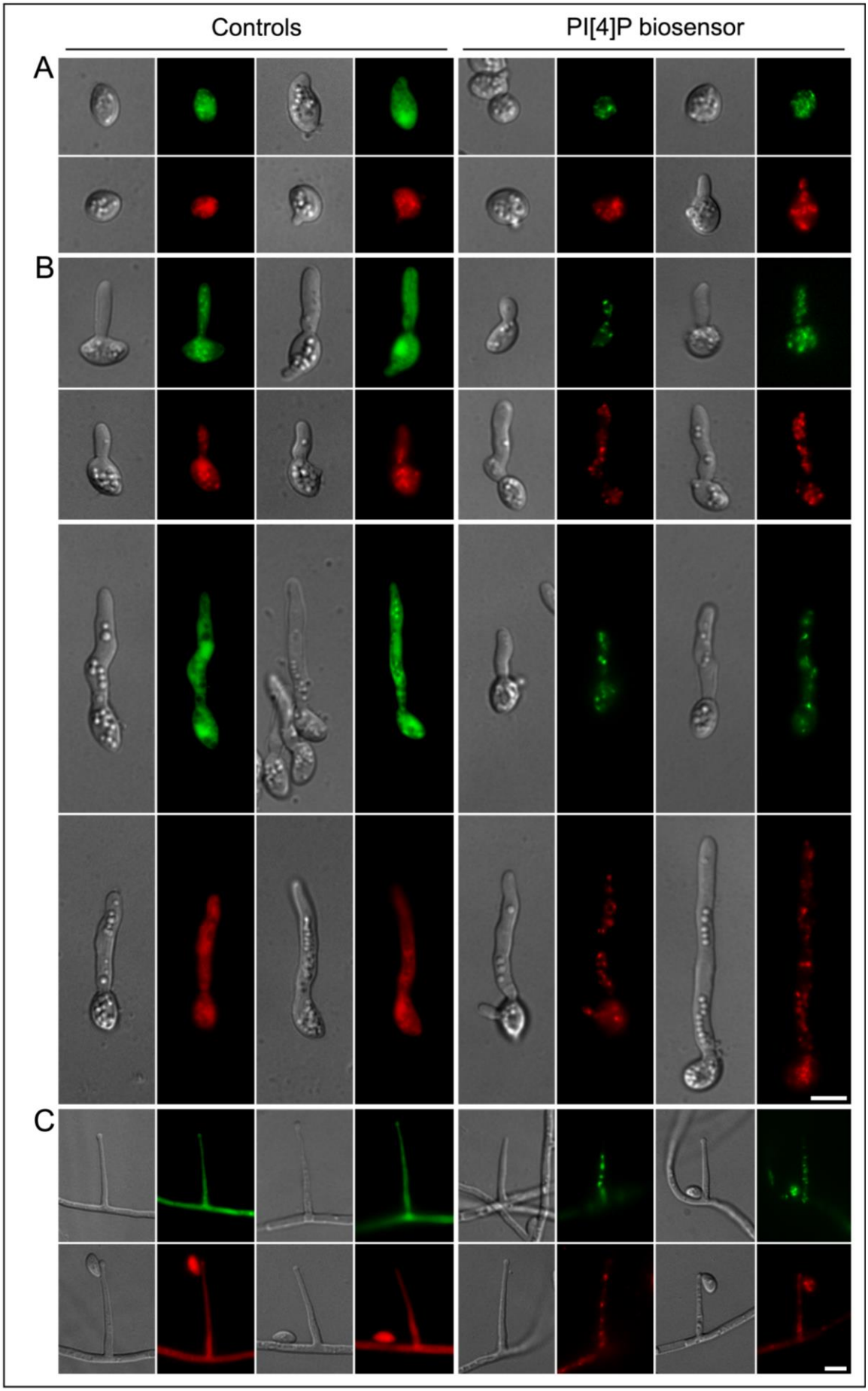
Controls
PI[4]P biosensor
A
B
C

Figure 3.19. Localisation of PI[4]P in *Epichloë festucae* (E2368) asexual conidia and phialides. Differential interference contrast and fluorescent microscopy images of the PI[4]P biosensor localisation in conidia (A), germinating conidia (B), and phialides (C). Images from control strains expressing cytoplasmic mCherry (EFS84) and eGFP (EFS80, EFS81, EFS82, and EFS83) and independent transformants expressing the PI[4]P biosensor either N-terminally fused mCherry (EFS66, EFS67, and EFS68) or C-terminally fused to eGFP (EFS65) have been included. Fluorescence signals have been pseudocoloured green or red and the DIC signal appears in grey scale. Conidia were obtained by scrubbing fungal colonies grown on PD agar for 7-9 days, plating onto 1.5% (w/v) water agar, and grown over night for 15-20 hours at 22°C. Plates were then left a further 3-4 nights for phialides to develop. Bars = 5 μm. Bar in (B) also applies to (A).

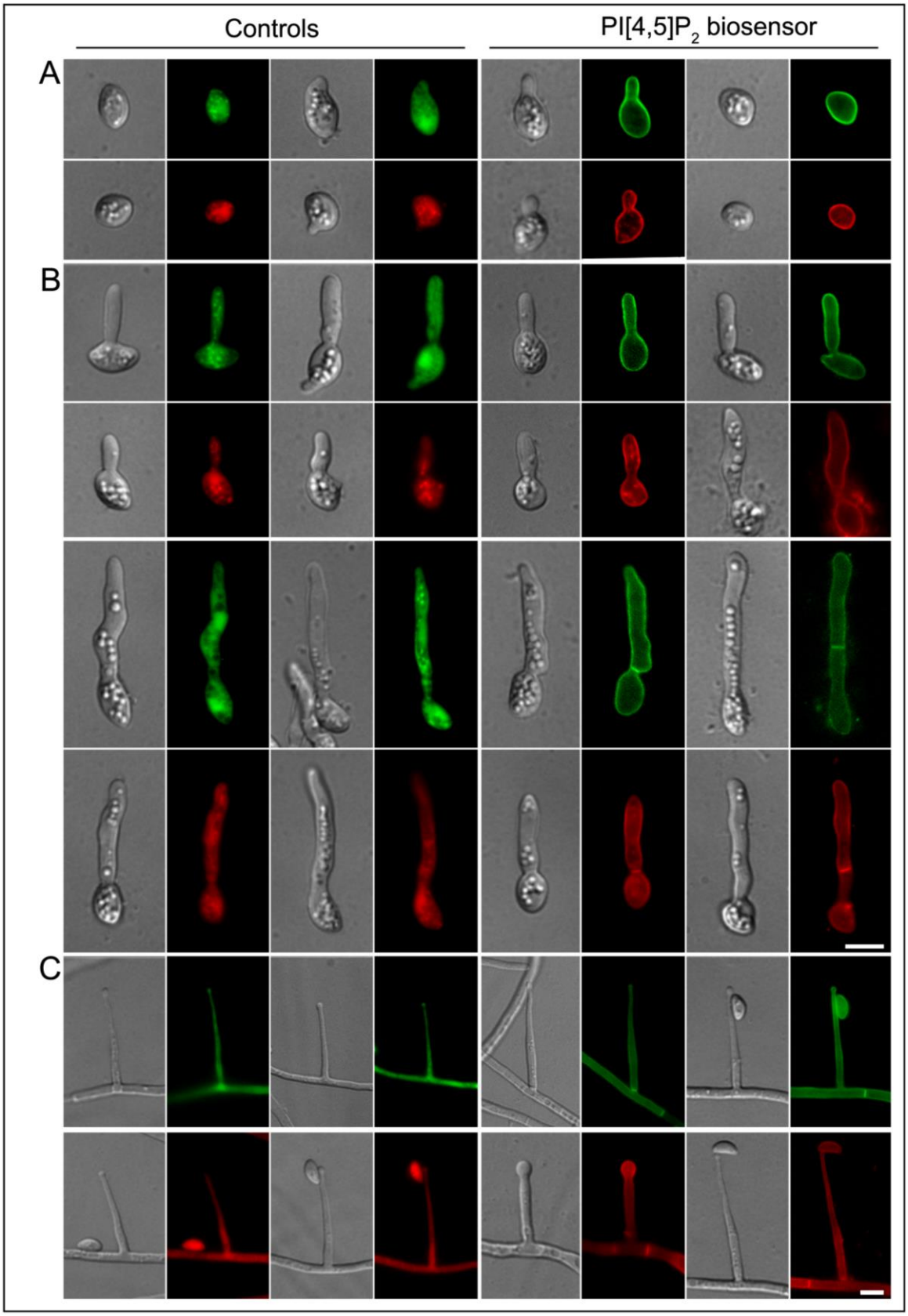

Figure 3.20. Localisation of PI[4,5]P_2 in *Epichloë festucae* asexual conidia and phialides. Differential interference contrast and fluorescent microscopy images of the PI[4,5]P_2 biosensor localisation in conidia (A), germinating conidia (B), and phialides (C). Images from control strains expressing cytoplasmic mCherry (EFS84) and eGFP (EFS80, EFS81, EFS82, and EFS83) and

independent transformants expressing the PI[4,5]P_2 biosensor either N-terminally fused mCherry (EFS77 and EFS78) or C-terminally fused to eGFP (EFS75 and EFS76) have been included. Fluorescence signals have been pseudocoloured green or red and the DIC signal appears in grey scale. Conidia were obtained by scrubbing fungal colonies grown on PD agar for 7-9 days, plating onto 1.5% (w / v) water agar, and grown over night for 15-20 hours at 22°C. Plates were then left a further 3-4 nights for phialides to develop. Bars = 5 μm. Bar in (B) also applies to (A).

3.2.4 Localisation *in planta*

Each biosensor strain was inoculated into 40 perennial ryegrass seedlings (Section 2.9.2), and the healthiest 20 seedlings were planted and grown under controlled environmental conditions for 6-9 weeks. Plants were immunoblotted (Section 2.9.3) between 10-15 weeks post inoculation to identify infected plants. inner sections of sheath tissue were harvested, mounted in deionised water, and then analysed on a scanning confocal microscope (Section 2.10.3). For each biosensor at least three independently infected plants were analysed to ensure observations made were robust.

3.2.4.1 PI[3]P biosensor

Localisation of the PI[3]P biosensor was only performed for the mCherry-LBD construct as all LBD-eGFP strains inoculated into plants failed to fluoresce. This was particularly unfortunate due to the differences in localisation seen between mCherry- and -eGFP biosensors in germinating conidiospores (Section 3.2.3.1). While the fluorescence observed from the mCherry-LBD biosensors was indistinguishable from that of the mCherry control *in planta* (Figure 3.21), without observations for the LBD-eGFP biosensors it is difficult to be certain about the presence or absence of this PPI in membranes of hyphae growing *in planta*.

3.2.4.2 PI[3,4]P_2 biosensor

As seen in culture, fluorescence of the PI[3,4]P_2 biosensors was indistinguishable from the control strains (Figure 3.22), suggesting this PPI was either absent or inaccessible in membranes of hyphae growing *in planta*.

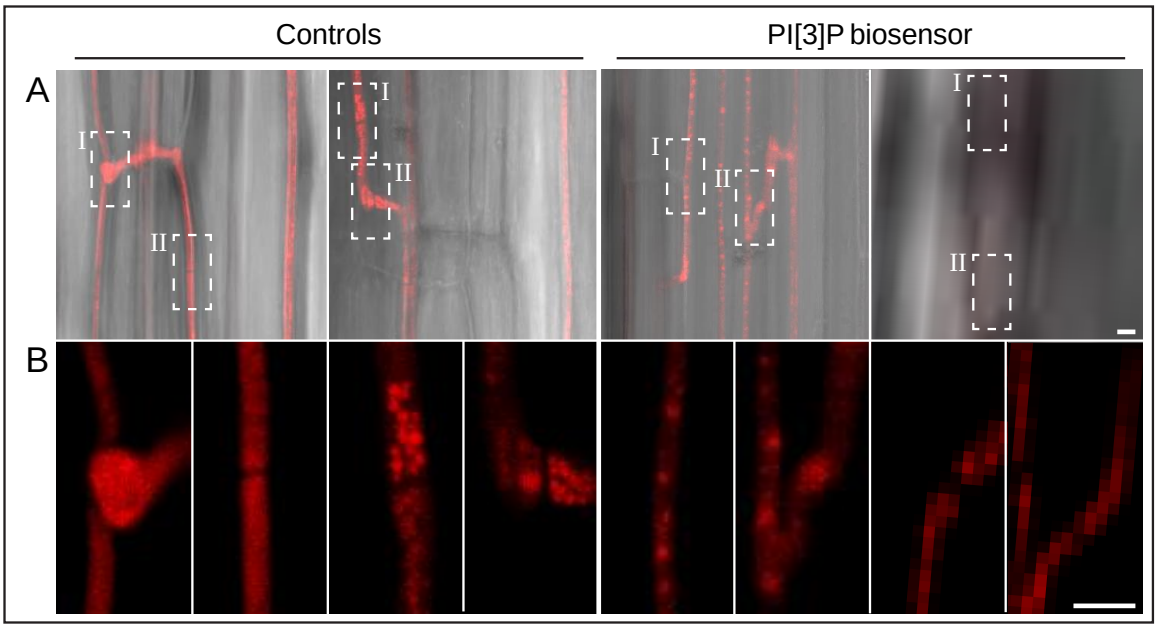

Figure 3.21. Localisation of the PI[3]P biosensor *in planta*. Confocal scanning laser microscopy images of the PI[3]P biosensor *in planta*. (A) Maximum intensity projections of 4-8 optical sections from control strain expressing cytoplasmic mCherry (EFS34) and an independent transformant expressing the PI[3]P biosensor N-terminally fused mCherry (EFS20). Fluorescence signals have been pseudocoloured green or red and the DIC signal appears in grey scale. (B) Selected and enlarged single optical planes from the boxed areas in (A). Samples were freshly harvested from the innermost layer of the pseudostem 9-14 weeks post inoculation and mounted in deionised water for analysis. Bars = 5 µm.

3.2.4.3 PI[3,4,5]P_3 biosensor

As for PI[3,4]P_2, fluorescence seen in the PI[3,4,5]P_3 biosensor strains *in planta* mirrored that of the control strains, indicating that this PPI was either not present or inaccessible to the biosensor in membranes of hyphae growing *in planta* (Figure 3.23).

3.2.4.4 PI[4]P biosensor

Both the mCherry-LBD and LBD-eGFP PI[4]P biosensors localised to vesicle-like structures of varying sizes, very similar to the localisation seen in the control strains (Figure 3.24). The localisation of the mCherry-LBD was indistinguishable from that of the control (Figure 3.24C and D). However, the vesicular localisation in the LBD-eGFP biosensor was clearer and more prevalent than in the eGFP control, which suggested the localisation may be due to the presence of PI[4]P

(Figure 3.24A and B). While the LBD biosensor localisation was very similar to that of the controls, PI[4]P may be present *in planta* in vesicle-like structures as previously seen in culture, conidiospores, and phialides (Sections 3.2.2.4 and 3.2.3.4). Further analysis will be required to confirm vesicular localisation.

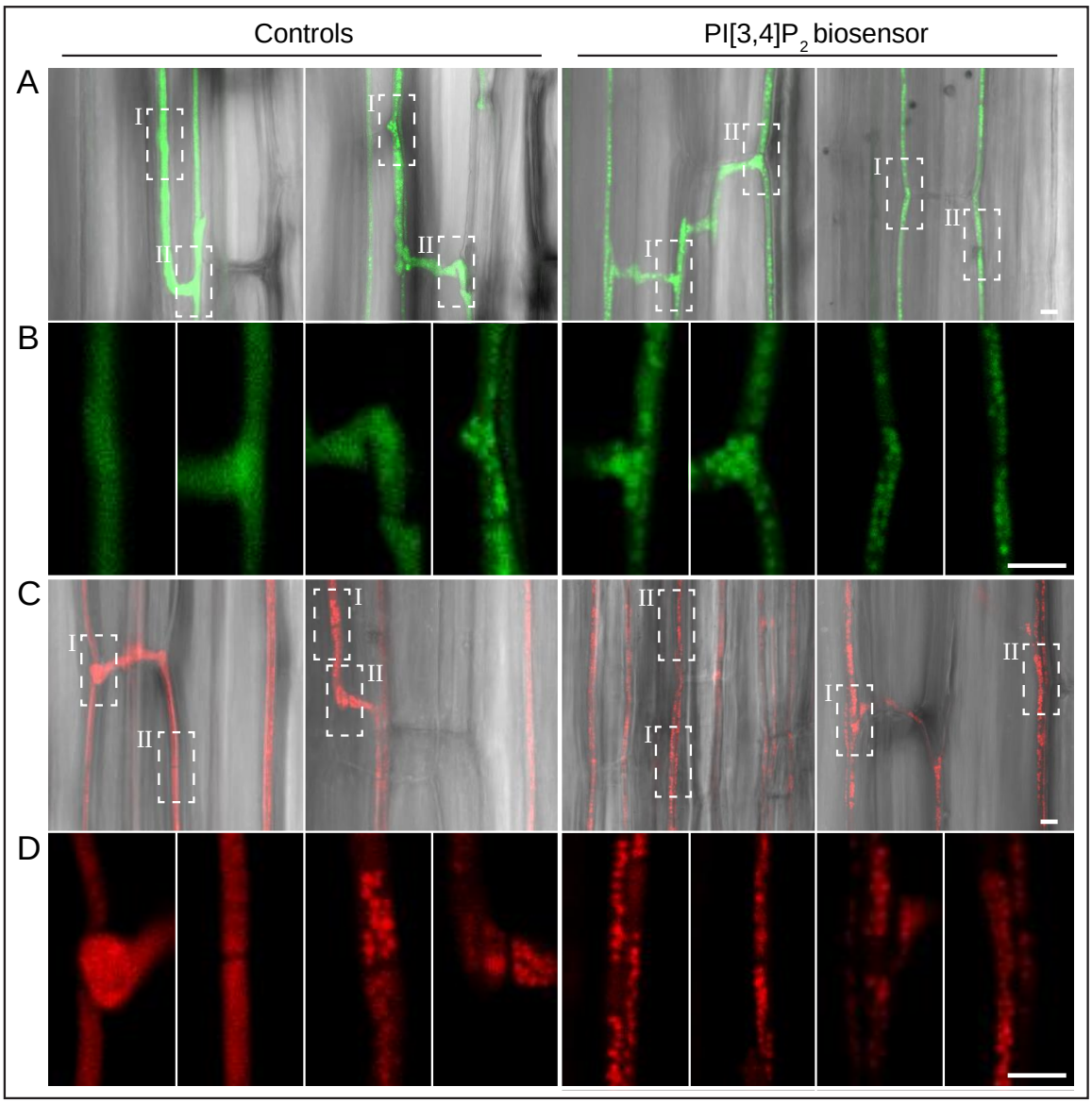

Figure 3.22. Localisation of the PI[3,4]P$_2$ biosensor *in planta*. Confocal scanning laser microscopy images of the PI[3,4]P$_2$ biosensor *in planta*. (A) and (C) Maximum intensity projections of 4-8 optical sections from control strains expressing cytoplasmic eGFP (EFS33)or mCherry (EFS34) and independent transformants expressing the PI[3,4]P$_2$ biosensor either C-terminally fused to eGFP (EFS10) or N-terminally fused to mCherry (EFS27). Fluorescence signals have been pseudocoloured green or red and the DIC signal appears in grey scale. (B) and (D) Selected and enlarged single optical planes from the boxed areas in (A) and (C). Samples were freshly harvested from the innermost layer of the pseudostem 9-14 weeks post inoculation and mounted in deionised water for analysis. Bars = 5 µm.

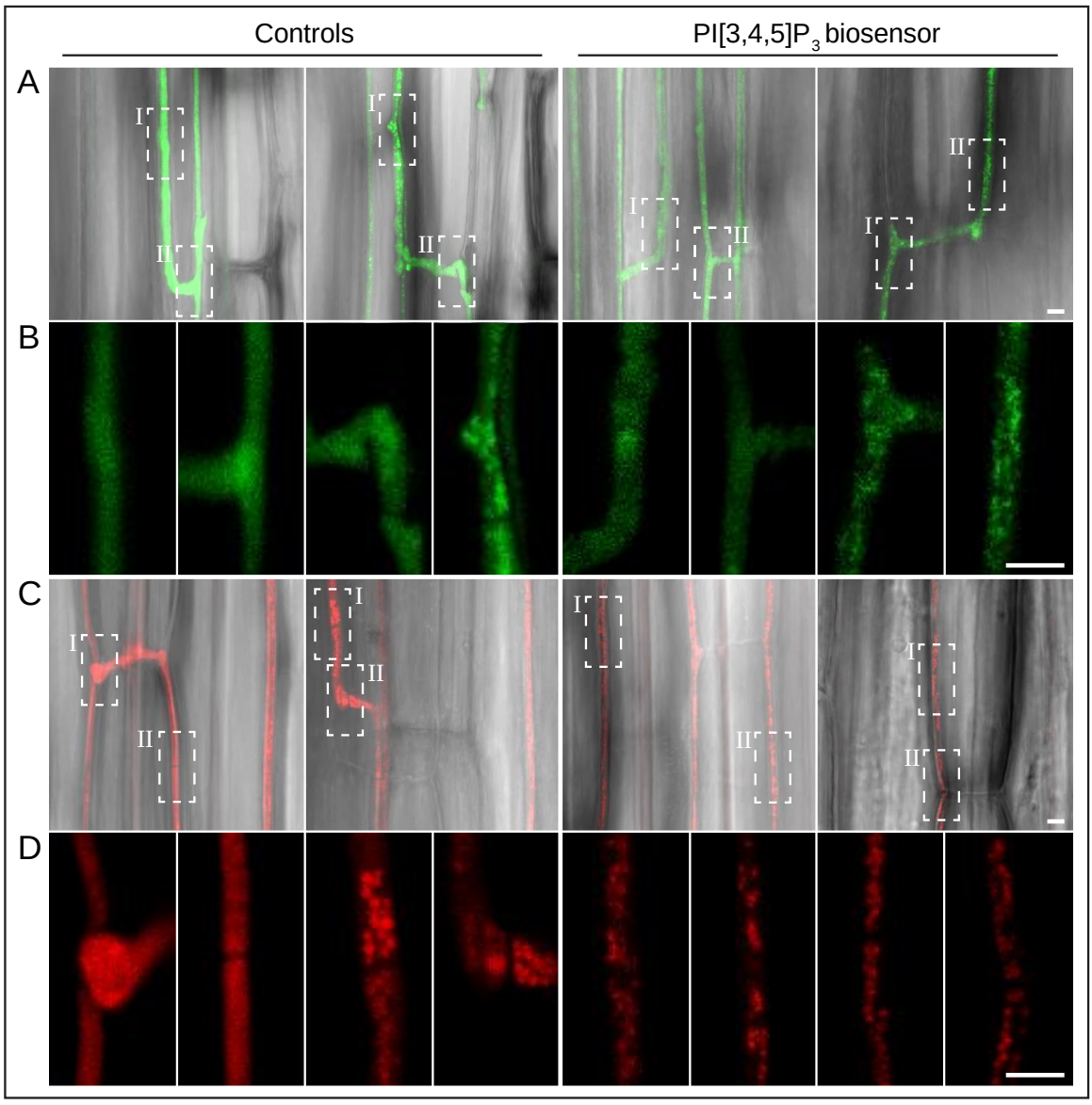

Figure 3.23. Localisation of the PI[3,4,5]P_3 biosensor *in planta*. Confocal scanning laser microscopy images of the PI[3,4,5]P_3 biosensor *in planta*. (A) and (C) maximum intensity projections of 4-8 optical sections from control strains expressing cytoplasmic eGFP (EFS33)or mCherry (EFS34) and independent transformants expressing the PI[3,4,5]P_3 biosensor either C-terminally fused to eGFP (EFS7 and EFS8) or N-terminally fused to mCherry (EFS22 and EFS24). Fluorescence signals have been pseudocoloured green or red and the DIC signal appears in grey scale. (B) and (D) Selected and enlarged single optical planes from the boxed areas in (A) and (C). Samples were freshly harvested from the innermost layer of the pseudostem 9-14 weeks post inoculation and mounted in deionised water for analysis. Bars = 5 µm.

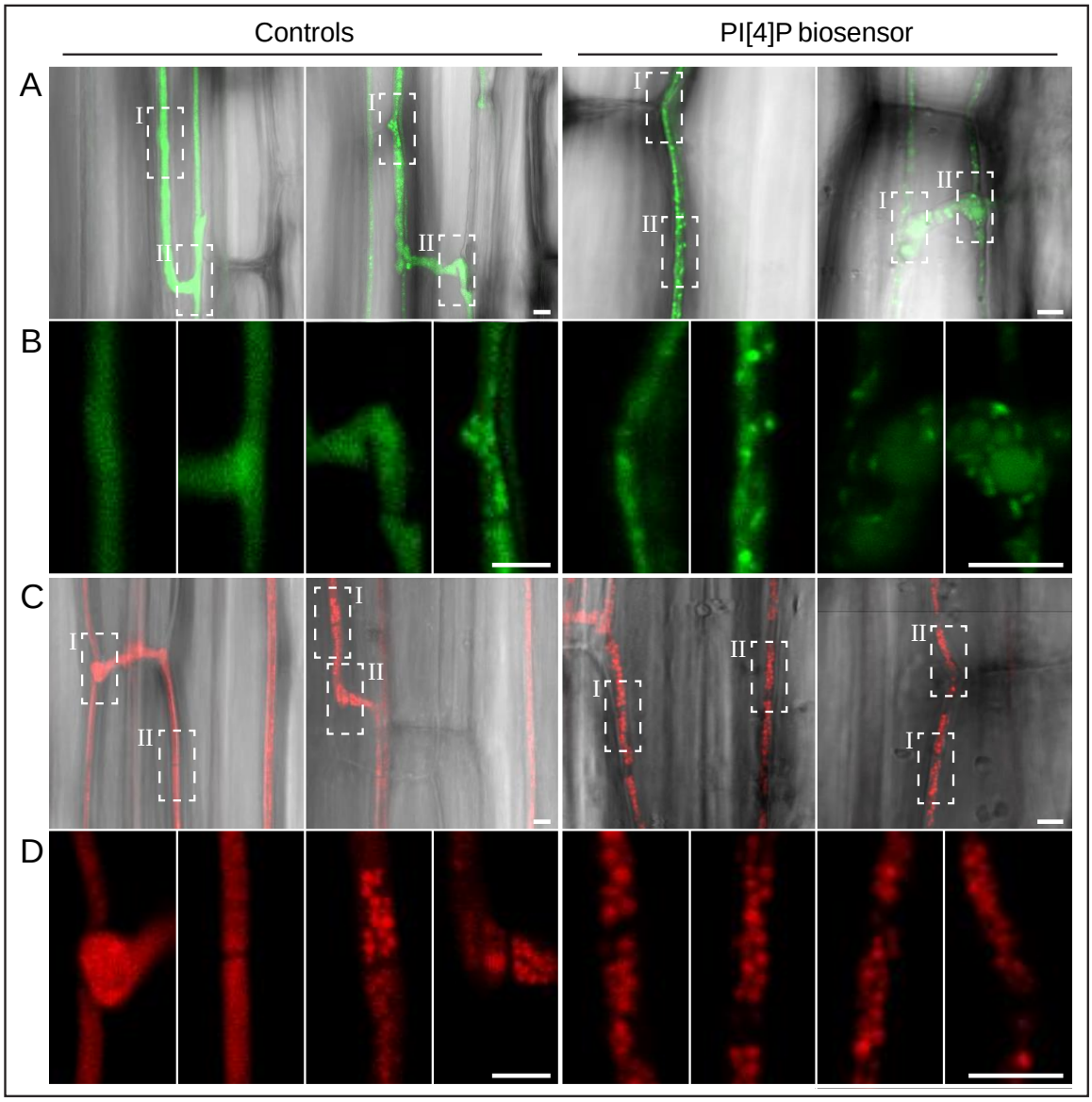

Figure 3.24. Localisation of the PI[4]P biosensor *in planta.* Confocal scanning laser microscopy images of the PI[4]P biosensor *in planta*. (A) and (C) maximum intensity projections of 4-8 optical sections from control strains expressing cytoplasmic eGFP (EFS33)or mCherry (EFS34) and independent transformants expressing the PI[4]P biosensor either C-terminally fused eGFP (EFS13) or N-terminally to fused mCherry (EFS30). Fluorescence signals have been pseudocoloured green or red and the DIC signal appears in grey scale. (B) and (D) Selected and enlarged single optical planes from the boxed areas in (A) and (C). Samples were freshly harvested from the innermost layer of the pseudostem 9-14 weeks post inoculation and mounted in deionised water for analysis. Bars = 5 µm.

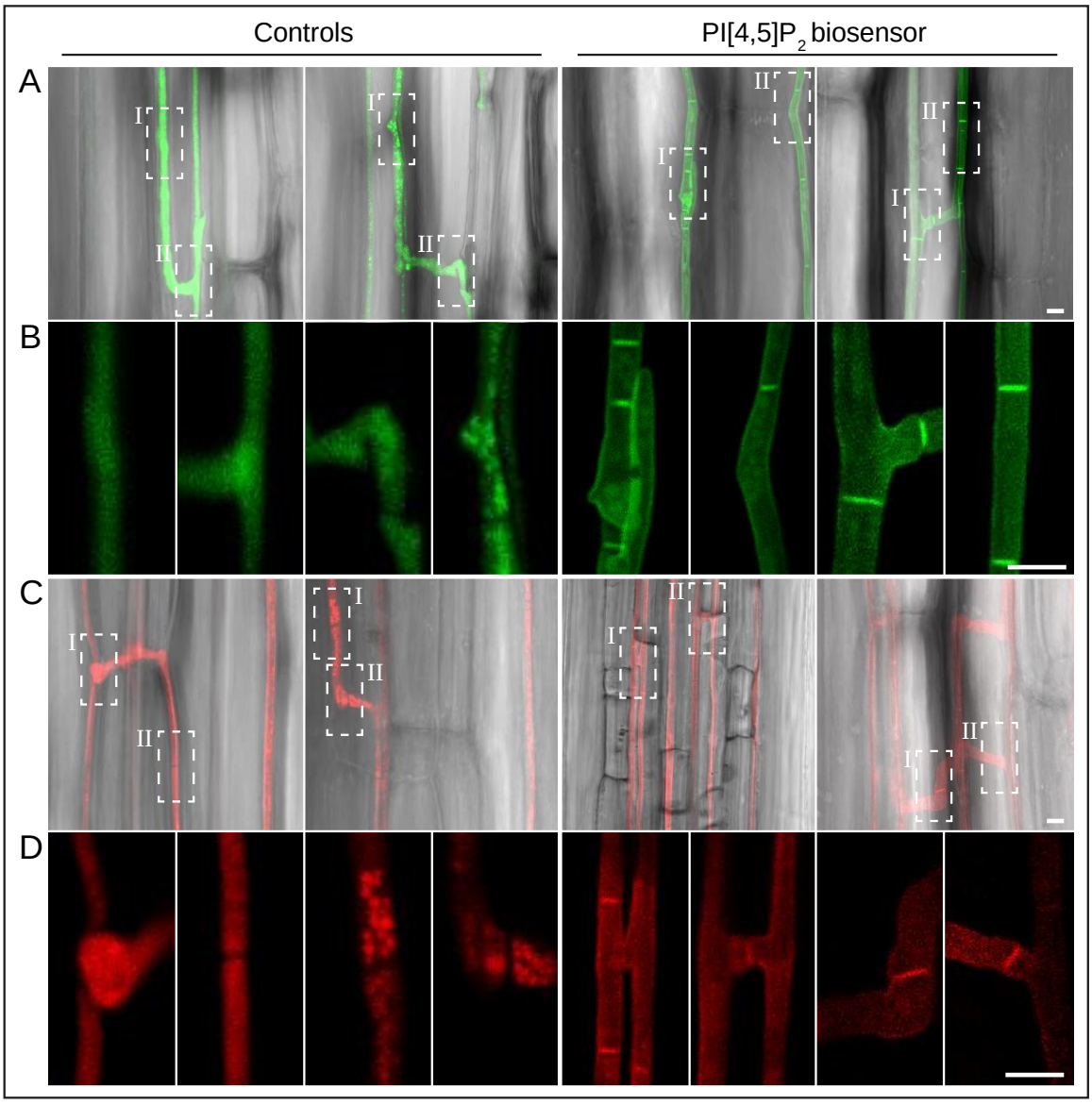

Figure 3.25. Localisation of the PI[4,5]P$_2$ biosensor *in planta.* Confocal scanning laser microscopy images of the PI[4,5]P$_2$ biosensor *in planta*. (A) and (C) maximum intensity projections of 4-8 optical sections from control strains expressing cytoplasmic eGFP (EFS33)or mCherry (EFS34) and independent transformants expressing the PI[4,5]P$_2$ biosensor either C-terminally fused to eGFP (EFS1) or N-terminally fused to mCherry (EFS16). Fluorescence signals have been pseudocoloured green or red and the DIC signal appears in grey scale. (B) and (D) Selected and enlarged single optical planes from the boxed areas in (A) and (C). Samples were freshly harvested from the innermost layer of the pseudostem 9-14 weeks post inoculation and mounted in deionised water for analysis. Bars = 5 µm.

3.2.4.5 PI[4,5]P_2 biosensor

The PI[4,5]P_2 biosensor clearly localised to the plasma membrane and septa of hyphae *in planta* (Figure 3.25). Again, the biosensor was more enriched at septa, which resulted in a stronger fluorescent signal (Sections 3.2.2.5 and 3.2.3.5). This provided strong evidence for the presence of PI[4,5]P_2 at the cell membrane and septa of *E. festucae in planta*.

3.3 Identification and characterisation of MssD in *E. festucae*

In fungi, several cytosolic proteins of the Nox complex localise to the tip of the hyphae (48). Additionally, production of ROS occurs primarily at the apical and sub-apical regions of the hyphal tip (46). These observations provide strong evidence that the tip region of hyphae is a site for assembly and activation of the Nox complex. The presence of PI[4,5]P_2 in a sub-apical gradient along the cell membrane suggests it may be involved in Nox complex assembly and activation. In *S. cerevisiae, mss4* encodes a phosphatidylinositol-4-phosphate 5-kinase enzyme which converts PI[4]P to PI[4,5]P_2. It is hypothesised that increasing the expression of this gene and consequently the amount of PI[4,5]P_2 will change the distribution of the PPI at the hyphal tip, affecting the assembly of the Nox complex, resulting in a break down in the mutualistic symbiosis between *E. festucae* and perennial ryegrass.

3.3.1 Identification of *mssD* gene

To identify the gene encoding the homologue of the *mss4* phosphatidylinositol-4-phosphate 5-kinase in *E. festucae* an initial tBLASTn analysis of the *E. festucae* Fl1 genome was performed using the protein sequence of *S. cerevisiae* Mss4 (YDR208W) as the query. This search identified a candidate *E. festucae* homologue (EfM3.031950, *E*-value 0). A reciprocal BLASTp analysis in Fungal DB with the predicted protein sequence confirmed that it was the correct homologue. In accordance with *E. festucae* nomenclature (162) the gene was designated *mssD* (EfM3.031950). *E. festucae mssD* was found to contain two introns, and encodes a predicted polypeptide of 963 amino acids, which is 183 amino acids (aa) longer than *S. cerevisiae* Mss4 (Figure 26A). InterProScan predicts *E. festucae* MssD has a

highly conserved phosphatidylinositol-4-phosphate 5-kinase domain (IPR023610). Additionally, the whole protein shares 71.8%, 51.0%, 54.6%, and 36.2% amino acid sequence identity with homologues from *Neurospora crassa* (NCU02295), *Magnaporthe oryzae* (MGG_06572), *Fusarium graminearum* (FGSG_10792), and more distantly related *S. cerevisiae* (YDR208W), respectively (Section 2.11; Figure 3.26B and C; Appendix 6.7).

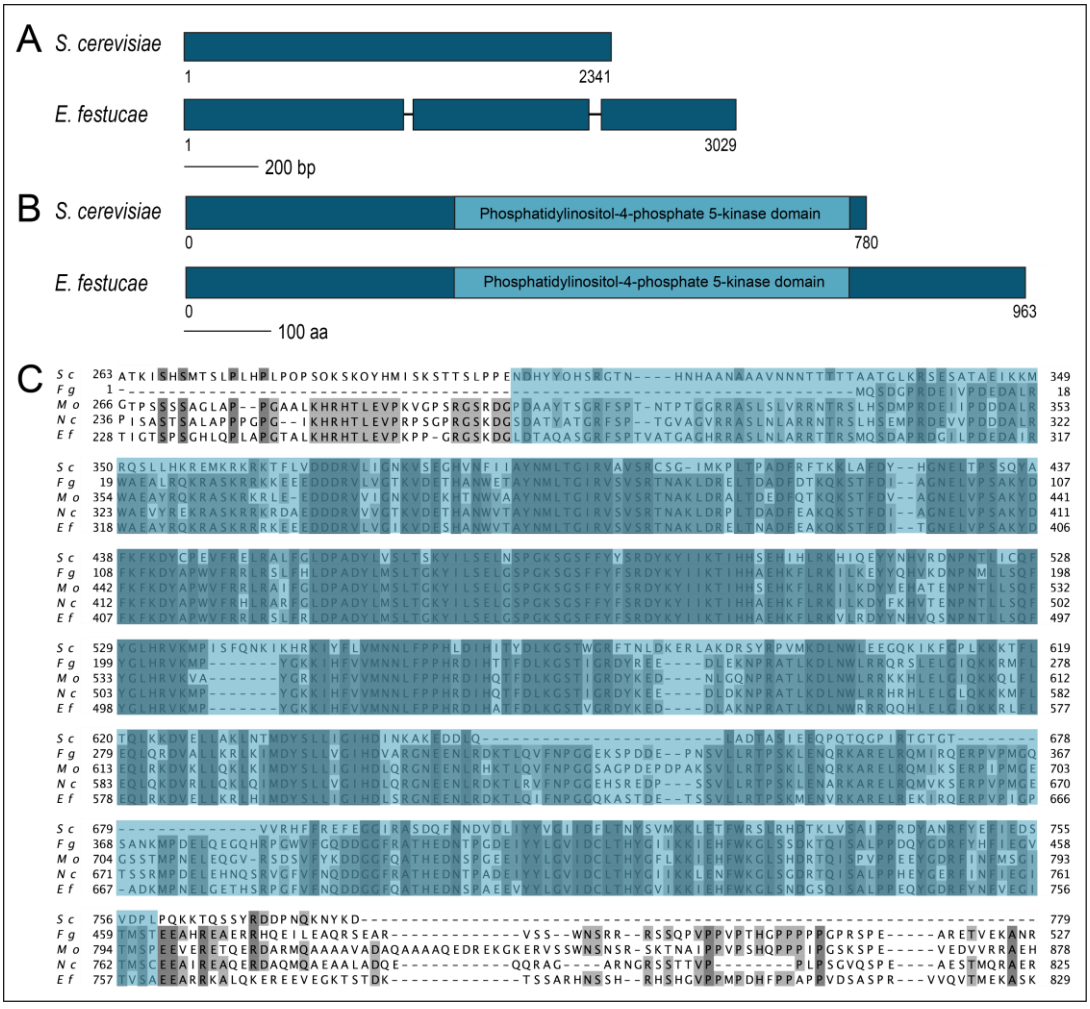

Figure 3.26. *mssD* gene structure, predicted protein structure, and multiple sequence alignment. (A) *Saccharomyces cerevisiae MSS4* and *Epichloë festucae mssD* gene structures. *mssD* is 3029 bp in length and contains 3 exons separated by 2 introns of 71 bp and 70 bp. (B) *S. cerevisiae* Mss4p and predicted *E. festucae* MssD polypeptides. The phosphatidylinositol-4-phosphate 5-kinase domain (IPR023610), as predicted by InterProScan, is 780 amino acids (aa) long in *S. cerevisiae* and 963 aa in *E. festucae*. (C) Multiple sequence alignment of MssD homologues from *E. festucae* (Ef; EfM3.031950), *Neurospora crassa* (Nc; NCU02295), *Magnaporthe oryzae* (Mo; MGG_06572), *Fusarium graminearum* (Fg; FGSG_10792), and *S. cerevisiae* (Sc; YDR208W). The degree of grey shading is indicative of the amino acid percentage identity. Blue shading indicates the position of the *E. festucae* kinase domain.

3.3.2 Generation of *mssD* over expression strains

To investigate whether an increase in P[4,5]P_2 impacts the development of *E. festucae* in culture or the interaction with its host *L. perenne* an overexpression (OE) construct for *mssD*, pCE101, was generated by Dr Carla Eaton (Appendices 6.2.3 and 6.3.3.1). This plasmid was introduced into protoplasts of *E. festucae* strain Fl1 by co-transforming with pSF16.17 (Section 2.7, Appendix 6.3.4.1). Geneticin resistant transformants were picked and nuclear purified by three rounds of sub-culturing. Crude genomic DNA was extracted from these strains (Section 2.3.2) and used as template in a PCR reaction to screen for transformants with the plasmid. Three primer pairs spanning the 5', middle, and 3' areas of the construct were used to confirm whether the OE construct had successfully integrated into the genome (Section 2.6.1; Figure 3.27). Transformants found to contain bands corresponding to the predicted sizes for each of these reactions, indicating a complete copy of the *mssD* OE construct, were selected for further analysis.

3.3.3 Expression levels of OE mutants

To confirm if *mssD* was overexpressed in these strains RT-qPCR analysis (Sections 2.6.2 and 2.6.3) was carried out using total RNA extracted from mycelia of these transformants (Section 2.5.1). Increased expression of *mssD* was observed for four transformants (#17, 20, 32, and 53) and three of these (#17, 53, and 20), representing high, medium, and low levels of OE, were selected for further analysis (Figure 3.28; Appendix 6.8).

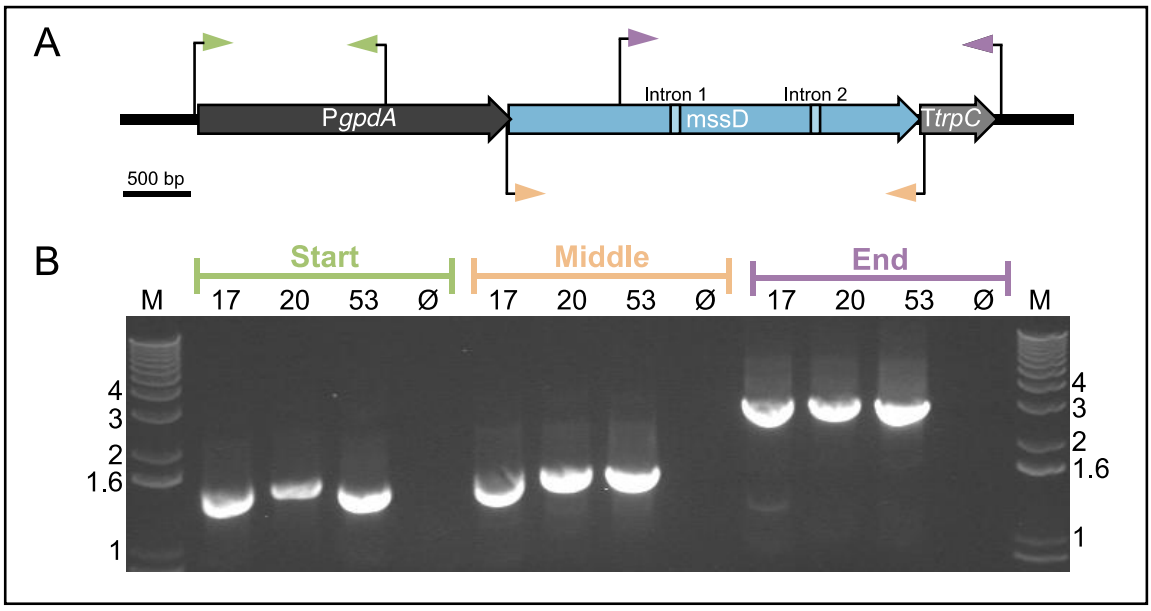

Figure 3.27. PCR screen of *mssD* overexpression transformants. (A) Strategy for screening the *mssD* OE construct, pCE101, using three primer pairs covering the start (pRS426-Pgpd-F/Pgpd-R, 1412 bp; green arrows), middle (mss5/mss6, 1474 bp; orange arrows), and end (mss7/pRS426-TtrpC, 2819 bp; purple arrows) of the construct. (B) Gel electrophoresis of PCR screen with primers pairs amplifying the start, middle, and end of the mCherry construct. Ø = negative control. M = 1kb plus ladder. Approximate fragment sizes are given in kilobases.

3.3.4 Culture phenotype

To investigate the effect of overexpressing of *mssD*, the OE strains were analysed in culture for any changes in cell morphology or PI[4,5]P_2 localisation, and *in planta*, to determine the impact on fungal-plant symbiosis.

3.3.4.1 Hyphal morphology analysis

The OE strains and WT were sub-cultured onto 1.5% (w/v) water agar slide plates, grown for 6-9 days, stained with Calcofluor white, and analysed on the fluorescent microscope (Section 2.10.1). Both the culture growth and cellular morphology of the hyphal tip, branch points, fusion sites, and coils were indistinguishable from WT (Figure 3.29). This suggests that OE of *mssD* has no impact on mycelial growth under the conditions examined.

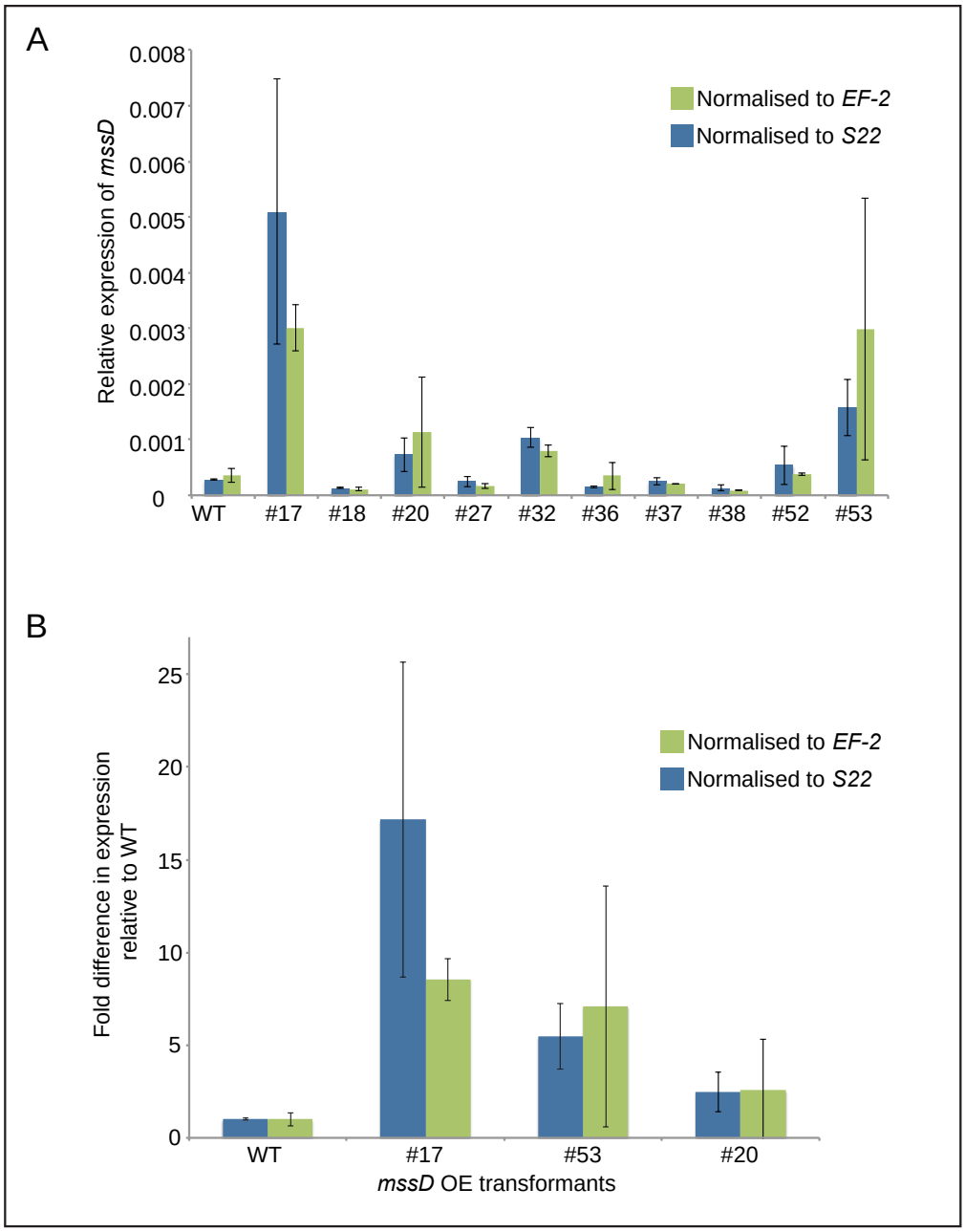

Figure 3.28. Expression of *mssD* transcript in WT and *mssD* overexpression strains. Mycelia were grown in 2.4% (w/v) potato dextrose media for 3 days at 22°C and total RNA extracted from mycelia was used to synthesise cDNA and used for qRT-PCR analysis. (A) Relative expression levels of *mssD* in WT and *mssD* OE transformants. Values were quantified by the $2^{(\Delta Cp)}$ method normalised to the expression levels of two reference genes, 40S ribosomal protein 22 (*S22*) and elongation factor 2 (*EF-2*) relative to *mssD* expression. Data are representative of two technical replicates from a single biological sample. Y-axis represents the expression of *mssD* relative to *S22* and *EF-2*. (B) Fold difference in expression of *mssD* relative to WT in strains selected to represent high (#17, EFS85), medium (#53, EFS87), and low (#20, EFS86) levels of overexpression. Error bars represent the S.D. from two technical replicates.

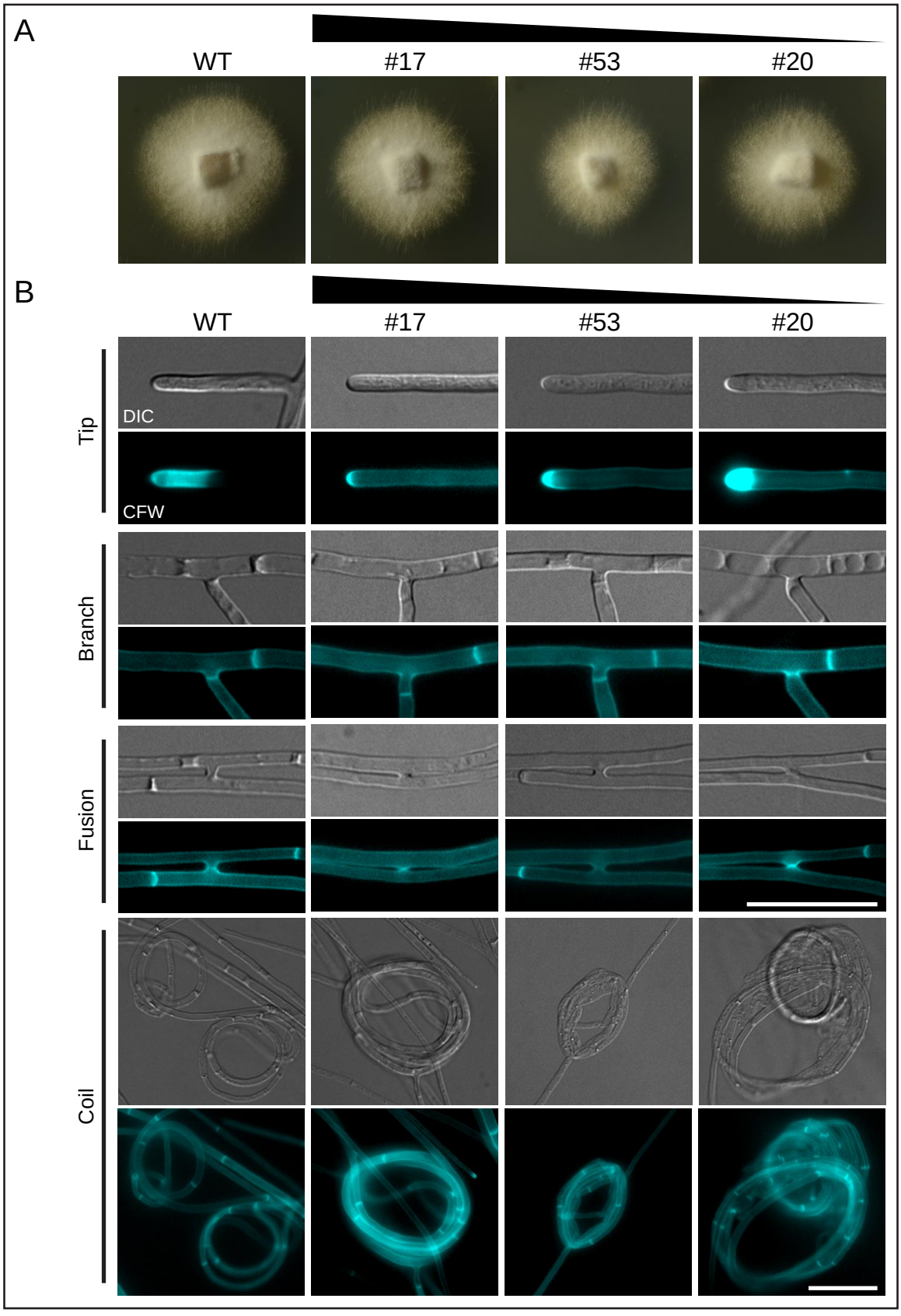

Figure 3.29. Culture phenotype of *mssD* overexpression strains. (A) Culture phenotype of *Epichloë festucae* WT and three independent *mssD* OE strains grown on PD agar for 9 days. Strains #17, #53, and #20 represent high, medium, and low, levels of overexpression, respectively. (B)

Inverted fluorescence and differential interference contrast (DIC) microscopy images of hyphal morphology of *E. festucae* WT and *mssD* OE strains grown on 1.5% (w/v) water agar for 7 days. Width of arrows represents the level of overexpression. Cultures were stained with Calcofluor white (CFW) as indicated. Bars = 20μm

3.3.4.2 Localisation of the PI[4,5]P_2 biosensor in *mssD* OE strain

Protoplasts obtained (Section 2.7.1) from strain #17, which had the greatest increase in *mssD* expression, were co-transformed with pSF15.15 (Hygromycin resistance; Appendix 6.3.4.2) and either the eGFP PI[4,5]P_2 biosensor construct or free eGFP construct. Hygromycin resistant transformants were picked then nuclear purified with one round of sub-culturing and screened for fluorescence, initially on the darkreader blue light transilluminator then on the fluorescent microscope. One transformant for both eGFP and the biosensor were found to fluoresce. Each strain was sub-cultured onto 1.5% (w/v) water agar slide plates, grown for 6-9 days, and analysed on the fluorescent microscope (Section 2.10.1). The localisation of both the control and LBD constructs were the same as WT with comparable patterns of expression in all cell structures, including the hyphal tip, fusion sites, branch points, and mature hyphae (Figure 3.30A). Similarly, the gradient of the LBD biosensor seen in the sub-apical region of the hyphal tip (Figure 3.30B) was identical between the WT and *mssD* OE strain, suggesting that OE of *mssD* had no effect on localisation of PI[4,5]P_2.

3.3.5 Plant phenotype

To investigate whether the OE of *mssD* affected the fungal-plant symbiosis, perennial ryegrass plants were infected with WT and *mssD* OE #17, #20, and #53 strains (Section 2.9.2). Plants were immunoblotted (Section 2.9.3) at 13 weeks post-inoculation to identify infected plants. Unfortunately, whole-plant phenotype analyses 14 weeks post inoculation yielded conflicting results (Figure 3.31A; Appendix 6.9). Plants infected with the highest overexpressing strain, *mssD* OE #17, 18 fold, had significantly less tillers than WT infected plants (p-value = 0.046), however, plants infected with medium (*mssD* OE #53, 8 fold) and low (*mssD* OE #20, 3 fold) OE strains, had significantly more tillers (p-values = 0.0037, 0.029, respectively) (Figure 3.31C). Analysis of the tiller lengths showed that tillers grew

significantly longer in plants infected with *mssD* OE #17 compared to WT infected plants (*p*-value = 0.00023), whereas, the tiller length of plants infected *mssD* OE #53 and #20 were not significantly different from that of WT infected plants (Figure 3.31B). This experiment needs to be repeated in the future to confirm results.

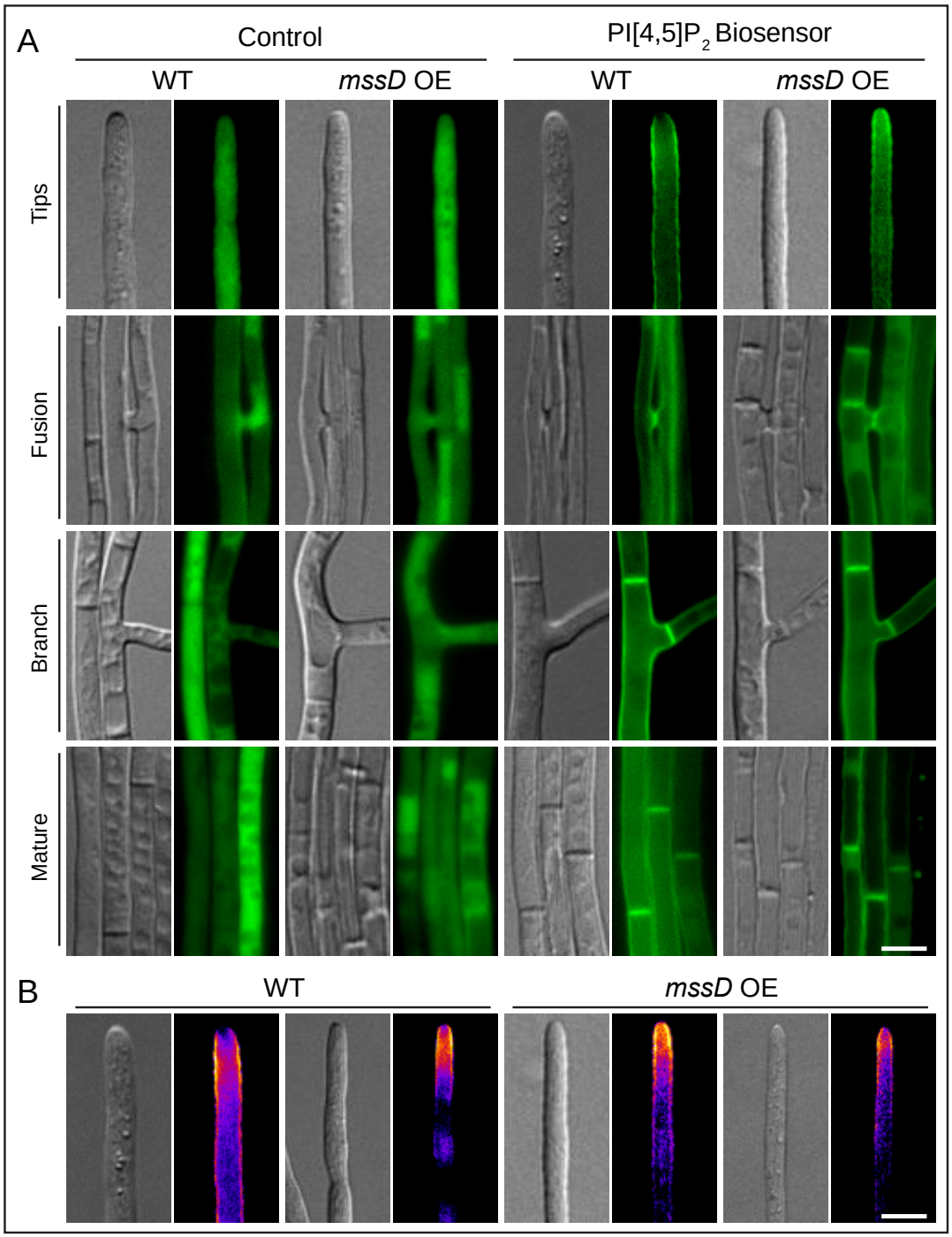

Figure 3.30. Localisation of PI[4,5]P$_2$ in *mssD* overexpression strain. Differential interference contrast and fluorescent microscopy images of WT and *mssD* OE strain #17 (EFS85) expressing cytoplasmic eGFP (EFS33 and EFS95; controls) and the PI[4,5]P$_2$ eGFP biosensor (EFS3 and EFS96).

Fluorescence signals have been pseudocoloured green and the DIC signal appears in grey scale. (B) Representative images of the asymmetric localisation of the PI[4,5]P_2 biosensor at hyphal tips in WT and *mssD* OE strains, pseudocoloured to indicate the saturation of each pixel from 0 to 255 (fully saturated). Cultures were grown on 1.5% (w/v) water agar for 6-9 days. Bars = 5 µm.

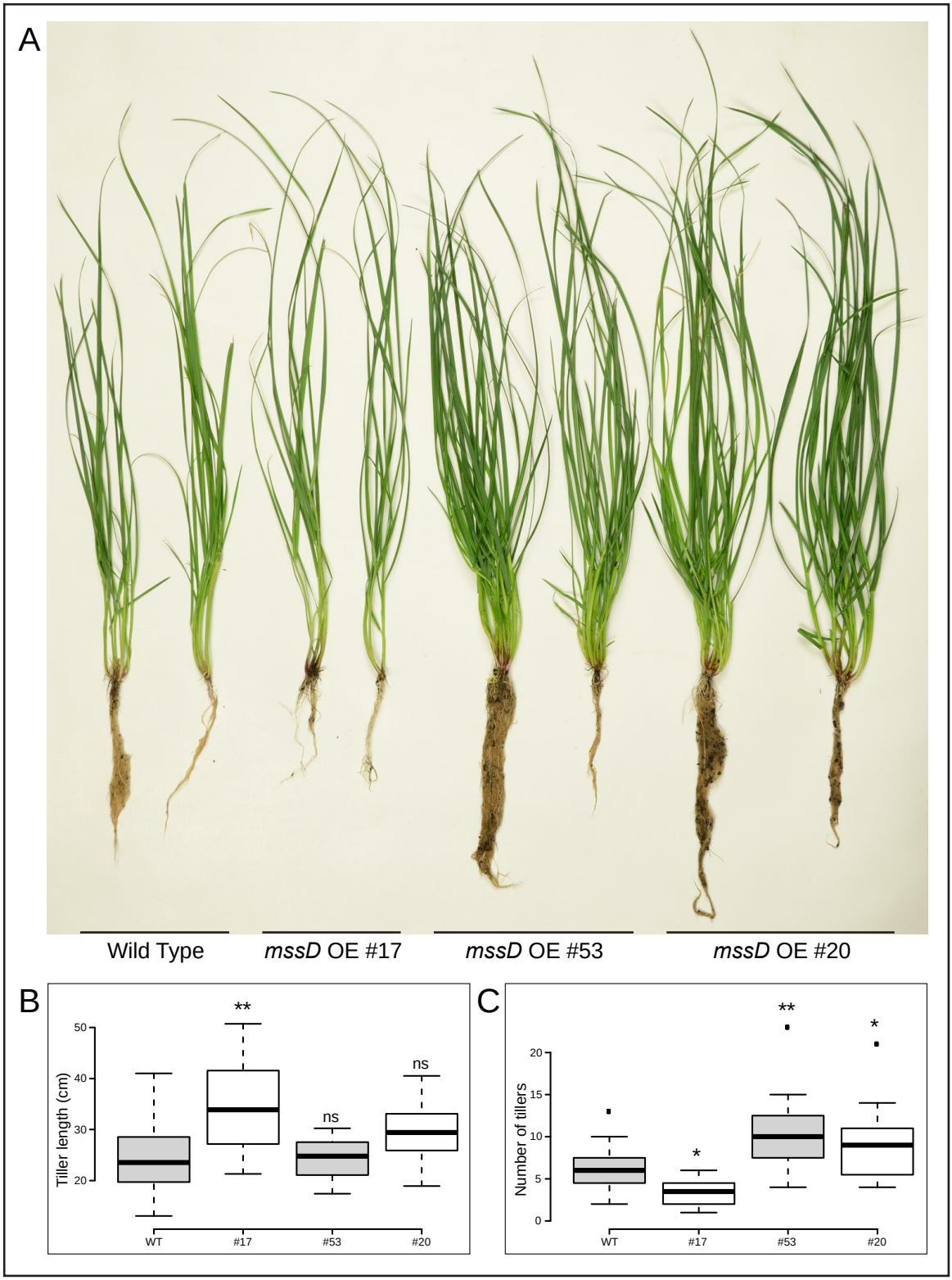

Figure 3.31. Phenotype of perennial ryegrass plants infected with WT and *mssD* overexpression strains. (A) Plants were infected with the indicated endophyte strains and the

photograph taken at 15 weeks post-inoculation. (B and C) Box plots showing the range of (B) tiller lengths and (C) tiller number. Statistical significance in comparison to the WT strain was determined using a Tukey Test where *p*-value < 0.05 is significant (* = 0.05-0.01, ** = 0.01-0.0001, ns = non-significant).

3.4 Deletion of the *E. festucae mssD* gene

To further examine the function of MssD in *E. festucae*, attempts were made to create a gene replacement mutant for *mssD* using the split marker method. This method is reported to yield around 33-74% targeted gene deletions in *E. festucae*, compared to around only 25% for standard homologous recombination (163). Transformants were previously generated by Dr Carla Eaton by co-transforming WT *E. festucae* protoplasts with two overlapping fragments amplified from the *mssD* replacement cassette, pCE98 (Appendices 6.2.4 and 6.3.3.2). This construct was designed to replace the *mssD* gene with an *hph* (hygromycin B phosphotransferase) cassette, which confers hygromycin resistance (Figure 3.32A). Putative Δ*mssD* mutants were selected for on PD plates containing hygromycin (Section 2.2.2.3). Out of the resulting transformants, 34 strains with reduced radial growth were selected for further analysis. Crude gDNA was extracted for PCR screening (Section 2.3.2) using primer pair mss12/mss13, which yields a 3376 bp fragment in WT, 1487 bp fragment in *mssD* mutants, and both fragments in ectopic transformants (Figure 3.32A). Most strains contained both bands, indicating ectopic integration of the construct. Transformant #22 initially failed to amplify either fragment, but when analysed again was shown to possess both bands. Transformant #29 had only a WT band present suggesting it did not contain the plasmid and was presumably sensitive to hygromycin, explaining why it grew so poorly on media containing hygromycin (Figure 3.32B). The failure to obtain a Δ*mssD* strain, even using a split marker approach, suggests this gene is likely essential in *E. festucae* as it is in yeast (84). However, additional transformants would need to be generated and screened to confirm this.

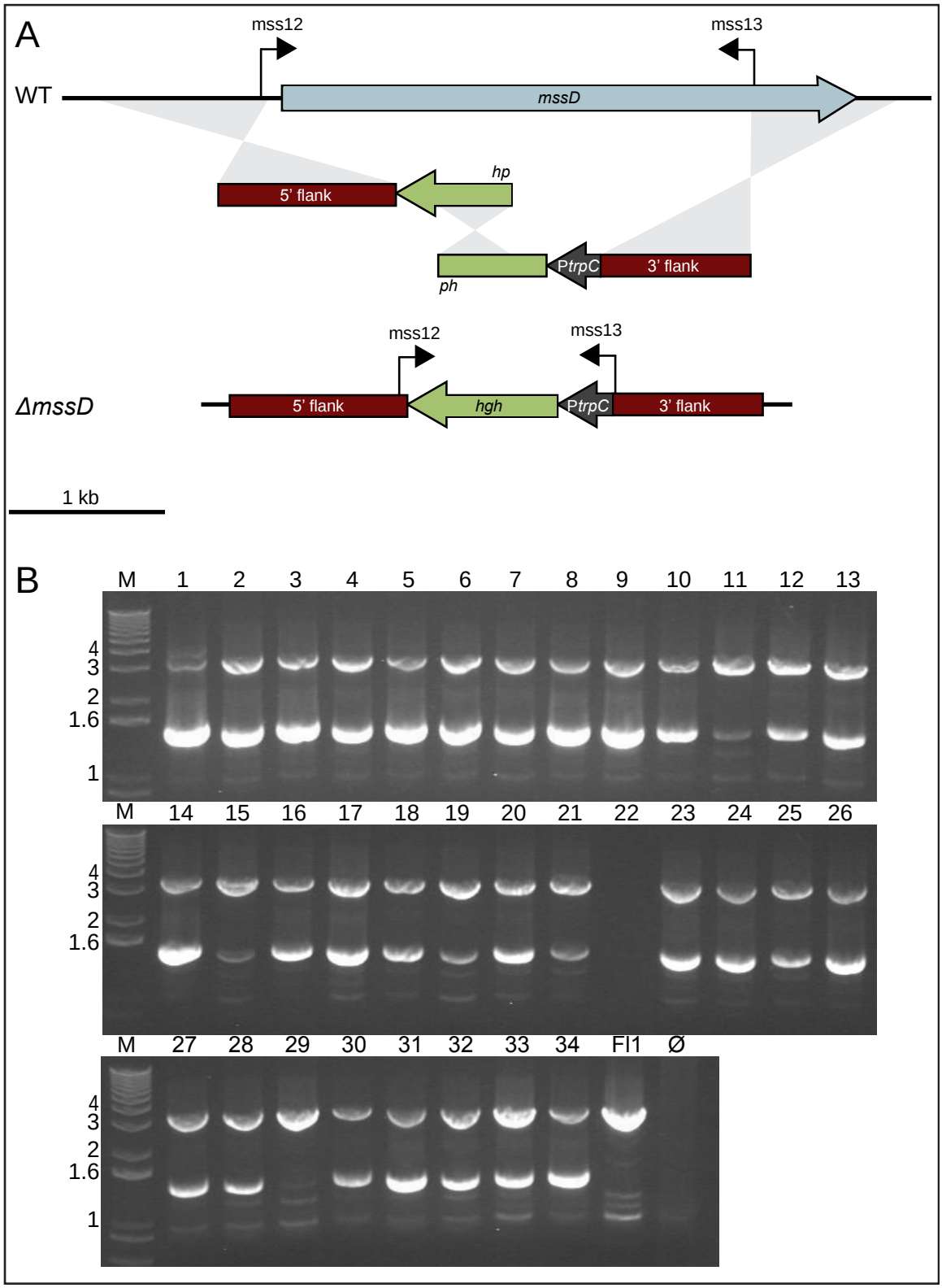

Figure 3.32. PCR screen of putative Δ*mssD* mutants. (A) Map of the *mssD* replacement strategy using two fragments amplified from the KO cassette, pCE98. Arrows indicate the location of the primer pair used to PCR screen for mutants. (B) Gel electrophoresis of PCR screen of 34 Δ*mssD* transformants using the primer pair mss12/mss13, which generates a 3376 bp fragment in WT, 1487 bp in Δ*mssD*, and both fragments in ectopic mutants. Ø = negative control. M = 1kb plus ladder. Approximate fragment sizes are given in kilobases.

4. Discussion

In *E. festucae* production of ROS by the Nox complex plays an essential role in regulating growth and development both in culture and *in planta*. However, little is known about how production of ROS by this complex is controlled. In mammals and plants, lipid signalling plays a key role in regulating complex assembly and activation, through the recruitment of its cytosolic proteins (53). Homology between the mammalian, plant, and fungal Nox complexes provides strong evidence that a similar regulatory mechanism is conserved in fungi. To examine the role lipid signalling plays in the *E. festucae* Nox complex, the ability of Cdc24, a cytosolic Nox protein, to be recruited through LBDs was confirmed and membrane lipid composition was analysed to identify potential PPI targets.

The first step towards understanding the regulation of the fungal Nox complex was to determine whether the cytosolic Nox complex proteins could be recruited to localised regions of certain modified PPIs. In the mammalian Nox2 complex, three cytosolic proteins, p67^{phox}, p47^{phox}, and p40^{phox}, play an essential role in complex assembly through protein-protein and protein-lipid interactions (53). An unknown stimulus results in phosphorylation of the proteins exposing their PX LBDs, allowing them to translocate to the plasma membrane (PM) (164). *E. festucae* does not have any direct homologues for p47^{phox} and p40^{phox}. Instead, yeast polarity establishment homologues Cdc24 and BemA were found to physically interact with p67^{phox} homologue, NoxR (48). BemA was originally proposed to be the functional homologue of p47^{phox} and p40^{phox}. It contains the protein and lipid interaction domains found in the mammalian counterparts, necessary for binding other cytosolic proteins and transporting them to the PM (48, 165). However, *bemA* mutants do not have the same phenotype as *noxA* mutants in *A. nidulans* or *E. festucae* and the PX domain is unnecessary for localisation in *N. crassa*, suggesting BemA is dispensable for Nox function (48, 71, 166). In *E. festucae*, Cdc24 contains a putative lipid-binding PH (Pleckstrin Homology) domain as well as a protein binding PB1 (Phox and Bem1) domain making it a possible functional homolog of p47^{phox}, and p40^{phox}. PH domains exhibit a range of specificity and affinity to different PPIs, making the target of the Cdc24 PH domain hard to predict (154). Whilst the PPI target(s) is unclear, this domain is necessary for correct cellular localisation in *S. cerevisiae* (72). To determine whether the PH domain of Cdc24 is

similarly responsible for localisation in *E. festucae*, two constructs were designed to visualise the localisation of fluorescently tagged Cdc24 with (Cdc24-eGFP) and without (Cdc24ΔPH-eGFP) the PH domain. Transformants expressing the Cdc24-eGFP fusion protein consistently displayed fluorescence at the centre of the hyphal septa and also infrequently in an arch at the apex of the hyphal tip as seen previously (48). In contrast, transformants expressing the Cdc24ΔPH-eGFP fusion protein exhibited fluorescence non-specifically throughout the cytoplasm and did not fluoresce at the hyphal tip or at the centre of the septa. However, large vacuoles compressing the cytoplasm against septa made it difficult to discern whether localisation was completely absent. Confirmation that the PH domain of Cdc24 is required for protein localisation seen in this study strongly suggests that Cdc24 may be the central protein delivering NoxR-BemA-Cdc24 to the membrane in *E. festucae*. Work is ongoing to determine the lipid specificity of the Cdc24 PH domain using a simple protein-lipid overlay assay that utilises PIP strips (68). The PH domain of Cdc24 will be exposed to a range of immobilised PPIs and visualise which lipid(s) it binds using a secondary antibody. The main PPI targets of PH domains are PI[4,5]P_2, PI[3,4,5]P_3, and PI[3,4]P_2 in mammals (167).

The next step towards understanding the role lipid signalling plays in regulating the production of ROS by the fungal Nox complex was to analyse the lipid composition in the membranes of *E. festucae*, enabling the prediction of the Cdc24 PH domain target. In this study, five lipid-biosensors were used to investigate the presence and distribution of specific PPIs at different developmental stages in *E. festucae*. Three PPIs, PI[3]P, PI[4]P, and PI[4,5]P_2 were found to be present in hyphae growing in a variety of developmental and environmental conditions. Two PPIs, PI[3,4]P_2 and PI[3,4,5]P_3, were not identified in any condition tested.

Using a biosensor for PI[4]P, based on the PH domain of mouse Plekha3 (134), this PPI was found to localise to highly mobile vesicle-like structures throughout the hyphae of axenically grown cultures of *E. festucae* Fl1. Work in the human pathogen *C. albicans* as well as mammalian cell lines has shown that PI[4]P is commonly found in *trans*-Golgi vesicles (78, 82, 83). Balla, Kim (168) identified that there are in fact two pools of PI[4]P maintained by different PIKs in mammalian cells, one in the membrane of golgi vesicles and the other in the PM.

The first pool of PI[4]P in the membranes of Golgi vesicles is crucial for the anterograde Golgi-to-PM phase of the secretory pathway in yeast (82, 87) and may also be involved in facilitating the formation of clathrin-coated vesicles alongside PI[4,5]P_2 (169). Golgi membranes have the highest PI4K activity compared to other organelles in mammals (170) and when the amount of PI[4]P is decreased, Golgi-to-PM, as well as Golgi-to-vacuole transport is inhibited (75, 80). FM4-64 staining (171) will be required to confirm that the localisation seen in this study is to the Golgi network.

The second pool of PI[4]P to the PM was originally proposed as a precursor for PI[4,5]P_2 synthesis (172, 173). However, recent studies show that the PM pool is not actually required for PI[4,5]P_2 synthesis but is required for targeting specific proteins to the PM (82, 161, 169, 174, 175). PI[4]P in the PM has a distinct role in vacuole morphology, actin cytoskeleton organization, cell wall integrity, and receptor mediated endocytosis in yeast and mammals (75, 169, 174, 176, 177). Presence of PI[4]P in the PM was not consistently observed in this study, although in some mature hyphae a PM-like localisation can be seen. However, it is unclear whether this is a distinct localisation of PI[4]P or cleaved biosensor resulting in free fluorophore in the cytoplasm being squashed against the periphery of the cell by large vacuoles. It may also be that the particular biosensor used for PI[4]P, the PH domain of mouse Plekha3, is unable to bind PM localised PI[4]P, as work by (161) showed that it was necessary to use two different biosensors to target the distinct foci; oxysterol-binding protein homologs (OSH), PH_{OSH2} for *trans*-golgi network and PH_{OSH2x2} for PM pools of PI[4]P. It would be interesting to use a variety of PI[4]P biosensors in *E. festucae* to ascertain whether PM localisation is present and if it changes.

In mammals PI[4]P is the most abundant mono-phosphorylated inositide (175, 178) and is generated by two types of PI 4-kinases (PI4Ks), types II and III. Within these there are also different isoforms, and each displays differential localisation patterns. Yeast possess three PI4Ks; Pik1p, Stt4p, and Lsb6. Pik1 and Stt4p are essential for yeast viability and neither can substitute for the other, which indicates that each isoform has a specialised role (179). Pik1p localises on cytoplasmic puncta as part of the *trans*-Golgi complex as well as in the nucleus (87,

180). The function of Pik1 in the nuclear compartment is unknown, but is essential for yeast viability. Stt4p localises to the PM and generates the PM pool of PI[4]P (75, 176, 180, 181). Unlike Pik1 and Stt4p, Lsb6 is not essential (179). It appears to localise at the PM and vacuolar membranes and is thought to supply PI[4]P as a precursor to $PI[4,5]P_2$, a reaction necessary for homotypic vacuolar fusion or endosome motility (87, 182, 183). Homologues of Pik1p, Stt4p, Lsb6 have been identified in *E. festucae*, *pikA* (EfM3.004190), *sttD* (EfM3.023090), and *lsbF* (EfM3.068110) respectively. It would be interesting to investigate the localisation of the homologs in *E. festucae* to determine their importance in developing the different pools of PI[4]P.

The PI[4]P biosensor also localised to highly mobile vesicle-like structures in germinating asexual conidia and phialides of *E. festucae* strain E2368. This closely related strain (34, 35) was used for analysing biosensor localisation in germinating conidia as it more readily forms conidia than Fl1 (32). The highly mobile nature of the vesicle like structures in phialides is consistent with cytoskeleton trafficking (184). In the future it will be necessary to co-localise the LBD-eGFP biosensor with markers such as VPS-52 (185) and Sec-7 (186) (late Golgi markers), Sec-23 and Sec-13 (ER-exit site markers), or RAB-4 and TLG-1 (early endosome markers) (187) to determine where the PI[4]P vesicles are derived from. The endocytic dye, FM4-64 can be used to determine whether the biosensor undergoes endocytosis from the PM (188). Additionally, it would be interesting to co-localise PI[4]P biosensor strains with Lifeact-TagRFP and tubulin-mCherry to determine the mode of vesicle transport (188).

To see whether localisation of PI[4]P changed when the fungus is grown in its natural condition *in planta*, *E. festucae* strains carrying the PI[4]P biosensors were inoculated into perennial ryegrass and the localisation analysed in hyphae undergoing intercalary growth. The eGFP biosensor localised to vesicles similar to in culture. However, problems were encountered with the mCherry biosensor where it appeared no different from the control. One possible reason for this difference is that many RFPs tend to form aggregates, accumulating in lysosomes (189), thereby disrupting secretory pathways and organelle structures (190-193). mCherry is generally not suitable for Golgi localised membrane fusion proteins as

it often localises to punctate structures leading to misidentification of protein localisation (189). It is unclear why this is an issue *in planta* but not in culture. Overall, this work suggests there is no difference in localisation between mature hyphae, germinating conidia, and *in planta* localisation so it appears to have a 'stable' localisation. The fact that PI[4]P was detected in all developmental stages examined would suggest that as in mammals and yeast, it has a core role in fungal hyphal development and growth. It would be interesting to delete the genes responsible for PI[4]P generation, PikA, SttD, and Lsb6, to visualise the effect on fungal growth.

The putative presence of PI[4]P in the membranes of Golgi vesicles is potentially significant to Nox signalling. NoxA has been localised to the nuclear envelope and endoplasmic reticulum (ER) in *Botrytis cinerea* (194). However, the overlay of fluorescence from ER-Tracker™ and NoxA-GFP fusion protein is not exact. This may be because NoxA is transported from the ER to the Golgi complex before being delivered to the PM (195). If this is the case, NoxA may be co-transported with PI[4]P in Golgi vesicles to the tip of the hyphae. Work is ongoing to determine whether PI[4]P and NoxA co-localise in these vesicles using the PI[4]P biosensor and a NoxA-eGFP fusion protein.

All PI[4]P biosensor strains exhibited background fluorescence in hyphae under all conditions analysed. It is likely that rather than being due to cytoplasmic localisation of PI[4]P it is due to free eGFP or mCherry as western blot analysis revealed significant cleavage of both biosensors. Whilst this is a common observation for localisation studies using fusion proteins (196), the mechanism responsible for cleavage is not entirely understood. This is possibly related to the presence of a linker between the protein of interest and the fluorophore, and the inherent susceptibility of this linker to cleavage (156); the eGFP biosensors have a five glycine linker and the mCherry biosensors have a six glycine linker.

Using a biosensor for PI[4,5]P_2, based on the PH domain of mouse phospholipase C-δ1 (136), this lipid was found to localise at the PM and septa in all developmental conditions analysed in *E. festucae* Fl1 and E2368. PI[4,5]P_2 is known to be present in the inner leaflet of the PM in both mammals and yeast (85-

90). This lipid controls a myriad of cellular processes in yeast and mammals including, endocytosis, exocytosis, establishment of cell polarity, cytoskeletal dynamics, apoptosis, and insertion of ion channels (90, 92-94). Dramatic changes in total cellular $PI(4,5)P_2$ levels rarely occur during normal cell signalling, suggesting cells establish and maintain specific subcellular pools of $PI(4,5)P_2$ (92). For example, mammalian epithelial cells maintain different $PI(4,5)P_2$ concentrations at apical and basolateral membranes by a combination of mechanisms including: $PI(4,5)P_2$ synthesis in different regions, restriction of diffusion of PPI through epithelial tight junctions, localisation of the actin cytoskeleton or clathrin scaffold, and sequestering of $PI(4,5)P_2$ by proteins which restrict and concentrate $PI(4,5)P_2$ locally (92).

In this study, striking asymmetric localisation of the $PI[4,5]P_2$ biosensor was observed in vegetatively growing hyphal tips, where there was little to no signal at the hyphal apex followed by a strong signal in the sub-apical region, indicative of elevated $PI[4,5]P_2$, which became uniform in intensity further down the sides of the tip. This localisation pattern was also seen in germinating conidia, however, it is more difficult to quantify due to the 3D nature of hyphal protrusions making it difficult to differentiate between a natural fluorescent gradient and a false gradient due to distance from the focal plane. In phialides, the biosensor was enriched in the PM of developing conidiospores, indicating an increase in $PI[4,5]P_2$ in the membrane. This increase is likely due to the rapid expansion of the membrane and the need for membrane recycling and specific signalling as seen in *C. albicans* and *S. cerevisiae*, where disruption of the lipid gradient inhibits invasive filamentous growth (96, 197). However, the localisation gradients seen in both *C. albicans* and *S. cerevisiae* show strong fluorescence signals at the hyphal apex, which contrasts with this study. This difference could be because neither *C. albicans* nor *S. cerevisiae* have a Nox complex (52). In tobacco pollen tubes, where growth is analogous to that of fungal hyphae, $PI[4,5]P_2$ was observed in two gradients (99). In actively growing pollen tubes, $PI[4,5]P_2$ was asymmetrically distributed with a lower fluorescence intensity at the tube apex as seen in this study and in non-growing pollen tubes $PI[4,5]P_2$ was most intense at the tube apex (99). This change in $PI[4,5]P_2$ may have role in assembly and activation of the Nox complex, leading

to outgrowth of the pollen tube. Determining whether the distribution of $PI[4,5]P_2$ changes between growing and non-growing hyphae would be an interesting focus of future research.

The elevated levels of $PI[4,5]P_2$ in the sub-apical region of the hyphal tip coincides with an active zone of endocytosis, a major pathway for selective internalization and recycling of PM receptors during hyphal tip growth (81, 86, 169, 198-204). For efficient polarised tip growth in *Nicotiana tabacum* pollen tubes, multiple signalling factors are involved, including a calcium ion (Ca^{2+}) gradient, reactive oxygen species (ROS), Rho-family GTPase, and recycling of membranes (205, 206). These factors have overlapping activities/actions and influence each other. For example the Rac-Rop-type Rho family small GTPases specifically accumulate at the tip PM of the pollen tube, and interact with a lipid kinase to produce $PI[4,5]P_2$ (207). The product of PLC breakdown of $PI[4,5]P_2$, IP_3, induces Ca^{2+} release from internal stores into the cytoplasm which in turn promote growth (208-211).

While the cause of this asymmetry is unknown, there are several possibilities. It may be related to localisation of phospholipase C (PLC) which gives rise to an asymmetric localisation of $PI[4,5]P_2$ in the tips of growing pollen tubes in *N. tabacum* and *Petunia hybrida* (207, 208, 212). Interestingly, Helling, Possart (208) demonstrated that in rapidly elongating pollen tubes, $PI[4,5]P_2$ is produced at the pollen tube apex of *N. tabacum*, while PLC1, the enzyme which breaks $PI[4,5]P_2$ into IP_3 and DAG, is preferentially localised in the sub-apical region. Inhibition and overexpression of PLC1 causes diffusion of $PI[4,5]P_2$ down the sides of the pollen tube tip, resulting in the loss of polarised growth (208, 212). This observation contrasts with the findings of this study, where the $PI[4,5]P_2$ biosensor accumulates in the sup-apical region and is in low levels or absent at the tip apex. Thus, it would be interesting to examine PLC localisation in *E. festucae*, with the expectation that it would be present at the tip apex.

The asymmetric localisation of $PI[4,5]P_2$ observed in this study may also be caused by the action of the PTEN homologue TepA, a phosphatase which converts $PI[3,4,5]P_3$ to $PI[4,5]P_2$. There are very few reports of identification of $PI[3,4,5]P_3$ in fungi. However, in *S. pombe*, deletion of the PTEN homolog, *ptn1*, enables

detection of PI[3,4,5]P_3 at comparable levels to those seen in mammalian cells (131). This was unexpected as yeast lack the class I PI3Ks which generate PI[3,4,5]P_3 (213). Yeast are able to generate PI[3,4,5]P_3 by an alternative pathway which evolved before the appearance of class I PI3Ks by using two kinase enzymes, Vps34p (PI 3-kinase) and Its3p (a PI[4]P 5-kinase). However, rapid turnover by PTEN prevents the PPI from being detected (91, 131, 214). In this study PI[3,4,5]P_3 was not observed under the conditions analysed, however, as *E. festucae* has a Vps34p homolog, VpsA, it is likely that this PPI is produced by the same pathway as in yeast and may not have been seen in this study because of the rapid turnover by the PTEN homolog, TepA, for membrane recycling. Campbell, Liu (215) found that PI[4,5]P_2 enhances phosphatase activity of the PTEN, TepA homologue, resulting in a positive feedback loop to deplete PI[3,4,5]P_3 in mammals making it plausible that PI[3,4,5]P_3 is similarly at the fungal hyphal apex (215-217). It would be interesting to analyse the localisation of TepA in growing hyphal tips of *E. festucae*. Work is ongoing to analyse the impact of knocking out TepA on the concentration of PI[3,4,5]P_3 in *E. festucae*.

Another possible cause of the asymmetric localisation may be asymmetric localisation of MssD, the kinase enzyme which converts PI[4]P to PI[4,5]P_2. Work in *S. cerevisiae* and *C. albicans* both demonstrate localisation of the MssD homologue, Mss4, to the PM and hyphal tip, respectively. When this localisation was disrupted both actin organisation and the PI[4,5]P_2 gradient was lost resulting in inhibition of the yeast-to-hypha transition (95, 96). A key focus of future work will be to determine the localisation of MssD in *E. festucae* and analyse the impact changing the abundance of MssD has on the PI[4,5]P_2 gradient.

In an attempt to further determine if PI[4,5]P_2 is the target of lipid signalling, *mssD* was overexpressed in *E. festucae* and the effect on Nox complex regulation was analysed through studying fungal growth both in culture and *in planta*. Mammals possess three PI5Ks, α, β, and γ, whereas yeast have a single PI5K, MSS4, which is essential (87, 218). *E. festucae mssD* was overexpressed using the constitutive *gpdA* promoter. Three strains were selected that had high (18 fold), medium (8 fold), and low (3 fold) levels of overexpression, respectively. Using these strains, no evidence was found to suggest that overexpressing *mssD* affected cell

morphology, PI[4,5]P_2 distribution in *E. festucae* or association with perennial ryegrass. The analysis of ryegrass plants infected with WT versus *mssD* OE strains provided no clear phenotypic differences caused by OE of *mssD.* While some differences were observed, these were not significantly different between the treatments and are likely due to biological variation. This is possibly because OE of *mssD* in *E. festucae* is detrimental, allowing only small increases in *mssD* expression, which do not affect the morphology or cell integrity, before becoming lethal. Alternatively, it could be because OE of the *mssD* gene does not translate into more protein or that the extra protein is not active so is redundant. Attempts were also made to knock out *mssD* using the split marker technique. This proved unsuccessful, yielding only ectopic integrations suggesting that *mssD* is likely an essential gene as it is in yeast (84). To examine the role of this essential kinase, past studies have utilised temperature sensitive (ts) mutants to both decrease and increase PI5K activity (84, 87, 95, 201, 219, 220). Desrivières, Cooke (219) found that *MSS4*^{ts} yeast cells were defective in fluid-phase endocytosis and had aberrant cell morphology and loss of cell integrity, all due to disorganisation of the actin cytoskeleton.

Future attempts to examine the role of PI[4,5]P_2 in lipid signalling through its kinase MssD, should focus on using an inducible promoter to control *mssD* expression, such as the Tet-on or the copper inducible system, where tetracycline or copper, respectively, is added to fungal cultures to induce expression of the gene of interest, in this case a multi-copy array of *mssD* (221, 222). This would allow the fungus to develop normally then visualise the change in morphology and PI[4,5]P_2 distribution when OE is induced. Strict controls will be necessary to ensure the added compound does not affect fungal or host growth.

The PI[4,5]P_2 gradient seen in this study opens up many possibilities for the lipid target of the Cdc24 PH domain. As all cytosolic Nox complex proteins localise to the apex of the hyphal tip (in addition to other locations) and ROS is primarily produced at the hyphal tip, the hyphal tip is most likely the site of Nox complex activation (223). We now know that PI[4,5]P_2 is at the tip, albeit in the sub-apical region, and that there is an unknown PPI at the apex of the tip which was undetectable under the conditions in this study. As mentioned above this lipid is

likely to be either PI[3,4,5]P_3 or PI[4]P, and different methods, including overexpressing and deletion of key kinases as well as utilising different LBDs to target different lipid pools, are being used to identify the apical lipid.

PI[4,5]P_2 has been identified in additional subcellular compartments including the nucleus, endosomes, lysosomes, autolysosomes, autophagic precursor membranes, ER, mitochondria, and the Golgi complex in mammalian cells (90, 175, 224-226). The presence of PPI pools in these other compartments was not observed in this study, possibly because the PPI in these locations was inaccessible to the biosensor due to interactions with endogenous PI[4,5]P_2 binding proteins. Alternatively, the other PPI pools may be very transient, which appears to be the case in the Golgi complex where there is an apparent absence of stable Golgi-associated PIP5K and presence of 5-phosphatases (80, 90). To view this PPI in locations other than the PM will require high-resolution microscopy techniques such as immunoelectron microscopy, where samples are fixed thereby blocking the lipid dynamics that prevents observation by standard microscopy (224, 227, 228).

The localisation of PI[4,5]P_2 to septa of *E. festucae* was not surprising as this PPI has been previously shown to play an important role in the formation of fungal septa and in cytokinesis (229, 230). Septum formation is a well-regulated and conserved developmental event in filamentous fungi, yeast, and mammals. The process in *N. crassa* has been broken down into 3 distinct stages: 1) septal actomyosin tangle assembly, 2) contractile ring (CR) formation, 3) CR constriction together with PM ingrowth and cell wall construction (229, 231, 232). PI[4,5]P_2 and the enzymes which generate this phospholipid are enriched in the division site of mammalian and yeast cells (233-236). In mammalian cells, depletion of PI[4,5]P_2 in the PM results in disassociation of the actin cytoskeleton and sliding of the CR, indicating that CR anchoring and septal placement is dependent upon the PPI (234). The presence of PI[4,5]P_2 at septa observed in this study suggests that the role of the PPI in septation is conserved in *E. festucae*.

PI[4,5]P_2 also localised to the PM and septa *in planta*. Samples used for this analysis were taken from the cell expansion zone of the leaf sheath where hyphae switch from tip to intercalary growth, a mechanism which synchronises fungal growth

with that of the host plant to effectively avoid mechanical shear as the leaf expands (38, 237). While hyphae are undergoing intercalary growth, they remain metabolically active and still require mobilisation of the polarity complex to actively growing regions to allow extension of the hyphae (237). It is proposed that septa act as the recruitment hub for machinery to allow hyphal extension. Under all biological conditions PI[4,5]P_2 is enriched at the septa and likely has an important role in septation, signalling, and protein recruitment, and may indeed support the role of septa as the hub for hyphal extension. It would be interesting to investigate the effect of depleting septal PI[4,5]P_2 pools , potentially through knocking down MssD, on tip and intercalary hyphal growth.

The presence of PI[4,5]P_2 at the PM and septa under a range of environmental conditions strongly suggests that the PPI plays an essential role in several biological processes including tip growth, endocytic membrane recycling, and septa formation, as seen in mammals and plants. PI[4,5]P_2 may also be a target of lipid signalling in the assembly and activation of the Nox complex. However, the absence of the PPI at the apex of the hyphae opens up possibilities for other PPIs to be present such as PI[4]P and PI[3,4,5]P_3. Work to delete and overexpress the enzymes that affect the production and turnover of these PPIs, such as TepA, is ongoing to help elucidate their role in lipid signalling.

Using a biosensor for PI[3]P, comprised of the FYVE domain of mouse hepatocyte growth factor-regulated tyrosine kinase substrate (134), this lipid was found to display two distinct localisation patterns between mature hyphal cells and hyphal tip cells of axenically grown cultures. In mature hyphal cells, the biosensor localised to the periphery of vacuole-like structures of various sizes as well to the membrane of small punctate structures both in the cytoplasm and inside vacuoles. Previous studies in yeast and mammals, indicate that PI[3]P is highly enriched on early endosomes and in the internal vesicles of both multivesicular endosomes and vacuoles (102-105) and additionally to the TGN in plant cells (106). PI[3]P has been implicated in key roles throughout the endosomal system where cargo may either be recycled to the cell surface (238), trafficked retrogradely to the TGN (239), or sorted to MVBs/late endosomes for lysosomal degradation (105, 109, 240, 241). Regulatory proteins of endocytosis and endosomal trafficking are

shown to contain the two main types of domains that specifically recognize PI[3]P, FYVE and PX domains (81, 102, 242-245). For example, PI[3]P regulates early endosomal fusion by recruiting tethering factor EEA1 with the help of rab5-GTP through PX and FYVE binding domains (246-249). In the tip cell, the biosensor localised exclusively to highly mobile vesicular structures. As discussed above, in other organisms PI[3]P in vesicles is involved in fusion and delivery of cargo to endosomes and vacuoles (102, 103). Given the tip cell does not contain many vacuoles, localisation is primarily to vesicles and is likely part of the endomembrane system delivering cargo to the Spitzenkörper at the rapidly growing tip cell (250). Studies in filamentous fungi have demonstrated that FM4-64 transiently stains the Spitzenkörper (251-253). Indeed, endocytic recycling via early endosomes is essential for proper hyphal morphology and pathogenicity, as seen in the corn smut *Ustilago maydis* (254). Therefore, it appears that the hyphal apex not only is a site of exocytosis but presumably also participates in membrane recycling processes that support tip growth (250). It would be interesting to investigate whether the PI[3]P vesicles are associated with the Spitzenkörper.

Based on previous work in yeast and mammals, the large organelles containing PI[3]P in the membrane are likely vacuoles and the vesicle structures are likely endosomes targeted to either the TGN, cell surface, or to the vacuole/MVB/lysosomes (102). To confirm the localisation of PI[3]P to vacuoles, endosomes and MVBs, co-localisation studies with PI[3]P eGFP biosensor and organelle markers such as VMA-1 (vacuole and prevacuolar compartment (PVC) marker), RAB-4 and TLG-1 (early endosome markers) (187), and FM4-64 to visualise the Spitzenkörper (250) will be needed.

Mammals possess three classes of phosphoinositide 3-kinases (PI3Ks) with different substrate specificities, class I produce PI[3,4,5]P_3, class II generates PI[3,4]P_2 and PI[3]P, and class III exclusively forms PI[3]P (105, 255). Only a single PI3K has been identified in yeast, vps34p which synthesizes PI[3]P (131). As previously mentioned, *E. festucae* has a vps34p homologue, VpsA, making it very likely PI[3]P is biologically important in filamentous fungi. When Vps34p is inactivated, fusion of endosomal transport intermediates with the vacuole are impaired, suggesting PI[3]P is an essential second messenger in vacuolar protein

transport, playing a role in the endosome to vacuole transport (103). Work is ongoing to overexpress *vpsA* and study the effect this has on fungal growth, PPI distribution, and interaction with the plant host.

In *E. festucae* conidiospores the PI[3]P biosensor displayed differential localisation between the eGFP and mCherry fusions, as seen for PI[4]P *in planta*. The mCherry PI[3]P biosensor localised exclusively to mobile vesicles, whereas the eGFP version localised to either putative vesicles or to a circular organelle. This organelle is thought to be the nucleus as there was just one 'spot' present per cell in germinating conidia, which are known to be uninucleate (256). However, DAPI and FM4-64 staining must be used to confirm the nuclear and vesicular localisation results, respectively. Vesicular localisation is to be expected, as conidiospores are fast growing cells, much like the hyphal tip in axenic cultures where vesicular localisation was also observed. The reason for putative localisation of this biosensor to the nucleus is not clear, however, a study in mammalian cells detected nuclear labelling PI[3]P when the probe was highly expressed (102). The inconsistent localisation to the nucleus seen in this study could be due to the level of expression of each biosensor; western blots comparing the expression of each biosensor would be necessary to confirm this hypothesis. Electron microscopy of mammalian cells detected PI[3]P within the nucleus and in the nuclear envelope (102). Coincidentally, Cdc24 has been identified in the nucleus in yeast (72). While not observed in this study the possibility that PI[3]P co-localises with Cdc24 in the nucleus of germinating conidia should be investigated. In phialides, this difference in localisation appears to be resolved with both biosensors localising to vacuolar membranes and mobile vesicles as seen in mature hyphal cells in axenic culture.

Localisation of PI[3]P *in planta* proved inconclusive. All strains of the LBD-eGFP biosensor failed to fluoresce *in planta* and there was no difference in fluorescence between the control and mCherry-LBD biosensor. The mCherry results suggest that PI[3]P may be absent from hyphal cells *in planta*. However, this is very unlikely due to the biological importance of this PPI in other organisms and its specific localisation in cells of axenic cultures of *E. festucae.* Given it is unclear where PI[3]P is localised *in planta* this section of the work will need to be repeated with new transformants in the future.

The localisation of PI[3]P observed in this study make it unlikely that this PPI is a target of lipid signalling in the recruitment of the cytosolic Nox proteins. Instead the lipid likely plays a key role in the endosomal system trafficking as seen in mammalian and yeast systems.

In contrast to PI[3]P, PI[4]P and PI[4,5]P_2, no specific localisation signal could be seen for PI[3,4]P_2 and PI[3,4,5]P_3. Cytoplasmic localisation was observed but this is likely due to free fluorophore, as seen by western blot analysis. Three possible explanations for this are: the target PPIs are not present, the biosensors may not have an affinity to the PPI, or the biosensor cannot access the PPI. It would be very surprising if the PPIs were not present as these PPIs are important in both yeast and mammals (115, 120). PI[3,4]P_2 is expected to localise in the PM playing an important role in cancer metastasis in mammals and endosomal trafficking in yeast. (89, 120, 127). PI[3,4,5]P_3 is found at the PM of the leading edge in mammalian cells (80, 89, 257), where it serves as a potent signal for survival and proliferation (91, 128, 129), and is associated with cytoskeletal rearrangements (130). As previously mentioned, while there is no distinct class I PI3Ks to produce PI[3,4,5]P_3, it is possible that the PPI is generated along an alternative pathway, as seen in yeast, and is present at the hyphal apex where it is rapidly turned over to PI[4,5]P_2 by TepA (131). Yeast also do not have a PI3K enzyme for the synthesis of PI[3,4]P_2, but there may be alternative pathways for generating this PPI as found for PI[3,4,5]P_3 (131). Alternatively, the biosensors may not have an affinity to the PPI in *E. festucae*. To detect PI[3,4]P_2 and PI[3,4,5]P_3 the second PH domain of pleckstrin homology domain-containing family A member 2 (Plekha2) and Bruton's tyrosine kinase (BTK) were used, respectively. The affinity and localisation of these PH domains have been confirmed using affinity assays as well as co-localisation studies in both yeast and mammals (167, 258-263). In future, the specificity of biosensors used in this study will be confirmed. This may be done using PIP strips (Echelon Biosciences, P-6001), an affinity blotting assay; by co-localising biosensors with antibodies specific for a PPI (122); or by making new biosensors based on other mammalian domains known to bind these PPIs. Lastly, it is possible that the PPI was inaccessible to the biosensor due to PPI-protein interactions preventing the biosensor from binding and specific localisation from

being observed. In the future, experiments using higher resolution microscopy techniques such as immunoelectron microscopy, coupled with deletion and overexpression analysis of the enzymes involved in producing these PPIs could be used. While PI[3,4,5]P_3 is not observed in this study it is likely a very important PPI in *E. festucae*. The absence of a lipid at the hyphal tip apex makes it very likely that PI[3,4,5]P_3 is at the apex, and is rapidly turned over to PI[4,5]P_2 by TepA preventing detection, as seen in yeast (131). If this PPI is indeed at the hyphal apex, it could be a potential target of Cdc24. This could be confirmed using the PIP strips mentioned above. Work is ongoing to delete and overexpress TepA to visualise the effect this has on PI[3,4,5]P_3 localisation.

In conclusion, this study represents the first comprehensive analysis of PPI composition in filamentous fungi using biosensors. The knowledge of the spatial PPI composition gained provides a crucial step towards understanding which processes are regulated in *E. festucae* via lipid signalling, including Nox signalling. Deletion of Cdc24 PH domain of Cdc24, abolished localisation to the hyphal tip and septa, suggesting localisation of Cdc24, and activation of the Nox complex, is reliant on the interaction of the PH domain with its lipid target, and therefore lipid signalling.

Using a suite of biosensors, three lipids were identified in *E. festucae*: PI[4]P, in golgi vesicles; PI[4,5]P_2, in the plasma membrane and septa; and PI[3]P, in the vacuolar and endosome membranes. While these structures require confirmation, the localisation of these lipids is well documented in plants, mammals, and yeast. An important focus of future studies will be to confirm identity of these structures using fluorescent markers as indicated above. PI[4,5]P_2 had an asymmetric gradient at the hyphal tip where the PPI was enriched in the sub-apical region with little to no signal at the apex. It is possible that lipids PI[4]P or PI[3,4,5]P_3 are present at the apex, and may be the target of Cdc24, but are not observed as are rapidly turned over. It is also suspected that PI[4]P co-localises with NoxA/NoxD in the golgi vesicles before delivery to the plasma membrane. A co-localisation study between PI[4]P and NoxA as well as affinity assays for the lipid-binding domains, Cdc24 PH domain and BemA PX domain, are underway to identify the lipid target(s). The effects of deleting and overexpressing the enzymes involved in

generating these lipids, *mssD*, *vpsA*, and *tepA*, are being analysed. So far the PI5K which generates PI[4,5]P_2, *mssD*, has been overexpressed and shows no clear impact on the culture growth, phenotype, PPI distribution, or plant-fungal symbiosis. Attempts have been made to delete *mssD*, however it is likely that it is an essential gene. An inducible knockout system is being developed to observe the effect of lowering PI[4,5]P_2 concentrations.

The regulation of the fungal Nox complex has been a hot topic since its discovery in *E. festucae* in 2006 due to its crucial role in regulating the fungal growth *in planta* (46). This study confirms that lipid signalling does play an important role in the assembly of the Nox complex. The potential importance of PI[4]P and PI[3,4,5]P_3 in recruiting cytosolic Nox proteins to the membrane opens up several exciting avenues for future research.

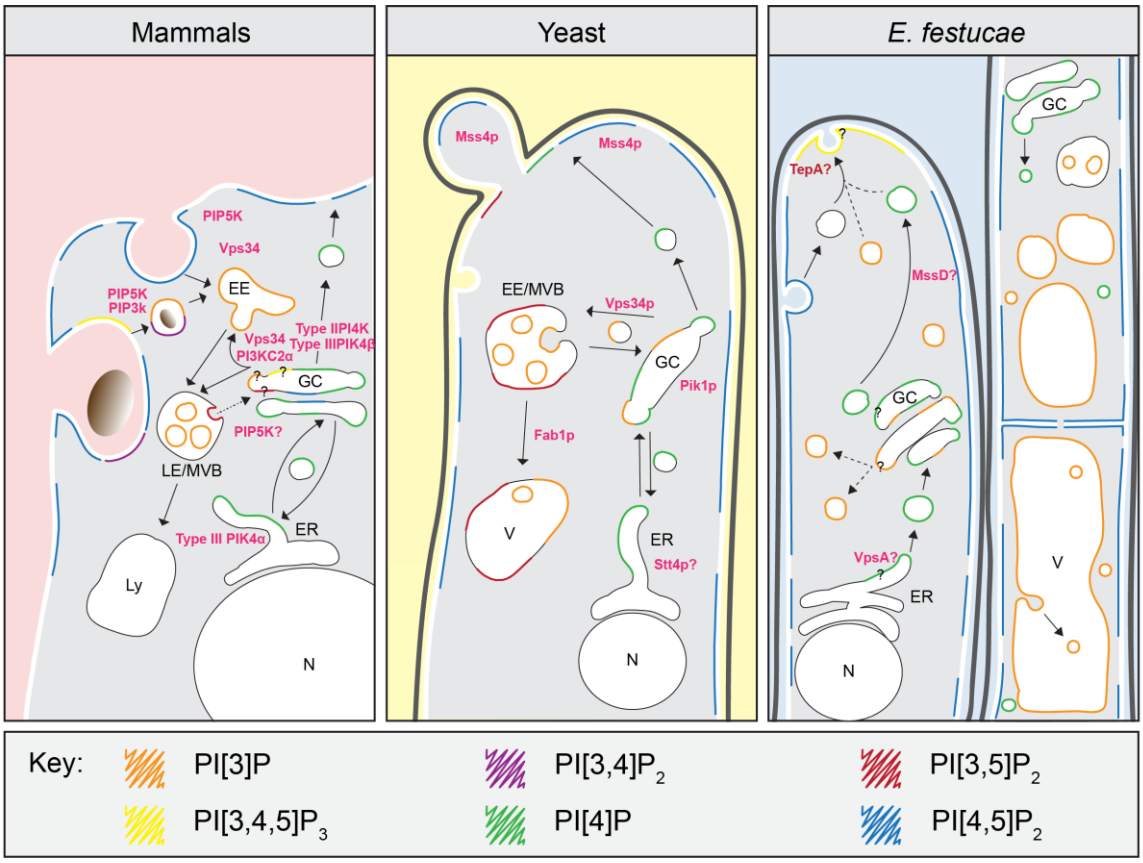

Figure 4.1. Distribution of phosphoinositides in the membranes of mammals, yeast, and fungus, *Epichloë festucae*, cells. Different PIKs (in pink) and phosphatases (in red) are localised to their proposed site of action. The coloured rings around subcellular structures indicate their specificities for different PPIs described in the key. EE, early endosome; LE, late endosome; MVB, multivesicular body; GC, Golgi complex; V, vacuole; Ly, lysosome; ER, endoplasmic reticulum; N, nucleus. Question marks indicate the proposed, yet unconfirmed, localisation of a PPI or PIK. Note: the membrane compartments to which PPIs localise to in the *E. festucae* model are purely based off the literature and results from this study; co-staining is required to confirm compartment identity. Adapted from De Matteis, Godi (80).

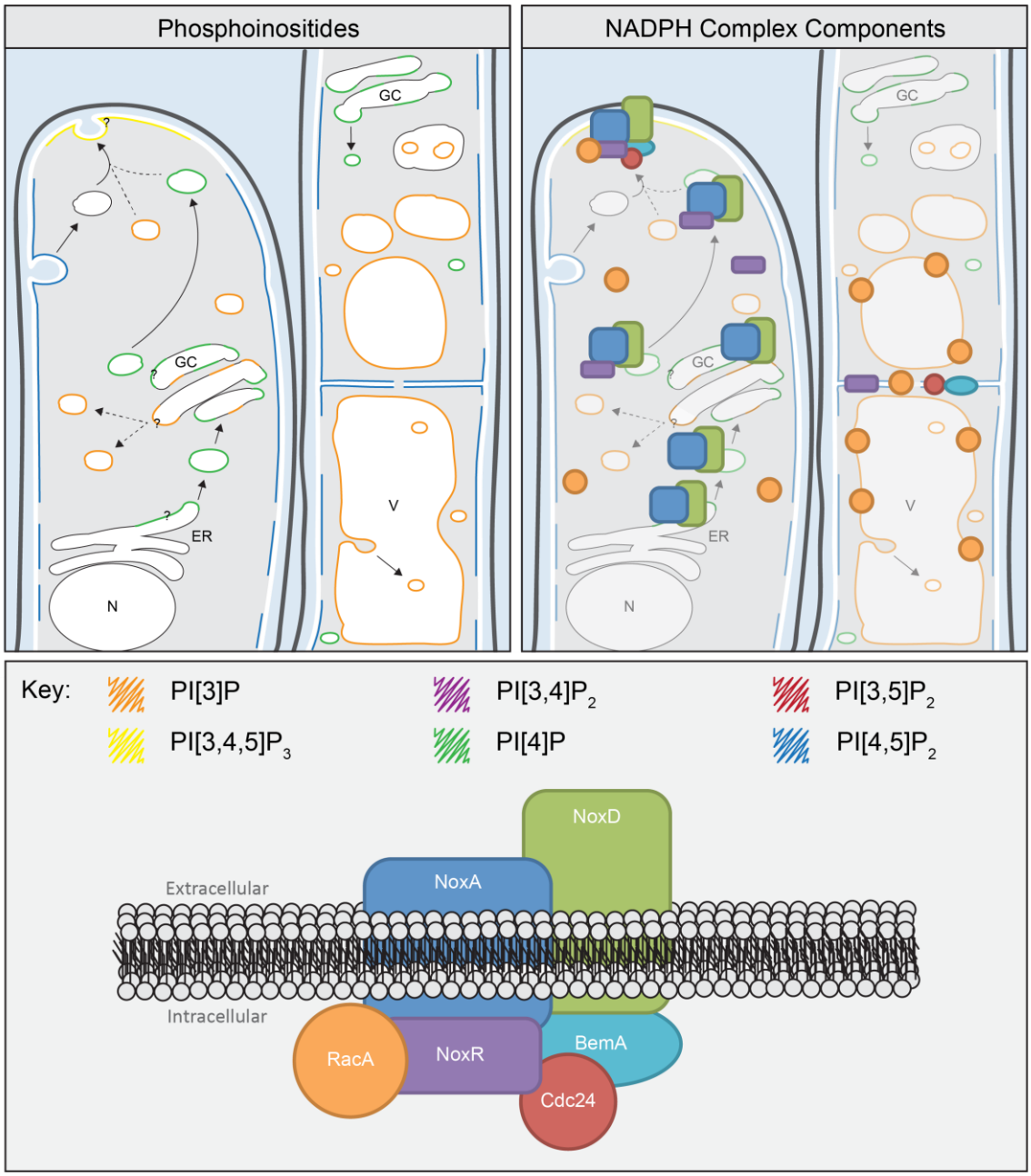

Figure 4.2. Subcellular localisation of phosphoinositides and NADPH oxidase complex subunits in *Epichloë festucae*. Coloured rings represent localisation of different PPIs and solid coloured shapes represent localisation Nox complex subunits within the *E. Festucae* fungal hyphae. Identity of PPIs and Nox complex subunits as indicated in the key. GC, Golgi complex; ER, endoplasmic reticulum; N, nucleus. Note: the membrane compartments to which PPIs localise to and the co-localisation of PPIs and Nox complex subunits are purely based off the literature and results from this study; co-staining and co-localisation studies are required for conformation.

5. Bibliography

1. Clay K, Schardl C. (**2002**) Evolutionary origins and ecological consequences of endophyte symbiosis with grasses. Am Nat 160:99-127.
2. Guérin P. (**1898**) Sur la présence d'un champignon dans l'ivraie. J Botanique 12:230-8.
3. Clay K, Holah J. (**1999**) Fungal endophyte symbiosis and plant diversity in successional fields. Science 285:1742-4.
4. Redecker D, Kodner R, Graham LE. (**2000**) Glomalean fungi from the Ordovician. Science 289:1920-1.
5. Parniske M. (**2008**) Arbuscular mycorrhiza: the mother of plant root endosymbioses. Nat Rev Microbiol 6:763-75.
6. Saikkonen K, Young CA, Helander M, Schardl CL. (**2016**) Endophytic *Epichloë* species and their grass hosts: From evolution to applications. Plant Mol Biol 90:665-75.
7. Wilson D. (**1995**) Endophyte: The evolution of a term, and clarification of its use and definition. Oikos 73:274-6.
8. Charlton D. Pastures - ryegrasses. Encyclopedia of New Zealand 2008.
9. Schardl CL. (**2001**) *Epichloë festucae* and related mutualistic symbionts of grasses. Fungal Genet Biol 33:69-82.
10. Dupont P-Y, Eaton CJ, Wargent JJ, Fechtner S, Solomon P, Schmid J, et al. (**2015**) Fungal endophyte infection of ryegrass reprograms host metabolism and alters development. New Phytol 208:1227-40.
11. Schardl CL, Leuchtmann A, Spiering MJ. (**2004**) Symbioses of grasses with seedborne fungal endophytes. Annu Review Plant Biol 55:315-40.
12. Takemoto D, Tanaka A, Scott B. (**2006**) A p67*Phox*-like regulator is recruited to control hyphal branching in a fungal–grass mutualistic symbiosis. Plant Cell 18:2807-21.
13. Schardl CL. (**1996**) Epichloë species: Fungal symbionts of grasses. Annu Rev Phytopathol 34:109-30.
14. Eaton C, Mitic M, Scott B. (**2012**) Signalling in the *Epichloë festucae*: Perennial ryegrass mutualistic symbiotic interaction. Signaling and communication in plant symbiosis: Springer; p. 143-81.
15. Vázquez-de-Aldana BR, García-Ciudad A, García-Criado B, Vicente-Tavera S, Zabalgogeazcoa I. (**2013**) Fungal endophyte (*Epichloë festucae*) alters the nutrient content of *Festuca rubra* regardless of water availability. PLoS One 8:e84539.
16. Eaton CJ, Dupont P-Y, Solomon P, Clayton W, Scott B, Cox MP. (**2015**) A core gene set describes the molecular basis of mutualism and antagonism in *Epichloë* spp. Mol Plant Micobe In 28:218-31.
17. Tanaka A, Takemoto D, Chujo T, Scott B. (**2012**) Fungal endophytes of grasses. Curr Opin Plant Biol 15:462-8.
18. Kogel K-H, Franken P, Hückelhoven R. (**2006**) Endophyte or parasite – what decides? Curr Opin Plant Biol 9:358-63.
19. Leuchtmann A, Bacon CW, Schardl CL, White JF, Tadych M. (**2014**) Nomenclatural realignment of *Neotyphodium* species with genus *Epichloë*. Mycologia 106:202-15.
20. Scott B, Becker Y, Becker M, Cartwright G. Morphogenesis, growth, and development of the grass symbiont *Epichlöe festucae*. 2012. In: Morphogenesis and Pathogenicity in Fungi Topics in current Genetics [Internet]. Springer, Berlin, HeidelbergTopics in Current Genetics; [243 - 64].

21. Bony S, Pichon N, Ravel C, Durix A, Balfourier F, Guillaumin J-J. (**2001**) The relationship between mycotoxin synthesis and isolate morphology in fungal endophytes of *Lolium perenne*. New Phytol 152:125-37.
22. Christensen MJ, Latch GCM, Tapper BA. (**1991**) Variation within isolates of *Acremonium* endophytes from perennial rye-grasses. Mycol Res 95:918-23.
23. Scott B, Takemoto D, Tanaka A. (**2007**) Fungal endophyte production of reactive oxygen species is critical for maintaining the mutualistic symbiotic interaction between *Epichloë festucae* and perennial ryegrass. Plant Signal Behav 2:171-3.
24. Christensen MJ, Ball OJ-P, Bennett RJ, Schardl CL. (**1997**) Fungal and host genotype effects on compatibility and vascular colonization by *Epichloë festucae*. Mycol Res 101:493-501.
25. Scott B, Green K, Berry D. (**2018**) The fine balance between mutualism and antagonism in the *Epichloë festucae*–grass symbiotic interaction. Curr Opin Plant Biol 44:32-8.
26. Philipson MN, Christey MC. (**1986**) The relationship of host and endophyte during flowering, seed formation, and germination of *Lolium perenne*. New Zeal J Bot 24:125-34.
27. Oberhofer M. (**2012**) Significance of hybridization in *Epichloë* endophytes of *Hordelymus europaeus* [Doctoral Thesis]: Universität Wien.
28. White JF, Jr. (**1988**) Endophyte-host associations in forage grasses. XI. A proposal concerning origin and evolution. Mycologia 80:442-6.
29. Bultman TL, White JF, Jr., Bowdish T, I, Welch A, M, Johnston J. (**1995**) Mutualistic transfer of *Epichloë* spermatia by phorbia flies. Mycologia 87:182-9.
30. Brem D, Leuchtmann A. (**1999**) High prevalence of horizontal transmission of the fungal endophyte *Epichloë sylvatica*. Bull Geobot Inst ETH 65:3-12.
31. Christensen MJ, Spiering MJ, Schmid J. (**2000**) Metabolic activity, distribution, and propagation of grass endophytes in planta: investigations using the GUS reporter gene system. Microbial endophytes: CRC Press; p. 309-36.
32. Green KA, Becker Y, Fitzsimons HL, Scott B. (**2016**) An *Epichloë festucae* homologue of MOB3, a component of the STRIPAK complex, is required for the establishment of a mutualistic symbiotic interaction with *Lolium perenne*. Mol Plant Pathol 17:1480-92.
33. Glass NL, Rasmussen C, Roca MG, Read ND. (**2004**) Hyphal homing, fusion and mycelial interconnectedness. Trends Microbiol 12:135-41.
34. Wilkinson HH, Siegel MR, Blankenship JD, Mallory AC, Bush LP, Schardl CL. (**2000**) Contribution of fungal loline alkaloids to protection from aphids in a grass-endophyte mutualism. Mol Plant Microbe In 13:1027-33.
35. Young CA, Aiken GE, McCulley RL, Strickland JR, Schardl CL. (**2012**)l Epichloae, endophytes of cool season grasses: implications, utilization and biology. Ardmore: Samuel Roberts Noble Foundation. 137 p.
36. Kayano Y, Tanaka A, Akano F, Scott B, Takemoto D. (**2013**) Differential roles of NADPH oxidases and associated regulators in polarized growth, conidiation and hyphal fusion in the symbiotic fungus *Epichloë festucae*. Fungal Genet Biol 56:87-97.
37. Bacon CW, Hinton DM. (**1988**) Ascosporic iterative germination in *Epichloe typhina*. T Brit Mycol Soc 90:563-9.

38. Christensen MJ, Bennett RJ, Ansari HA, Koga H, Johnson RD, Bryan GT, et al. (**2008**) *Epichloë* endophytes grow by intercalary hyphal extension in elongating grass leaves. Fungal Genet Biol 45:84-93.
39. Voisey CR. (**2010**) Intercalary growth in hyphae of filamentous fungi. Fungal Biol Rev 24:123-31.
40. Becker M, Becker Y, Green K, Scott B. (**2016**) The endophytic symbiont *Epichloë festucae* establishes an epiphyllous net on the surface of *Lolium perenne* leaves by development of an expressorium, an appressorium-like leaf exit structure. New Phytol 211:240-54.
41. Moy M, Belanger F, Duncan R, Freehoff A, Leary C, Meyer W, et al. (**2000**) Identification of epiphyllous mycelial nets on leaves of grasses infected by clavicipitaceous endophytes. Symbiosis (Rehovot) 28:291-302.
42. Becker Y, Eaton CJ, Brasell E, May KJ, Becker M, Hassing B, et al. (**2015**) The fungal cell-wall integrity MAPK cascade is crucial for hyphal network formation and maintenance of restrictive growth of *Epichloë festucae* in symbiosis with *Lolium perenne*. Mol Plant Microbe In 28:69-85.
43. Eaton CJ, Cox MP, Ambrose B, Becker M, Hesse U, Schardl CL, et al. (**2010**) Disruption of signaling in a fungal-grass symbiosis leads to pathogenesis. Plant Physiol 153:1780-94.
44. Voisey CR, Christensen MT, Johnson LJ, Forester NT, Gagic M, Bryan GT, et al. (**2016**) cAMP signaling regulates synchronised growth of symbiotic *Epichloë* fungi with the host grass *Lolium perenne*. Front Plant Sci 7:1546.
45. Mitic M, Berry D, Brasell E, Green K, Young CA, Saikia S, et al. (**2017**) Disruption of calcineurin catalytic subunit (*cnaA*) in *Epichloë festucae* induces symbiotic defects and intrahyphal hyphae formation. Mol Plant Pathol 19:1414-26.
46. Tanaka A, Christensen MJ, Takemoto D, Park P, Scott B. (**2006**) Reactive oxygen species play a role in regulating a fungus–perennial ryegrass mutualistic interaction. Plant Cell 18:1052-66.
47. Tanaka A, Takemoto D, Hyon G-S, Park P, Scott B. (**2008**) NoxA activation by the small GTPase RacA is required to maintain a mutualistic symbiotic association between *Epichloë festucae* and perennial ryegrass. Mol Microbiol 68:1165-78.
48. Takemoto D, Kamakura S, Saikia S, Becker Y, Wrenn R, Tanaka A, et al. (**2011**) Polarity proteins Bem1 and Cdc24 are components of the filamentous fungal NADPH oxidase complex. P Natl Acad Sci USA 108:2861-6.
49. Smith SE, Smith FA. (**2012**) Fresh perspectives on the roles of arbuscular mycorrhizal fungi in plant nutrition and growth. Mycologia 104:1-13.
50. Christensen MJ, Bennett RJ, Schmid J. (**2002**) Growth of *Epichloë* / *Neotyphodium* and p-endophytes in leaves of *Lolium* and *Festuca* grasses. Mycol Res 106:93-106.
51. Ryder LS, Dagdas YF, Mentlak TA, Kershaw MJ, Thornton CR, Schuster M, et al. (**2013**) NADPH oxidases regulate septin-mediated cytoskeletal remodeling during plant infection by the rice blast fungus. P Natl Acad Sci USA 110:3179-84.
52. Takemoto D, Tanaka A, Scott B. (**2007**) NADPH oxidases in fungi: Diverse roles of reactive oxygen species in fungal cellular differentiation. Fungal Genet Biol 44:1065-76.
53. Sumimoto H. (**2008**) Structure, regulation and evolution of Nox-family NADPH oxidases that produce reactive oxygen species. FEBS J 275:3249-77.

54. Jaishy B, Zhang Q, Chung HS, Riehle C, Soto J, Jenkins S, et al. (**2015**) Lipid-induced NOX2 activation inhibits autophagic flux by impairing lysosomal enzyme activity. J Lipid Res 56:546-61.
55. Lambeth JD. (**2004**) NOX enzymes and the biology of reactive oxygen. Nature Reviews Immunology 4:181-9.
56. Lacaze I, Lalucque H, Siegmund U, Silar P, Brun S. (**2014**) Identification of NoxD/Pro41 as the homologue of the p22phox NADPH oxidase subunit in fungi. Mol Microbiol 95:1006-24.
57. Siegmund U, Marschall R, Tudzynski P. (**2014**) BcNoxD, a putative ER protein, is a new component of the NADPH oxidase complex in *Botrytis cinerea*. Mol Microbiol 95:988-1005.
58. Scott B. (**2015**) Conservation of fungal and animal nicotinamide adenine dinucleotide phosphate oxidase complexes. Mol Microbiol 95:910-3.
59. de Mendez I, Garrett MC, Adams AG, Leto TL. (**1994**) Role of p67-*phox* SH3 domains in assembly of the NADPH oxidase system. J Biol Chem 269:16326-32.
60. Kitada M, Koya D, Sugimoto T, Isono M, Araki S-i, Kashiwagi A, et al. (**2003**) Translocation of glomerular p47*phox* and p67*phox* by protein kinase C-β activation is required for oxidative stress in diabetic nephropathy. Diabetes 52:2603-14.
61. Nitti M, Furfaro AL, Cevasco C, Traverso N, Marinari UM, Pronzato MA, et al. (**2010**) PKC delta and NADPH oxidase in retinoic acid-induced neuroblastoma cell differentiation. Cell Signal 22:828-35.
62. Benna JE, Dang PM-C, Gaudry M, Fay M, Morel F, Hakim J, et al. (**1997**) Phosphorylation of the respiratory burst oxidase subunit p67*phox* during human neutrophil activation: Regulation by protein kinase C-dependent and independent pathways. J Biol Chem 272:17204-8.
63. Ellson CD, Gobert-Gosse S, Anderson KE, Davidson K, Erdjument-Bromage H, Tempst P, et al. (**2001**) PtdIns(3)P regulates the neutrophil oxidase complex by binding to the PX domain of p40*phox*. Nat Cell Biol 3:679-82.
64. Karathanassis D, Stahelin RV, Bravo J, Perisic O, Pacold CM, Cho W, et al. (**2002**) Binding of the PX domain of p47*phox* to phosphatidylinositol 3,4-bisphosphate and phosphatidic acid is masked by an intramolecular interaction. Embo J 21:5057-68.
65. Ago T, Takeya R, Hiroaki H, Kuribayashi F, Ito T, Kohda D, et al. (**2001**) The PX domain as a novel phosphoinositide- binding module. Biochem Bioph Res Co 287:733-8.
66. Ago T, Kuribayashi F, Hiroaki H, Takeya R, Ito T, Kohda D, et al. (**2003**) Phosphorylation of p47*phox* directs phox homology domain from SH3 domain toward phosphoinositides, leading to phagocyte NADPH oxidase activation. P Natl Acad Sci USA 100:4474-9.
67. Stahelin RV, Burian A, Bruzik KS, Murray D, Cho W. (**2003**) Membrane binding mechanisms of the PX domains of NADPH oxidase p40*phox* and p47*phox*. J Biol Chem 278:14469-79.
68. Kanai F, Liu H, Field SJ, Akbary H, Matsuo T, Brown GE, et al. (**2001**) The PX domains of p47*phox* and p40*phox* bind to lipid products of PI(3)K. Nat Cell Biol 3:675-8.
69. Madden K, Snyder M. (**1998**) Cell polarity and morphogenesis in budding yeast. Annu Rev Microbiol 52:687-744.
70. Kawahara T, Lambeth JD. (**2007**) Molecular evolution of *Phox*-related regulatory subunits for NADPH oxidase enzymes. BMC Evol Biol 7:178.

71. Schürg T, Brandt U, Adis C, Fleißner A. (**2012**) The *Saccharomyces cerevisiae* BEM1 homologue in *Neurospora crassa* promotes co-ordinated cell behaviour resulting in cell fusion. Mol Microbiol 86:349-66.
72. Toenjes KA, Sawyer MM, Johnson DI. (**1999**) The guanine-nucleotide-exchange factor Cdc24p is targeted to the nucleus and polarized growth sites. Curr Biol 9:1183-6.
73. Lu S, Chen L, Tao K, Sun N, Wu Y, Lu X, et al. (**2013**) Intracellular and extracellular phosphatidylinositol 3-phosphate produced by *Phytophthora* species is important for infection. Mol Plant 6:1592-604.
74. Prior SL, Cunliffe BW, Robson GD, Trinci APJ. (**1993**) Multiple isomers of phosphatidyl inositol monophosphate and inositol bis- and trisphosphates from filamentous fungi. FEMS Microbiol Lett 110:147-52.
75. Audhya A, Foti M, Emr SD. (**2000**) Distinct roles for the yeast phosphatidylinositol 4-kinases, Stt4p and Pik1p, in secretion, cell growth, and organelle membrane dynamics. Mol Biol Cell 11:2673-89.
76. Godi A, Pertile P, Meyers R, Marra P, Di Tullio G, Iurisci C, et al. (**1999**) ARF mediates recruitment of PtdIns-4-OH kinase-β and stimulates synthesis of PtdIns(4,5)P2 on the Golgi complex. Nat Cell Biol 1:280-7.
77. Balla A, Tuymetova G, Tsiomenko A, Várnai P, Balla T. (**2005**) A plasma membrane pool of phosphatidylinositol 4-phosphate is generated by phosphatidylinositol 4-kinase type-III alpha: Studies with the ph domains of the oxysterol binding protein and FAPP1. Mol Biol Cell 16:1282-95.
78. Ghugtyal V, Garcia-Rodas R, Seminara A, Schaub S, Bassilana M, Arkowitz RA. (**2015**) Phosphatidylinositol-4-phosphate-dependent membrane traffic is critical for fungal filamentous growth. P Natl Acad Sci USA 112:8644-9.
79. Simon MLA, Platre MP, Marquès-Bueno MM, Armengot L, Stanislas T, Bayle V, et al. (**2016**) A PtdIns(4)P-driven electrostatic field controls cell membrane identity and signalling in plants. Nat Plants 2.
80. De Matteis MA, Godi A, Corda D. (**2002**) Phosphoinositides and the golgi complex. Curr Opin Cell Biol 14:434-47.
81. Simonsen A, Wurmser AE, Emr SD, Stenmark H. (**2001**) The role of phosphoinositides in membrane transport. Curr Opin Cell Biol 13:485-92.
82. Hama H, Schnieders EA, Thorner J, Takemoto JY, DeWald DB. (**1999**) Direct involvement of phosphatidylinositol 4-phosphate in secretion in the yeast *Saccharomyces cerevisiae*. J Biol Chem 274:34294-300.
83. Walch-Solimena C, Novick P. (**1999**) The yeast phosphatidylinositol-4-OH kinase Pik1 regulates secretion at the Golgi. Nat Cell Biol 1:523-5.
84. Desrivières S, Cooke FT, Parker PJ, Hall MN. (**1998**) MSS4, a phosphatidylinositol-4-phosphate 5-kinase required for organization of the actin cytoskeleton in *Saccharomyces cerevisiae*. J Biol Chem 273:15787-93.
85. Martin-Belmonte F, Gassama A, Datta A, Yu W, Rescher U, Gerke V, et al. (**2007**) PTEN-mediated apical segregation of phosphoinositides controls epithelial morphogenesis through Cdc42. Cell 128:383-97.
86. Di Paolo G, De Camilli P. (**2006**) Phosphoinositides in cell regulation and membrane dynamics. Nature 443:651-7.
87. Strahl T, Thorner J. (**2007**) Synthesis and function of membrane phosphoinositides in budding yeast, *Saccharomyces cerevisiae*. Biochim Biophys ACTA 1771:353-404.

88. Koushik AB, Powell RR, Temesvari LA. (**2013**) Localization of phosphatidylinositol 4,5-bisphosphate to lipid rafts and uroids in the human protozoan parasite *Entamoeba histolytica*. Infect Immun 81:2145-55.
89. Sharma VP, DesMarais V, Sumners C, Shaw G, Narang A. (**2008**) Immunostaining evidence for PI(4,5)P2 localization at the leading edge of chemoattractant-stimulated HL-60 cells. J Leukocyte Biol 84:440-7.
90. Tan X, Thapa N, Choi S, Anderson RA. (**2015**) Emerging roles of PtdIns(4,5)2 – beyond the plasma membrane. J Cell Sci 128:4047-56.
91. Gericke A, Leslie NR, Lösche M, Ross AH. (**2013**) PtdIns(4,5)P2-mediated cell signaling: Emerging principles and PTEN as a paradigm for regulatory mechanism. In: Capelluto DGS, editor. Lipid-mediated Protein Signaling. Dordrecht: Springer Netherlands; p. 85-104.
92. van den Bout I, Divecha N. (**2009**) PIP5K-driven PtdIns(4,5)2 synthesis: regulation and cellular functions. J Cell Sci 122:3837-50.
93. Huang C-L. (**2007**) Complex roles of PIP2 in the regulation of ion channels and transporters. Am J Physiol-Renal 293:F1761-F5.
94. Schramp M, Hedman A, Li W, Tan X, Anderson R. (**2012**) PIP kinases from the cell membrane to the nucleus. In: Balla T, Wymann M, York JD, editors. Phosphoinositides I: Enzymes of synthesis and degradation. Dordrecht: Springer Netherlands; p. 25-59.
95. Homma K, Terui S, Minemura M, Qadota H, Anraku Y, Kanaho Y, et al. (**1998**) Phosphatidylinositol-4-phosphate 5-kinase localized on the plasma membrane is essential for yeast cell morphogenesis. J Biol Chem 273:15779-86.
96. Vernay A, Schaub S, Guillas I, Bassilana M, Arkowitz RA. (**2012**) A steep phosphoinositide bis-phosphate gradient forms during fungal filamentous growth. J Cell Biol 198:711-30.
97. Eaton CJ. Marsden Grant. 2015.
98. Mähs A, Ischebeck T, Heilig Y, Stenzel I, Hempel F, Seiler S, et al. (**2012**) The essential phosphoinositide kinase MSS-4 is required for polar hyphal morphogenesis, localizing to sites of growth and cell fusion in *Neurospora crassa*. PLoS ONE 7:e51454.
99. Ischebeck T, Stenzel I, Heilmann I. (**2008**) Type B phosphatidylinositol-4-phosphate 5-kinases mediate *Arabidopsis* and *Nicotiana tabacum* pollen tube growth by regulating apical pectin secretion. Plant cell 20:3312-30.
100. Stenzel I, Ischebeck T, Quint M, Heilmann I. (**2012**) Variable regions of PI4P 5-kinases direct PtdIns(4,5)P2 toward alternative regulatory functions in tobacco pollen tubes. Front Plant Sci 2:1-14.
101. Potocký M, Pejchar P, Gutkowska M, Jiménez-Quesada MJ, Potocká A, Alché JdD, et al. (**2012**) NADPH oxidase activity in pollen tubes is affected by calcium ions, signaling phospholipids and Rac/Rop GTPases. J Plant Physiol 169:1654-63.
102. Gillooly DJ, Morrow IC, Lindsay M, Gould R, Bryant NJ, Gaullier J-M, et al. (**2000**) Localization of phosphatidylinositol 3-phosphate in yeast and mammalian cells. Embo J 19:4577-88.
103. Wurmser AE, Emr SD. (**1998**) Phosphoinositide signaling and turnover: PtdIns(3)P, a regulator of membrane traffic, is transported to the vacuole and degraded by a process that requires lumenal vacuolar hydrolase activities. Embo J 17:4930-42.
104. Odorizzi G, Babst M, Emr SD. (**2000**) Phosphoinositide signaling and the regulation of membrane trafficking in yeast. Trends Biochem Sci 25:229-35.

105. Marat AL, Haucke V. (**2016**) Phosphatidylinositol 3-phosphates—at the interface between cell signalling and membrane traffic. Embo J 35:561-79.
106. Kim DH, Eu Y-J, Yoo CM, Kim Y-W, Pih KT, Jin JB, et al. (**2001**) Trafficking of phosphatidylinositol 3-phosphate from the trans-Golgi network to the lumen of the central vacuole in plant cells. Plant Cell 13:287-301.
107. Kihara A, Kabeya Y, Ohsumi Y, Yoshimori T. (**2001**) Beclin–phosphatidylinositol 3‐kinase complex functions at the *trans*‐Golgi network. EMBO reports 2:330-5.
108. Ono F, Nakagawa T, Saito S, Owada Y, Sakagami H, Goto K, et al. (**1998**) A novel class II phosphoinositide 3-kinase predominantly expressed in the liver and its enhanced expression during liver regeneration. J Biol Chem 273:7731-6.
109. Schu PV, Takegawa K, Fry MJ, Stack JH, Waterfield MD, Emr SD. (**1993**) Phosphatidylinositol 3-kinase encoded by yeast VPS34 gene essential for protein sorting. Science 260:88-91.
110. Bréchard S, Plançon S, Tschirhart EJ. (**2013**) New insights into the regulation of neutrophil NADPH oxidase activity in the phagosome: A focus on the role of lipid and Ca(2+) signaling. Antioxid Redox Sign 18:661-76.
111. Bissonnette SA, Glazier CM, Stewart MQ, Brown GE, Ellson CD, Yaffe MB. (**2008**) Phosphatidylinositol 3-phosphate-dependent and -independent functions of p40*phox* in activation of the neutrophil NADPH oxidase. J Biol Chem 283:2108-19.
112. Liu J, Zhou J, Xing D. (**2012**) Phosphatidylinositol 3-kinase plays a vital role in regulation of rice seed vigor via altering nadph oxidase activity. PLoS ONE 7:e33817.
113. Park K-Y, Jung J-Y, Park J, Hwang J-U, Kim Y-W, Hwang I, et al. (**2003**) A role for phosphatidylinositol 3-phosphate in abscisic acid-induced reactive oxygen species generation in guard cells. Plant Physiol 132:92-8.
114. Leshem Y, Seri L, Levine A. (**2007**) Induction of phosphatidylinositol 3-kinase-mediated endocytosis by salt stress leads to intracellular production of reactive oxygen species and salt tolerance. Plant J 51:185-97.
115. Li H, Marshall AJ. (**2015**) Phosphatidylinositol (3,4) bisphosphate-specific phosphatases and effector proteins: A distinct branch of PI3K signaling. Cell Signal 27:1789-98.
116. Nakahira M, Tanaka T, Robson BE, Mizgerd JP, Grusby MJ. (**2007**) Regulation of signal transducer and activator of transcription signaling by the tyrosine phosphatase PTP-BL. Immunity 26:163-76.
117. Servant G, Weiner OD, Herzmark P, Balla T, Sedat JW, Bourne HR. (**2000**) Polarization of chemoattractant receptor signaling during neutrophil chemotaxis. Science 287:1037-40.
118. Meili R, Ellsworth C, Lee S, Reddy TBK, Ma H, Firtel RA. (**1999**) Chemoattractant‐mediated transient activation and membrane localization of Akt/PKB is required for efficient chemotaxis to cAMP in Dictyostelium. Embo J 18:2092-105.
119. Li H, Wu X, Hou S, Malek M, Kielkowska A, Noh E, et al. (**2016**) Phosphatidylinositol-3,4-bisphosphate and its binding protein lamellipodin regulate chemotaxis of malignant B lymphocytes. J Immunol 196:586-95.
120. Fukumoto M, Ijuin T, Takenawa T. (**2017**) PI(3,4)P2 plays critical roles in the regulation of focal adhesion dynamics of MDA-MB-231 breast cancer cells. Cancer Sci 108:941-51.

121. Bae YH, Ding Z, Das T, Wells A, Gertler F, Roy P. (**2010**) Profilin1 regulates PI(3,4)P2 and lamellipodin accumulation at the leading edge thus influencing motility of MDA-MB-231 cells. P Natl Acad Sci USA 107:21547-52.
122. Posor Y, Eichhorn-Gruenig M, Puchkov D, Schöneberg J, Ullrich A, Lampe A, et al. (**2013**) Spatiotemporal control of endocytosis by phosphatidylinositol-3,4-bisphosphate. Nature 499:233-7.
123. Bendris N, Schmid SL. (**2017**) Endocytosis, metastasis and beyond: Multiple facets of SNX9. Trends Cell Biol 27:189-200.
124. Schöneberg J, Lehmann M, Ullrich A, Posor Y, Lo W-T, Lichtner G, et al. (**2017**) Lipid-mediated PX-BAR domain recruitment couples local membrane constriction to endocytic vesicle fission. Nature Commun 8:1-17.
125. Lo W-T, Vujičić Žagar A, Gerth F, Lehmann M, Puchkov D, Krylova O, et al. (**2017**) A coincidence detection mechanism controls PX-BAR domain-mediated endocytic membrane remodeling via an allosteric structural switch. Dev Cell 43:522-9.
126. Daumke O, Roux A, Haucke V. (**2014**) BAR domain scaffolds in dynamin-mediated membrane fission. Cell 156:882-92.
127. Wallroth A, Haucke V. (**2017**) Phosphoinositide conversion in endocytosis and the endolysosomal system. J Biol Chem 293:1526-35.
128. Vanhaesebroeck B, Leevers SJ, Ahmadi K, Timms J, Katso R, Driscoll PC, et al. (**2001**) Synthesis and function of 3-phosphorylated inositol lipids. Annu Rev Biochem 70:535-602.
129. Iijima M, Devreotes P. (**2002**) Tumor suppressor PTEN mediates sensing of chemoattractant gradients. Cell 109:599-610.
130. Cai HQ, Devreotes PN. (**2011**) Moving in the right direction: How eukaryotic cells migrate along chemical gradients. Semin Cell Dev Biol 22:834-41.
131. Mitra P, Zhang Y, Rameh LE, Ivshina MP, McCollum D, Nunnari JJ, et al. (**2004**) A novel phosphatidylinositol(3,4,5)P(3) pathway in fission yeast. J Cell Biol 166:205-11.
132. Vanhaesebroeck B, Stephens L, Hawkins P. (**2012**) PI3K signalling: the path to discovery and understanding. Nat Rev Mol Cell Biol 13:195-203.
133. Audhya A, Emr SD. (**2003**) Regulation of PI4,5P(2) synthesis by nuclear–cytoplasmic shuttling of the Mss4 lipid kinase. Embo J 22:4223-36.
134. Vermeer JE, van Leeuwen W, Tobeña-Santamaria R, Laxalt Ana M, Jones DR, Divecha N, et al. (**2006**) Visualization of PtdIns3P dynamics in living plant cells. Plant J 47:687-700.
135. Lakin-Thomas PL. (**1993**) Effects of inositol starvation on the levels of inositol phosphates and inositol lipids in *Neurospora crassa*. Biochem J 292:805-11.
136. Van Leeuwen W, Vermeer JE, Gadella TWJ, Munnik T. (**2007**) Visualization of phosphatidylinositol 4,5-bisphosphate in the plasma membrane of suspension-cultured tobacco BY-2 cells and whole Arabidopsis seedlings. Plant J 52:1014-26.
137. Potocký M, Pleskot R, Pejchar P, Vitale N, Kost B, Žárský V. (**2014**) Live-cell imaging of phosphatidic acid dynamics in pollen tubes visualized by Spo20p-derived biosensor. New Phytol 203:483-94.
138. Yao J, Chen Y, Wang N, Jiang D, Zheng J. (**2014**) Lipid A-based affinity biosensor for screening anti-sepsis components from herbs. Biosci Rep 34:e00109.

139. Vermeer JE, Thole JM, Goedhart J, Nielsen E, Munnik T, Gadella TWJ. (**2009**) Imaging phosphatidylinositol 4-phosphate dynamics in living plant cells. Plant J 57:356-72.
140. Auger KR, Carpenter CL, Cantley LC, Varticovski L. (**1989**) Phosphatidylinositol 3-kinase and its novel product, phosphatidylinositol 3-phosphate, are present in *Saccharomyces cerevisiae*. J Biol Chem 264:20181-4.
141. Dove SK, Cooke FT, Douglas MR, Sayers LG, Parker PJ, Michell RH. (**1997**) Osmotic stress activates phosphatidylinositol-3,5-bisphosphate synthesis. Nature 390:187-92.
142. Serunian LA, Auger KR, Cantley LC. (**1991**) Identification and quantification of polyphosphoinositides produced in response to platelet-derived growth factor stimulation. Methods in Enzymology. 198: Academic Press; p. 78-87.
143. Christianson TW, Sikorski RS, Dante M, Shero JH, Hieter P. (**1992**) Multifunctional yeast high-copy-number shuttle vectors. Gene 110:119-22.
144. Saikia S, Scott B. (**2009**) Functional analysis and subcellular localization of two geranylgeranyl diphosphate synthases from *Penicillium paxilli*. Mol Genet Genomics 282:257-71.
145. Young CA, Bryant MK, Christensen MJ, Tapper BA, Bryan GT, Scott B. (**2005**) Molecular cloning and genetic analysis of a symbiosis-expressed gene cluster for lolitrem biosynthesis from a mutualistic endophyte of perennial ryegrass. Mol Genet Genomics 274:13-29.
146. Lorang JM, Tuori RP, Martinez JP, Sawyer TL, Redman RS, Rollins JA, et al. (**2001**) Green fluorescent protein is lighting up fungal biology. Appl Environ Microbiol 67:1987-94.
147. Miller J. (**1972**)l Experiments in molecular genetics. New York: Cold Spring Harbor Laboratory Press.
148. Byrd AD, Schardl CL, Songlin PJ, Mogen KL, Siegel MR. (**1990**) The β-tubulin gene of *Epichloë typhina* from perennial ryegrass (*Lolium perenne*). Curr Genet 18:347-54.
149. Livak KJ, Schmittgen TD. (**2001**) Analysis of relative gene expression data using Real-Time Quantitative PCR and the 2−ΔΔCT method. Methods 25:402-8.
150. Itoh Y, Johnson R, Scott B. (**1994**) Integrative transformation of the mycotoxin-producing fungus, *Penicillium paxilli*. Curr Genet 25:508-13.
151. Latch GCM, Christensen MJ. (**1985**) Artificial infection of grasses with endophytes. Ann Appl Biol 107:17-24.
152. Schardl CL, Young CA, Hesse U, Amyotte SG, Andreeva K, Calie PJ, et al. (**2013**) Plant-symbiotic fungi as chemical engineers: Multi-genome analysis of the clavicipitaceae reveals dynamics of alkaloid loci. PLoS Genet 9:e1003323.
153. Brandes RP, Weissmann N, Schröder K. (**2014**) Nox family NADPH oxidases: Molecular mechanisms of activation. Free Radical Bio Med 76:208-26.
154. Lemmon MA. (**2007**) Pleckstrin homology (PH) domains and phosphoinositides. Biochem Soc Symp 74:81-93.
155. Stahelin RV. (**2009**) Lipid binding domains: More than simple lipid effectors. J Lipid Res 50:S299-S304.
156. Holzer T, Liffers K, Rahm K, Trageser B, Özbek S, Gradl D. (**2012**) Live imaging of active fluorophore labelled Wnt proteins. FEBS Lett 586:1638-44.
157. Rella A, Farnoud AM, Del Poeta M. (**2016**) Plasma membrane lipids and their role in fungal virulence. Prog Lipid Res 61:63-72.

158. Ryder LS, Talbot NJ. (**2015**) Regulation of appressorium development in pathogenic fungi. Curr Opin Plant biol 26:8-13.
159. Shafrir Y, ben-Avraham D, Forgacs G. (**2000**) Trafficking and signaling through the cytoskeleton: A specific mechanism. J Cell Sci 113:2747-57.
160. Nebenführ A, Gallagher LA, Dunahay TG, Frohlick JA, Mazurkiewicz AM, Meehl JB, et al. (**1999**) Stop-and-go movements of plant Golgi stacks are mediated by the acto-myosin system. Plant Physiol 121:1127-41.
161. Dickson EJ, Jensen JB, Hille B. (**2014**) Golgi and plasma membrane pools of PI(4)P contribute to plasma membrane PI(4,5)P2 and maintenance of KCNQ2/3 ion channel current. P Natl Acad Sci USA 111:E2281.
162. Schardl C, Scott B, editors. Recommendations for gene nomenclature for *Epichloë* species and related Clavicipitaceae. Epichloae, endophytes of cool season grasses: implications, utilization and biology Proceedings of the 7th International Symposium on Fungal Endophytes of Grasses, Lexington, Kentucky, USA, 28 June to 1 July 2010; 2010: Samuel Roberts Noble Foundation.
163. Rahnama M, Forester N, Ariyawansa KGSU, Voisey CR, Johnson LJ, Johnson RD, et al. (**2017**) Efficient targeted mutagenesis in *Epichloë festucae* using a split marker system. J Microbiol Meth 134:62-5.
164. Inanami O, Johnson JL, McAdara JK, Benna JE, Faust LRP, Newburger PE, et al. (**1998**) Activation of the leukocyte NADPH oxidase by phorbol ester requires the phosphorylation of p47*Phox* on serine 303 or 304. J Biol Chem 273:9539-43.
165. Marcotte EM, Pellegrini M, Ng H-L, Rice DW, Yeates TO, Eisenberg D. (**1999**) Detecting protein function and protein-protein interactions from genome sequences. Science 285:751-3.
166. Leeder AC, Turner G. (**2008**) Characterisation of *Aspergillus nidulans* polarisome component BemA. Fungal Genet Biol 45:897-911.
167. Rameh LE, Arvidsson A-k, Carraway KL, Couvillon AD, Rathbun G, Crompton A, et al. (**1997**) A comparative analysis of the phosphoinositide binding specificity of pleckstrin homology domains. J Biol Chem 272:22059-66.
168. Balla A, Kim YJ, Varnai P, Szentpetery Z, Knight Z, Shokat KM, et al. (**2008**) Maintenance of hormone-sensitive phosphoinositide pools in the plasma membrane requires phosphatidylinositol 4-kinase IIIα. Mol Biol Cell 19:711-21.
169. Yamamoto W, Wada S, Nagano M, Aoshima K, Siekhaus DE, Toshima JY, et al. (**2018**) Distinct roles for plasma membrane PtdIns(4)P and PtdIns(4,5)P2 during receptor-mediated endocytosis in yeast. J Cell Sci 131:1-12.
170. Cockcroft S, Taylor JA, Judah JD. (**1985**) Subcellular localisation of inositol lipid kinases in rat liver. Biochim Biophys ACTA 845:163-70.
171. Shen G, Zhou E, Alspaugh JA, Wang P. (**2012**) Wsp1 is downstream of Cin1 and regulates vesicle transport and actin cytoskeleton as an effector of Cdc42 and Rac1 in *Cryptococcus neoformans*. Eukaryot Cell 11:471-81.
172. Hammond Gerald R V, Schiavo G, Irvine Robin F. (**2009**) Immunocytochemical techniques reveal multiple, distinct cellular pools of PtdIns4P and PtdIns(4,5)P2. Biochem J 422:23-35.
173. Weixel KM, Blumental-Perry A, Watkins SC, Aridor M, Weisz OA. (**2005**) Distinct Golgi populations of phosphatidylinositol 4-phosphate regulated by phosphatidylinositol 4-kinases. J Biol Chem 280:10501-8.
174. Hammond GRV, Fischer MJ, Anderson KE, Holdich J, Koteci A, Balla T, et al. (**2012**) PI4P and PI(4,5)P2 are essential but independent lipid determinants of membrane identity. Science 337:727-30.

175. D'Angelo G, Vicinanza M, Di Campli A, De Matteis MA. (**2008**) The multiple roles of PtdIns(4) – not just the precursor of PtdIns(4,5)2. J Cell Sci 121:1955-63.
176. Audhya A, Emr SD. (**2002**) Stt4 PI 4-kinase localizes to the plasma membrane and functions in the Pkc1-mediated MAP kinase cascade. Dev Cell 2:593-605.
177. Foti M, Audhya A, Emr SD. (**2001**) Sac1 lipid phosphatase and Stt4 phosphatidylinositol 4-kinase regulate a pool of phosphatidylinositol 4-phosphate that functions in the control of the actin cytoskeleton and vacuole morphology. Mol Biol Cell 12:2396-411.
178. Lemmon MA. (**2008**) Membrane recognition by phospholipid-binding domains. Nat Rev Mol Cell Biol 9:99-111.
179. Jesch SA, Gaspar ML, Stefan CJ, Aregullin MA, Henry SA. (**2010**) Interruption of inositol sphingolipid synthesis triggers Stt4p-dependent protein kinase C signaling. J Biol Chem 285:41947-60.
180. Strahl T, Hama H, DeWald DB, Thorner J. (**2005**) Yeast phosphatidylinositol 4-kinase, Pik1, has essential roles at the Golgi and in the nucleus. J Cell Biol 171:967-79.
181. Sheri M R, Margaret M R, Kimberly T, Kellie E R, Carl M, Olivier R, et al. (**2005**) Nonclassical PITPs activate PLD via the Stt4p PtdIns-4-kinase and modulate function of late stages of exocytosis in vegetative yeast. Traffic 6:1157-72.
182. Mayer A, Scheglmann D, Dove S, Glatz A, Wickner W, Haas A. (**2000**) Phosphatidylinositol 4,5-bisphosphate regulates two steps of homotypic vacuole fusion. Mol Biol Cell 11:807-17.
183. Shelton SN, Barylko B, Binns DD, Horazdovsky BF, Albanesi JP, Goodman JM. (**2003**) *Saccharomyces cerevisiae* contains a Type II phosphoinositide 4-kinase. Biochem J 371:533-40.
184. Zajac AL, Goldman YE, Holzbaur ELF, Ostap EM. (**2013**) Local cytoskeletal and organelle interactions impact molecular motor-driven early endosomal trafficking. Cur Biol 23:1173-80.
185. Bowman BJ, Draskovic M, Freitag M, Bowman EJ. (**2009**) Structure and distribution of organelles and cellular location of calcium transporters in *Neurospora crassa*. Eukaryot cell 8:1845-55.
186. Sánchez‐León E, Bowman B, Seidel C, Fischer R, Novick P, Riquelme M. (**2015**) The Rab GTPase YPT‐1 associates with Golgi cisternae and Spitzenkörper microvesicles in *Neurospora crassa*. Mol Microbiol 95:472-90.
187. Bowman BJ, Draskovic M, Schnittker RR, El-Mellouki T, Plamann MD, Sánchez-León E, et al. (**2015**) Characterization of a novel prevacuolar compartment in *Neurospora crassa*. Eukaryot Cell 14:1253-63.
188. Jonkers W, Fischer MS, Do HP, Starr TL, Glass NL. (**2016**) Chemotropism and cell fusion in *Neurospora crassa* relies on the formation of distinct protein complexes by HAM-5 and a novel protein HAM-14. Genetics 203:319-34.
189. Costantini LM, Baloban M, Markwardt ML, Rizzo M, Guo F, Verkhusha VV, et al. (**2015**) A palette of fluorescent proteins optimized for diverse cellular environments. Nature Commun 6:7670-.
190. Costantini LM, Snapp EL. (**2013**) Fluorescent proteins in cellular organelles: Serious pitfalls and some solutions. DNA Cell Biol 32:622-7.
191. Snapp E. (**2005**) Design and use of fluorescent fusion proteins in cell biology. Curr Protocol Cell Biol 27:1-13.

192. Yanushevich YG, Staroverov DB, Savitsky AP, Fradkov AF, Gurskaya NG, Bulina ME, et al. (**2001**) A strategy for the generation of non-aggregating mutants of *Anthozoa* fluorescent proteins. FEBS Lett 511:11-4.
193. Landgraf D, Okumus B, Chien P, Baker TA, Paulsson J. (**2012**) Segregation of molecules at cell division reveals native protein localization. Nat Meth 9:480-2.
194. Siegmund U, Heller J, van Kann JAL, Tudzynski P. (**2013**) The NADPH oxidase complexes in *Botrytis cinerea*: Evidence for a close association with the ER and the tetraspanin Pls1. PLoS ONE 8:e55879.
195. Alberts B, Johnson A, Lewis J, Raff M, Roberts K, Walter P. (**2002**) Transport from the *trans* Golgi network to the cell exterior: Exocytosis. Molecular Biology of the Cell. 4th edition ed. New York: Garland Science; p.
196. Huang L, Pike D, Sleat DE, Nanda V, Lobel P. (**2014**) Potential pitfalls and solutions for use of fluorescent fusion proteins to study the lysosome. PLoS ONE 9:e88893.
197. Guillas I, Vernay A, Vitagliano J-J, Arkowitz RA. (**2013**) Phosphatidylinositol 4,5-bisphosphate is required for invasive growth in *Saccharomyces cerevisiae*. J Cell Sci 126:3602-14.
198. Jost M, Simpson F, Kavran JM, Lemmon MA, Schmid SL. (**1998**) Phosphatidylinositol-4,5-bisphosphate is required for endocytic coated vesicle formation. Curr Biol 8:1399-404.
199. Hill E, van der Kaay J, Downes CP, Smythe E. (**2001**) The role of dynamin and its binding partners in coated pit invagination and scission. J Cell Biol 152:309-23.
200. Marks B, Stowell MHB, Vallis Y, Mills IG, Gibson A, Hopkins CR, et al. (**2001**) GTPase activity of dynamin and resulting conformation change are essential for endocytosis. Nature 410:231-5.
201. Roth MG. (**2004**) Phosphoinositides in constitutive membrane traffic. Physiol Rev 84:699-730.
202. Haucke V. (**2005**) Phosphoinositide regulation of clathrin-mediated endocytosis. Biochem Soc T 33:1285-9.
203. Abe N, Inoue T, Galvez T, Klein L, Meyer T. (**2008**) Dissecting the role of PtdIns(4,5)2 in endocytosis and recycling of the transferrin receptor. J Cell Sci 121:1488-94.
204. Saavedra L. (**2014**) PtdIns4P and PtdIns(4,5)P2 as signalling phosphoinositides involved in tip growth. In: Hakeem KR, Rehman RU, Tahir I, editors. Plant signaling: Understanding the molecular crosstalk. New Delhi: Springer India; p. 75-91.
205. Kusano H, Tominaga R, Wada T, Kato M, Aoyama T. (**2014**) Phosphoinositide signaling in root hair tip growth. Plant Cell Wall Patterning and Cell Shape. Wiley Online Books.
206. Brand A, Gow NAR. (**2009**) Mechanisms of hypha orientation of fungi. Curr Opin Microbiol 12:350-7.
207. Kost B, Lemichez E, Spielhofer P, Hong Y, Tolias K, Carpenter C, et al. (**1999**) Rac homologues and compartmentalized phosphatidylinositol 4, 5-bisphosphate act in a common pathway to regulate polar pollen tube growth. J Cell Biol 145:317-30.
208. Helling D, Possart A, Cottier S, Klahre U, Kost B. (**2006**) Pollen tube tip growth depends on plasma membrane polarization mediated by tobacco PLC3 activity and endocytic membrane recycling. Plant Cell 18:3519-34.

209. Clapham DE. (**1995**) Calcium signaling. Cell 80:259-68.
210. Yang C, Kazanietz MG. (**2003**) Divergence and complexities in DAG signaling: Looking beyond PKC. Trends Pharmacol Sci 24:602-8.
211. Cole RA, Fowler JE. (**2006**) Polarized growth: Maintaining focus on the tip. Curr Opin Plant Biol 9:579-88.
212. Dowd PE, Coursol S, Skirpan AL, Kao T-h, Gilroy S. (**2006**) *Petunia* phospholipase C1 is involved in pollen tube growth. Plant Cell 18:1438-53.
213. Takegawa K, DeWald DB, Emr SD. (**1995**) *Schizosaccharomyces pombe* Vps34p, a phosphatidylinositol-specific PI 3-kinase essential for normal cell growth and vacuole morphology. J Cell Sci 108:3745-56.
214. Vazquez F, Matsuoka S, Sellers WR, Yanagida T, Ueda M, Devreotes PN. (**2006**) Tumor suppressor PTEN acts through dynamic interaction with the plasma membrane. P Natl Acad Sci USA 103:3633-8.
215. Campbell RB, Liu FH, Ross AH. (**2003**) Allosteric activation of PTEN phosphatase by phosphatidylinositol 4,5-bisphosphate. J Biol Chem 278:33617-20.
216. Singh G, Odriozola L, Guan H, Kennedy CR, Chan AM. (**2011**) Characterization of a novel PTEN mutation in MDA-MB-453 breast carcinoma cell line. Bmc Cancer 11:1-11.
217. Odriozola L, Singh G, Hoang T, Chan AM. (**2007**) Regulation of PTEN activity by its carboxyl-terminal autoinhibitory domain. J Biol Chem 282:23306-15.
218. Divecha N. (**2010**) Lipid kinases: Charging PtdIns(4,5)P2 synthesis. Curr Biol 20:R154-R7.
219. Desrivières S, Cooke FT, Morales-Johansson H, Parker PJ, Hall MN. (**2002**) Calmodulin controls organization of the actin cytoskeleton via regulation of phosphatidylinositol (4,5)-bisphosphate synthesis in *Saccharomyces cerevisiae*. Biochem J 366:945-51.
220. Winzeler EA, Shoemaker DD, Astromoff A, Liang H, Anderson K, Andre B, et al. (**1999**) Functional characterization of the S. cerevisiae genome by gene deletion and parallel analysis. Science 285:901-6.
221. Gossen M, Bujard H. (**1992**) Tight control of gene expression in mammalian cells by tetracycline-responsive promoters. P Natl Acad Sci USA 89:5547-51.
222. McKenzie MJ, Mett V, Reynolds PHS, Jameson PE. (**1998**) Controlled cytokinin production in transgenic tobacco using a copper-inducible promoter. Plant Physiol 116:969-77.
223. Semighini CP, Harris SD. (**2008**) Regulation of apical dominance in *Aspergillus nidulans* hyphae by reactive oxygen species. Genetics 179:1919-32.
224. Watt SA, Kular G, Fleming IN, Downes CP, Lucocq JM. (**2002**) Subcellular localization of phosphatidylinositol 4,5-bisphosphate using the pleckstrin homology domain of phospholipase C δ1. Biochem J 363:657-66.
225. Wang H, Sun H-Q, Zhu X, Zhang L, Albanesi J, Levine B, et al. (**2015**) GABARAPs regulate PI4P-dependent autophagosome:lysosome fusion. P Natl Acad Sci USA 112:7015-20.
226. Sridhar S, Patel B, Aphkhazava D, Macian F, Santambrogio L, Shields D, et al. (**2013**) The lipid kinase PI4KIIIβ preserves lysosomal identity. The EMBO Journal 32:324.
227. Lemmon MA, Ferguson KM. (**2000**) Signal-dependent membrane targeting by pleckstrin homology (PH) domains. Biochem J 350:1-18.

228. Vicinanza M, Di Campli A, Polishchuk E, Santoro M, Di Tullio G, Godi A, et al. (**2011**) OCRL controls trafficking through early endosomes via PtdIns4,5P2-dependent regulation of endosomal actin. Embo J 30:4970-85.
229. Field SJ, Madson N, Kerr ML, Galbraith KAA, Kennedy CE, Tahiliani M, et al. (**2005**) PtdIns(4,5)P2 functions at the cleavage furrow during cytokinesis. Curr Biol 15:1407-12.
230. Snider CE, Willet AH, Brown HT, Gould KL, Lew DJ. (**2018**) Analysis of the contribution of phosphoinositides to medial septation in fission yeast highlights the importance of PI(4,5)P2 for medial contractile ring anchoring. Mol Biol Cell 29:2137-242.
231. Delgado-Álvarez DL, Bartnicki-García S, Seiler S, Mouriño-Pérez RR. (**2014**) Septum development in *Neurospora crassa*: The septal actomyosin tangle. PLoS ONE 9:e96744.
232. Harris SD. (**2001**) Septum formation in *Aspergillus nidulans*. Curr Opin Microbiol 4:736-9.
233. Abe M, Makino A, Hullin-Matsuda F, Kamijo K, Ohno-Iwashita Y, Hanada K, et al. (**2012**) A role for sphingomyelin-rich lipid domains in the accumulation of phosphatidylinositol-4,5-bisphosphate to the cleavage furrow during cytokinesis. Mol Cell Biol 32:1396-407.
234. Snider CE, Willet AH, Chen J-S, Arpağ G, Zanic M, Gould KL. (**2017**) Phosphoinositide-mediated ring anchoring resists perpendicular forces to promote medial cytokinesis. J Cell Biol 216:3041-50.
235. Emoto K, Inadome H, Kanaho Y, Narumiya S, Umeda M. (**2005**) Local change in phospholipid composition at the cleavage furrow is essential for completion of cytokinesis. J Biol Chem 280:37901-7.
236. Zhang Y, Sugiura R, Lu Y, Asami M, Maeda T, Itoh T, et al. (**2000**) Phosphatidylinositol 4-phosphate 5-kinase Its3 and calcineurin Ppb1 coordinately regulate cytokinesis in fission yeast. J Biol Chem 275:35600-6.
237. Tan YY, Spiering MJ, Scott V, Lane GA, Christensen MJ, Schmid J. (**2001**) In planta regulation of extension of an endophytic fungus and maintenance of high metabolic rates in its mycelium in the absence of apical extension. Appl Environ Microb 67:5377-83.
238. Peterson MR, Burd CG, Emr SD. (**1999**) Vac1p coordinates Rab and phosphatidylinositol 3-kinase signaling in Vps45p-dependent vesicle docking/fusion at the endosome. Curr Biol 9:159-62.
239. Hickinson DM, Lucocq JM, Towler MC, Clough S, James J, James SR, et al. (**1997**) Association of a phosphatidylinositol-specific 3-kinase with a human *trans*-Golgi network resident protein. Curr Biol 7:987-90.
240. Jones AT, Mills IG, Scheidig AJ, Alexandrov K, Clague MJ. (**1998**) Inhibition of endosome fusion by wortmannin persists in the presence of activated rab5. Mol Biol Cell 9:323-32.
241. Fernandez-Borja M, Wubbolts R, Calafat J, Janssen H, Divecha N, Dusseljee S, et al. (**1999**) Multivesicular body morphogenesis requires phosphatidylinositol 3-kinase activity. Curr Biol 9:55-8.
242. De Matteis MA, Di Campli A, Godi A. (**2005**) The role of the phosphoinositides at the Golgi complex. Biochim Biophys ACTA 1744:396-405.
243. Kutateladze T, Overduin M. (**2001**) Structural mechanism of endosome docking by the FYVE domain. Science 291:1793-6.

244. Stenmark H, Aasland R, Driscoll PC. (**2002**) The phosphatidylinositol 3-phosphate-binding FYVE finger. FEBS Lett 513:77-84.
245. Traer CJ, Rutherford AC, Palmer KJ, Wassmer T, Oakley J, Attar N, et al. (**2007**) SNX4 coordinates endosomal sorting of TfnR with dynein-mediated transport into the endocytic recycling compartment. Nat Cell Biol 9:1370-80.
246. Simonsen A, Lippe R, Christoforidis S, Gaullier J-M, Brech A, Callaghan J, et al. (**1998**) EEA1 links PI(3)K function to Rab5 regulation of endosome fusion. Nature 394:494-8.
247. Rubino M, Miaczynska M, Lippé R, Zerial M. (**2000**) Selective membrane recruitment of EEA1 suggests a role in directional transport of clathrin-coated vesicles to early endosomes. J Biol Chem 275:3745-8.
248. Burd CG, Emr SD. (**1998**) Phosphatidylinositol(3)-phosphate signaling mediated by specific binding to RING FYVE domains. Mol Cell 2:157-62.
249. Xu H, Wickner W. (**2010**) Phosphoinositides function asymmetrically for membrane fusion, promoting tethering and 3Q-SNARE subcomplex assembly. J Biol Chem 285:39359-65.
250. Steinberg G. (**2007**) Hyphal growth: A tale of motors, lipids, and the Spitzenkorper. Eukaryot Cell 6:351-60.
251. Crampin H, Finley K, Gerami-Nejad M, Court H, Gale C, Berman J, et al. (**2005**) *Candida albicans* hyphae have a Spitzenkörper that is distinct from the polarisome found in yeast and pseudohyphae. J Cell Sci 118:2935-47.
252. Fischer-Parton S, Parton RM, Hickey PC, Dijksterhuis J, Atkinson HA, Read ND. (**2000**) Confocal microscopy of FM4-64 as a tool for analysing endocytosis and vesicle trafficking in living fungal hyphae. J Microsc-Oxford 198:246-59.
253. Hoffmann J, Mendgen K. (**1998**) Endocytosis and membrane turnover in the germ tube of *Uromyces fabae*. Fungal Genet Biol 24:77-85.
254. Fuchs U, Hause G, Schuchardt I, Steinberg G. (**2006**) Endocytosis is essential for pathogenic development in the corn smut fungus *Ustilago maydis*. Plant Cell 18:2066-81.
255. Munson MJ, Ganley IG. (**2016**) Determination of ellular phosphatidylinositol-3-phosphate (PI3P) levels using a fluorescently labelled selective PI3P binding domain (PX). Bio-protocol 6:e1903.
256. Shoji J-y, Charlton ND, Yi M, Young CA, Craven KD. (**2015**) Vegetative hyphal fusion and subsequent nuclear behavior in *Epichloë* grass endophytes. PLoS ONE 10:e0121875.
257. Venkateswarlu K, Oatey PB, Tavaré JM, Cullen PJ. (**1998**) Insulin-dependent translocation of ARNO to the plasma membrane of adipocytes requires phosphatidylinositol 3-kinase. Curr Biol 8:463-6.
258. Marshall AJ, Krahn AK, Ma K, Duronio V, Hou S. (**2002**) TAPP1 and TAPP2 are targets of phosphatidylinositol 3-kinase signaling in B cells: Sustained plasma membrane recruitment triggered by the B-cell antigen receptor. Mol Cell Biol 22:5479-91.
259. Lam P-y, Yoo SK, Green JM, Huttenlocher A. (**2012**) The SH2-domain-containing inositol 5-phosphatase (SHIP) limits the motility of neutrophils and their recruitment to wounds in zebrafish. J Cell Sci 125:4973-8.
260. Dowler S, Currie RA, Campbell DG, Deak M, Kular G, Downes CP, et al. (**2000**) Identification of pleckstrin-homology-domain-containing proteins with novel phosphoinositide-binding specificities. Biochem J 351:19-31.

261. Strijbis K, Tafesse FG, Fairn GD, Witte MD, Dougan SK, Watson N, et al. (**2013**) Bruton's tyrosine kinase (BTK) and Vav1 contribute to Dectin1-dependent phagocytosis of *Candida albicans* in macrophages. PLoS Pathog 9:e1003446.
262. Yip S-C, Eddy RJ, Branch AM, Pang H, Wu H, Yan Y, et al. (**2008**) Quantitation of PI[3,4,5]P3 dynamics in EGF-stimulated carcinoma cells: A comparison of PH domain-mediated versus immunological methods. Biochem J 411:441-8.
263. Isakoff SJ, Cardozo T, Andreev J, Li Z, Ferguson KM, Abagyan R, et al. (**1998**) Identification and analysis of PH domain-containing targets of phosphatidylinositol 3-kinase using a novel *in vivo* assay in yeast. Embo J 17:5374-87.
264. Gibson DG, Young L, Chuang R-Y, Venter JC, Hutchison Iii CA, Smith HO. (**2009**) Enzymatic assembly of DNA molecules up to several hundred kilobases. Nat Meth 6:343-5.
265. Goswami RS. (**2012**) Targeted gene replacement in fungi using a split-marker approach. In: Bolton MD, Thomma BPHJ, editors. Plant fungal pathogens: Methods and protocols. Totowa, NJ: Humana Press; p. 255-69.

6. Appendices

6.1 Summary of lipid binding domains used in this study

Mammalian protein	Lipid binding domain	Lipid target	Plasmids	Protein details	Reference
Hepatocyte growth factor-regulated tyrosine kinase substrate (HGS)	FYVE	PI[3]P	pCE106, pCE111	Accession NP_001152800, amino acids 155-222 based on longest prediction from InterPro v.55 (IPR013083)	(134)
Second PH domain of pleckstrin homology domain-containing family A member 2 (Plekha2; also known as TAPP2 (Tandem PH-domain-containing protein-2))	PH	PI[3,4]P_2	pCE108, pCE113	Accession NP_112547, amino acids 195-304 based on longest prediction from InterPro v.55 (IPR011993)	(260)
Bruton's tyrosine kinase (BTK)	PH	PI[3,4,5]P_3	pCE107, pCE112	Accession NP_038510, amino acids 3-169 based on longest prediction from InterPro v.55 (IPR011993)	(167)
PH domain of pleckstrin homology domain-containing family A member 3 (Plekha3; also known as FAPP1 (four phosphate-adapter protein 1))	PH	PI[4]P	pCE109, pCE114	Accession NP_112546, amino acids 1-96 based on longest prediction from InterPro v.55 (IPR011993)	(134)
Phospholipase C-δ1 (PLC-δ1)	PH	PI[4,5]P_2	pCE105, pCE110	Accession NP_062650, amino acids 13-139 based on longest prediction from InterPro v.55 (IPR011993)	(136)

6.2 Construct preparation

All constructs were designed and prepared by Dr Carla Eaton.

6.2.1 Cdc24 localisation constructs

Constructs expressing full length Cdc24 and Cdc24 with the PH domain removed (ΔPH) were generated using Gibson assembly. pCE127 (Appendix 6.3.3.1) was made by cloning the *gpdA* promoter, full length *cdc24*, eGFP, and the *trpC* terminator into the pRS426 backbone. pCE124 (Appendix 6.3.3.2) was made in the same fashion except *cdc24* was amplified in two pieces to exclude the PH domain. Primers were designed to include a 5xGly linker between Cdc24 and eGFP in each construct to allow for correct protein folding.

6.2.2 Biosensor constructs

The mouse lipid binding domains (LBDs) were codon optimised for expression in fungi using codon usage information generated for *E. festucae*. Codon usage frequency was determined by comparison of all *E. festucae* Fl1 coding sequences and corresponding protein sequences (Schardl et al, 2013). The codon optimised LBD were fused to mCherry at the N-terminus with a 6x glycine linker generated as inserts in the vector pUC57 by GenScript USA Inc. The LBD was then amplified from these constructs and fused to eGFP at the C-terminus with a 5x glycine linker using Gibson assembly (264). Gibson assembly was further used to clone the mCherry-6Gly-LBD and LBD-5Gly-eGFP fragments under the control of the *gpdA* promoter and *trpC* terminator, to generate either P*gpdA*-mCherry-6Gly-LBD-T*trpC* or P*gpdA*-LBD-5Gly-eGFP-T*trpC* fragments within the yeast vector pRS426 (Appendix 6.3.1.1-6.3.1.10). The 5 and 6xGly linkers were placed to allow for correct protein folding of both LBD and fluorophore. In addition, control constructs in which mCherry or eGFP were cloned under the control of P*gpdA* and T*trpC* were generated to express free mCherry and eGFP (Appendix 6.3.1.11 and 6.3.1.12).

6.2.3 *mssD* OE construct

The 3029 bp *mssD* coding sequence was cloned under control of P*gpdA* and T*trpC* using Gibson Assembly to generate a P*gpdA*-*mssD*-T*trpC* fragment within the yeast vector pRS426 (Appendix 6.3.2).

6.2.4 *mssD* KO construct

The *mssD* replacement construct, pCE98 was generated by Gibson assembly (Gibson et al, 2009; Gibson, 2011). A 1208 bp PCR fragment 5' of *mssD* and a 1020 bp PCR fragment 3' of *mssD* were amplified using Phusion High Fidelity DNA polymerase (Thermo Fisher). To facilitate Gibson assembly, primers for amplification of the 5' flanking fragment contained overlap to pRS426 (mss1) and to the *hph* hygromycin resistance cassette (mss2), and primers for amplification of the 3' flanking fragment contained overlap to the *hph* resistance cassette (mss3) and to pRS426 (mss4). For replacement of *mssD*, a split marker approach (265) was employed in which the *mssD* replacement fragment was amplified as two pieces (mss1/hph-split-R 2025 bp; hph-split-F/mss4 2155 bp) with a 501 bp overlap in the middle of the *hph* resistance cassette. Protoplasts were then transformed with 2.5 □g of each fragment and transformants selected on media containing hygromycin. Theoretically all resistant transformants should be gene replacement mutants as homologous recombination is required to generate the full length hygromycin resistance cassette.

6.3 Construct maps

Maps of vectors routinely used in this study are presented below.

6.3.1 Cdc24 constructs

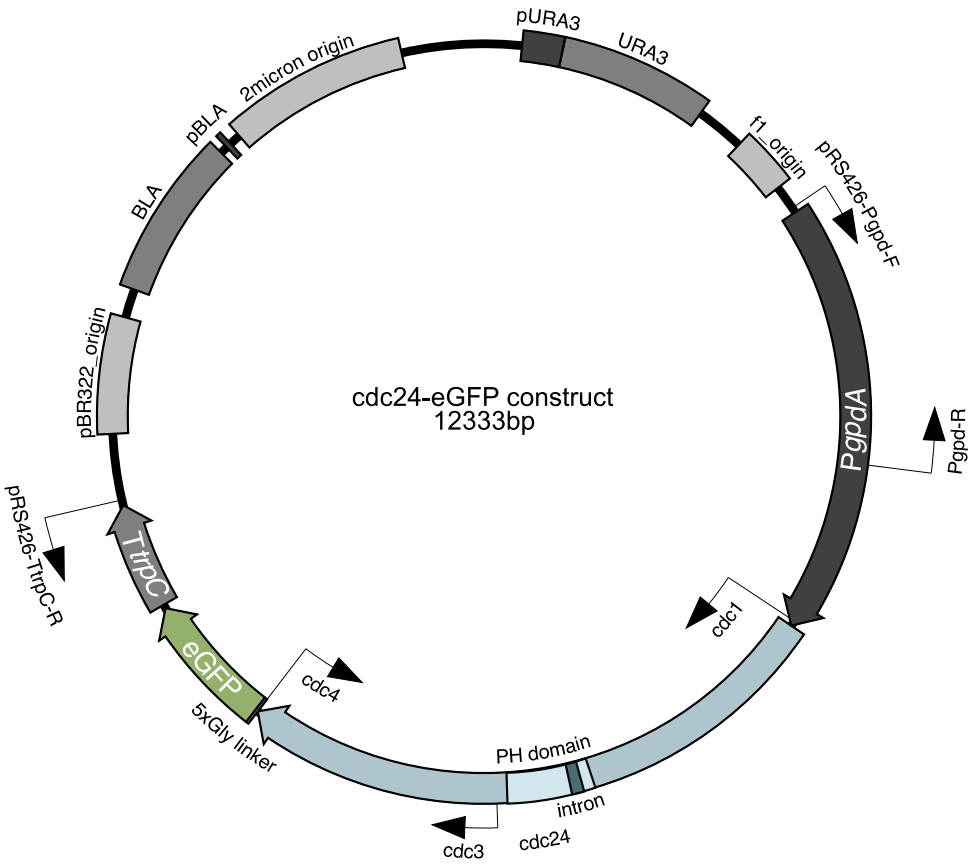

6.3.1.1 Cdc24-eGFP (pCE127)

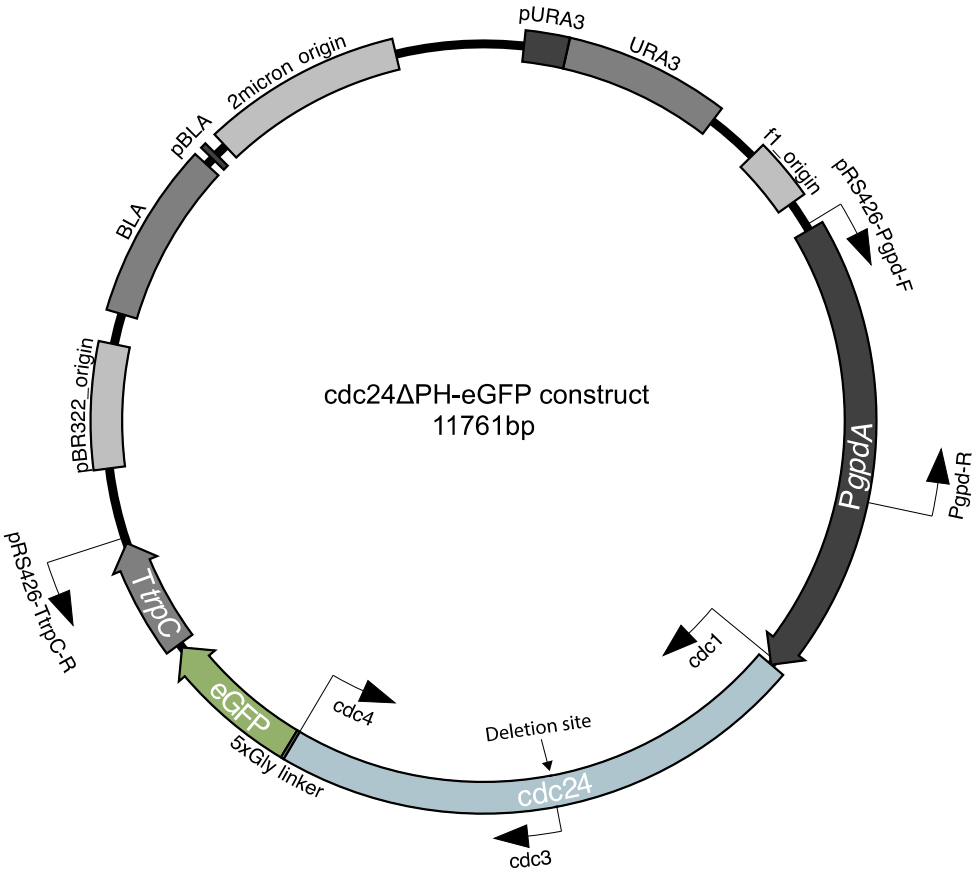

6.3.1.2 Cdc24ΔPH-eGFP (pCE124)

6.3.2 Biosensor constructs

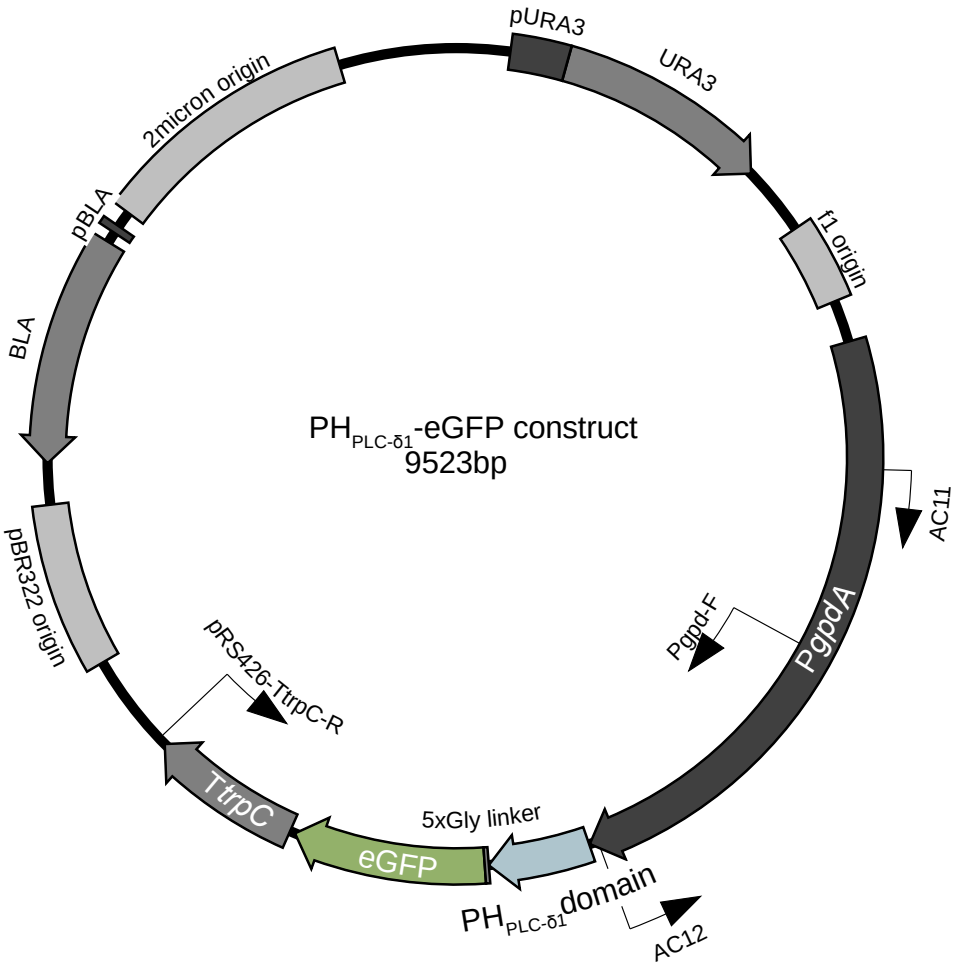

6.3.2.1 PI[4,5]P_2 eGFP biosensor (pCE105)

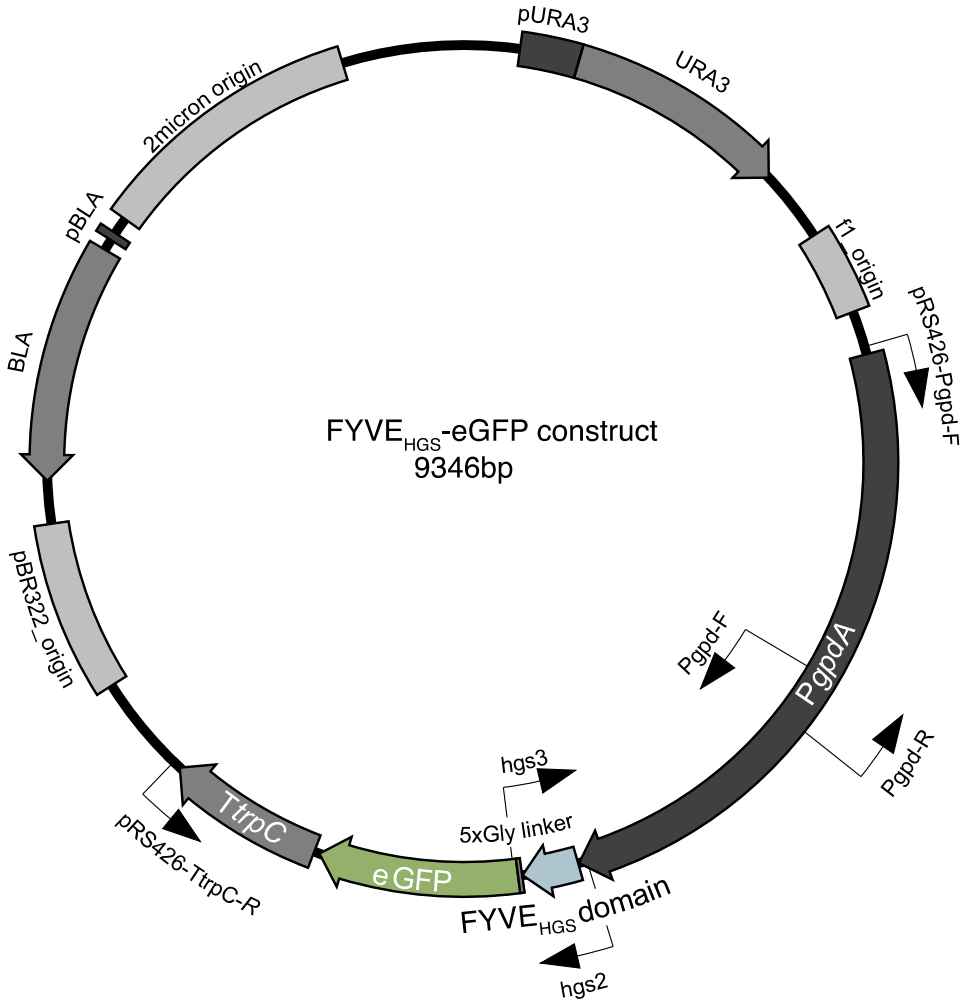

6.3.2.2 PI[3]P eGFP biosensor (pCE106)

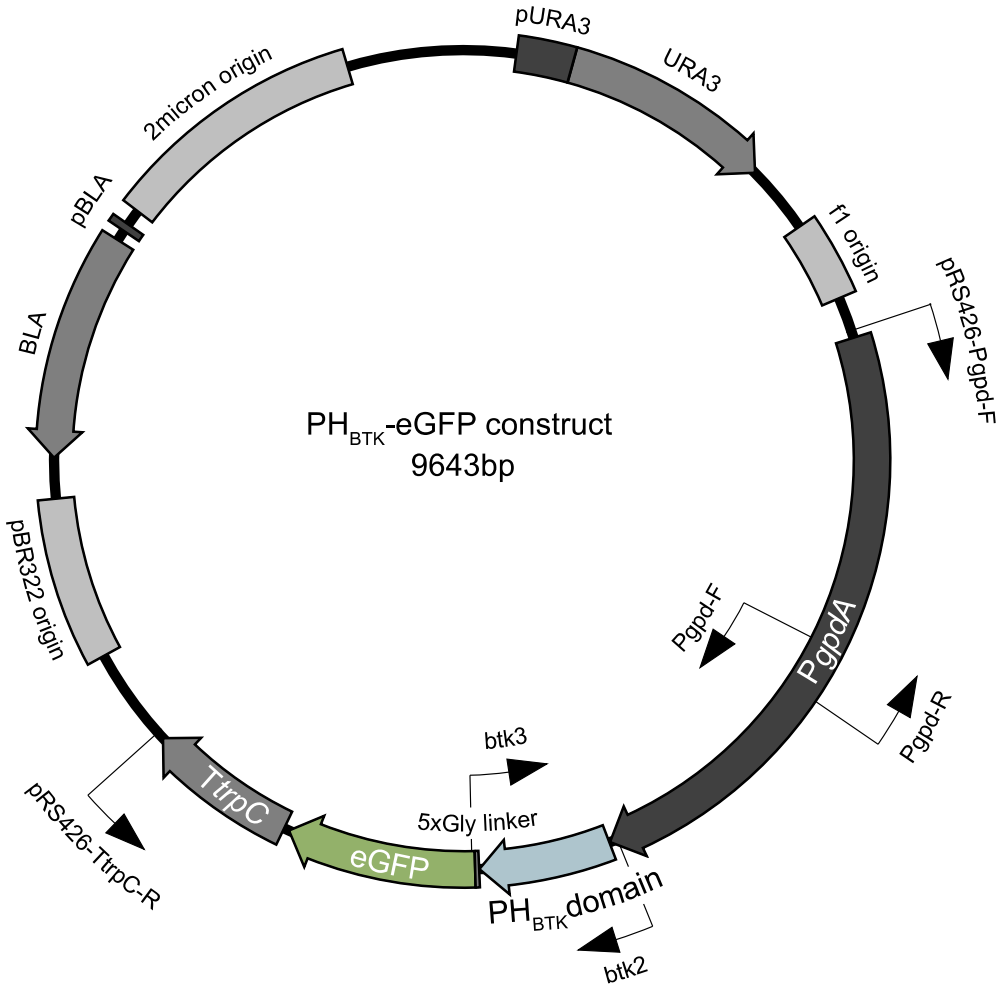

6.3.2.3 PI[3,4,5]P_3 eGFP biosensor (pCE107)

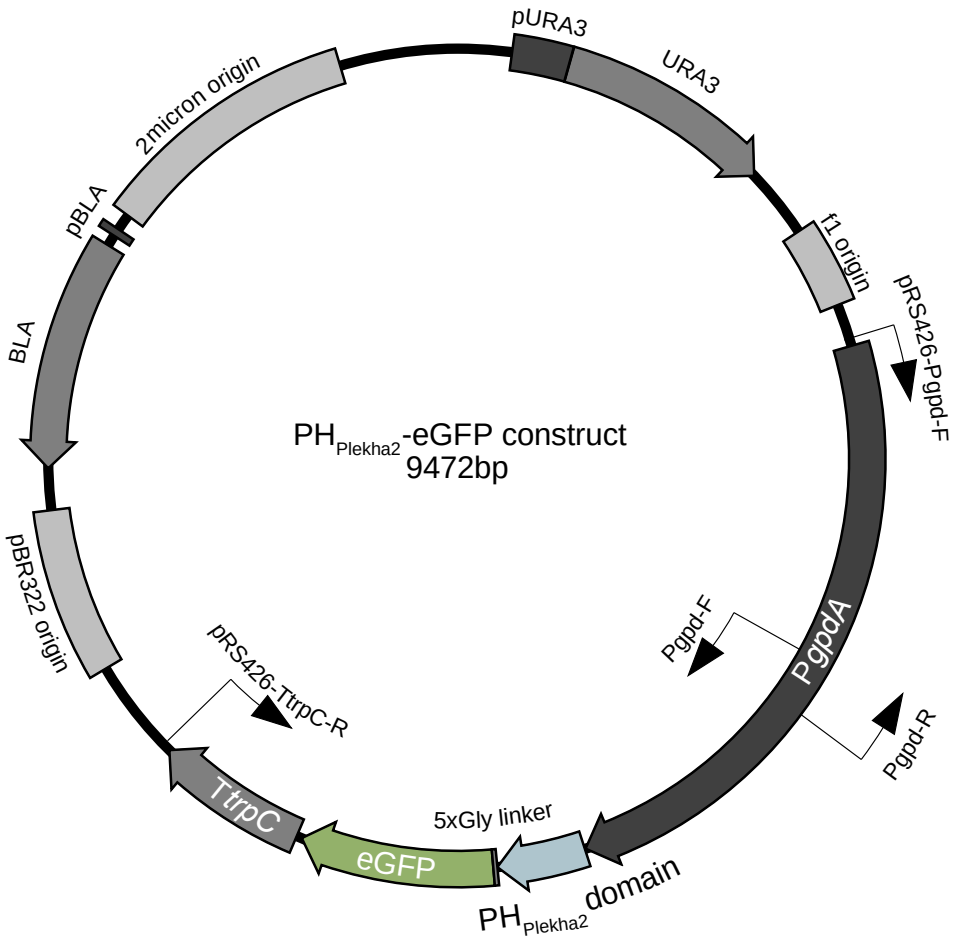

6.3.2.4 PI[3,4]P_2 eGFP biosensor (pCE108)

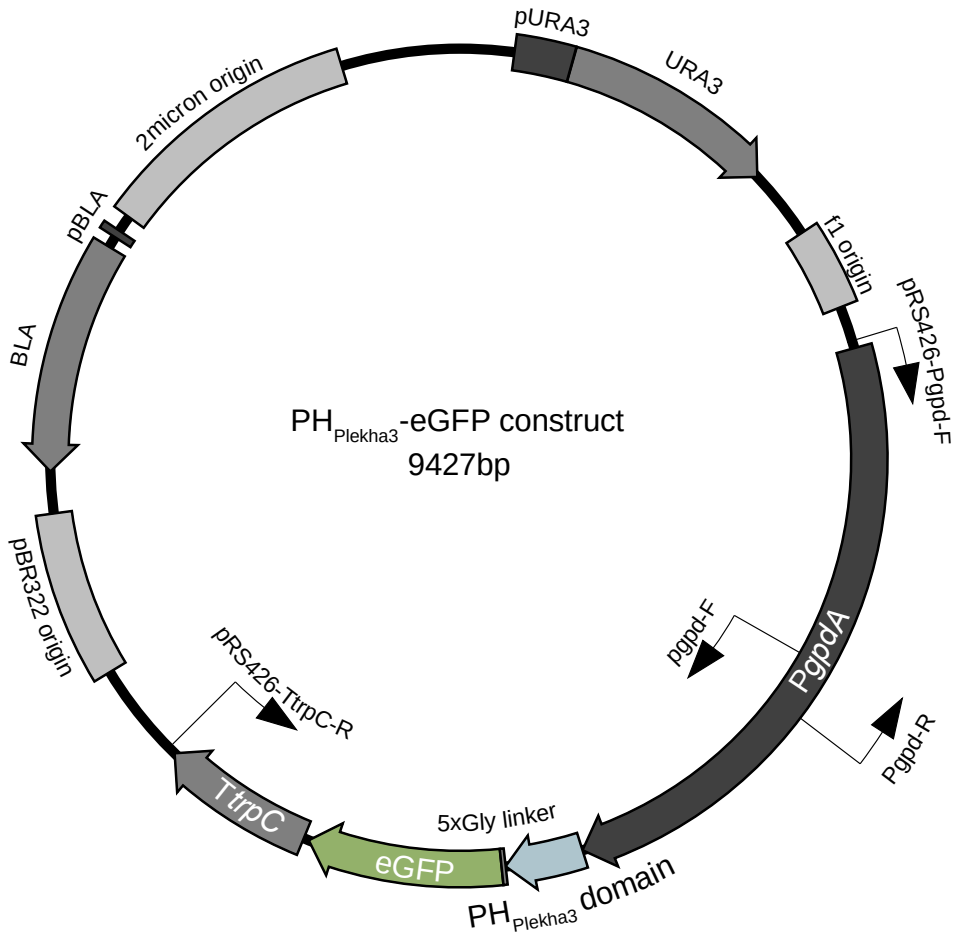

6.3.2.5 PI[4]P eGFP biosensor (pCE109)

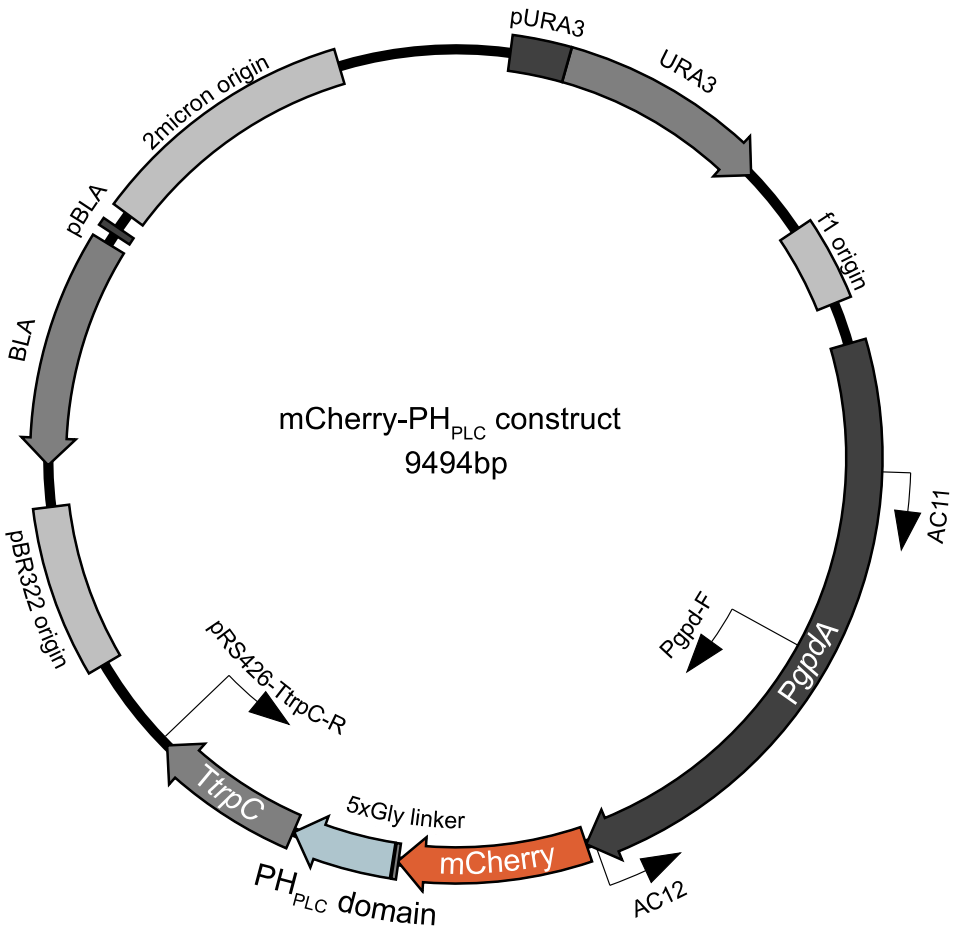

6.3.2.6 PI[4,5]P_2 mCherry biosensor (pCE110)

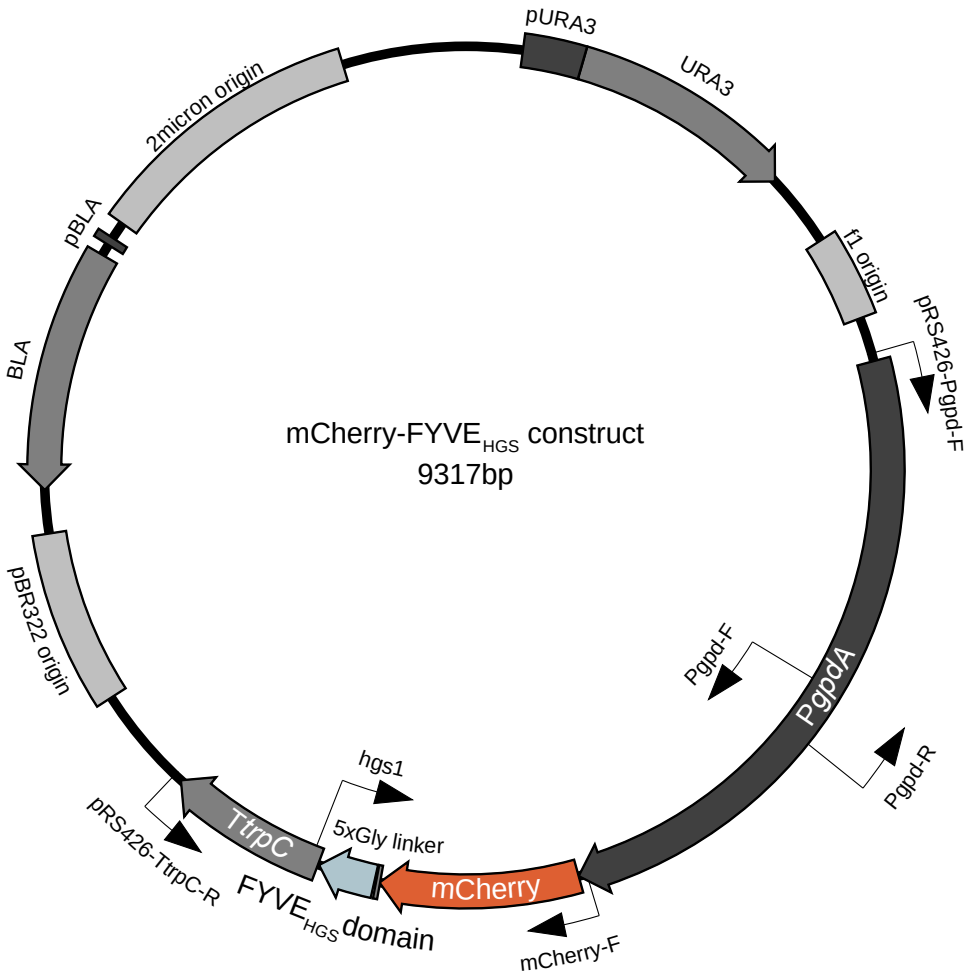

6.3.2.7 PI[3]P mCherry biosensor (pCE111)

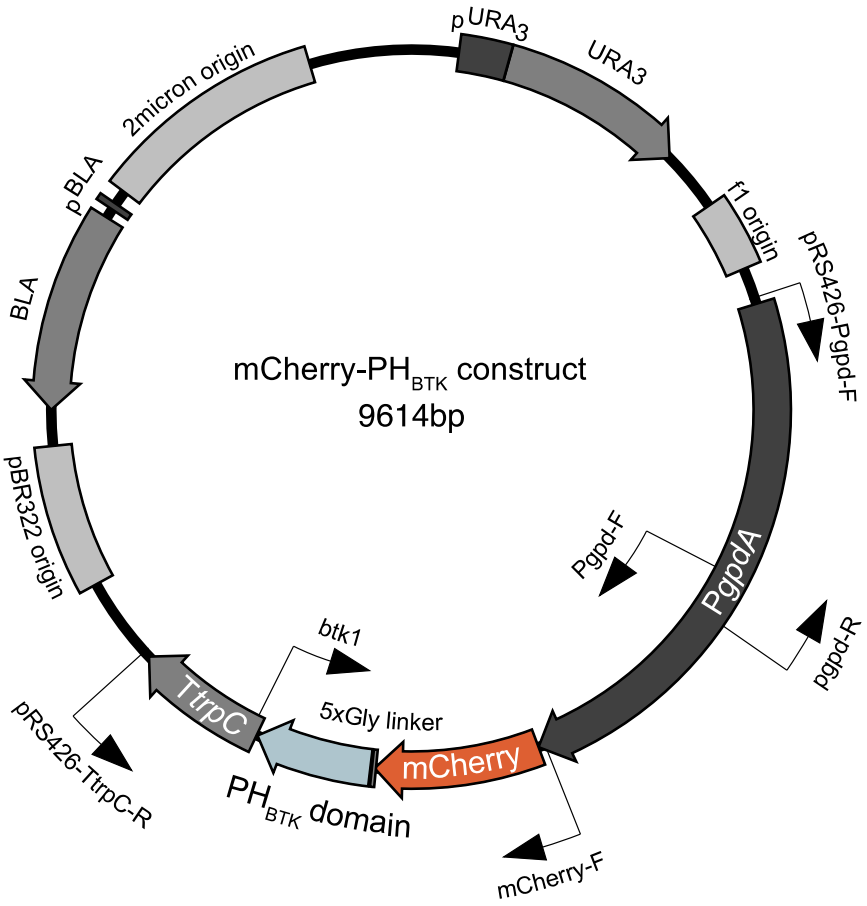

6.3.2.8 PI[3,4,5]P_3 mCherry biosensor (pCE112)

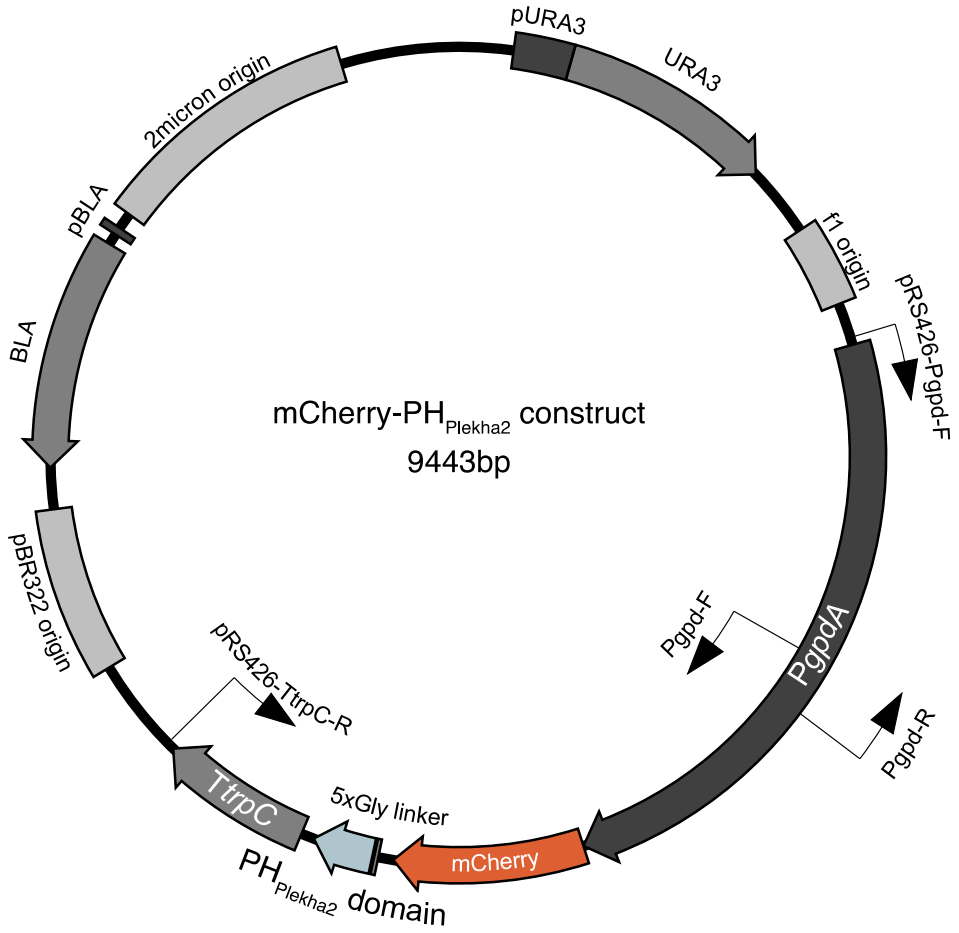

6.3.2.9 PI[3,4]P_2 mCherry biosensor (pCE113)

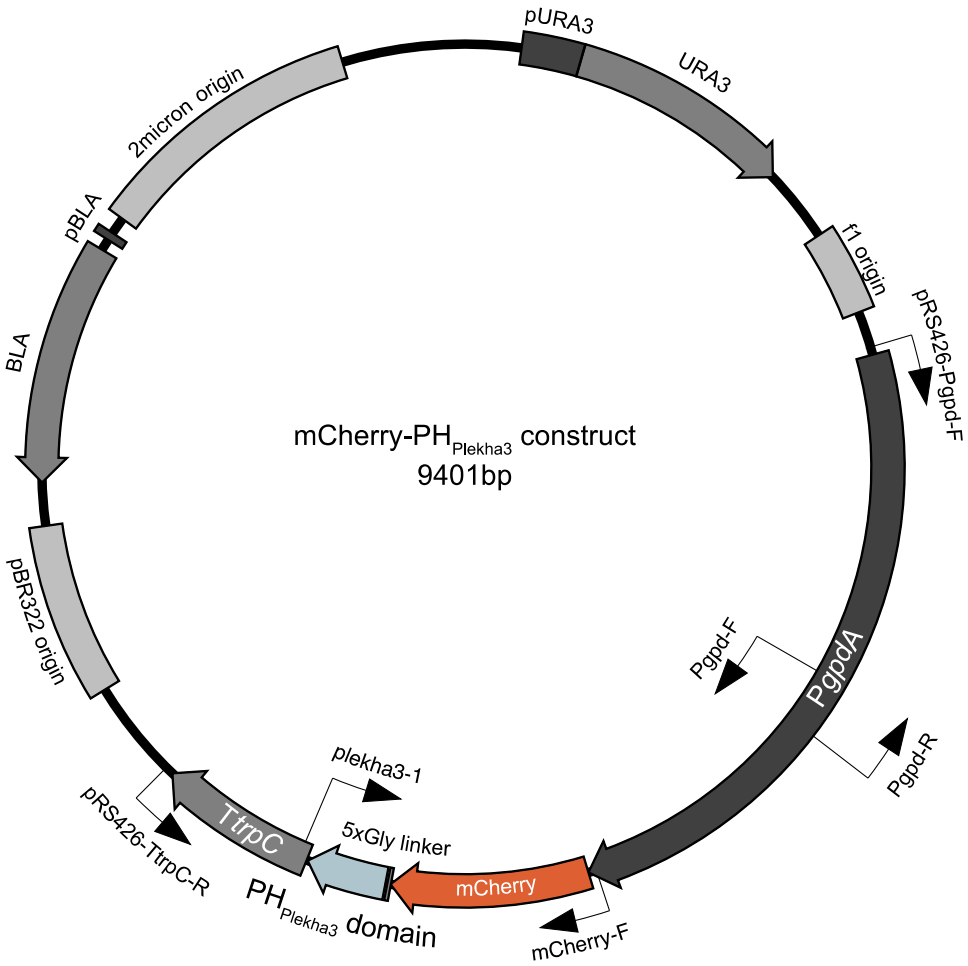

6.3.2.10 PI[4]P mCherry biosensor (pCE114)

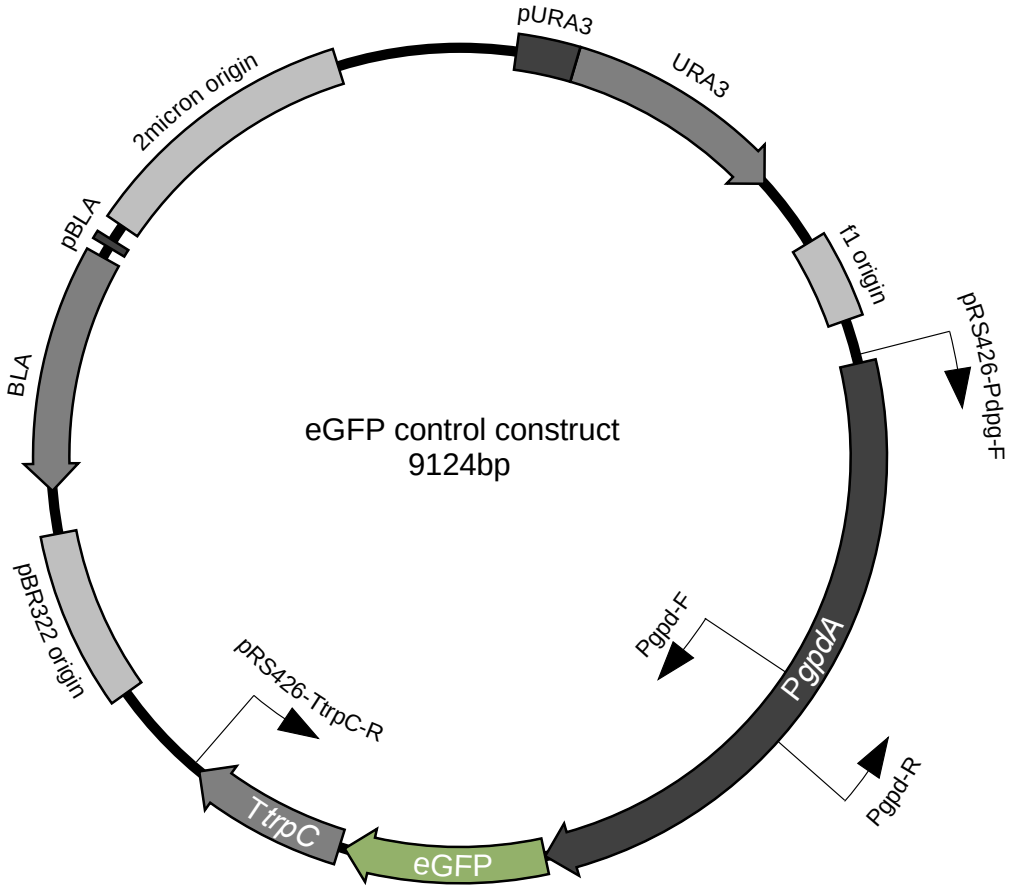

6.3.2.11 eGFP control (pCE125)

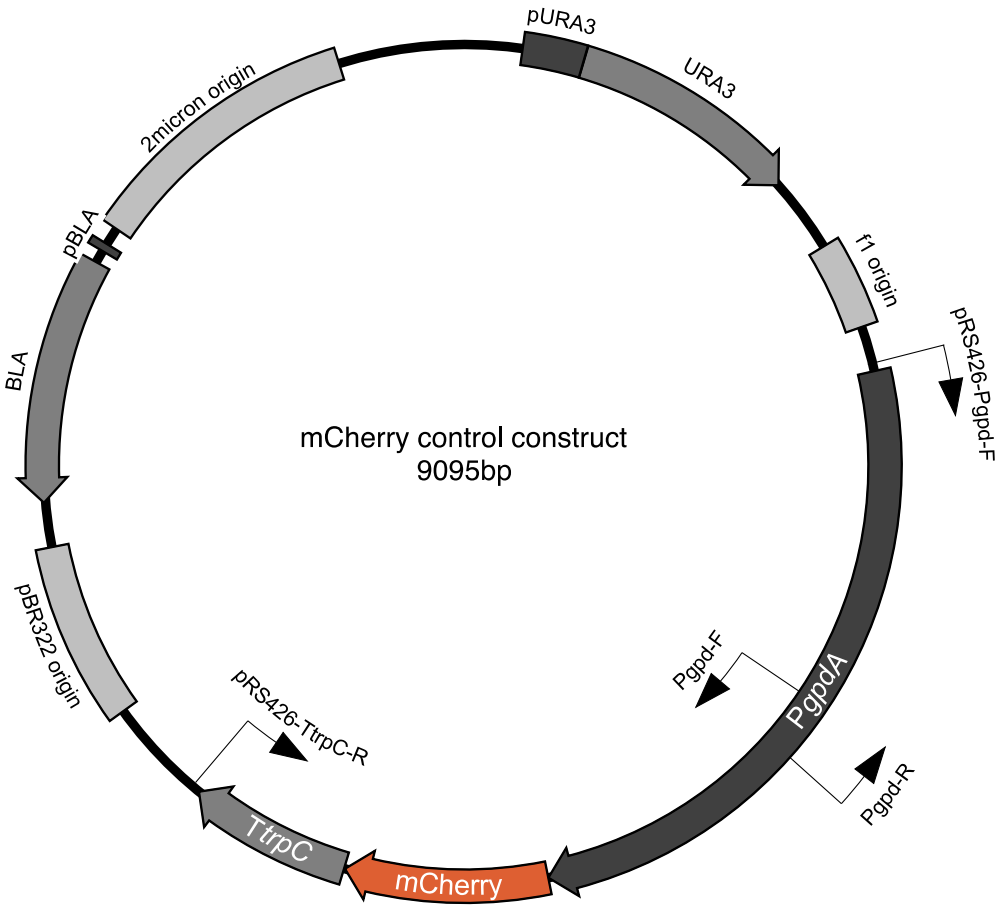

6.3.2.12 mCherry control (pCE1126)

6.3.3 MssD constructs

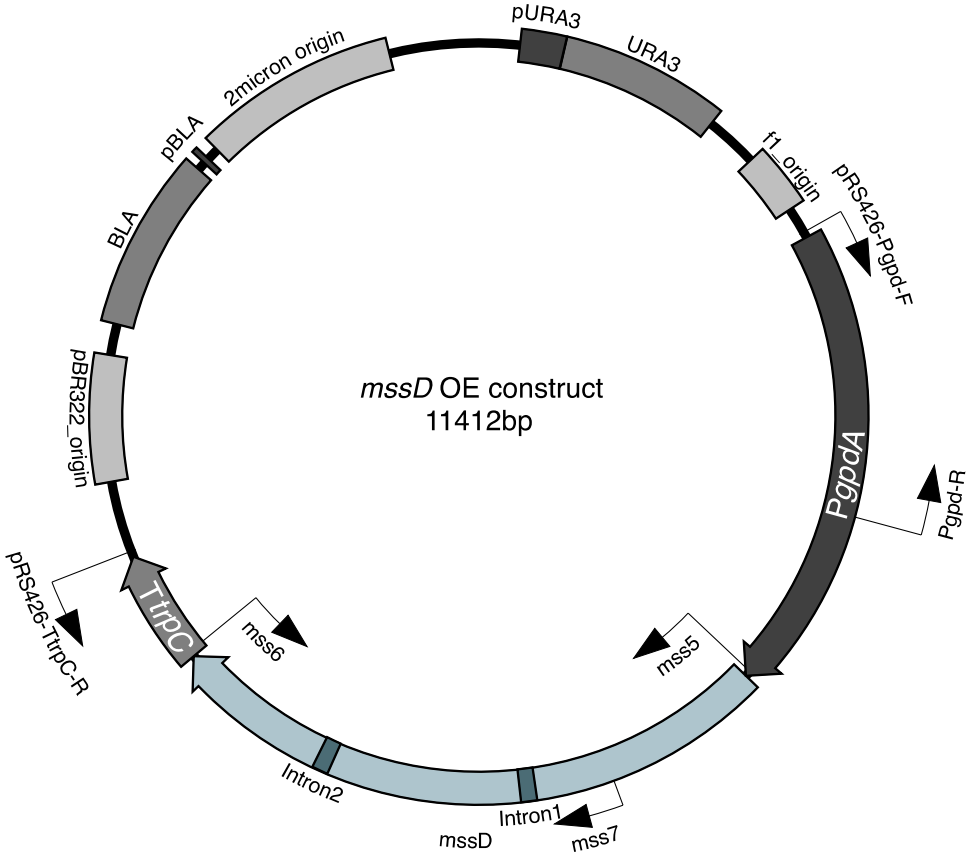

6.3.3.1 *mssD* OE construct (pCE101)

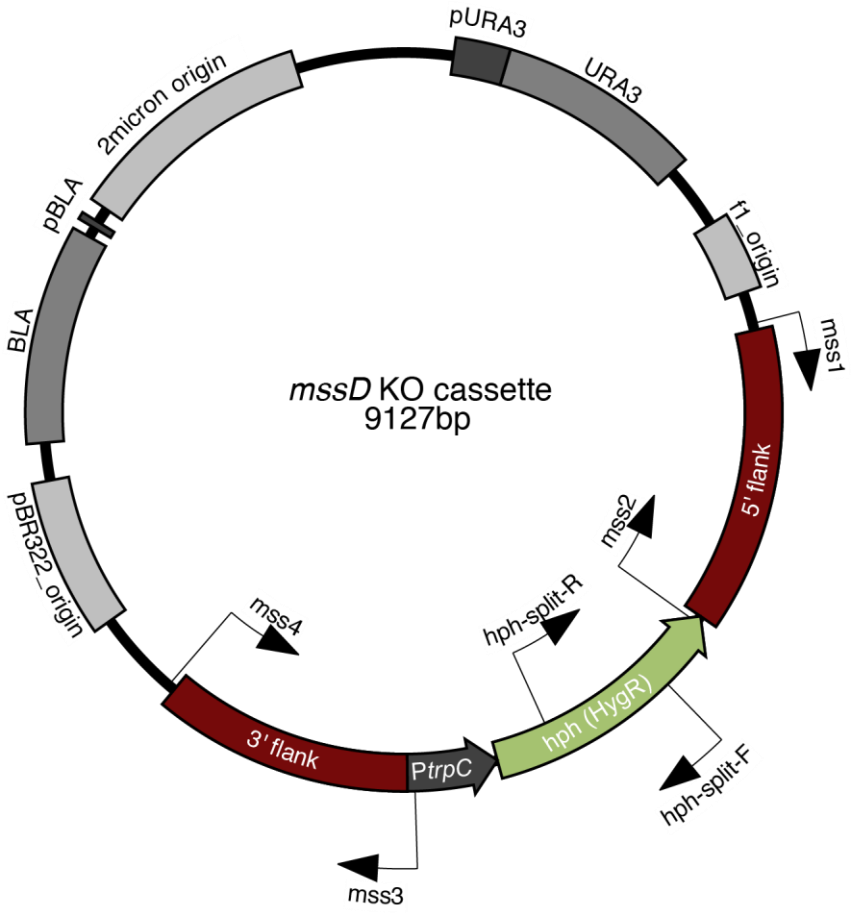

6.3.3.2 *mssD* KO cassette (pCE98)

6.3.4 Resistance plasmids

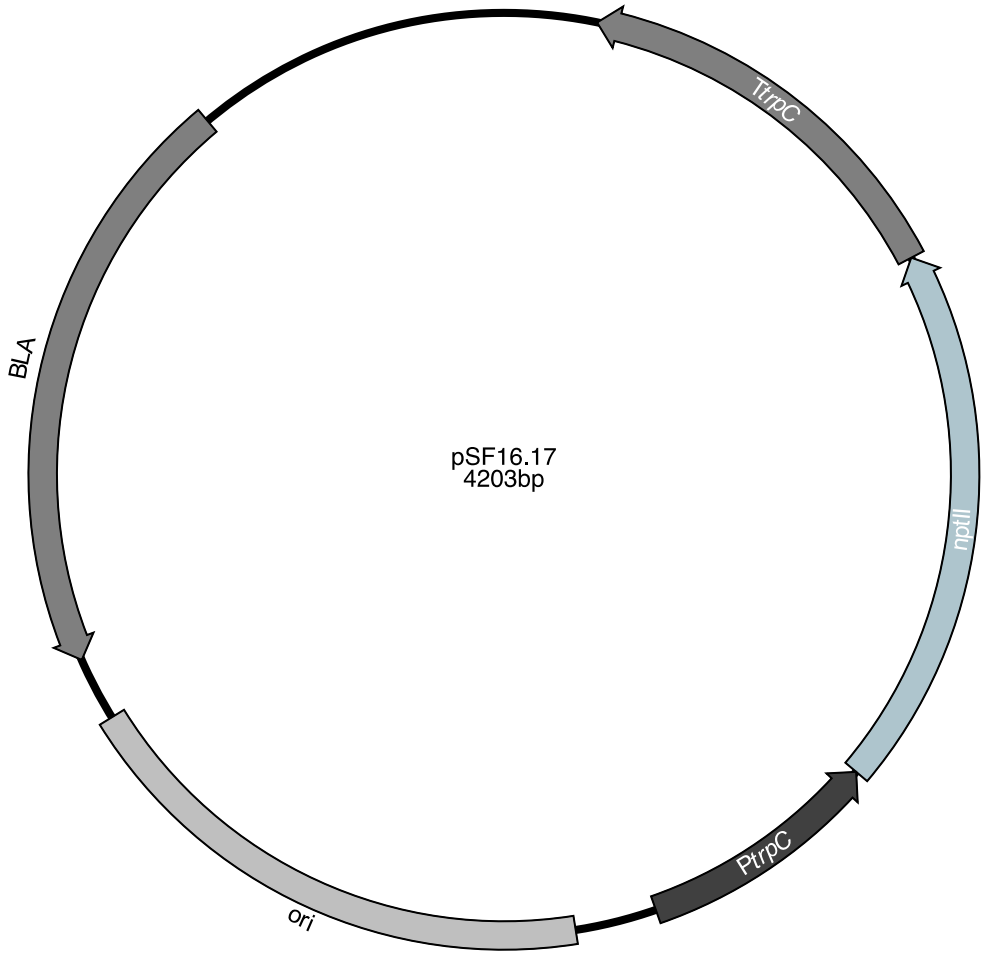

6.3.4.1 pSF16.17, geneticin resistance

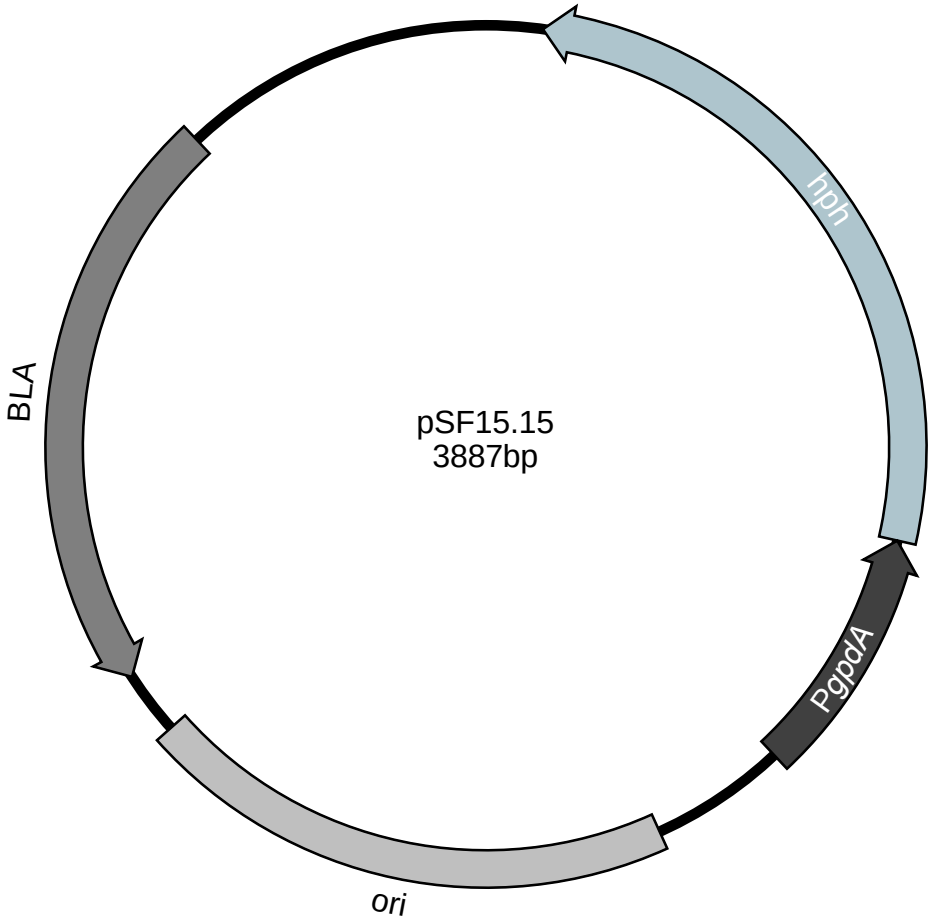

6.3.4.2 pSF15.15, hygromycin resistance

6.4 Supplementary images of Cdc24-eGFP and Cdc24ΔPH-eGFP localisation in culture.

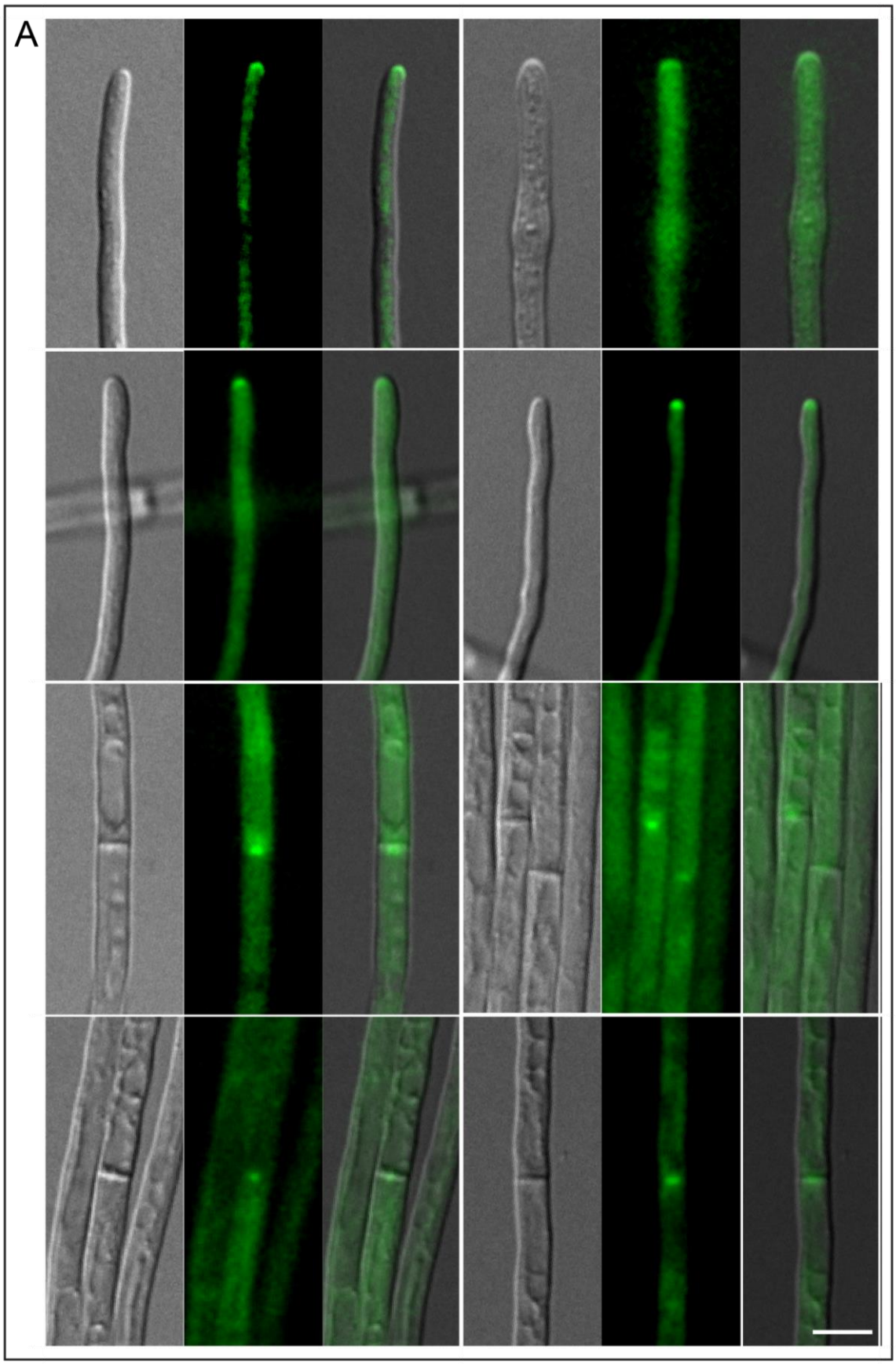

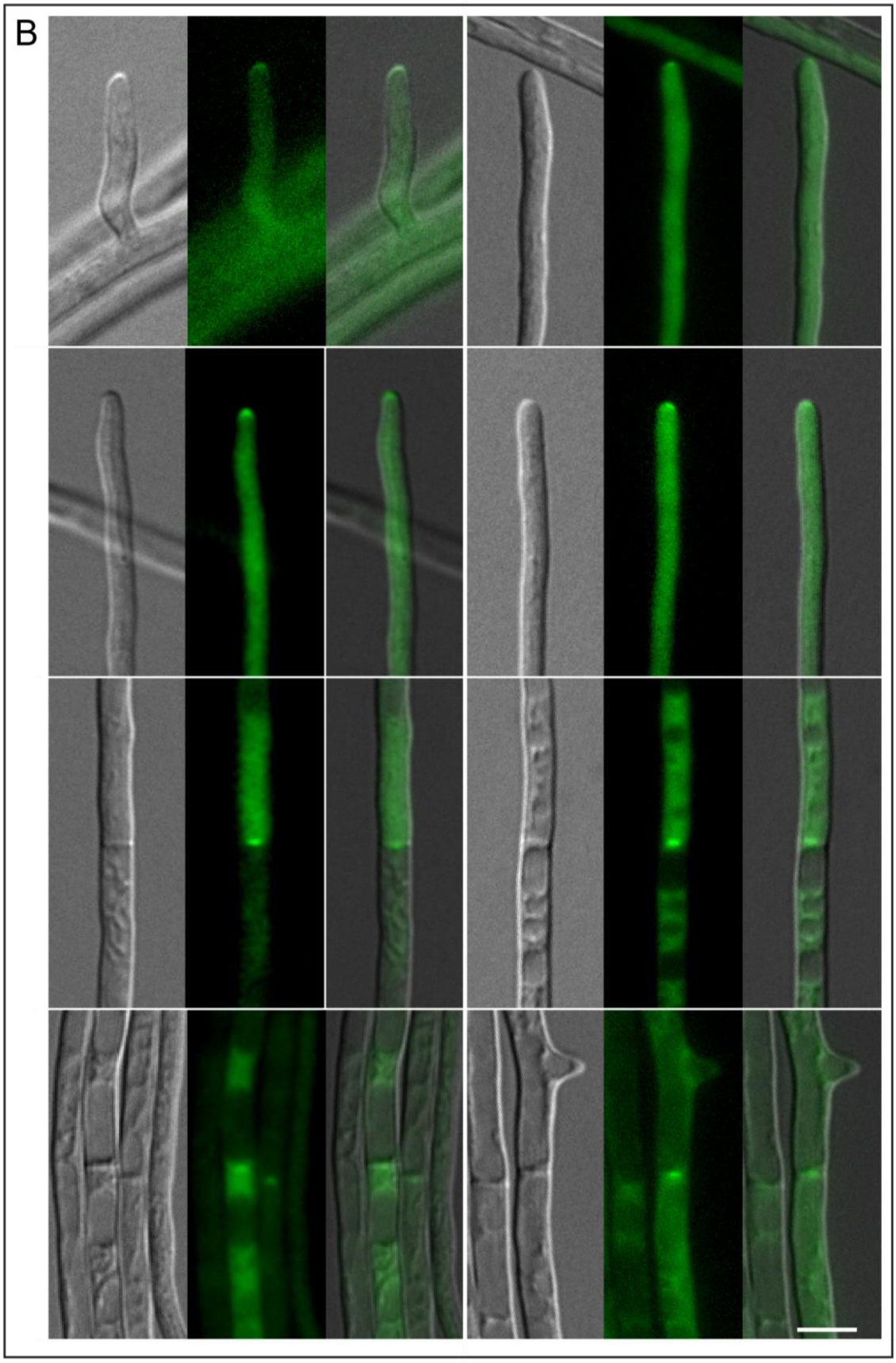
B

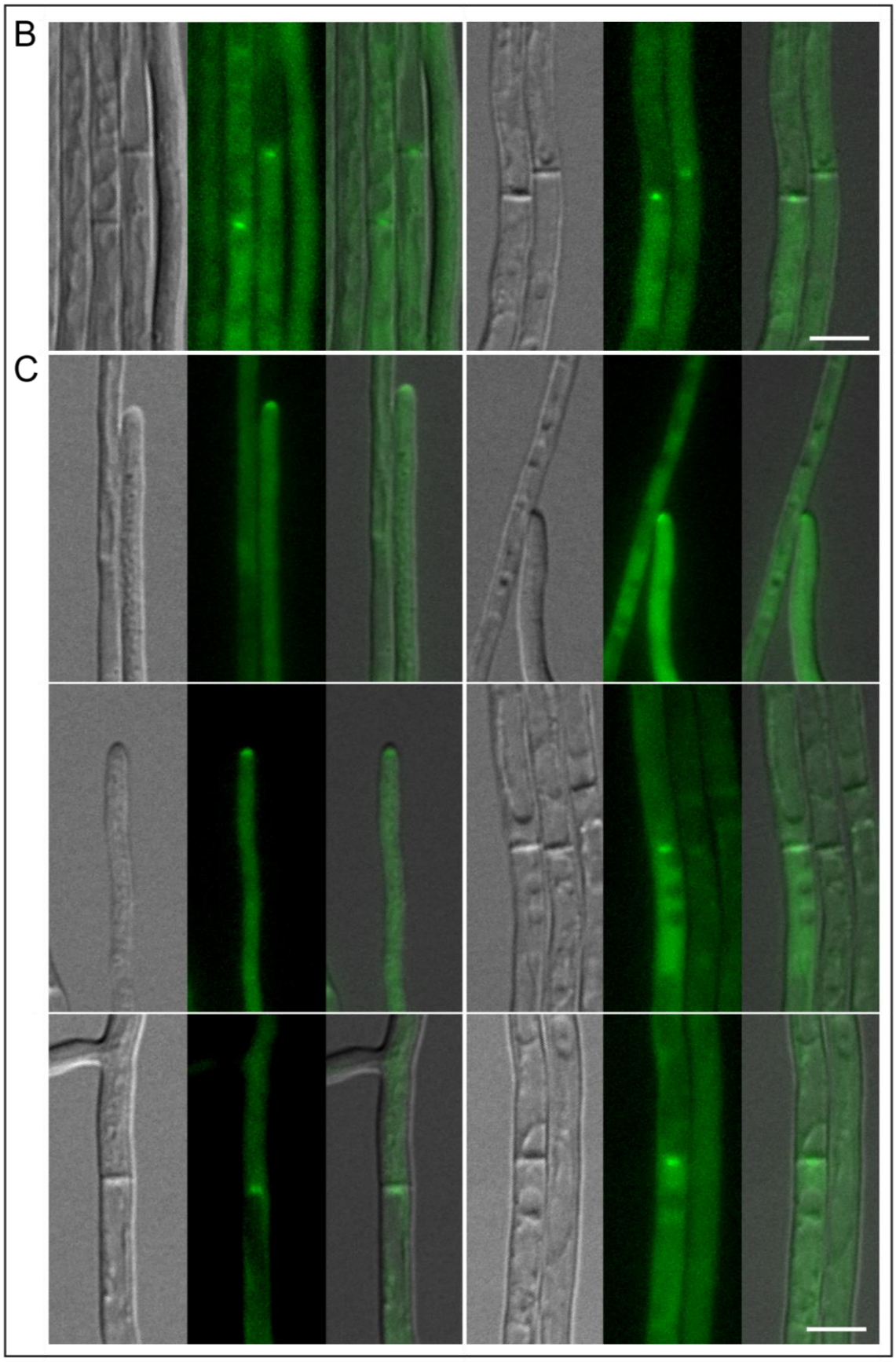
B
C

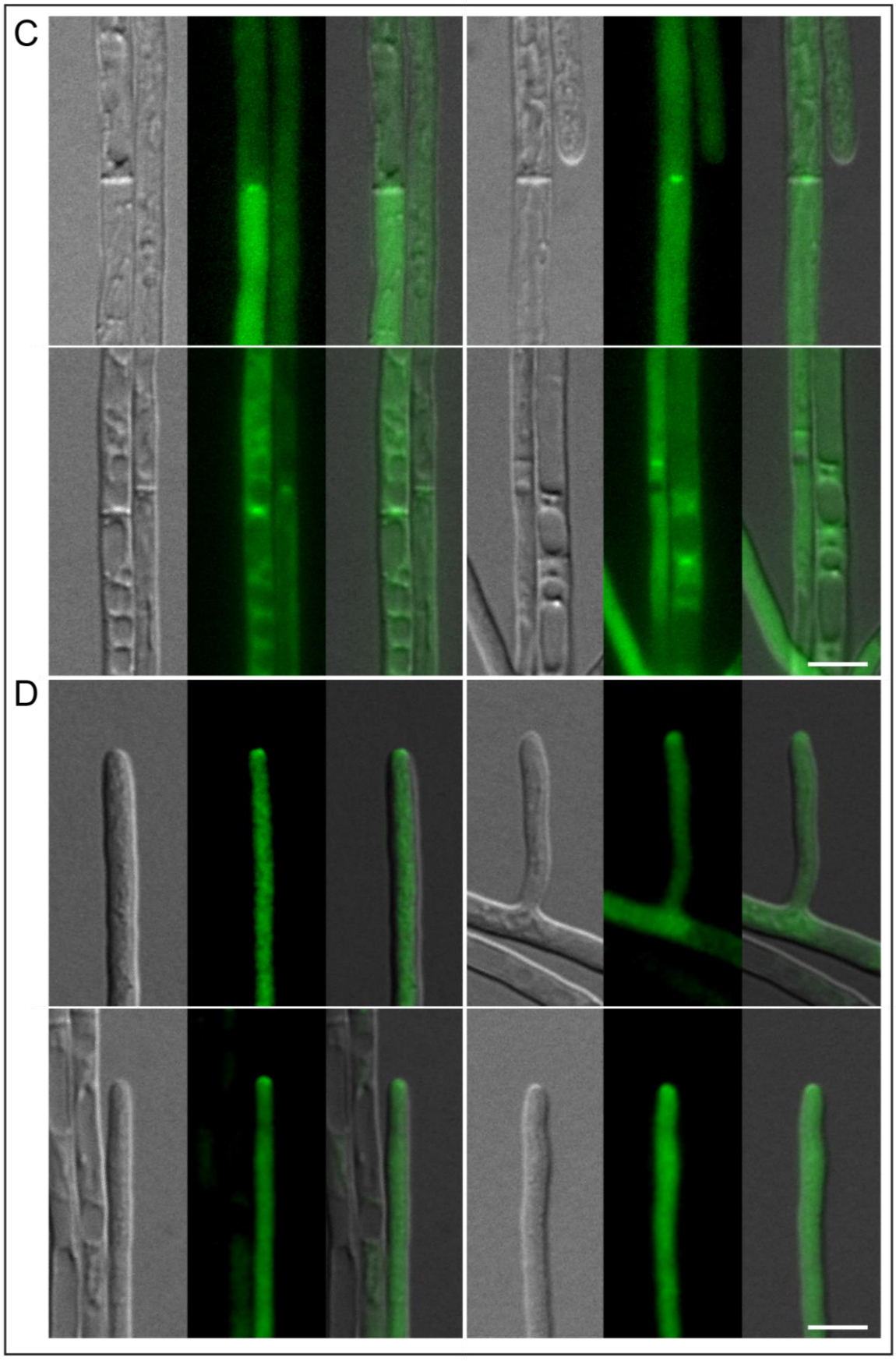
C
D

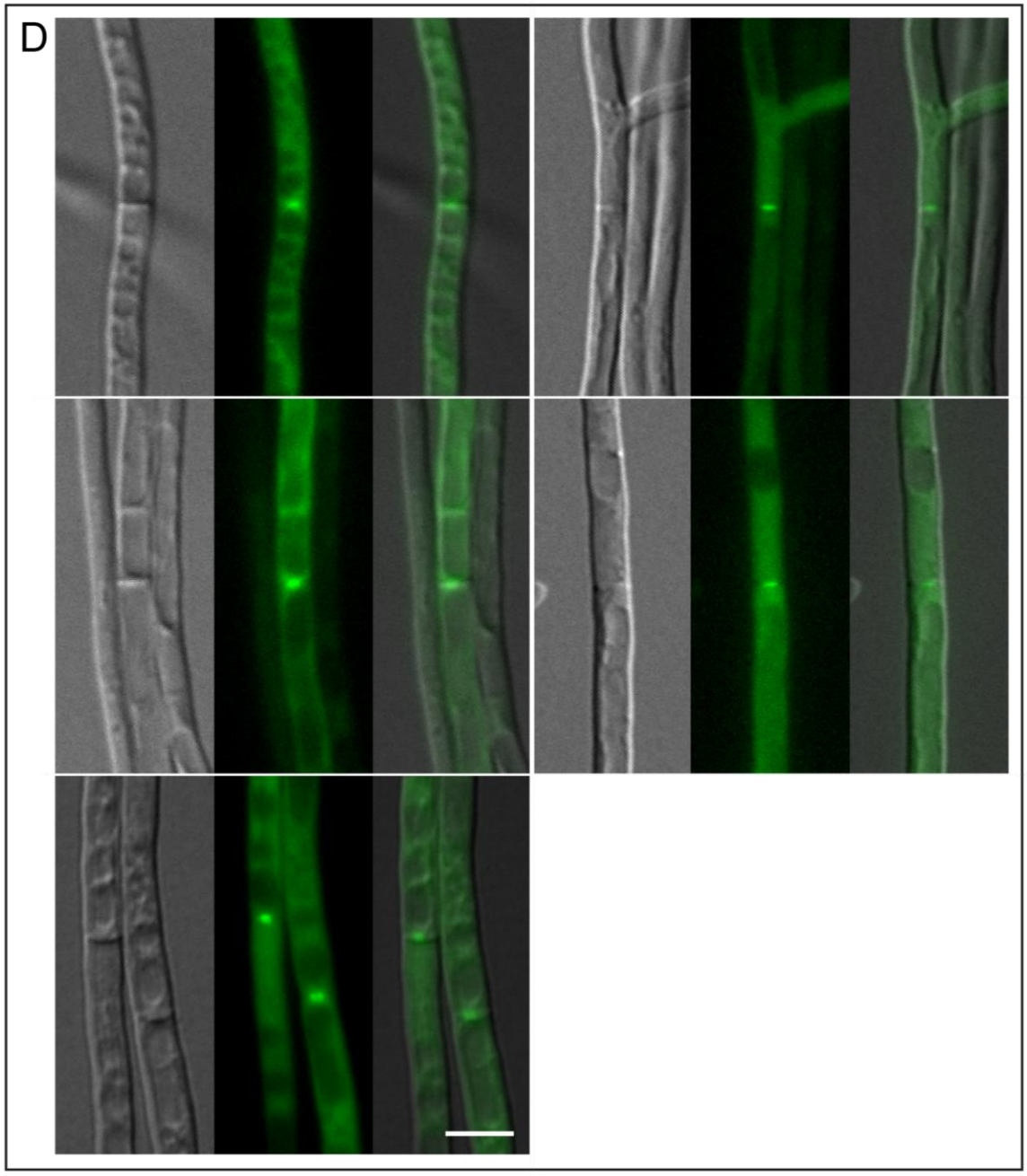

6.4.1 Cdc24-eGFP construct. Differential interference contrast and fluorescent microscopy images of Cdc24-eGFP in the following strains (A) EFS88, (B) EFS89, (C) EFS90, and (D) EFS91. Fluorescence signals have been pseudocoloured green and the DIC signal appears in grey scale. Cultures were grown on 1.5% (w/v) water agar for 6-9 days. Bars = 5 µm.

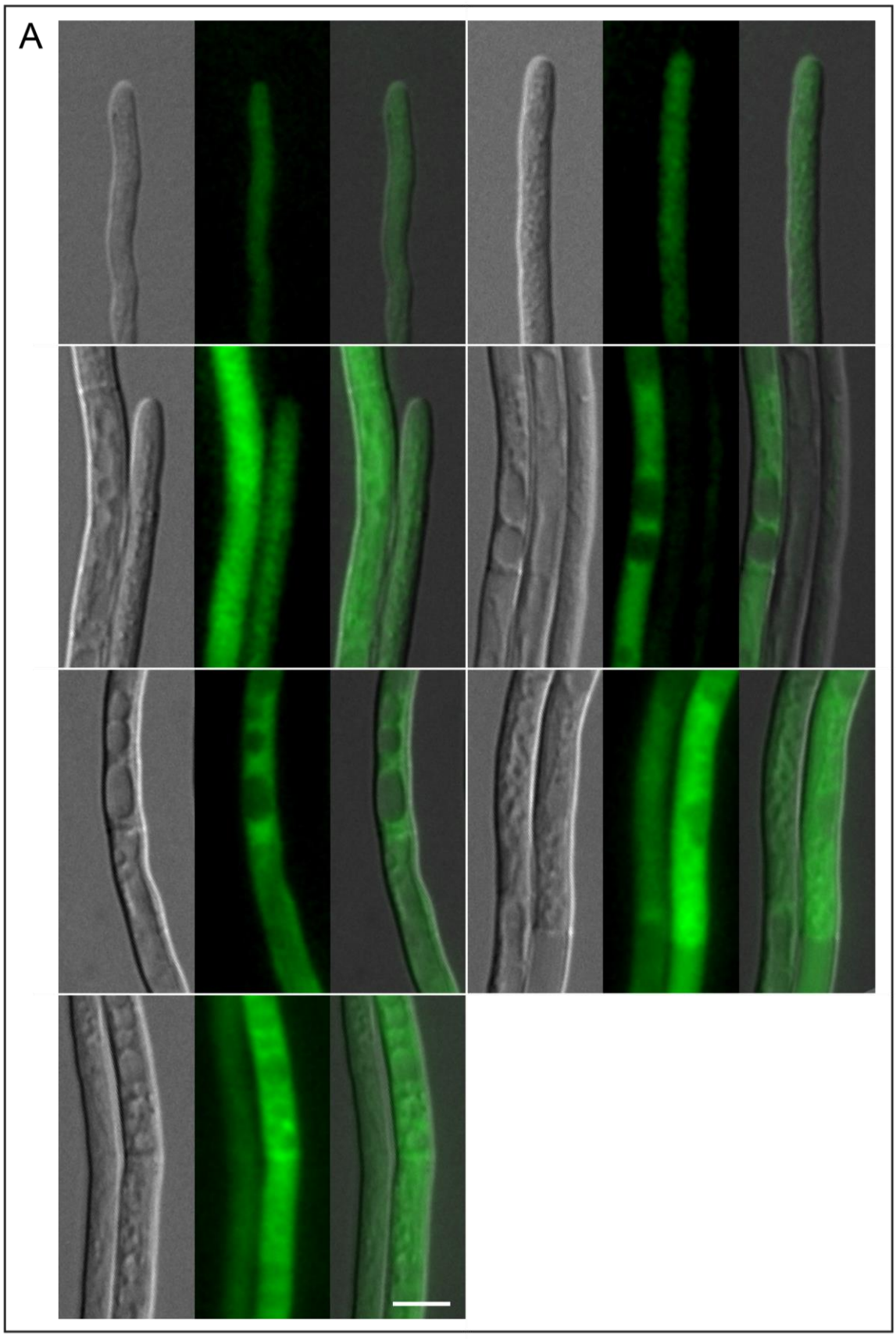
A

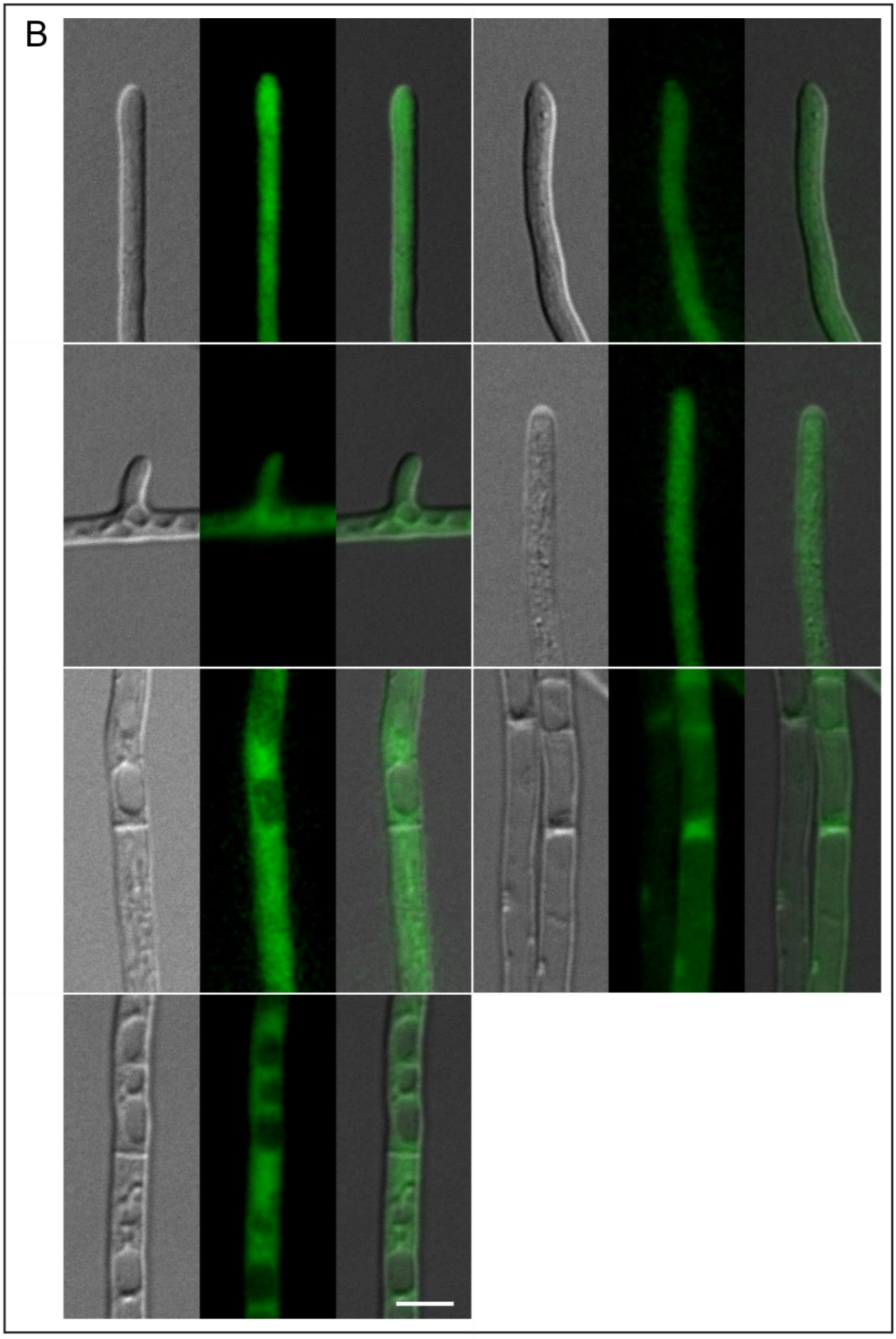
B

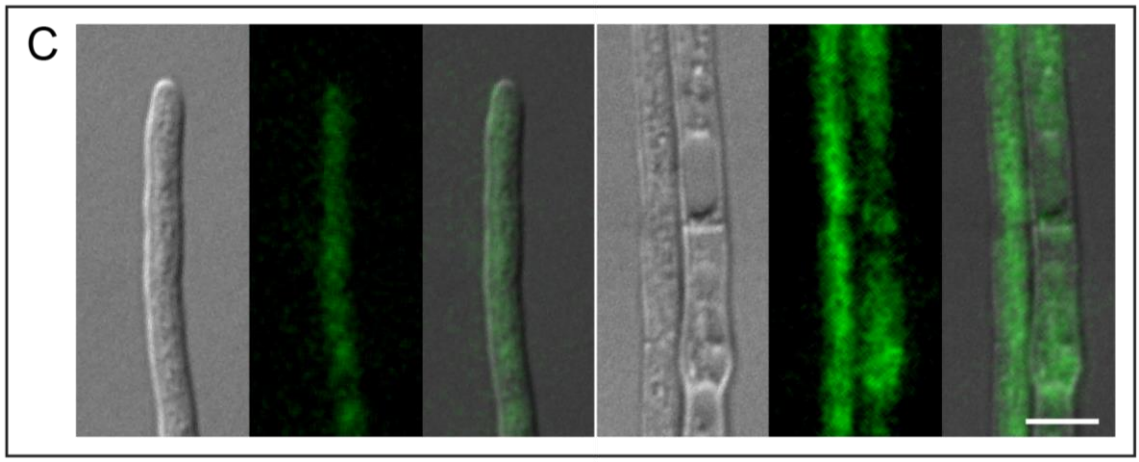

6.4.2 Cdc24ΔPH-eGFP construct. Differential interference contrast and fluorescent microscopy images of Cdc24ΔPH-eGFP in the following strains (A) EFS92, (B) EFS93, and (C) EFS94. Fluorescence signals have been pseudocoloured green and the DIC signal appears in grey scale. Cultures were grown on 1.5% (w/v) water agar for 6-9 days. Bars = 5 μm.

6.5 Western blots

A

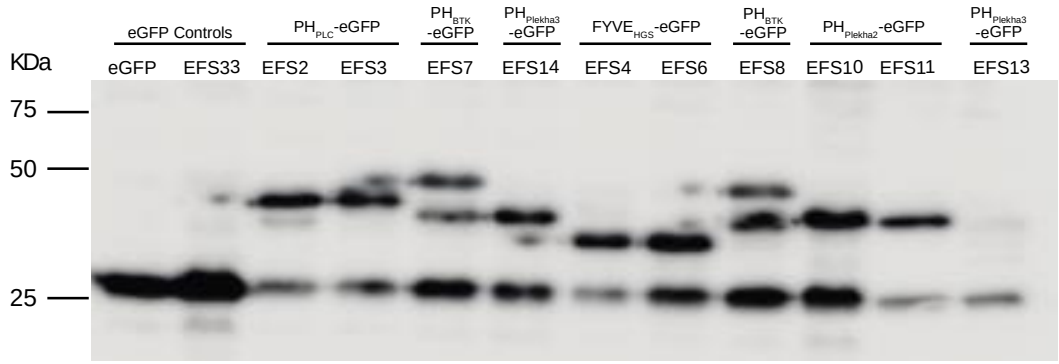

B

Construct	Domain Type	Target	Strain	EFS Number	Predicted MW (KDa)
eGFP	Control		PN4175	N/A	29.95
			19	EFS3	
PH_{PLC}-eGFP	PH	PI[4,5]P2	12	EFS2	42.34
			19	EFS3	
PH_{BTK}-eGFP	PH	PI[3,4,5]P3	9	EFS7	47.13
$PH_{Plekha3}$-eGFP	PH	PI[4]P	8	EFS14	38.19
$FYVE_{HGS}$-eGFP	FYVE	PI[3]P	9	EFS4	32.26
			24	EFS6	
PH_{BTK}-eGFP	PH	PI[3,4,5]P3	20	EFS8	47.13
$PH_{Plekha2}$-eGFP	PH	PI[3,4]P2	1	EFS10	40.01
			4	EFS11	
$PH_{Plekha3}$-eGFP	PH	PI[4]P	37	EFS15	38.19

6.5.1 Western blot analysis of eGFP biosensor strains. (A) Western blot of total protein extract of strains EFS33, EFS2, EFS3, EFS7, EFS14, EFS4, EFS6, EFS8, EFS10, EFS11, and EFS15, probed with the anti-GFP antibody (Invitrogen, A11122). Total protein extract of strain PN4175 expressing cytosolic GFP (pCT74) was used as a control (146). Per strain 50 µg of total protein were loaded and samples were separated on a 10% SDS Page gel. (B) Table of biosensor constructs and their expected weight (kDa) as calculated using https://www.bioinformatics.org/sms/prot_mw.html.

A

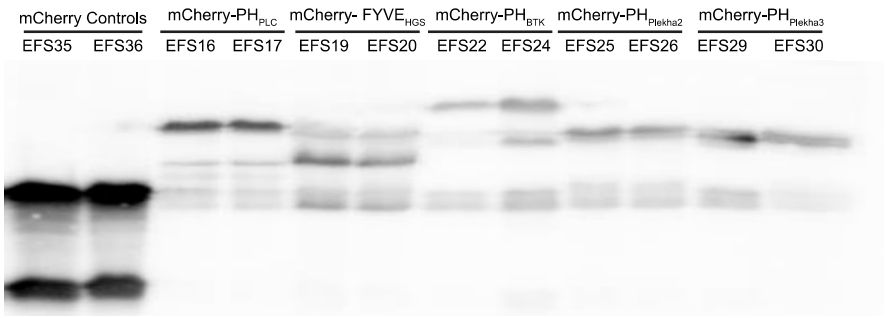

B

Construct	Domain Type	Target	Strain	EFS Number	Predicted MW (KDa)
mCherry	Control		2	EFS35	26.73
			15	EFS36	
mCherry-PH$_{PLC}$	PH	PI[4,5]P2	10	EFS16	42.04
			16	EFS17	
mCherry-FYVE$_{HGS}$	FYVE	PI[3]P	22	EFS19	34.97
			37	EFS20	
mCherry-PH$_{BTK}$	PH	PI[3,4,5]P3	16	EFS22	46.84
			33	EFS24	
mCherry-PH$_{Plekha2}$	PH	PI[3,4]P2	3	EFS25	39.72
			37	EFS26	
mCherry-PH$_{Plekha3}$	PH	PI[4]P	18	EFS29	38.03
			25	EFS30	

6.5.2 Western Blot analysis of mCherry biosensor strains. (A) Western blot of total protein extract of strains EFS35, EFS36, EFS16, EFS17, EFS19, EFS20, EFS22, EFS24, EFS25, EFS26, EFS29, and EFS30, probed with the anti-mCherry antibody (BioVision, 5993). Per strain 50 µg of total protein were loaded and samples were separated on a 10% SDS Page gel. (B) Table of biosensor constructs and their expected weight (kDa) as calculated using https://www.bioinformatics.org/sms/prot_mw.html.

6.6 Supplementary images of biosensor localisation in culture

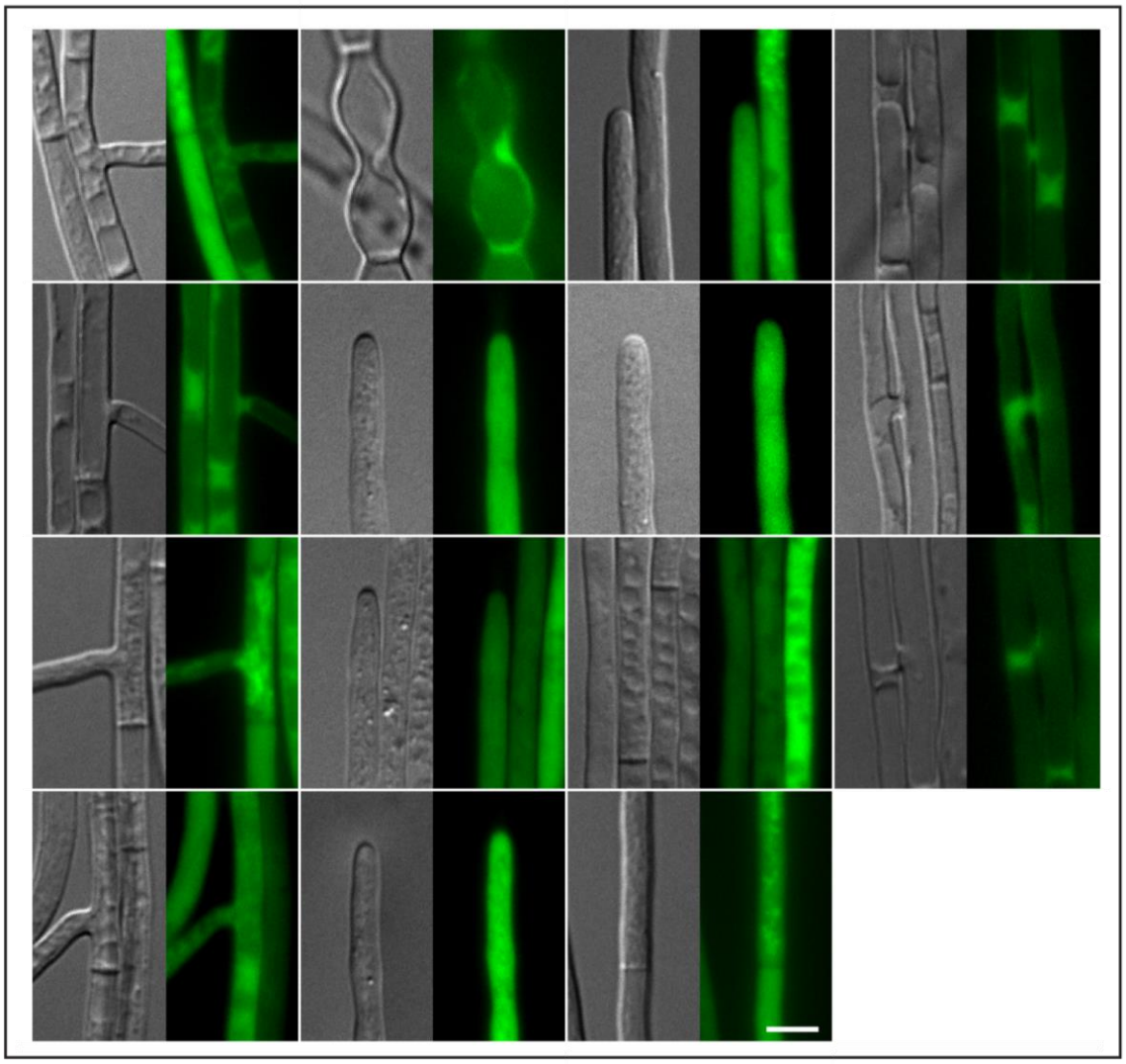

6.6.1 eGFP free fluorophore control. Differential interference contrast and fluorescent microscopy images of the free fluorophore controls in strain EFS33. Fluorescence signals have been pseudocoloured green and the DIC signal appears in grey scale. Cultures were grown on 1.5% (w/v) water agar for 6-9 days. Bars = 5 µm.

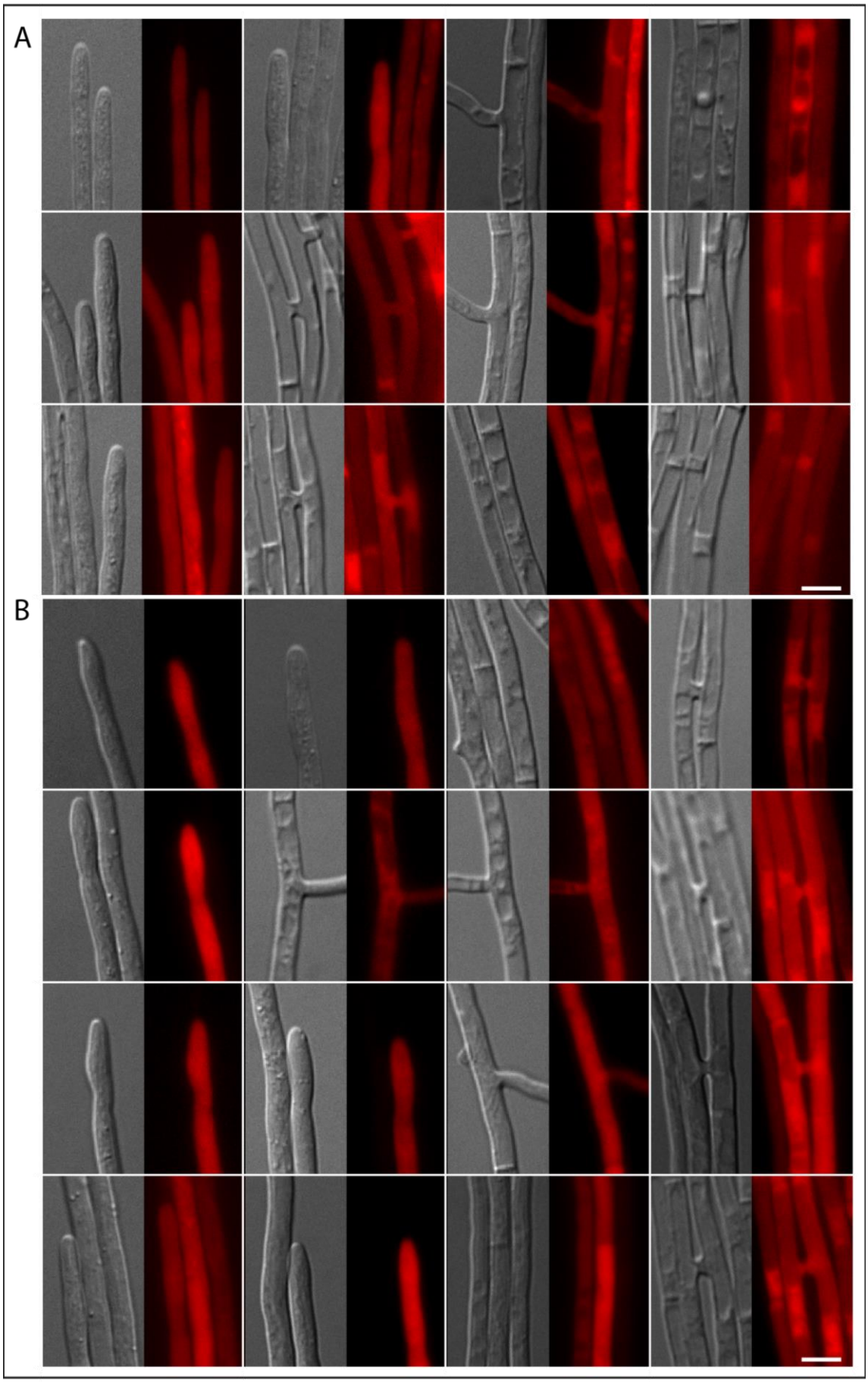
A
B

6.6.2 mCherry free fluorophore control. Differential interference contrast and fluorescent microscopy images of the free fluorophore controls in the following strains (A) EFS34 and (B) EFS35. Fluorescence signals have been pseudocoloured red and the DIC signal appears in grey scale. Cultures were grown on 1.5% (w/v) water agar for 6-9 days. Bars = 5 μm.

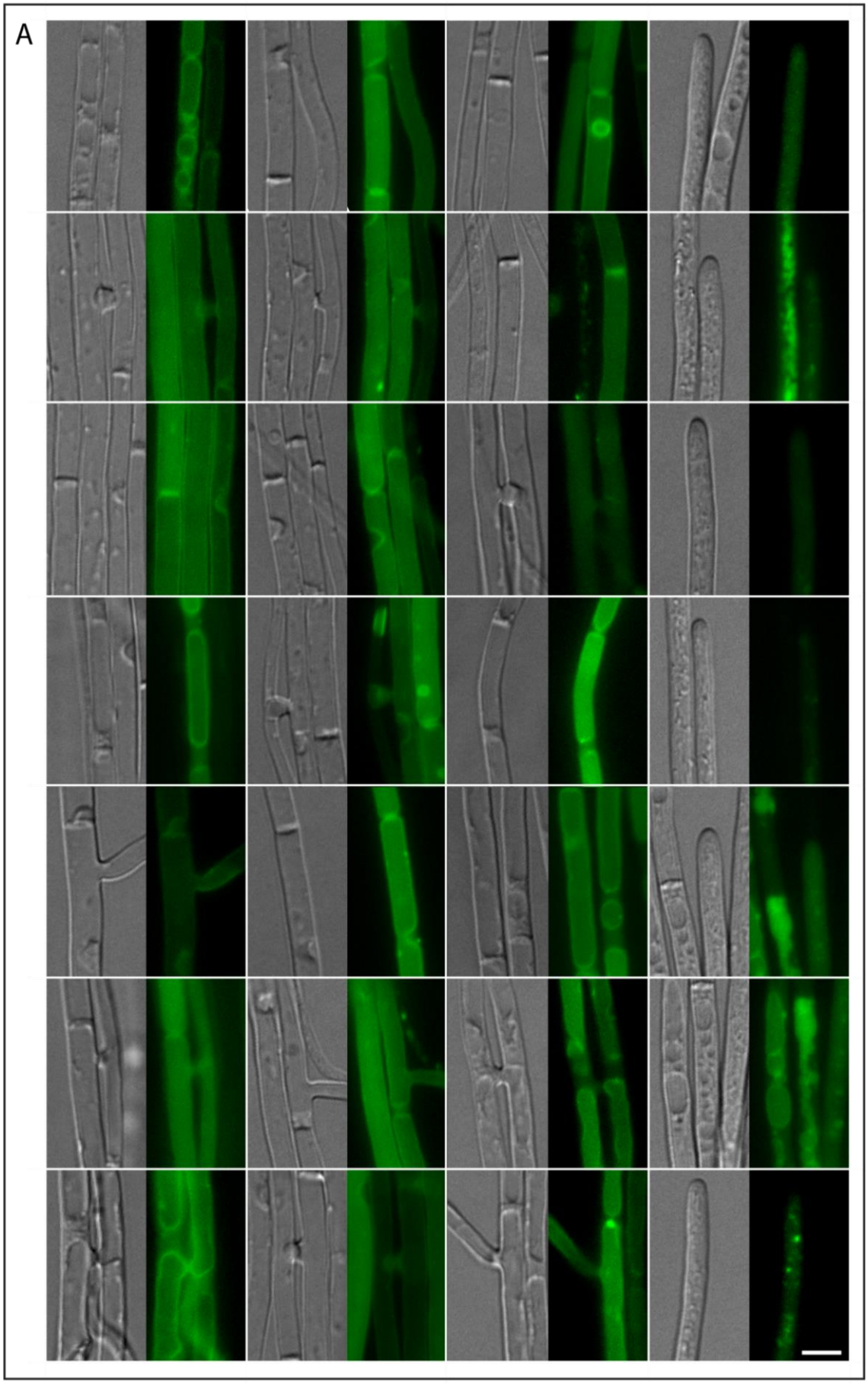
A

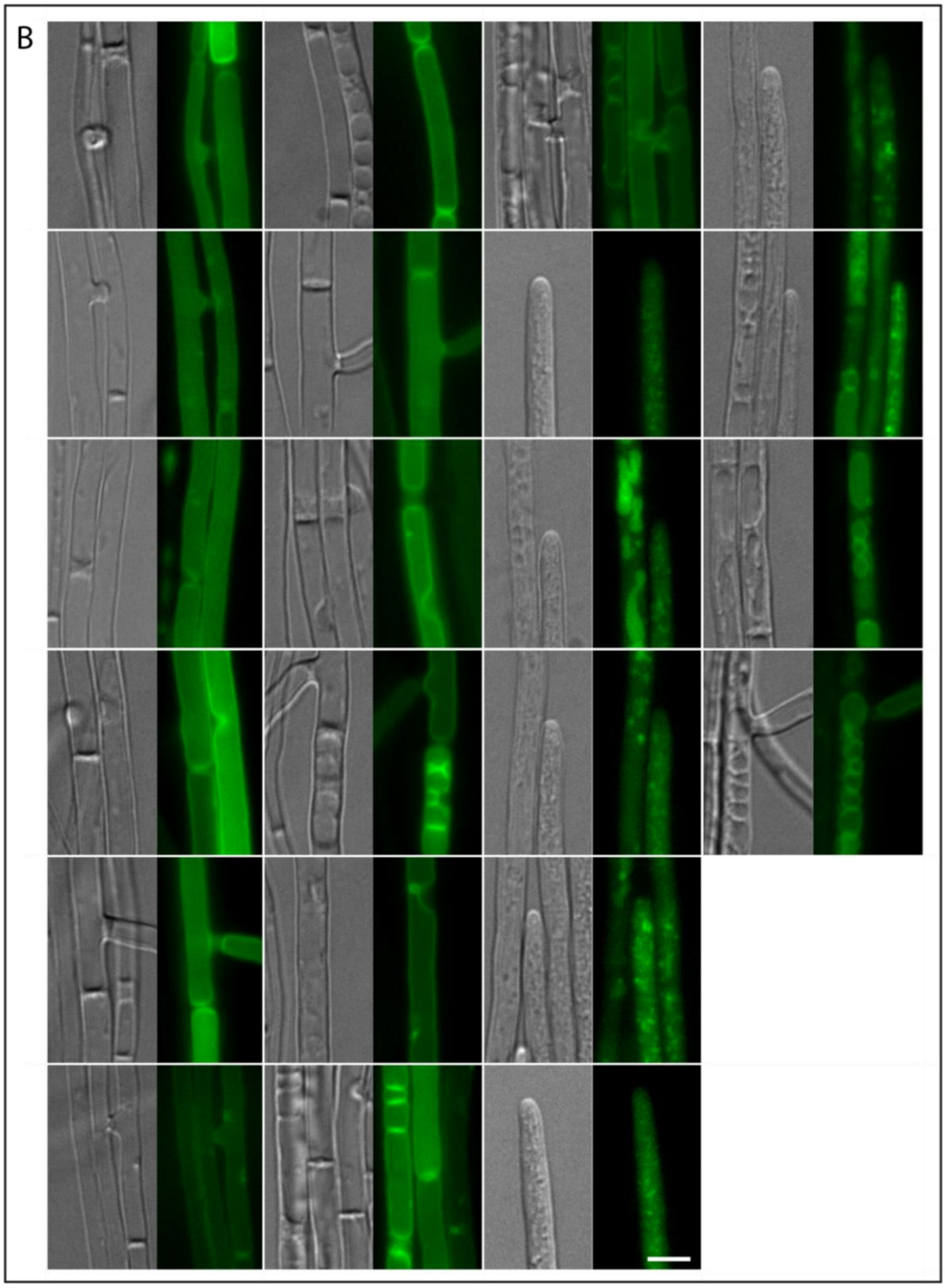

6.6.3 PI[3]P eGFP biosensor. Differential interference contrast and fluorescent microscopy images of the PI[3]P biosensor in the following strains (A) EFS4 and (B) EFS6. Fluorescence signals have been pseudocoloured green and the DIC signal appears in grey scale. Cultures were grown on 1.5% (w/v) water agar for 6-9 days. Bars = 5 μm.

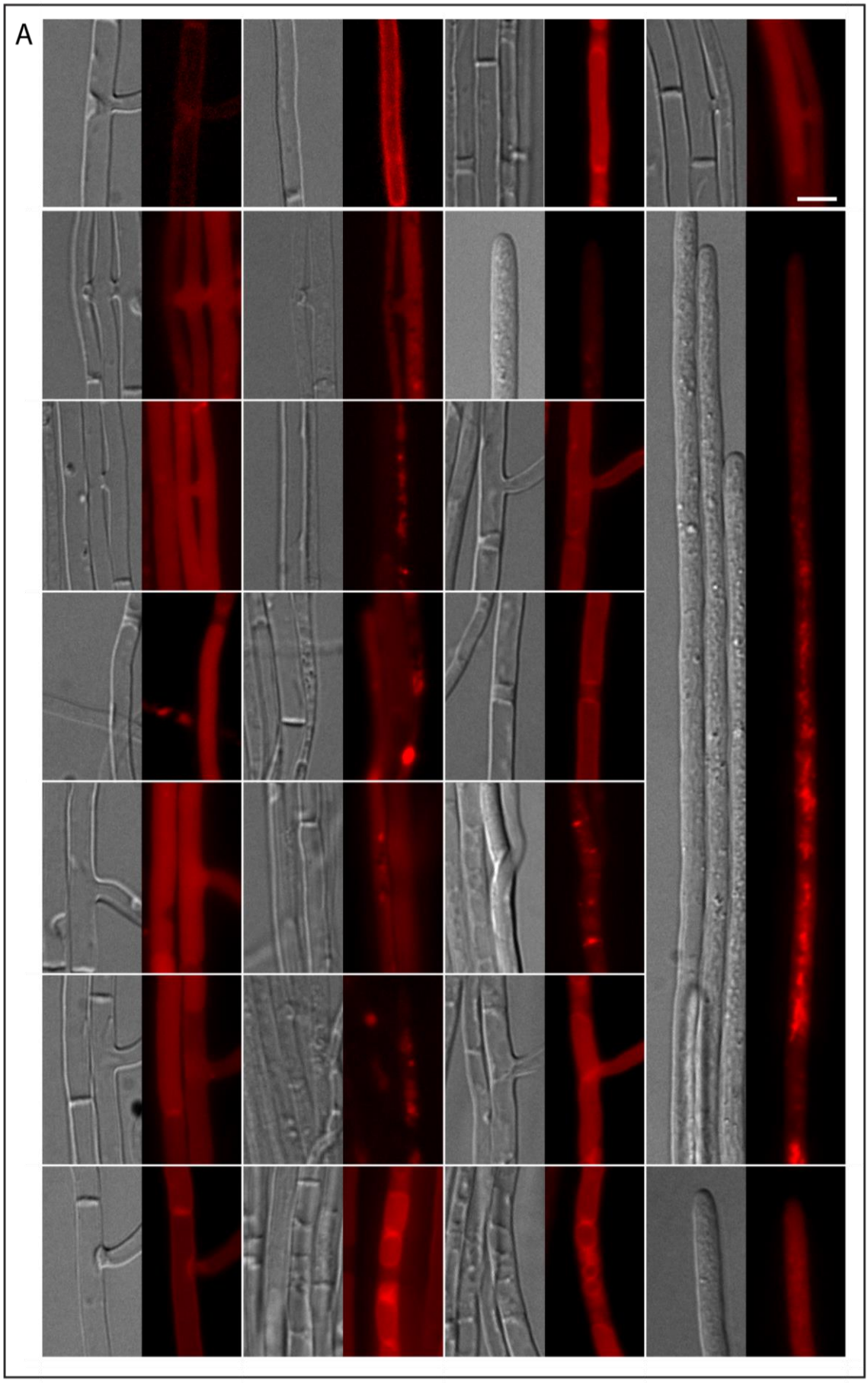
A

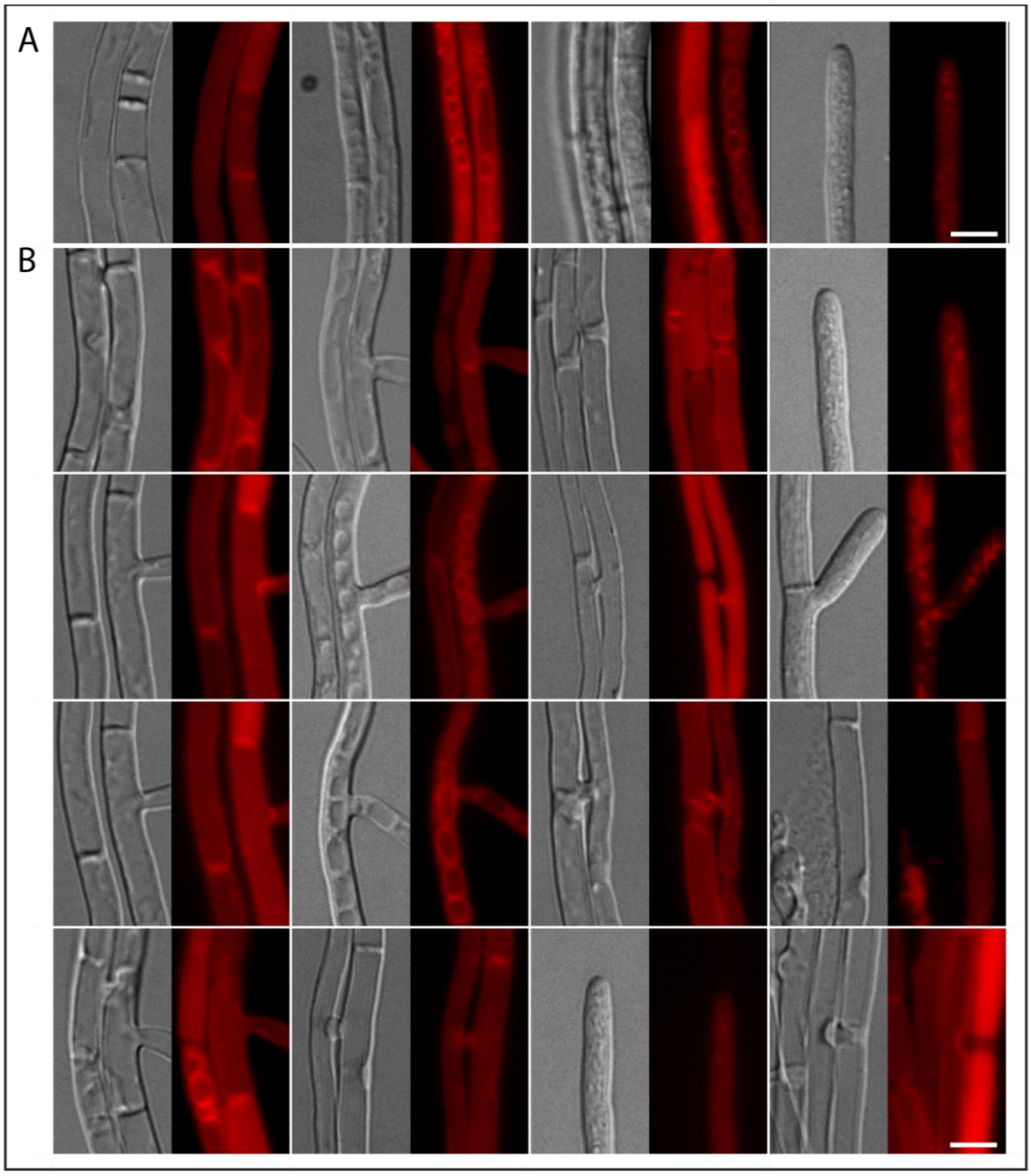

6.6.4 PI[3]P mCherry biosensor. Differential interference contrast and fluorescent microscopy images of the PI[3]P biosensor in the following strains (A) EFS18 and (B) EFS20. Fluorescence signals have been pseudocoloured red and the DIC signal appears in grey scale. Cultures were grown on 1.5% (w/v) water agar for 6-9 days. Bars = 5 µm.

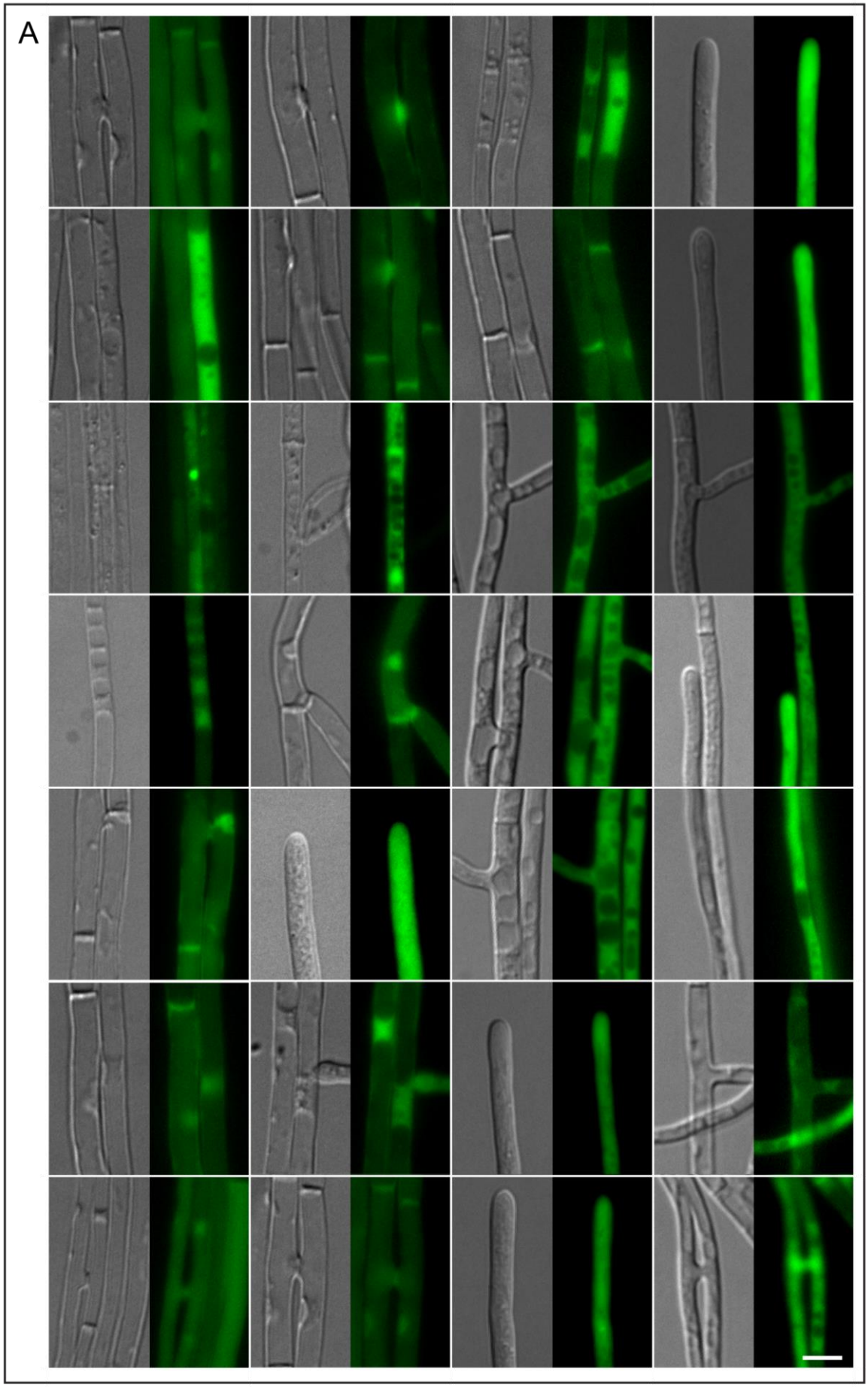
A

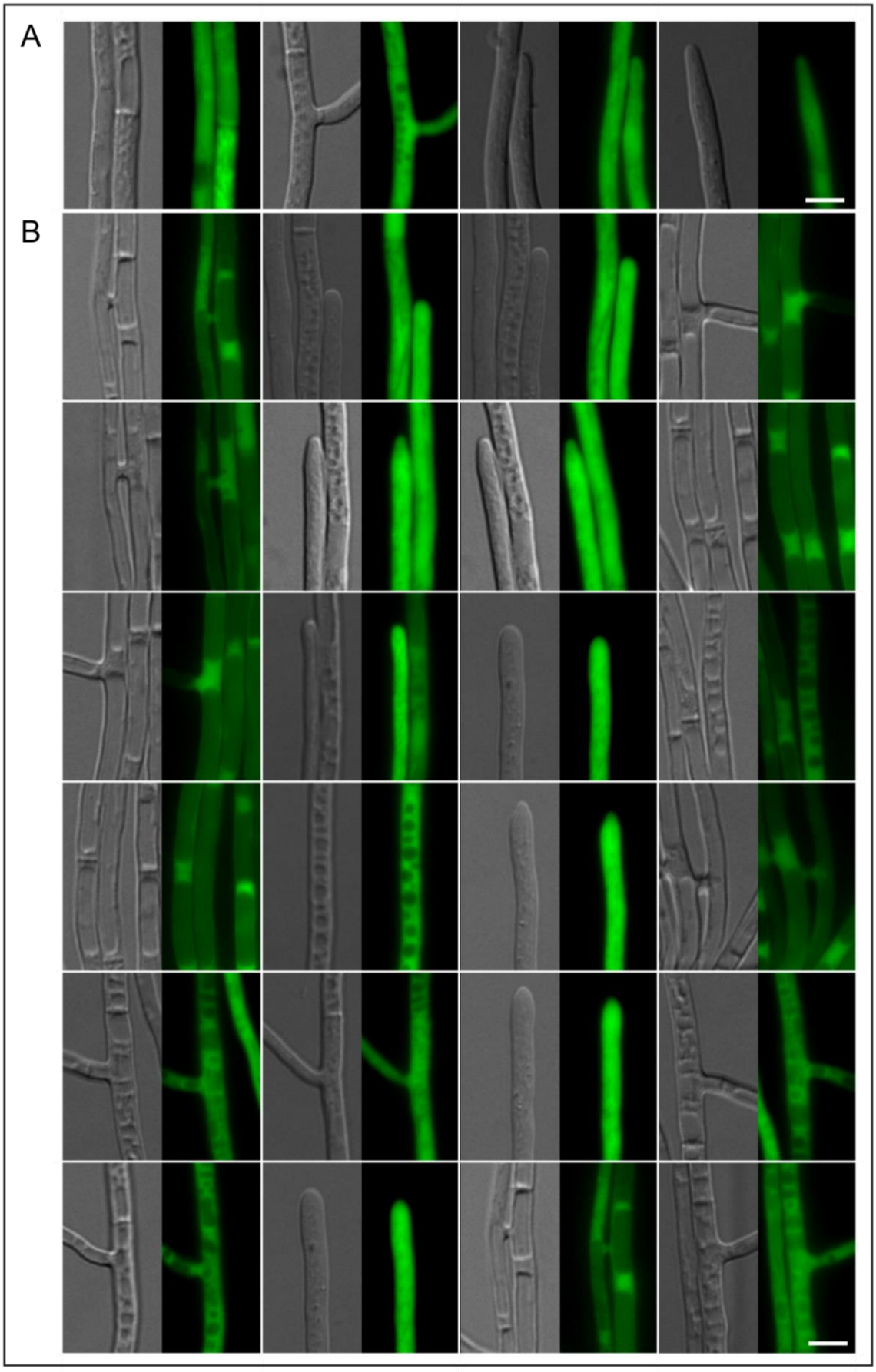
A
B

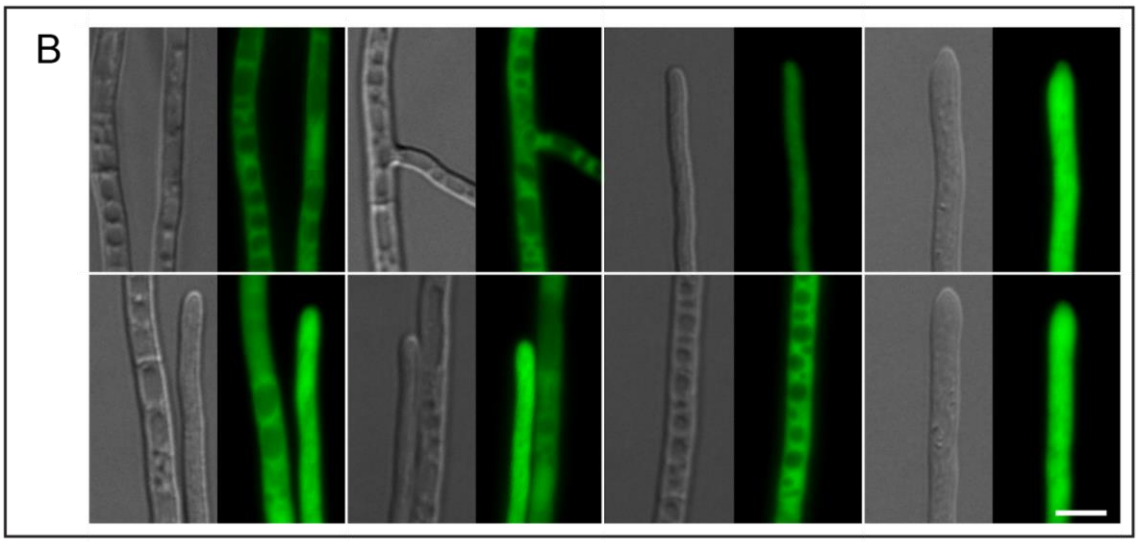

6.6.5 PI[3,4]P_2 eGFP biosensor. Differential interference contrast and fluorescent microscopy images of the PI[3,4]P_2 biosensor in the following strains (A) EFS10 and (B) EFS11. Fluorescence signals have been pseudocoloured green and the DIC signal appears in grey scale. Cultures were grown on 1.5% (w/v) water agar for 6-9 days. Bars = 5 μm.

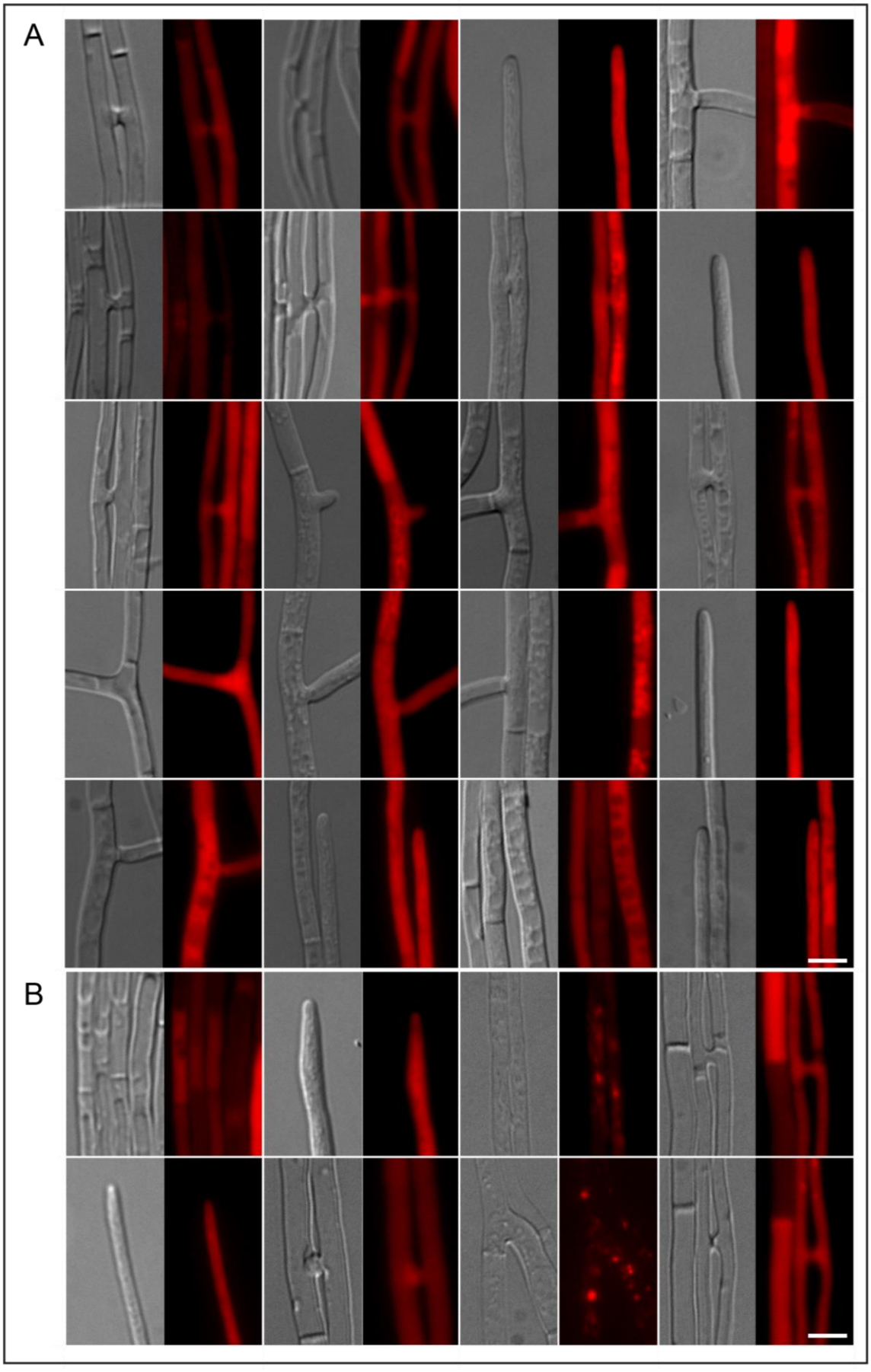
A
B

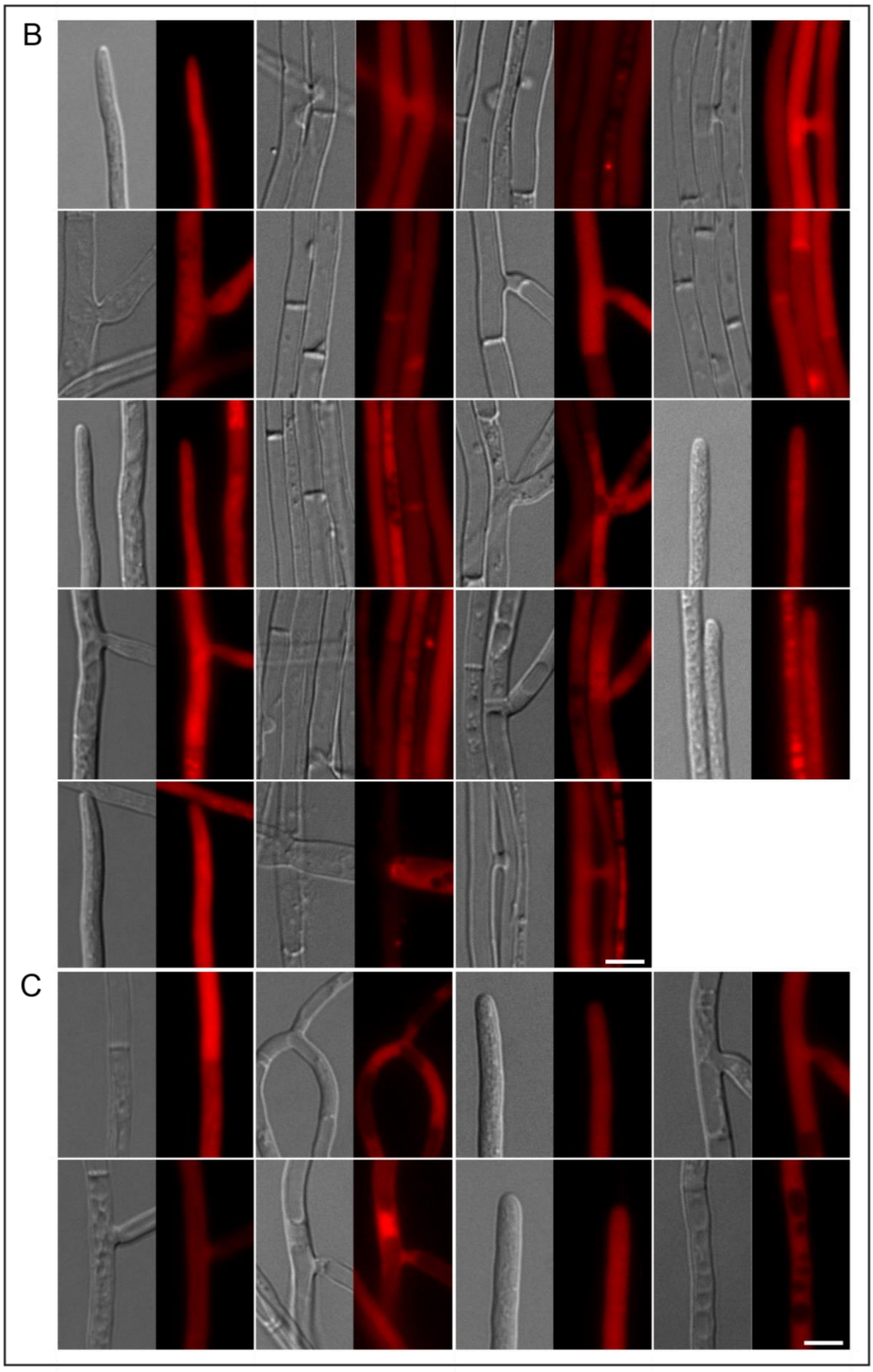
B
C

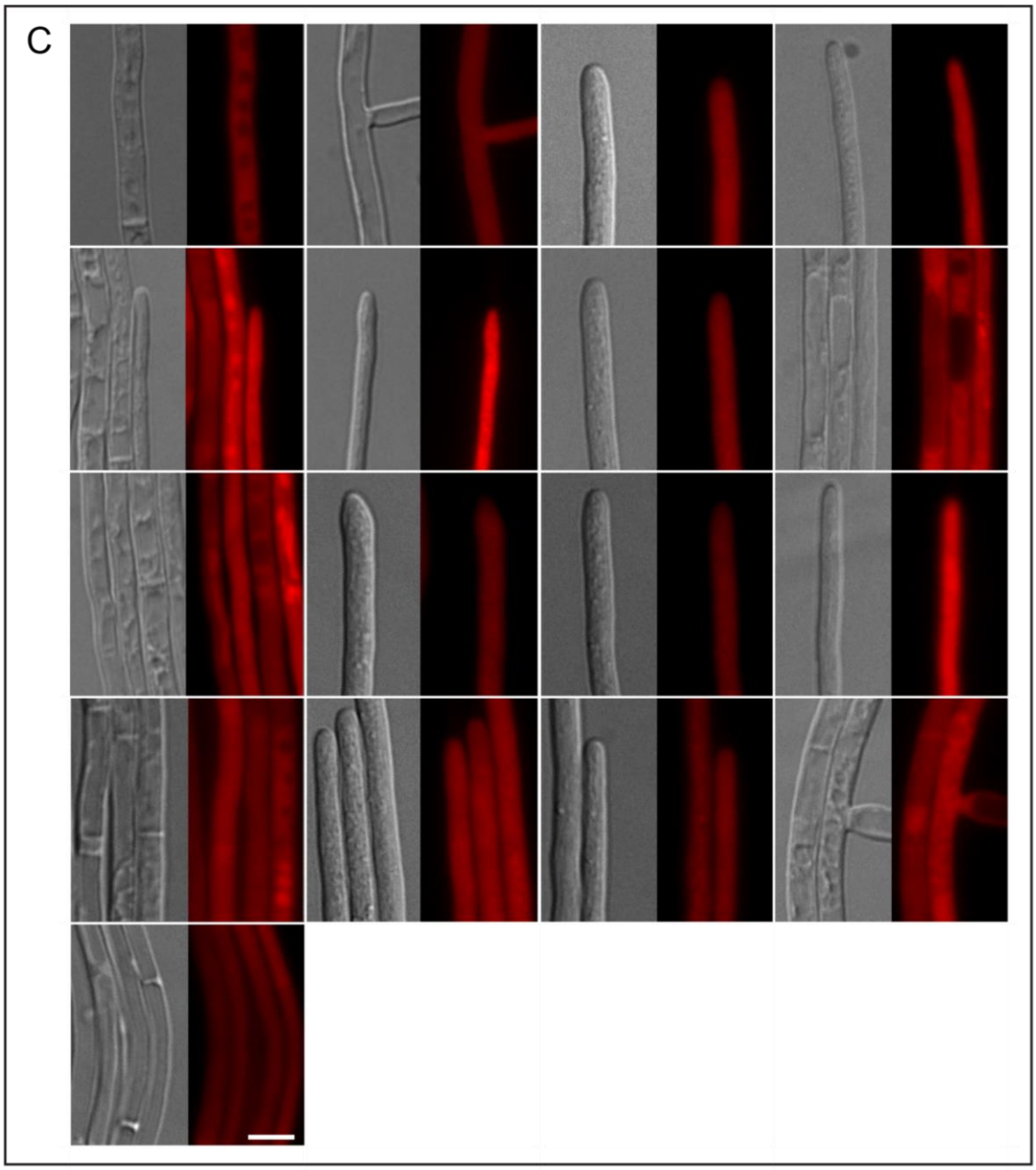

6.6.6 PI[3,4]P_2 mCherry biosensor. Differential interference contrast and fluorescent microscopy images of the PI[3,4]P_2 biosensor in the following strains (A) EFS25, (B) EFS26, and (C) EFS27. Fluorescence signals have been pseudocoloured red and the DIC signal appears in grey scale. Cultures were grown on 1.5% (w/v) water agar for 6-9 days. Bars = 5 µm.

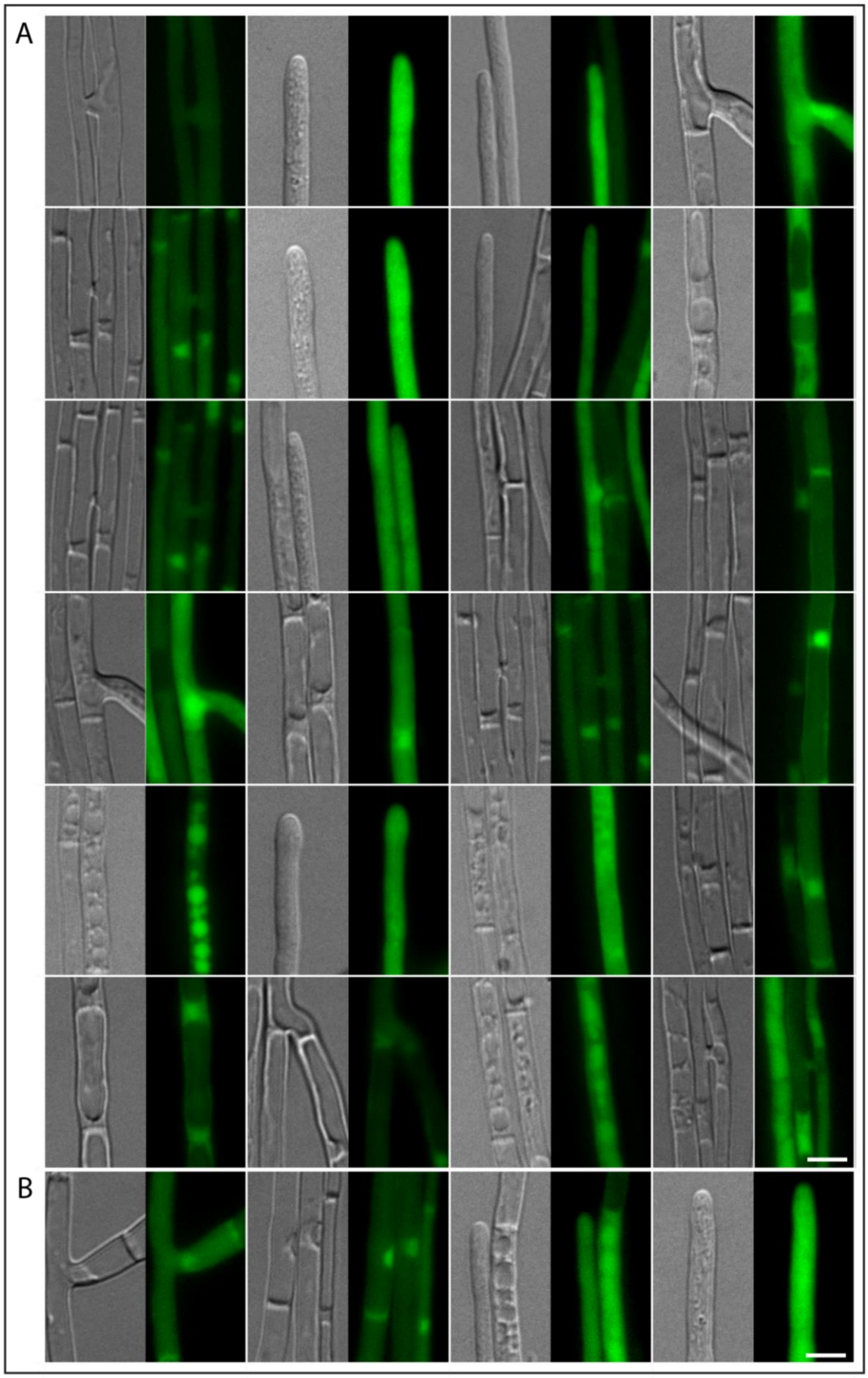
A
B

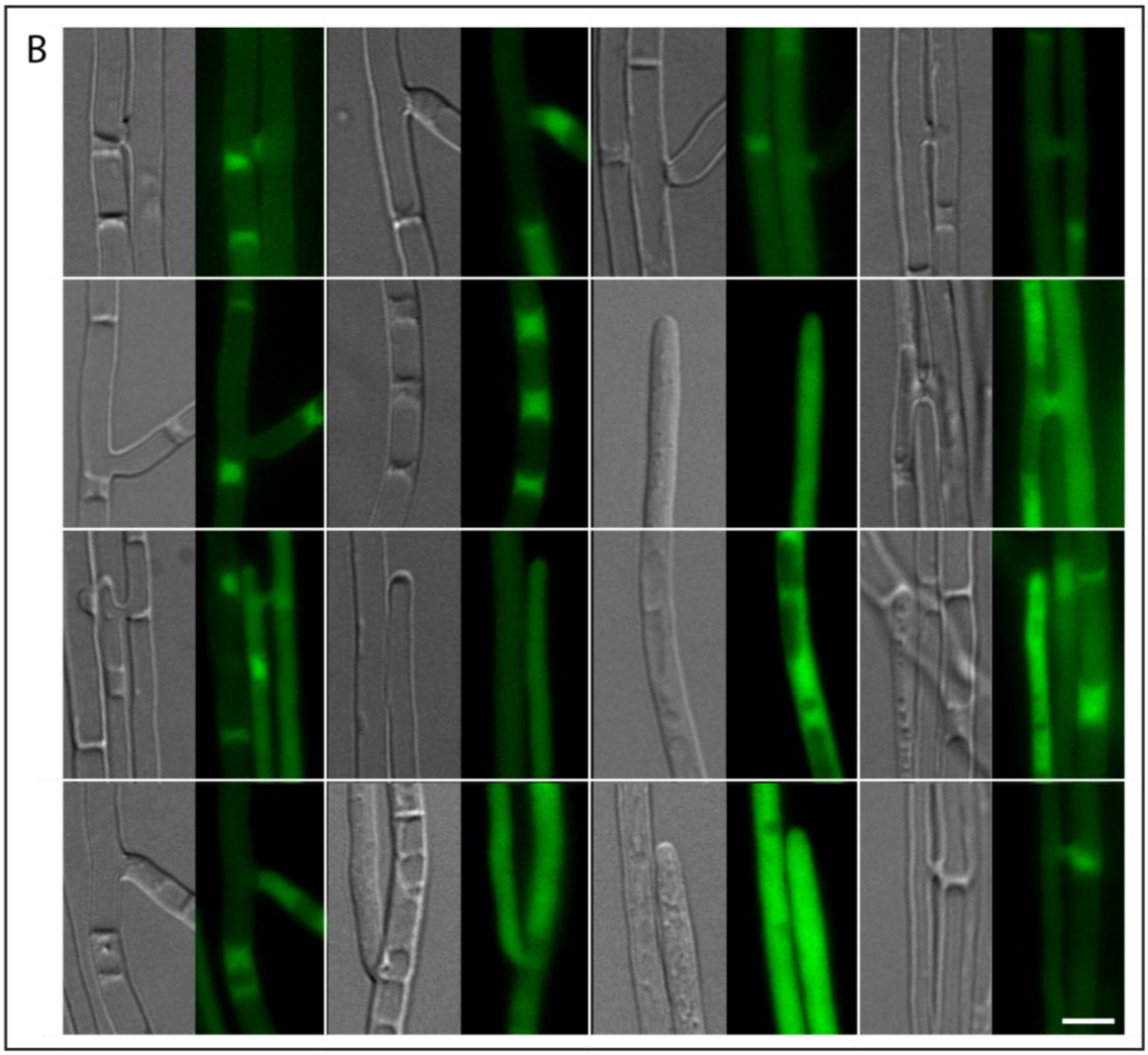

6.6.7 PI[3,4,5]P_3 eGFP biosensor. Differential interference contrast and fluorescent microscopy images of the PI[3,4,5]P_3 biosensor in the following strains (A) EFS7 and (B) EFS8. Fluorescence signals have been pseudocoloured green and the DIC signal appears in grey scale. Cultures were grown on 1.5% (w/v) water agar for 6-9 days. Bars = 5 μm.

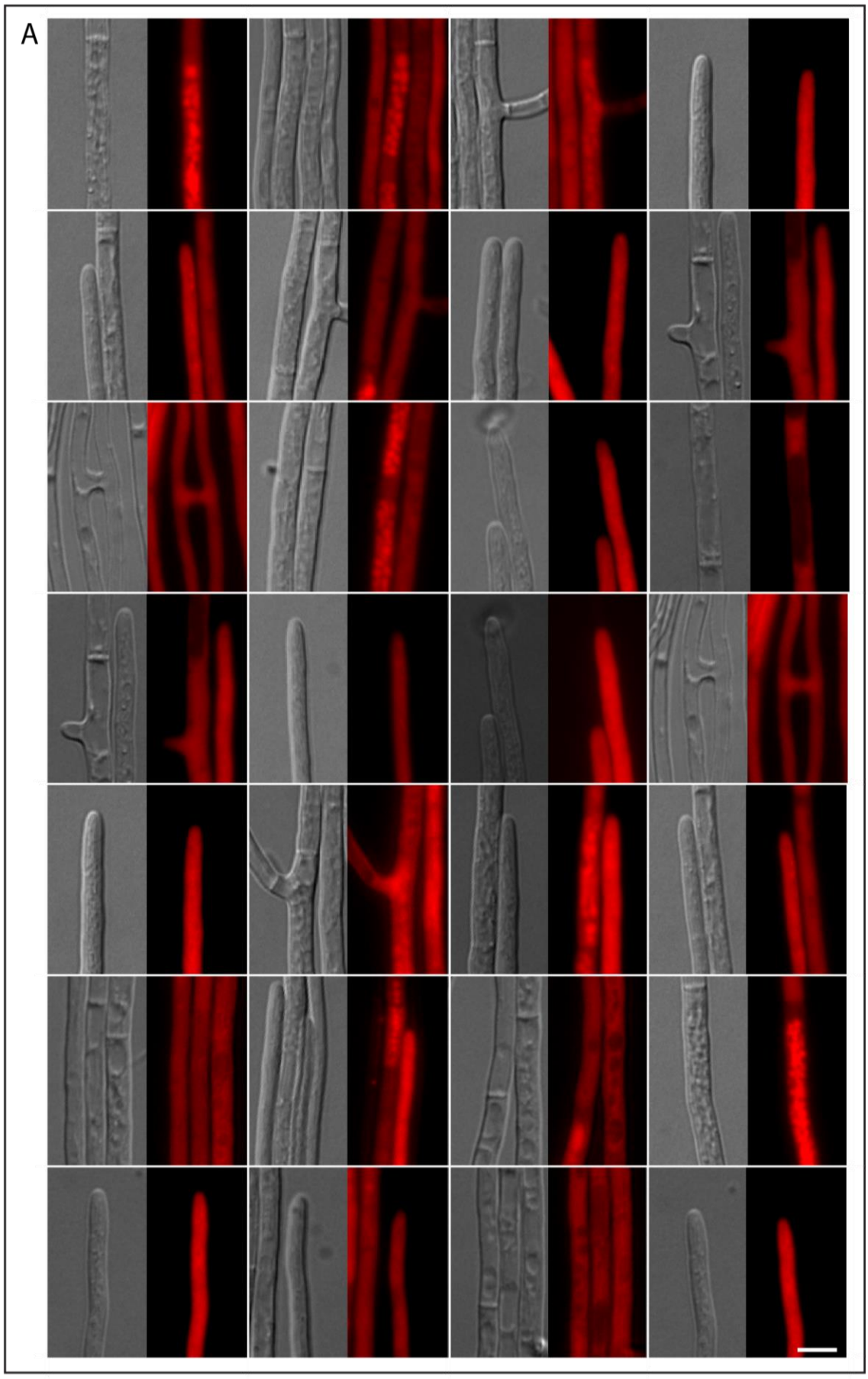
A

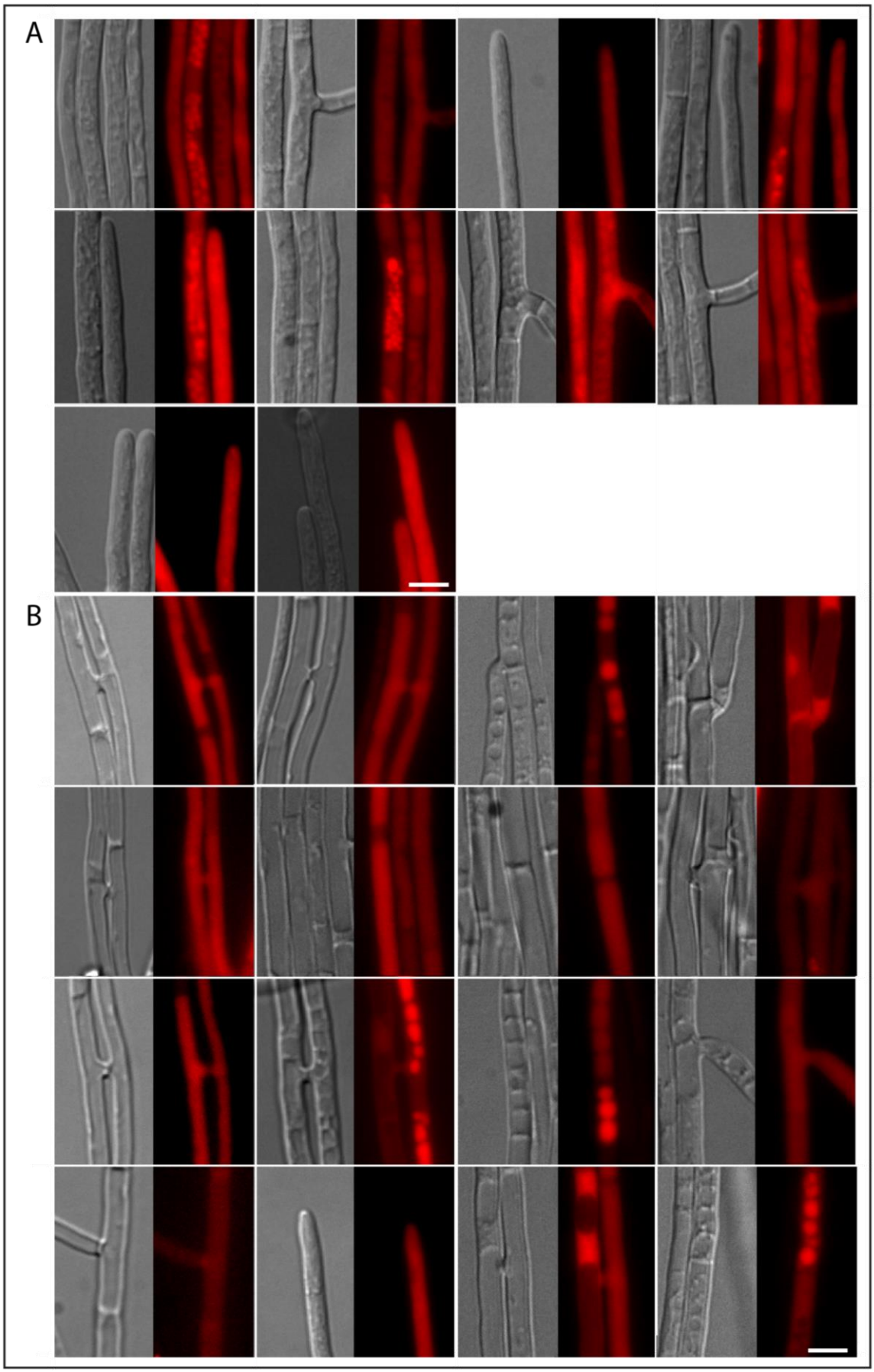
A
B

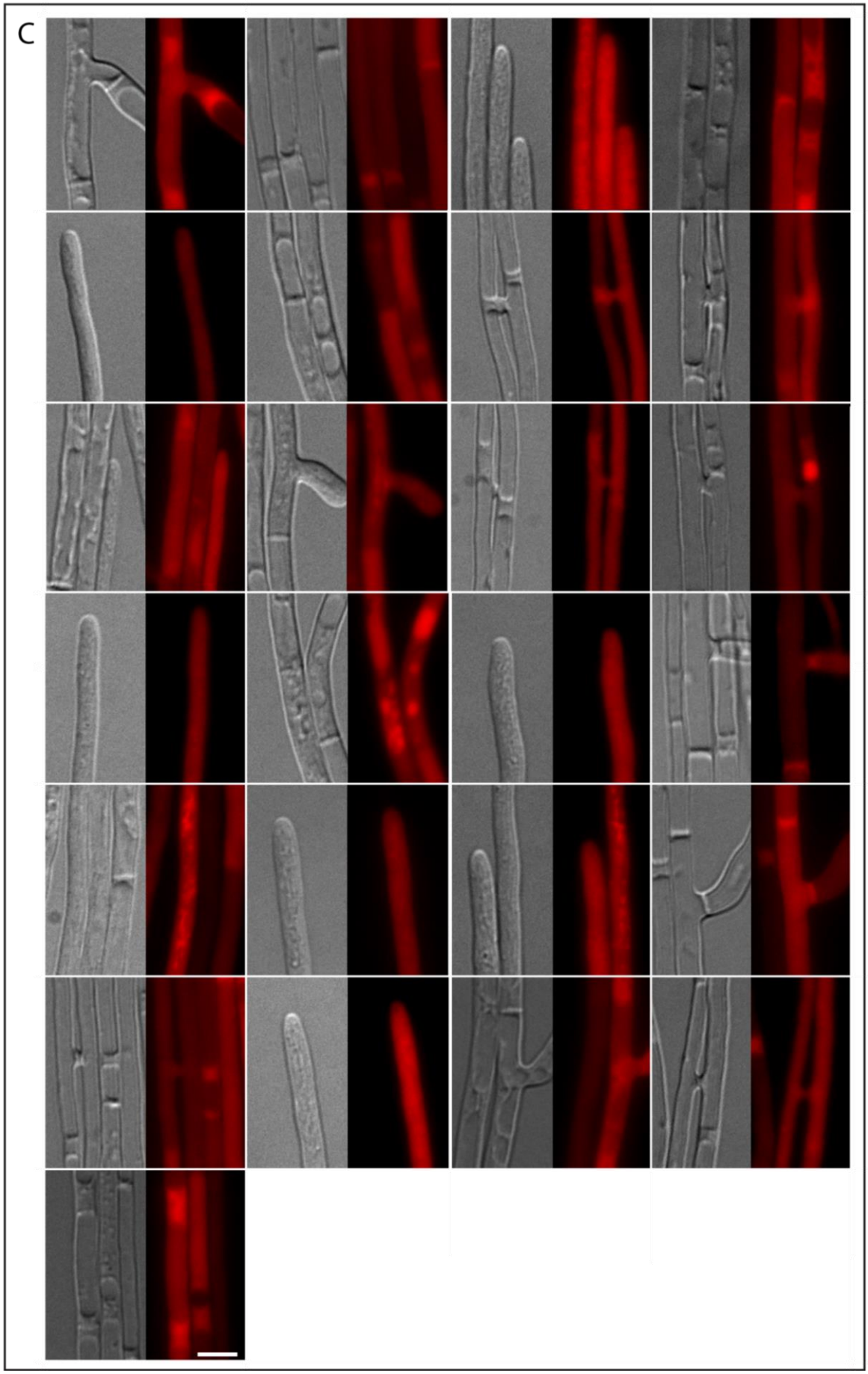
C

6.6.8 PI[3,4,5]P_3 mCherry biosensor. Differential interference contrast and fluorescent microscopy images of the PI[3,4,5]P_3 biosensor in the following strains (A) EFS22, (B) EFS23, and (C) EFS24. Fluorescence signals have been pseudocoloured red and the DIC signal appears in grey scale. Cultures were grown on 1.5% (w/v) water agar for 6-9 days. Bars = 5 μm.

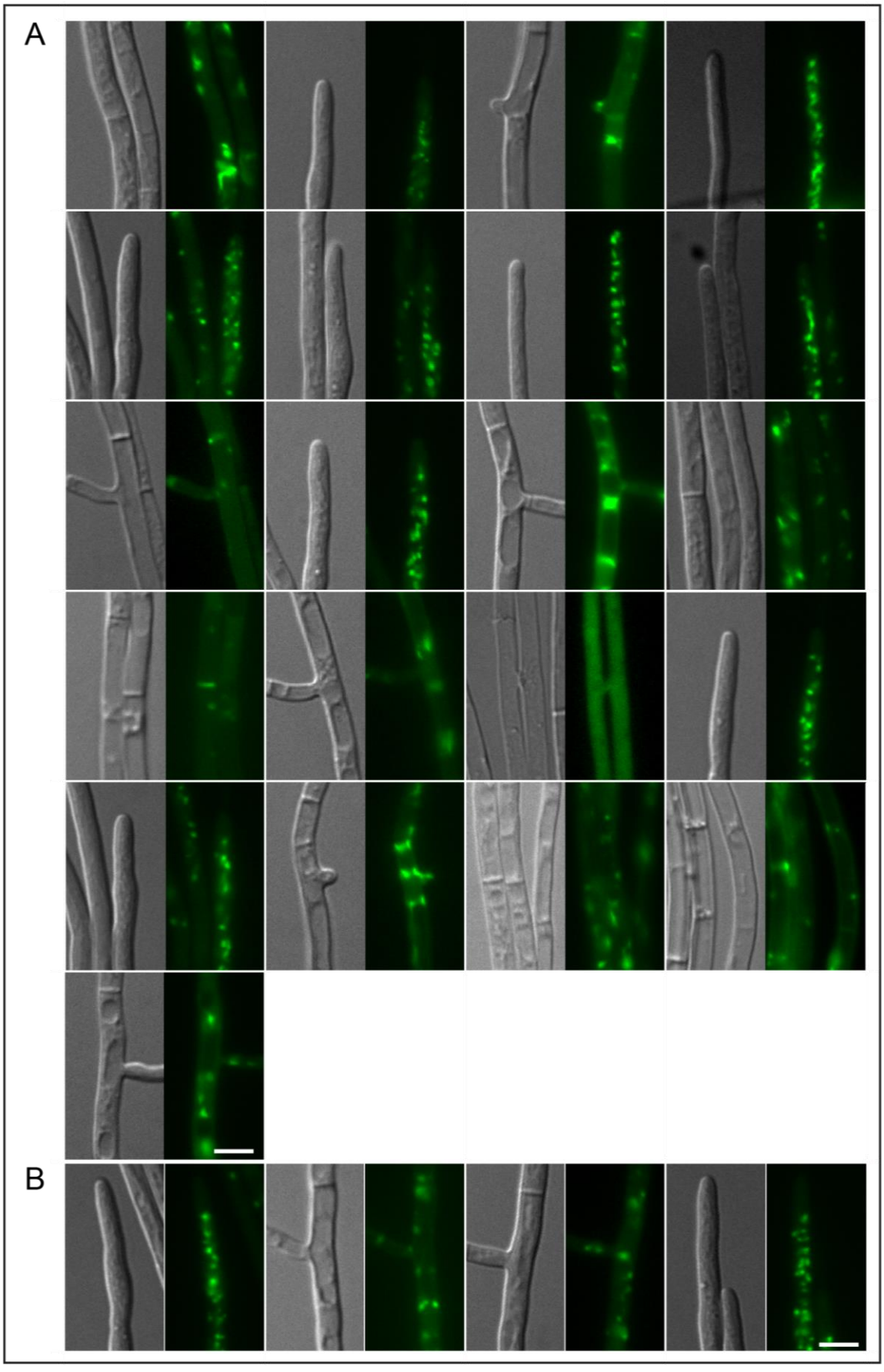
A
B

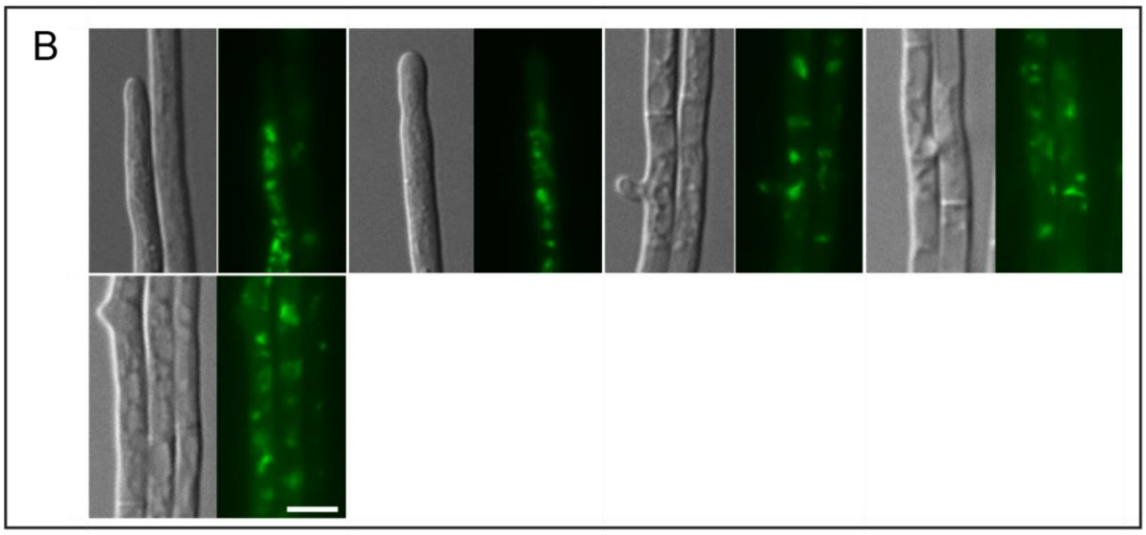

6.6.9 PI[4]P eGFP biosensor. Differential interference contrast and fluorescent microscopy images of the PI[4]P biosensor in the following strains (A) EFS13 and (B) EFS14. Fluorescence signals have been pseudocoloured green and the DIC signal appears in grey scale. Cultures were grown on 1.5% (w/v) water agar for 6-9 days. Bars = 5 μm.

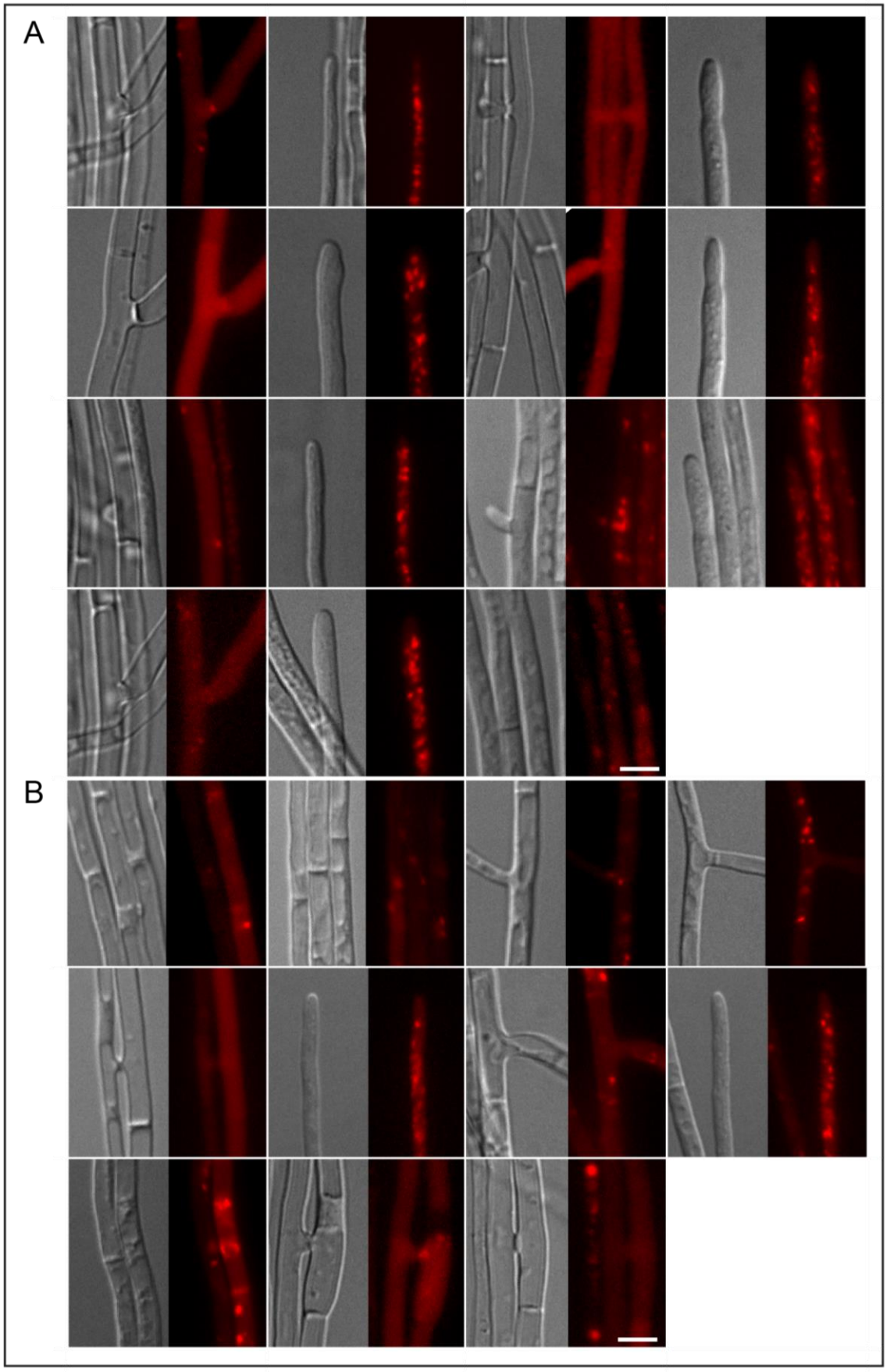
A
B

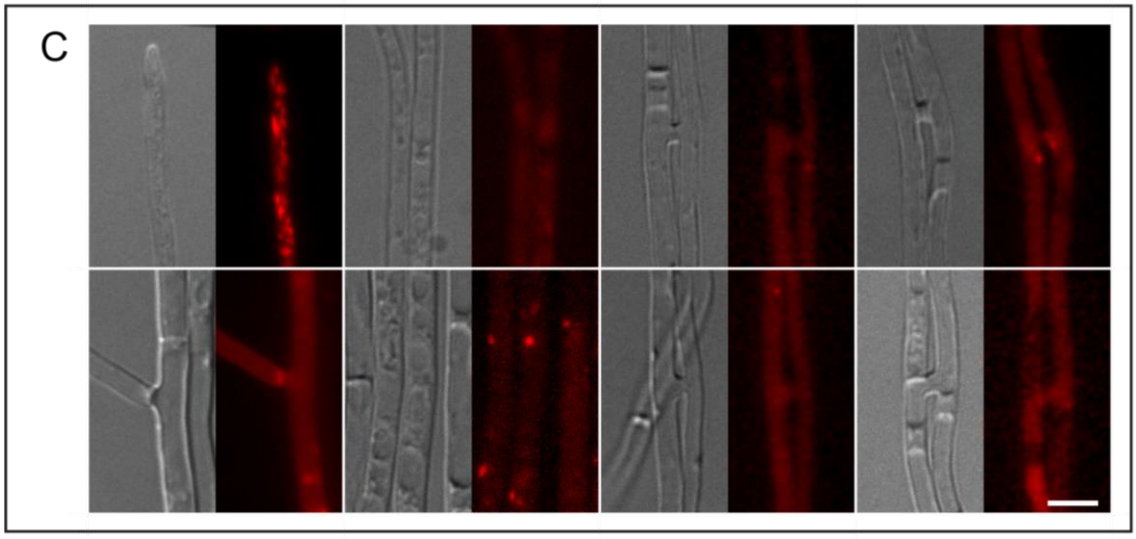

6.6.10 PI[4]P mCherry biosensor. Differential interference contrast and fluorescent microscopy images of the PI[4]P biosensor in the following strains (A) EFS29, (B) EFS30, and (C) EFS31. Fluorescence signals have been pseudocoloured red and the DIC signal appears in grey scale. Cultures were grown on 1.5% (w/v) water agar for 6-9 days. Bars = 5 µm.

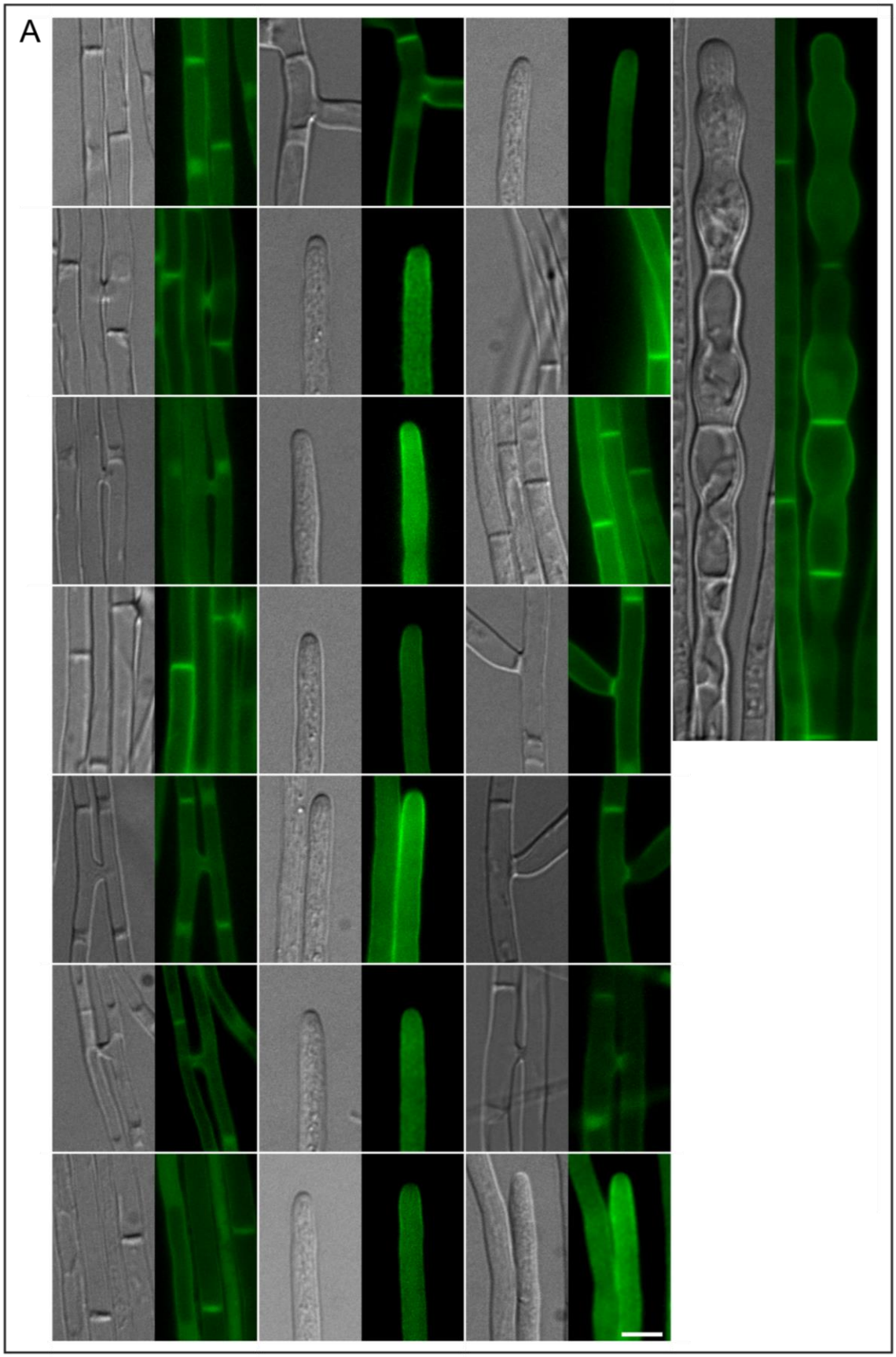
A

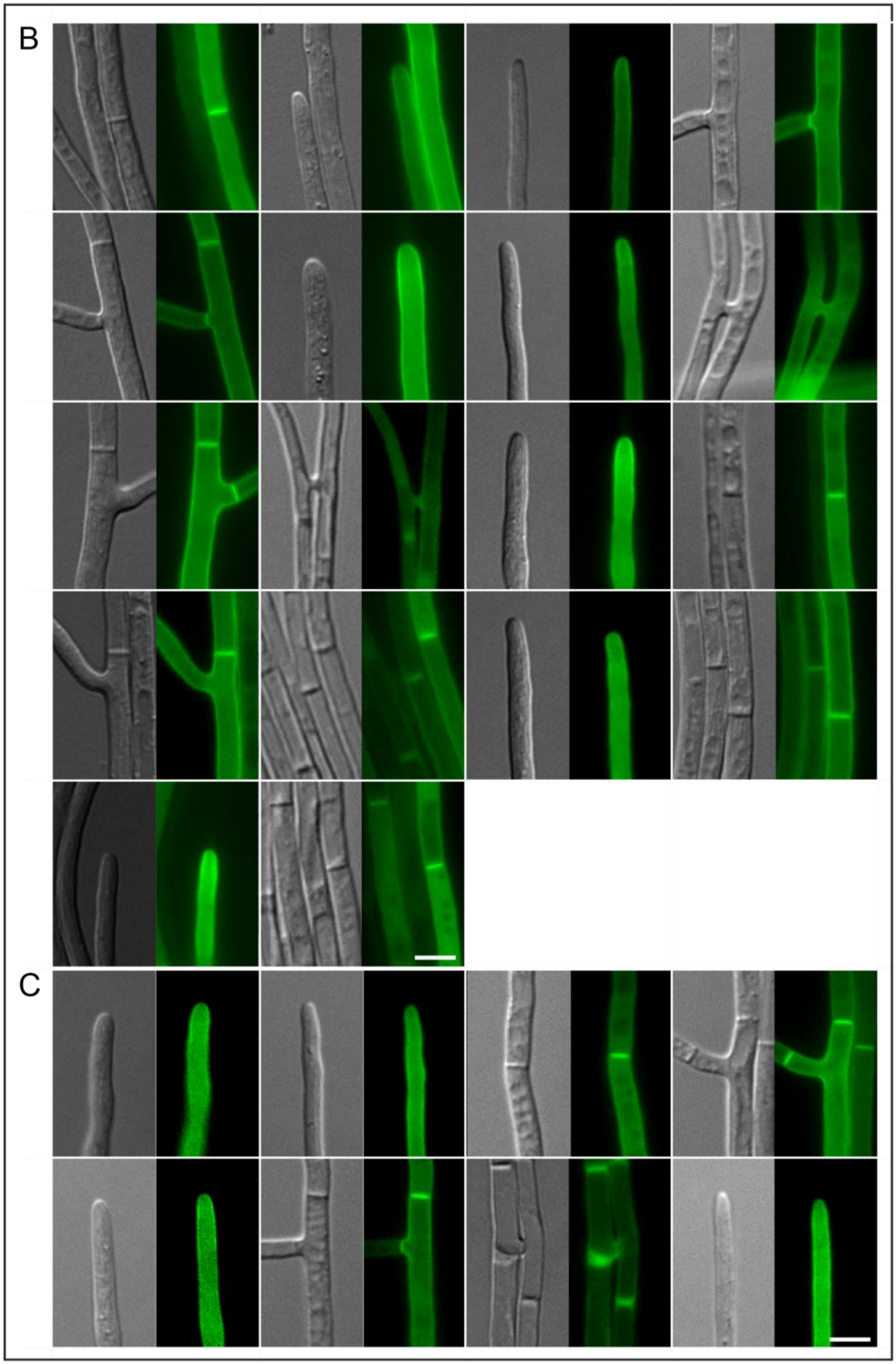
B
C

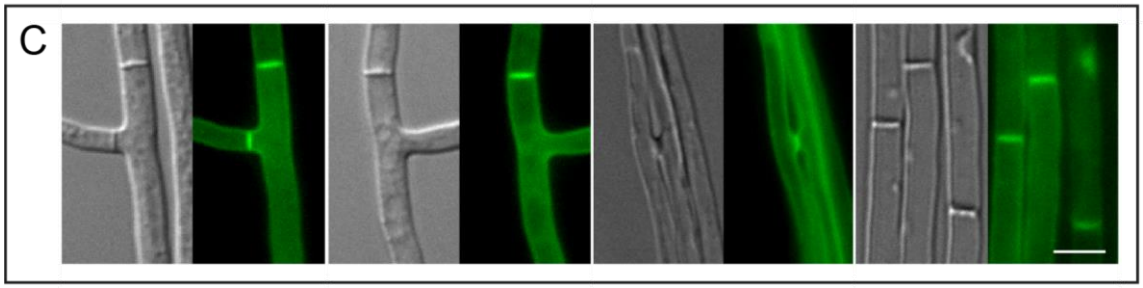

6.6.11 PI[4,5]P_2 eGFP biosensor. Differential interference contrast and fluorescent microscopy images of the PI[3]P biosensor in the following strains (A) EFS1, (B) EFS2, and (C) EFS3. Fluorescence signals have been pseudocoloured green and the DIC signal appears in grey scale. Cultures were grown on 1.5% (w/v) water agar for 6-9 days. Bars = 5 μm.

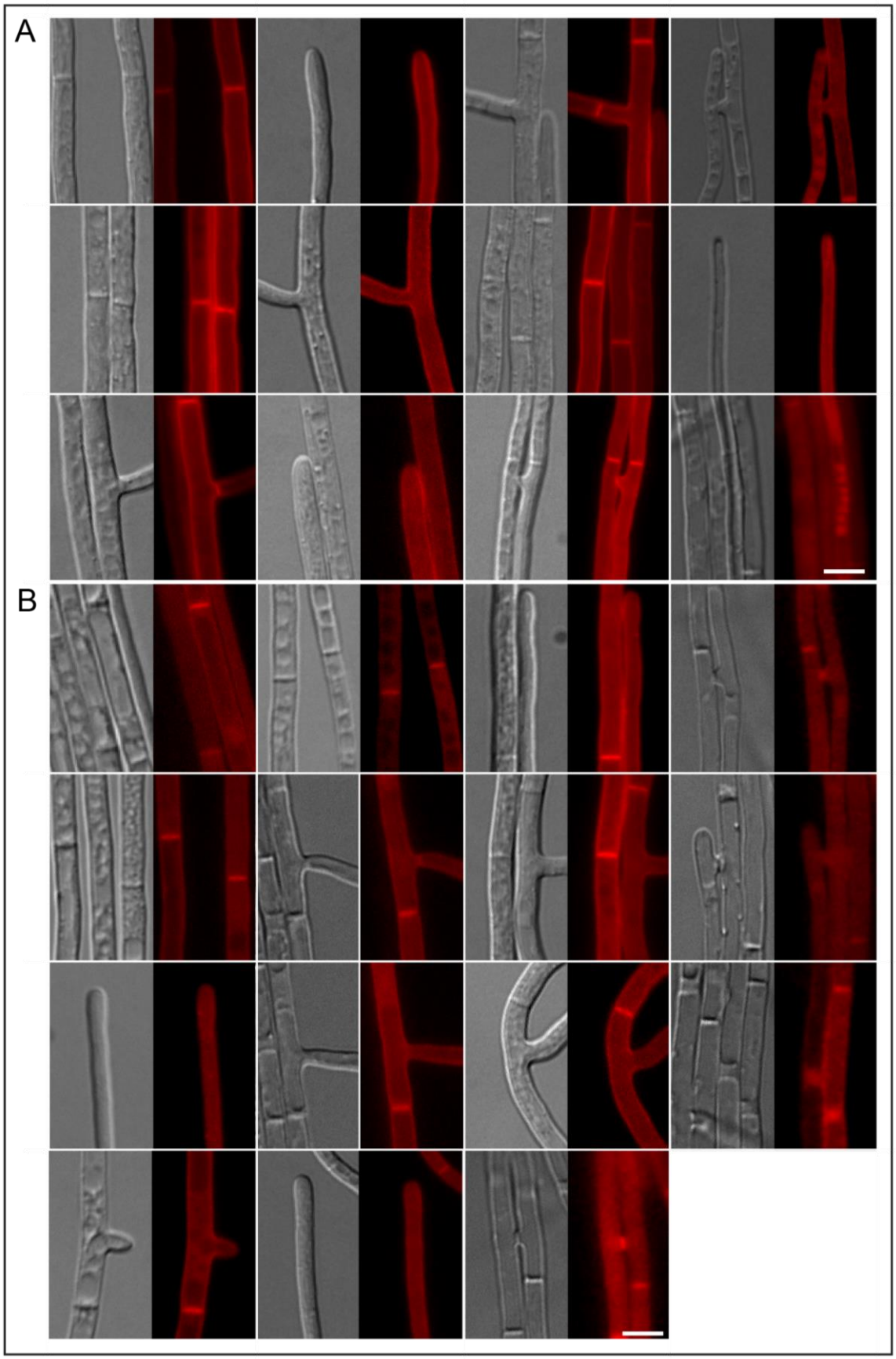
A
B

6.6.12 PI[4,5]P$_2$ mCherry biosensor. Differential interference contrast and fluorescent microscopy images of the PI[3]P biosensor in the following strains (A) EFS16 and (B) EFS17. Fluorescence signals have been pseudocoloured red and the DIC signal appears in grey scale. Cultures were grown on 1.5% (w/v) water agar for 6-9 days. Bars = 5 µm.

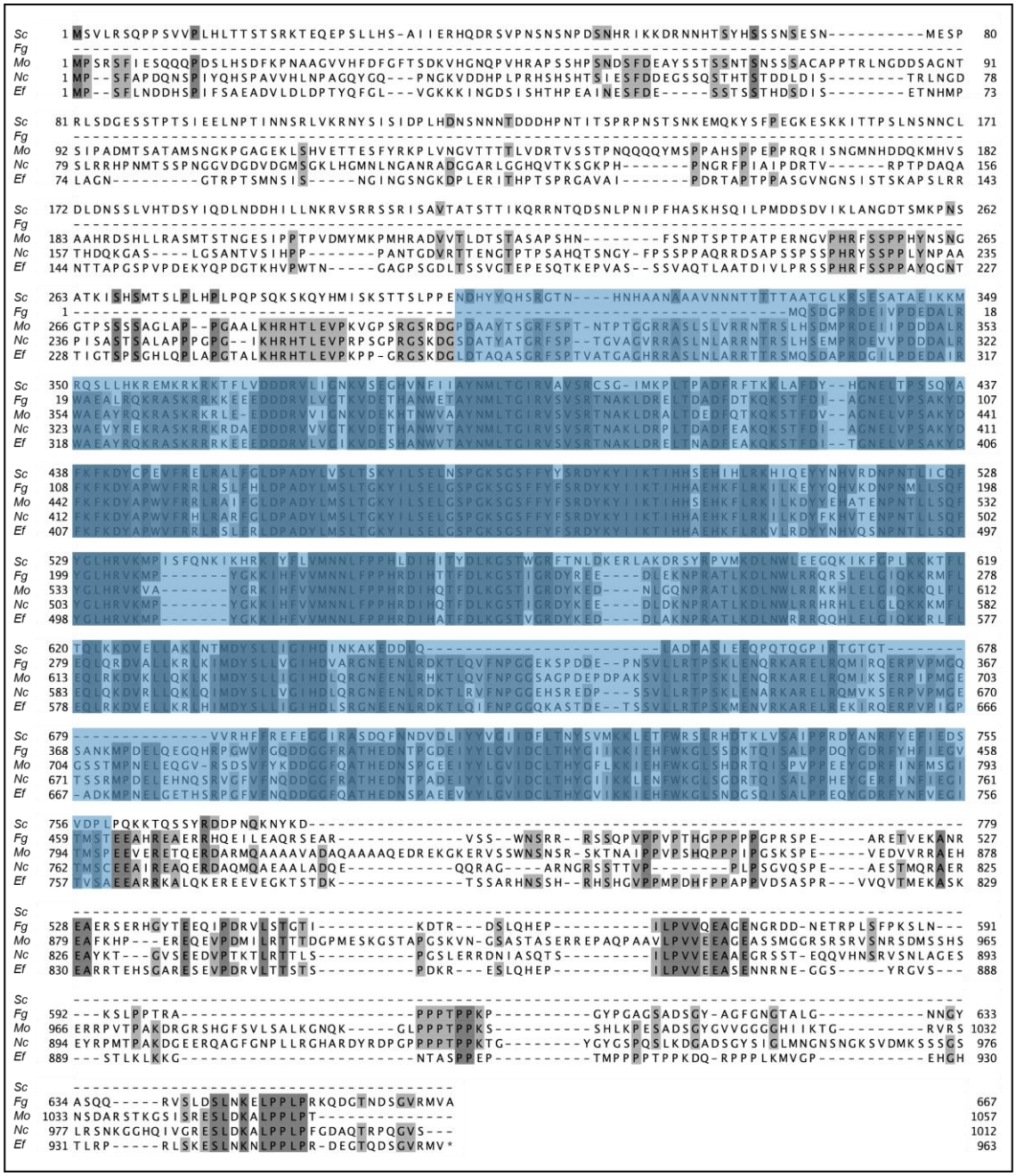

6.7 Multiple sequence alignment of fungal MssD proteins. Amino acid sequences of *S. cerevisiae* (Sc) YDR208W, Schizosaccharomyces pombe (Sp) SPAC19G12.14, *Fusarium graminearum* (Fg) FGSG_10792, *Magnaporthe*

oryzae (Mo) MGG_06572, *Neurospora crassa* (Nc) NCU02295, *Sordaria macrospora* (Sm) SMAC_08733, *Podospora anserina* (Pa) PODANS_5_9630, *E. festucae* (Ef) EfM3.031950. The degree of shading is indicative of the amino acid percentage identity. Blue boxing indicates the position of the kinase domain in *E. festucae* MssD as predicted by InterProScan (IPR023610).

6.8 qRT-PCR data for Figure 3.28. Expression of *mssD* in wild-type (Fl1) and three independent *mssD* OE transformants in culture.

Strain	MSSD		EF-2		*mssD*/EF-2					S22		*mssD*/S22				
	Cp	avg	Cp	Avg	2^(Cp reference-Cp target)	Avg	StDev	Fold WT	StDev	Cp	Avg	2^(Cp reference-Cp target)	Avg	StDev	Fold WT	StDev
#17	26.49	27.39	19.14	19	0.0033	0.003	0.00041	8.31	1.14	20.18	19.69	0.0068	0.0051	0.0024	18.16	8.48
#17	28.28		18.86		0.0027					19.19		0.0034				
#18	30.31	32.66	19.15	19.45	8.6E-05	0.00011	3.07E-05	0.30	0.085	19.85	19.76	0.00014	0.00013	0.000012	0.47	0.041
#18	35		19.74		0.00013					19.67		0.00012				
#20	27.11	30.07	20.98	19.94	0.0018	0.0011	0.00099	3.15	2.75	20.01	19.58	0.00094	0.00073	0.0003	2.59	1.07
#20	33.02		18.9		0.00044					19.14		0.00051				
#27	28.03	31.52	19.25	18.95	0.0002	0.00017	4.89E-05	0.47	0.14	19.88	19.49	0.00031	0.00025	9.37E-05	0.88	0.33
#27	35		18.65		0.00013					19.09		0.00018				
#32	28.19	29.69	19.53	19.39	0.00088	0.00080	0.00011	2.20	0.31	19.94	19.77	0.0012	0.001	0.00018	3.71	0.63
#32	31.18		19.24		0.00072					19.59		0.00091				
#36	30.12	32.56	21.66	20.85	0.00052	0.00035	0.00025	0.96	0.69	19.91	19.82	0.00016	0.00015	1.29E-05	0.52	0.046
#36	35		20.03		0.00017					19.73		0.00014				
#37	28.61	31.39	19.14	19.12	0.00021	0.0002	3.97E-06	0.56	0.011	19.71	19.43	0.0003	0.00026	6.93E-05	5.043	1.37
#37	34.17		19.1		0.0002					19.15		0.00021				
#38	30.13	32.57	19.13	19.14	9.029E-05	9.061E-05	4.44E-07	0.25	0.0012	20.11	19.645	0.00018	0.00014	5.98E-05	0.48	0.21
#38	35		19.14		9.092E-05					19.18		9.35E-05				
#52	30.76	31.29	20	19.93	0.0004	0.00038	2.62E-05	1.057	0.072	20.98	20.275	0.00079	0.00054	0.00035	1.94	1.24
#52	31.81		19.86		0.00036					19.57		0.0003				
#53	27.69	29.51	21.76	20.86	0.0046	0.003	0.0023	8.25	6.49	20.49	20.16	0.0019	0.0016	0.0005	5.6	1.78
#53	31.33		19.95		0.0013					19.83		0.0012				
Fl1	28.38	30.65	19.54	19.17	0.000452	0.00036	0.00013	1	0.35	18.9	18.85	0.00029	0.00028	1.37E-05	1	0.049
Fl1	32.92		18.8		0.00027					18.8		0.00027				

Cp = crossing point; StDev = Standard deviation

6.9 Statistical analysis

Results of the Tukey Test analyses used in Figure 3.28 are presented below. Statistical significance is deemed as a *p*-value <0.05.

Comparison	Tiller length				Tiller number			
	diff	lwr	upr	P adj	diff	lwr	upr	P adj
MssD OE 17-WT	9.67	3.88	15.46	0.00023**	-2.85	-5.66	-0.032	0.046*
MssD OE 20-WT	5.064	-0.85	10.97	0.12^{ns}	3.11	0.24	5.98	0.029*
MssD OE 53-WT	-0.38	-6.94	6.19	1^{ns}	4.32	1.13	7.52	0.0037**

diff = difference of the means , lwr and upr = 95% confidence interval, P adj = adjusted *p*-value, * = 0.05-0.01, ** = *p*-value 0.01-0.0001, ns = Non-significant.